Development and test of a method for the simultaneous measurement of heat capacity and thermal diffusivity by laser-flash technique at very high temperatures. Application to uranium dioxide.

by

Manuela Musella

Thesis

Submitted to the University of Warwick

For the degree of

Doctor of Philosophy

Department of Physics

June 1999

TABLE OF CONTENTS

ACKNOWLEDGMENTS

This research work was sponsored by the Human Capital and Mobility Program of the European Commission; I am most grateful for the financial support.

I would like to thank Prof. J. van Geel, Director of the Institute for Transuranium Elements (ITU, Joint Research Centre of the European Commission), Karlsruhe, Germany, for giving me the opportunity to perform the experimental part of the Thesis in such a prestigious facility, and Dr. Hj. Matzke for having me in his unit.

Special thanks go to my supervisors: Dr. Ronchi for introducing me to the world of the materials science and for guiding me through the whole research project, and Dr. Sheindlin for teaching me a great deal of experimental techniques and for providing useful and necessary advice and information. I would also like to convey my deep gratitude to my thesis adviser, Dr. G. Hyland, for his supervision through the years of study, for all the lectures on Physics and for trusting me to get on with things.

Many thanks go to Dr. B. Sätmark and Dr. R. Malmbeck for their help and for reading and correcting the whole Thesis!

I am particularly grateful to Dr. V.V. Rondinella and Dr. T. Wiss, who provided help and useful scientific discussions during the past years of study and experimental work, offered advice when I needed it, and provided relief, support and chocolate during the "dark periods". Concerning the use of computers, in case of emergency (that is, very frequently) Dr. T. Lam and R. Beukers were always available.

A special mention goes to the technical staff of ITU, especially (in alphabetic order): D. Halton, W. Heinz, M. Martellenghi, V. Meyritz, R. Selfslag, V. Tebaldi, H. Thiele for their kindness and help with the experimental work.

Finally, I would like to thank in a special way Luca for his tremendous help, his patience, loving support and encouragement.

This Thesis is dedicated to my grandfather who believed in me and in my research and is not here to celebrate the end of this work.

DECLARATIONS

This thesis is based on joint research carried out at the Institute for Transuranium Elements, Karlsruhe, Germany. My work consisted in carrying out the experimental part of the project and analysing the data obtained. During the research, I contributed with original ideas to the development of the apparatus and to improvements in the experimental protocol. I was also involved in the elaboration of the computer code used in the data analysis, and with the interpretation of the experimental results.

Part of this work was presented at the following conferences:

1. 13th Symposium on Thermophysical Properties, June 22-27 1997, Boulder, CO (USA) *"Universal laser-pulse apparatus for thermophysical measurement in refractory materials at very high temperature"*, C. Ronchi, W. Heinz, M. Musella, R. Selfslag, M. Sheindlin.
2. 14th European Conference on Thermophysical Properties, September 15-18 1996, Lyon, France *"Progress in Laser-Flash Applications for Thermophysical Measurements"*, D. Halton, H. Heinz, M. Musella, C. Ronchi, R. Selfslag, M. Sheindlin.
3. TEMPMEKO '96, September 10-12 1996, Turin, Italy, *"Development of New Laser-Pulse Techniques for Thermophysical Properties Measurements of Refractory Ceramics"*, D. Halton, H. Heinz, M. Musella, C. Ronchi, R. Selfslag, M. Sheindlin.

Some of the work was published under the titles:

1. *"Advances in the use of laser-flash techniques for thermal diffusivity measurement"*, M. Sheindlin, D. Halton, M. Musella, and C.Ronchi, *Rev. Sci. Instrum.* **69**, 1426 (1998).

2. *"Universal laser-pulse apparatus for thermophysical measurements in refractory materials at very high temperatures"*, C. Ronchi, W. Heinz, M. Musella, R. Selfslag, and M. Sheindlin, *Int. J. Thermophys.*, in press.
3. *"Thermal conductivity of uranium dioxide up to 2900 K from simultaneous measurement of the heat capacity and thermal diffusivity"*, C. Ronchi, M. Sheindlin, M. Musella, G.J. Hyland, *J. Appl. Phys.* **85,** 776 (1988).

No part of the work described in this thesis has been submitted in support of an application for a higher degree or qualification in this or in any other University.

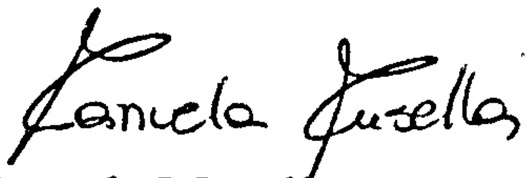

Manuela Musella

ABSTRACT

The "classical" laser-flash method is today the most used technique to measure the thermal diffusivity of a wide range of materials. This work describes the development of a new technique, based on the laser-flash method, which measures *simultaneously* on *the same sample* with an *absolute method* the *thermal diffusivity* and the *specific heat*, and its application to a number of high melting-point refractory materials.

The improvements of key components of the instrument and the use of a laser for both conditioning heating and probing made it possible to create more flexible and controllable experimental conditions, under which reliable measurements could be carried out. Thanks to these improvements, it was possible to apply an accurate analytical treatment to solve the heat transport equation.

In this work, a new data processing procedure, which takes radiative and conductive heat losses into consideration, is introduced, and the thermal diffusivity, a, and specific heat, c_P are determined by fitting the *entire* experimental transient temperature curve. The thermal conductivity is then calculated from the measured a and c_P values *via* the relationship $\lambda = a\rho c_P$, where ρ is the density of the material. For the calculation the measured room temperature values of ρ corrected to the temperature of interest *via* literature data on thermal expansion are used.

The new technique is applied to measure the specific heat, thermal diffusivity of POCO AXM 5Q graphite, zirconium dioxide and uranium dioxide (materials of scientific and technological interest) at very high temperatures (above 1800 K), from which thermal conductivity values can be calculated. The values obtained, having a precision of *~2%* in the case of the thermal diffusivity, and *~7%* for the specific heat and the thermal conductivity, are discussed and compared with literature data.
The results obtained for uranium dioxide are used for a critical analysis of the physical mechanisms underlying the heat transport in this material.

Chapter 1

1. INTRODUCTION

Thermophysical-property data are indispensable components in the design and technical evaluation of energy-producing and energy-converting systems.

In particular, in nuclear technology the necessity to know thermodynamic and thermophysical properties of reactor materials[i] up to the highest temperatures has now been extended beyond the original area of application, (*i.e.* consideration of the behaviour under *standard* reactor design conditions) to encompass a much wider scenario of new nuclear fuels[ii], and safety and risk analyses[iii]. In the recent years, a lot of projects, both experimental (*e.g.* PHEBUS, CEA, Cadarache, France) and computer based simulations have been developed to analyse and study *i*) different conditions which can lead to an accident, *ii*) different accident scenario - *i.e.* whether "protected" or "unprotected"[iv], *iii*) the worst conceivable accidents. In these studies, since all the accidents involve a large increase in temperature, knowledge of the thermophysical properties of the reactor materials up to their melting point is essential.

The heat capacity and the thermal conductivity are two of the most important parameters that control the response of the system. Under normal reactor operating conditions, they govern the basic processes underlying the eventual generation of steam. The energy produced by fission chain reactions is thermalized in the material containing the fissile isotopes (*i.e.* the fuel), and the temperature rise associated with a given deposition of neutronic energy is determined by the *heat capacity*, c_P, of the

---

[i] The term "reactor materials" refers to all the different materials used in a nuclear reactor: fuel, cladding, absorber materials, structural materials, coolants, concretes, *etc.*

[ii] Novel nuclear fuels: for instance MOX (Uranium-Plutonium Mixed Oxide), which are used in Light Water Reactor (LWR) to burn highly toxic plutonium. Measurements on MOX samples have been also performed during this study, the results, however, will be published separately.

[iii] Considerable attention has historically been given to the potential consequences of highly improbable accidents – events with such a low probability that they are termed "hypothetical" accidents. In these accidents the fuel temperature is expected to rapidly increase above the melting point. More recently, however, with the context of the advanced operating conditions of LWR's, milder accidents, are considered, which have re-opened and highlighted the problem of the behaviour of the fuel at high solid temperatures.

[iv] The term "protected" refers to the successful operation of the Plant Protection System (PPS) when brought into action, whereas "unprotected" implies failure of the PPS.

fuel. The transfer of this heat out of the fuel to a flowing coolant (which is then pumped away to raise the steam) is controlled by the *thermal conductivity*, λ. These two quantities are thus important parameters in the development and characterisation of new nuclear fuels. Additionally, they are of fundamental importance in risk and safety analyses. In the case of severe reactor accidents, in which rapid adiabatic core excursions are considered, the temperatures attained during the excursion are determined by the heat capacity of the nuclear fuel; on the other hand, the thermal conductivity plays a significant role in the *post accident* heat removal.

Despite the broad scientific and technological interest, measurements of the heat capacity and of the thermal conductivity at very high temperatures (above 2000K) have been plagued by experimental problems. The determination of these quantities at low temperatures are made using *steady-state* techniques, in which the specimen is subjected to high temperatures for relatively long periods of time (minutes to hours). Applications of these conventional techniques to measurements above 2000 K encounter severe problems due to the increased heat transfer, chemical reactions, evaporation, diffusion, *etc*. These disturbances effectively limit the use of the steady-state techniques to temperatures below about 1500 K in the case of heat capacity and about 2500 K in the case of thermal conductivity. Since most of the above-mentioned problems become more serious with increasing time, one approach (to reduce their effect) is to perform the experiments in shorter times. It is in this context that the majority of the high-speed techniques for the measurement of thermophysical properties at high temperatures were developed.

The most used high-speed technique for the measurements of the specific heat and thermal conductivity at very high temperature is the direct heating method. This method, however, is applicable only to electrical conductors, and not to refractory materials. For these, the usual way of determining specific heat is indirectly using the so-called enthalpy drop method, which being a steady-state technique, however, suffers from the above listed problems. In the case of thermal conductivity, the values are calculated from the thermal diffusivity, a, obtained using the *laser-flash* method, in conjunction with specific heat and density data, which are usually obtained from experiments on *different* samples. It can be seen that if the laser-flash method could be adapted to measure c_P as well as a, this undesirable features would

be removed, allowing more reliable values of thermal conductivity to be obtained, especially since, c_P and a, are not actually independent. The heat capacity is the sum of diverse energy absorption mechanisms (mainly lattice vibrations, crystal field transitions, point defect, and in the case of UO_2, also small polaron formation). Each of these has an associated conductivity, λ_i; however, only a few of them are effectively mobile, so that the others contribute to the total conductivity *only* through their interactions with the more mobile carriers. In the phenomenological heat flux equations, the individual diffusivities, a_i, (which are essentially in the nature of mobilities) are defined (see *e.g.* Ref. 1) as:

$$\rho c_P^i a_i = \frac{1}{T^2}\sum_k L_{ik} = \lambda_i + \sum_{i\neq k}\frac{L_{ik}}{T^2} \tag{1.1}$$

where L_{ik} are the cross-effect coefficients (*e.g.* involving the interaction of phonons with Frenkel defects, for example).

The various contributions to the *total* specific heat, c_P, are additive:

$$c_P = \sum c_P^i \quad , \tag{1.2}$$

while the average diffusivity appearing in the heat diffusion equation has the form:

$$a = \frac{\sum_i c_P^i a_i}{\sum_i c_P^i} \tag{1.3}$$

which indicates that the measured diffusivity is a function *not only* of the a_i, but also of the individual heat capacity contributions.

On account of this dependence, the evaluation of λ as the product of a and c_P entails a correlation of the errors of the latter two quantities, which can be hardly appreciated *a priori*[v]. This correlation is obviously more important at high

[v] Eq.(1.3) simplifies if the various effective diffusivities, a_i, are almost equal. This occurs if all the

temperatures, where the formation of Frenkel/Schottky point defects (very low mobility carriers) causes a marked upswing in c_P.

The idea of the simultaneous measurement of thermal diffusivity and heat capacity by laser-flash method is very old, dating from 1961 when *Parker et al.*[10] published the first paper on this subject. Yet, the instrumentation for sub-second measurements was at that time so rudimentary that the method was considered as merely hypothetical. With the progress of laser technology and fast pyrometry, the flash-method became more and more precise and reliable; however, for nearly three decades the extension of this technique to calorimetric measurements was still considered as unpracticable[vi].

Only at the end of the 80's in the *Institute of Technology of the Jet Propulsion Laboratory,* Pasadena (CA)[55] was a flash-method successfully applied, using a Xenon lamp, to heat capacity measurements up to 1300 K. The method was, however, based on a *comparative* empirical procedure, using POCO AXM-5Q graphite as a standard; moreover, the sample had to be sputtered with graphite in order to ensure the same energy absorption as in the standard. The weak point of this method was the sensitivity of the measurements to the positioning of the sample within the light beam.

A feasibility study was positively concluded in 1990, in the *National Laboratory of Metrology* of Ibaraki (Japan)[59], in which a laser-flash device was used to measure heat capacity. Again, a comparative method was used, whereby, thanks to the homogeneity of the laser beam used, the standard sample was now permanently mounted in a separate holder, in order to avoid position misalignments. In this set-up, the standard sample was essentially acting as a simple reference calorimeter.

It should be noted in both cases that an essential limitation of the applied method is set by heat losses, which may be different in the standard and in the measured

---

coefficients $\Sigma L_{ik} / T^2$ are similar to the maximum value of λ_i for $i=1$ (in the case of refractory materials, the phonon conductivity). This requires a very large cross section for inelastic scattering of phonons by lattice defects.

[vi] The calorimetric measurement requires a controllable, spatially homogeneous energy input system, as well as a very rapid and precise absolute temperature detector. In fact, accounting for the effective boundary conditions with the unavoidable heat losses necessitates a highly complex thermal analysis, which is only applicable to very accurate thermograms, obtained under highly symmetrical heat diffusion conditions.

sample; this can result in large systematic errors. A correction is to a certain extent possible; it requires, however, a rather complicated mathematical procedure, which practically annuls the advantages offered by the simplicity of the comparative method.

Furthermore, disturbing effects produced at very high temperatures were faced, entailing additional experimental difficulties. Firstly, because at these temperatures (independently of the intensity of the applied flash-perturbation) the heat losses are much higher, being proportional to the third power of temperature, and secondly, because thermal exposure of the standard sample would have changed its absorption properties, invalidating the energy measurements.

To overcome these difficulties, a new experimental set-up was constructed at the Institute of Transuranium Elements using advanced pyrometric techniques in conjunction with high quality laser beams and optical diagnostic equipment, previously unavailable. An absolute calorimetric method was implemented, in which the experimentally accesible information is fully exploited to simultaneously obtain thermal diffusivity and specific heat. A new data processing procedure, which takes radiative and conductive heat losses into consideration, was developed to enable thermal diffusivity and heat capacity values to be reliable obtained by fitting the *entire* transient temperature curve.

This thesis describes the development of the new technique and its application to a number of refractory materials.

The first step of the performed work was the refinement of the apparatus (originally built to measure the thermal diffusivity) to enable heat capacity measurements to be made. A calorimetric procedure was developed to measure the energy density of the laser probe beam, and a CCD camera was added to the device to check the spatial profile of the beam at each shot. A second pyrometer (in addition to the pyrometer looking at the rear surface of the specimen) was introduced to measure the temperature increase of the front surface of the specimen during the experiment, and allow more reliable measurements of thermophysical properties to be carried out. The experimental chamber was modified in order to carry out measurements in a slightly over-pressure (up to 5 bars) condition, by connecting to an inlet gas system;

in addition, this allowed different gaseous atmospheres to be used[vii]. To handle and study radioactive materials, a second experimental chamber was installed in a glove box[viii].

The data processing procedure (originally developed for thermal diffusivity measurements) was extended to permit specific heat measurements to be made; furthermore, the method was improved by using different solutions of the heat transport equation to describe the various experimental conditions, such as different modes of heat loss, finite pulse time effects and non-homogeneity of the flash beam profile.

The second step was to test the new technique (device and data analysis) on a reference material. The test material chosen was POCO AXM-5Q graphite, a recommended standard reference material for thermophysical measurements at high temperatures[ix]. The specific heat and the thermal diffusivity of POCO AXM-5Q were measured and compared with recommended values; the agreement was found to be excellent over the common temperature range - since the present experiments extended to much higher temperatures than did previous ones.

The technique was then applied to two materials for which the thermal diffusivity and the specific heat at temperature above 1800 K are *less* well established: (stabilised) zirconium dioxide and uranium dioxide.

Zirconium dioxide was chosen since is an important technological material[x], but one whose optical properties entail serious difficulties in the application of the laser-flash method for thermophysical properties measurements. Its high low temperature

---

[vii] The possibility to carry out experiments in over-pressure is important in the study of materials having high vapour pressure (*e.g.* graphite and uranium dioxide), since a slightly over-pressure can limit the sublimation of the material during the experiments. The use of different atmospheres (inert or reactive) is also of particular importance in the case of uranium dioxide in which the vaporisation is non-congruent,so that a suitable atmosphere is necessary to prevent a change in the composition of the material.

[viii] The glove-box is a metallic structure with plexiglass walls, which ensures shielding from α and β radiation. The manipulation of the sample is made trough holes covered with latex gloves.

[ix] Although several studies have been undertaken to establish a reference material for thermophysical properties measurements, as of now no reference material is available that is certified by official national and international organisations. One candidate reference material for measurements at high temperatures is POCO AXM-5Q graphite. "Round-Robin" measurements and several co-operative projects to measure thermophysical properties of this material were conducted and recommended values are given (see Ref.[68]).

[x] Plasma-sprayed stabilised zirconium dioxide is currently under investigation as a thermal barrier coating material for high temperature applications.

transparency (at the wavelength of the laser used) necessitates in fact very careful experimentation in order to ensure reliable results.

The study was then conducted on uranium dioxide, the most common nuclear reactor fuel. Though this material has been studied for several decades, its thermophysical properties at high temperature are, in fact, still controversial, and for temperatures above 2300 K the data are scanty and imprecise (the experimental dispersion of diffusivity and specific heat at high temperature are, respectively, 10-15% and 20-30%). Initially, this situation was not generally considered as a source of great concern, since these temperatures are far above the fuel operational range under normal reactor conditions. However, with the increasing demand for more information on mechanisms, together with the ongoing concern over the consequences of nuclear reactor accidents, the problem of obtaining a better understanding and definition of the thermophysical properties of the nuclear fuel up to very high temperatures has become a topic of great interest and importance.

<u>The thesis content is divided into two main sections.</u>

The first section (Chapters 2 and 3) is preparatory. Chapter 2 provides an introduction to specific heat, thermal diffusivity, and thermal conductivity, with a critical review of the methods used for their determination at very high temperatures. Chapter 3 describes, schematically, the principle of the laser flash method, with an overview of the different mathematical models used to analyse the experimental data (Section 3A). The principle of the laser-flash method, the model used to calculate thermal diffusivity for ideal conditions and corrections procedures for thermal losses, finite time pulse and non-uniform heating are presented. A summary of the calorimetric techniques based on the laser-flash principle is also presented (Section 3B).

The second part (Chapters 4 to 6) describes the new technique and the results obtained, and for the case of UO_2, considers their interpretation in terms of underlying physical processes. In particular:

Chapter 4 describes the features of the experimental set-up (Section 4A) and the method of data analysis used (Section 4B), emphasising the main improvements of the new technique and its advantages in comparison with the classical ones.

Chapters 5 presents the results on the measurements of thermal diffusivity, specific heat and thermal conductivity for graphite (Section 5A) and zirconium dioxide (Section 5B), their discussion, and a critical comparison with literature data.

In Chapter 6 are presented and discussed the results obtained on uranium dioxide, and an analysis is given of the physical mechanisms of heat transport, in the light of the new experimental data obtained.

Chapter 2

2. THERMOPHYSICAL PROPERTIES

2.1 Specific heat

2.1.1 *Definition of specific heat*

The heat capacity of a system of arbitrary mass, m, may be defined in terms of the following limit:

$$C = \lim_{\Delta T \to 0}\left(\frac{\Delta Q}{\Delta T}\right) \tag{2.1}$$

where ΔQ is the quantity of heat that must be added to the system to raise its temperature by an amount ΔT. In order to obtain a quantity that is independent of mass, Eq.(2.1) is divided by m to yield the specific heat capacity:

$$c = \frac{C}{m} = \frac{\delta q}{\delta T} \tag{2.2}$$

where δq is the quantity of heat required to raise the temperature of a unit mass of the system by an amount δT. The specific heat capacity is then the amount of heat, which a unit mass of substance has to exchange with its surroundings in order to change its temperature by one degree. In general, the required quantity of heat will depend upon the temperature of the system and the conditions under which it is exchanged. Since for an ideal fluid or for a solid the equation of state has the form $f(P,V,T)=0$, as T is increased, only one of the remaining two variables, P or V, can be kept constant. Consequently, there are two principal specific heats, one defined at constant volume, the other at constant pressure:

$$c_V = \left(\frac{\delta q}{\delta T}\right)_V \qquad c_P = \left(\frac{\delta q}{\delta T}\right)_P \tag{2.3}$$

in most theoretical calculations, the natural quantity to calculate is the 'heat capacity per mole' since this refers to a fixed number of particles. By convention, the molar specific heats are denoted by upper case symbols and are defined, as in Eq.(2.3), as:

$$C_V = \left(\frac{\delta Q}{\delta T}\right)_V \qquad C_P = \left(\frac{\delta Q}{\delta T}\right)_P \tag{2.4}$$

where δQ is the quantity of heat required to raise the temperature of one mole of the subtance by an amount δT under conditions of constant volume or constant pressure.

According to the first and second laws of thermodynamics C_V and C_P may be expressed as:

$$C_V = \left(\frac{\partial U}{\partial T}\right)_V \qquad C_P = \left(\frac{\partial H}{\partial T}\right)_P \tag{2.5}$$

where U and H are, respectively, the internal energy and the enthalpy of the material. The quantity C_V is of particular theoretical interest since a change in the internal energy of a substance with temperature can, in principle, be related by statistical methods to changes in the translational, vibrational, rotational, electronic and/or magnetic energy of its atoms. In the study of solids, however, it is very difficult to measure C_V directly and, thus, C_P is the quantity that is normally determined by experiment. The general relation between C_V and C_P is given by:

$$C_V = C_P - \left(\frac{\alpha^2 V_m}{\beta}\right) T \tag{2.6}$$

where α is the coefficient of volumetric expansion, β is the coefficient of isothermal compressibility, and V_m is the molar volume of the substance.

2.1.2 *Methods for measuring specific heat*

The calorimetric techniques used to measure heat capacity can be generally divided in two classes; one where specific heat is obtained directly from the measured quantities (adiabatic heating, temperature modulation, energy pulse, differential scanning) and another where the quantity directly measured is enthalpy and the heat capacity is obtained by differentiating the enthalpy with respect to temperature (drop or levitation). According to a second classification, the methods are divided into steady-state and transient calorimetry techniques. In the former the sample is kept under constant conditions for a period long enough to reach equilibrium conditions with the surrounding (during minutes to hours), while in the latter the measurement is made in a very short time period (usually less than one second).

The nature and the form of the specimen usually dictate a first selection of the applicable techniques. For example, in some of the more specialised methods, such as in temperature modulation and energy pulse, where resistive heating is used, the technique is limited to electrically conducting samples, which are shaped in the form of wires, rods, or tubes. In adiabatic and drop techniques, the specimen is generally contained in a capsule which enables the use of a specimen of any shape, and there is no restriction on the nature and properties of the material.

In the following paragraphs the direct heating and the drop method, the only two techniques applicable at high temperatures, will be briefly discussed. The laser-flash calorimetric technique, being the method used in this work, will be separately discussed in Chapter 3.

<u>The drop calorimetry method</u>

The drop calorimetry is a method generally used for measuring heat capacity of non-conductive material at high temperatures. Although drop calorimeters have been built to operate at temperatures as high as near 3000 K, the accuracy of this technique deteriorates rapidly above 2000 K.

In the drop calorimetry the specimen, brought to an initial thermodynamic equilibrium state in a furnace (outside the calorimeter), is translated rapidly into the

calorimeter boundary. As a result of this change, the calorimeter proceeds from its own initial thermodynamic equilibrium state prior to adding the specimen to some final state while containing the specimen. The specimen proceeds at the same time to its final equilibrium state within the calorimeter. In the ideal experiment, the specimen and the calorimeter each have the same temperature throughout in their final states. The physical quantity directly measured is the enthalpy change of the specimen upon entering the calorimeter. Under isobaric conditions the change in specimen enthalpy is equal to the heat transferred between the specimen and the calorimeter:

$$H_{T_i} - H_{T_e} = \int_{T_c}^{T_i} C_p dT \tag{2.7}$$

where T_i denotes the initial specimen temperature, and T_c denotes the final temperature common to both the specimen and the calorimeter.

In principle, it is possible to calculate the average heat capacity at the average temperature by evaluating $(H_2 - H_1)/(T_2 - T_1)$. In practice, this may produce a misleading large variant of the calculated heat capacity values due to the difference in size of the temperature intervals and the computation of $(H_2 - H_1)$ as a relatively small difference of two much large numbers. An example of the error introduced in the specific heat using this procedure is given by Hein *et al.*[2]. The mean specific heat calculated by Hein *et al.* for uranium dioxide with the formula $(H_T - H_{298.2})/(T - 298.2)$ compared with the recommended data[3], shows an error of 7% at 1500 K which rises up to 40% at 3100 K (see § 6.3.1).

A more satisfactory representation of the heat capacity can be obtained by first fitting some suitable function to the enthalpy data and then differentiating this function to obtain the heat capacity function. The algebraic form chosen to describe enthalpy as a function of temperature however, may influence to a great extent the heat capacity values derived. This point will be discussed in more detail in § 6.3.1, where some examples will be also given.

The transfer of the sample from the furnace to the calorimeter unavoidably involves a loss of heat to the surroundings, which is not detected by the calorimeter. At very high temperatures this loss can be a significant fraction of the total sample heat. The heat loss has a radiative component, and if not dropped in vacuum, conduction and convection components. The accuracy of the calculations after the heat losses from such a sample will depend on the successful modelling of the surroundings through which the sample travels on its path to the calorimeter. Encapsulating the specimen during measurement can reduce the amount of heat lost from the sample. Then it can be assumed that the enthalpy increment due to the sample alone is obtained by subtracting from the relative enthalpy determined for the sample plus its container, the corresponding relative enthalpy for the container alone (determined in a second experiment). This procedure implicitly assumes that no heat is lost by the sample itself in dropping into the calorimeter.

Although drop calorimetry is an appropriate technique for a broad range of substances, it does have important limitations. It is in general not applicable to samples that react chemically or dissociate in the temperature range of interest. Furthermore, it is desirable that the samples have negligible or low vapour pressure.

The direct electrical heating method

The direct electrical heating method has been developed to extend the limits of accurate measurements of specific heat of electrically conducting specimens to temperatures beyond the limits of other calorimetric techniques. Because of the extremely short experiment duration (subseconds to submilliseconds), this technique is immune from most of the high-temperature problems that arise from heat losses, chemical reactions, evaporation, etc. Pulse calorimetry is generally used at temperatures above 1000 K, and in the case of subsecond-duration techniques, the upper temperature limit is the melting point of the specimen.

The method is based on rapid resistive self-heating of the specimen in a controlled-environment chamber produced by the passage of a high electrical current through it. The measured quantities are the heating rate of the specimen's

temperature, the current flowing through the specimen and the voltage drop in the specimen. In general case, the power balance for the specimen may be expressed as:

Power Imparted = Power Stored + Power losses

which becomes:

$$VI = c_P m(dT/dt)_h + Q \tag{2.8}$$

and solving Eq. (2.8) for c_P

$$c_P = \frac{VI - Q}{m(dT/dt)_h} \tag{2.9}$$

where V is the voltage drop across the effective specimen, I is the current through the sample, m is the mass of the effective specimen, $(dT/dt)_h$ is the heating rate of the specimen and Q is the total power loss from the effective specimen.

The quantity Q may be obtained from data during the initial cooling period. Power balance for this period gives:

$$-c_P m(dT/dt)_c = Q \tag{2.10}$$

where $(dT/dt)_c$ is the cooling rate of the specimen. Substituting Eq.(2.10) in Eq(2.9) for Q, the specific heat can be calculated by:

$$c_P = \frac{VI}{m(dT/dt)_h(1+1/M)} \tag{2.11}$$

where

$$M = -\frac{(dT/dt)_h}{(dT/dt)_c}$$

At temperatures above 1500 K, in high-speed experiments of 0.001-1s duration, thermal radiation is the major source of power loss. In this case power loss may be estimated using the relation for thermal radiation:

$$Q_r = \varepsilon \sigma_S A_s (T^4 - T_0^4) \tag{2.12}$$

where ε is the hemispherical total emittance, σ_S is the Stephan-Boltzmann constant, A_s is the effective surface area, T is the specimen temperature, and T_0 is the ambient temperature. Although the general principle of all the direct heating methods is the same, there are considerable variations from each technique. In particular there are two different categories of pulse methods: methods were the specimen is initially at room temperature and methods were the specimen is preliminary heated initially under steady-state conditions at high temperature (in a furnace or by resistive self-heating).

The methods in the first category represent truly fast experiments, in the sense that the specimen and its immediate environment are initially at room temperature and only the specimen is heated to high temperatures during the very short pulse period. Thus, these techniques do not have the limitations of those in the second category, which, being a combination of steady-state and pulse methods, have the same limitations of the classical calorimetry techniques.

2.2 Thermal conductivity

2.2.1 *Definition of thermal conductivity*

The thermal conductivity is a phenomenological physical property of a substance, which characterises its ability to conduct heat.

The heat propagation in a material is described by the Fourier equation:

$$\vec{q} = - \| \lambda \| \nabla T \tag{2.13}$$

where $\vec{q}$ is the flux of thermal energy and ∇T is the temperature gradient. The proportionality matrix $\| \lambda \|$, is called *thermal conductivity* and it is represented by a symmetrical tensor of six independent components. For an isotropic medium, such as polycrystalline materials, $\| \lambda \|$ can be reduced to a constant and Eq.(2.13) is expressed by:

$$\vec{q} = - \lambda \nabla T \tag{2.14}$$

From Eq. (2.14) the thermal conductivity can be defined as the time rate of steady-state heat flow through a unit area of a homogeneous material induced by a unit temperature gradient in a direction perpendicular to that unit area[4].
The reciprocal of the thermal conductivity of a substance is called thermal resistivity.

2.2.2 *Methods for measuring thermal conductivity*

The methods used to measure thermal conductivity may be divided into two categories, static or dynamic, depending on whether the temperature distribution within the sample is time dependent or not. In the steady-state methods, the conductivity is directly measured, while in dynamic methods the property directly measured is the thermal diffusivity and the thermal conductivity is then derived by a separate measurement of the heat capacity.

In steady-state methods the test specimen is subjected to a temperature profile which is time invariant, and the thermal conductivity is determined by measuring the rate of heat flow per unit area as well as the temperature gradient after equilibrium has been reached. Several methods exist to measure the thermal conductivity in different ranges of temperatures for various classes of materials having different

ranges of thermal conductivity levels[5,6,7]. In the following paragraphs the radial flow and the direct electrical heating techniques, the only techniques that can be used for measurements at high temperature, will be briefly discussed. The dynamic methods will be presented in § 2.3.2

The radial heat flow method

The radial heat-flow method was first reported by Callendar and Nicholson in 1897[8]. This technique nowadays consists of a lot of variants, which differ basically on the specimen geometry (cylindrical, spherical, ellipsoidal, concentric cylinder, concentric sphere, plate). In the first method a specimen is used in the form of a circular cylinder with a coaxial central hole, which contains an electrical heater. The core heater is supposed to protrude from each end of the sample. A furnace to raise the average temperature of the system surrounds the specimen. Thermometers (usually thermocouples) are mounted in the specimen at a minimum of two radii near the specimen's midplane. A stable electrical current is passed through the core heater to generate heat, which is assumed to flow radially outward. This establishes a temperature difference between the thermometers. After the system reaches steady state the temperature gradient in the specimen is measured. The thermal conductivity is calculated from the formula:

$$\lambda = \left(\frac{P}{l}\right)\frac{\ln(r_2/r_1)}{2\pi(T_1 - T_2)} \tag{2.15}$$

where (P/l) is the power per unit length of the core heater and T_n is the temperature at radius r_n. This configuration will yield accurate data if the ratio of specimen length, l to diameter, d, is sufficiently large to ensure that the heat flow at the specimen midplane is fully radial. The great advantages of the radial flow technique are the wide range of applicability of the method for different temperatures and materials. It has also been employed to very high temperatures, generally with moderate to low thermal conductivity specimens. The greatest disadvantages of this method are the large specimen size required, and the long measurement time.

The direct electrical heating method

The direct electrical heating method (DEH) was first described by F. Kohlrausch in 1899[9]. The technique has several application variants; in the original one, the heat longitudinally flows, the sample being connected between two electrodes, and heated by the passing current. Under ideal conditions the thermal conductivity is calculated by:

$$\lambda = \frac{1}{8\rho}\frac{(V_1 - V_3)^2}{(T_2 - T_1)} \tag{2.16}$$

where ρ is the electrical resistivity of the sample, V_1 and V_3 are the electrical potentials at locations 1 and 3 on the specimen which are equidistant from the midpoint 2, and T_1 and T_2 are the temperature at locations 1 and 2.

Direct electrical heating method has advantages (attaining of very high temperatures, simple apparatus, small specimens, short time needed to reach equilibrium) that makes it preferable to other methods. In addition direct electrical heating techniques may be used to measure, simultaneously, or consecutively, also other physical properties such as specific heat (§ 2.1.2), electrical resistivity and emissivity. The major drawback is that the method can only be successfully applied to sufficiently good electrical conductors. Another disadvantage of this technique is that it usually yields thermal conductivity in terms of electrical conductivity, which is temperature-dependent. A more sophisticated analysis can be applied to DEH by assuming a temperature dependence of ρ, and calculating numerically, by using λ as a variable parameter, the radial temperature profile which fits to the measured temperatures.

2.3 Thermal diffusivity

2.3.1 *Definition of thermal diffusivity*

The linear law relating heat flow and temperature gradient, is adequate only for steady state phenomena, and gives only a partial description of the thermal processes involved in solids. In order to discuss time-varying phenomena requires the use of the principle of conservation of energy (first law of thermodynamics). Consider a small volume inside the conducting medium. If there is no work being done on this volume, the change in its internal energy will be given by the heat transfer across its boundaries. Thus, if ΔU_0 is the internal energy at the time $t = 0$, and ΔU_t that at the time t, then:

$$\Delta U = \Delta U_t - \Delta U_0 = \Delta Q \tag{2.17}$$

where ΔQ is the heat entering the small volume. This can be expressed in terms of the time derivative of the internal energy and the integration of the heat current over the total surface:

$$\frac{d(\Delta U)}{dt} = -\iint \vec{q} \cdot \vec{n} dS \tag{2.18}$$

where $\vec{n}$ is an outward directed normal to the surface. The term on the left-hand side can be replaced by a volume integral over the internal energy density U, and the right-hand side can be replaced by a volume integral, yielding:

$$\iiint \frac{\partial U}{\partial t} d^3x = \iiint div\vec{q} d^3x \tag{2.19}$$

or, since the integration volume is arbitrary,

$$\frac{\partial U}{\partial t} = -div\vec{q} \tag{2.20}$$

the changes in internal energy can be expressed in terms of the specific heat c_P[xi] multiplied by the density ρ:

$$\frac{\partial U}{\partial t} = c_P \rho \frac{\partial T}{\partial t} = -div\vec{q} \tag{2.21}$$

and combining with Fourier's law (Eq.2.13)

$$c_P \rho \frac{\partial T}{\partial t} = -div(\| \lambda \| \nabla T) \tag{2.22}$$

In case of isotropic medium and considering the thermal conductivity constant with temperature Eq.(2.22) may be written as:

$$c_P \rho \frac{\partial T}{\partial t} = \lambda \nabla^2 T \tag{2.23}$$

or

$$\frac{\partial T}{\partial t} = a \nabla^2 T \tag{2.24}$$

where

$$a = \frac{\lambda}{c_P \rho} \tag{2.25}$$

[xi] In this context c_V should be more appropriate, since work of any kind was excluded, which means no changes in volume. However, this is not the usual experimental situation, since it requires rigid constrains around the conductor to prevent the normal changes in volume by thermal expansion.

is the quantity called thermal diffusivity. All diffusivity processes can be represented by an equation similar to Eq.(2.24). In this respect, one can speak of "temperature diffusion", as a phenomenon essentially analogous to the movement of particles submitted to Brownian motion. When heat flows through a material under non-steady-state conditions, one may then visualise the thermal diffusivity as an indication of the ratio of the amount of heat flowing out of a volume of the material to the amount of heat retained within the volume.

Since Eq.(2.24) describes time-varying thermal phenomena but the energy flux does not compare in the equation, and since thermal diffusivity is simply correlated to thermal conductivity by Eq.(2.25), thermal diffusivity measurements are often utilised for the thermal conductivity determination. Thermal diffusivity, measured by non-steady-state methods, requires in fact the measurement of the time for a thermal perturbation to propagate a known distance. Thermal conductivity, measured by a steady-state method, requires the measurement of a thermal flux and a temperature gradient. Since lengths and time intervals can be measured more easily and accurately than heat fluxes and temperature gradients, it is often easier to measure thermal diffusivity than thermal conductivity. Further, because thermal diffusivity experiments are usually short, dynamic methods are preferable to use under extreme conditions. This is often the case at very high temperatures where a short test-time is desirable to avoid heat losses and complications due to any structural and chemical changes occurring in the specimen.

2.3.2 *Methods for measuring thermal diffusivity*

Thermal diffusivity is measured by non-steady state methods. These methods are based on the analysis of the temperature response of the specimen subjected to transient thermal conditions. According to the nature of the temperature perturbation at the specimen boundary, they may be divided into two basically separate large groups, transient heat flow methods and periodic heat flow methods. Transient heat

---

Using the condition of constant pressure, the place of internal energy U must be taken by the enthalpy H.

flow methods include the flash or pulse method, where the duration of the perturbation is very short compared with the transient. All periodic heat flow methods are based on the measurement of the attenuation or the phase shift of temperature waves along the path of their propagation through the material. They are, however, arbitrarily divided into two groups, according to the temperature range of application and the mode of energy supply. The first, called temperature wave techniques are applicable to lower and medium temperatures, and are suitable for generating a number of thermophysical measurements in one single experiment. The second group constitutes the high temperature variants, where the modulated energy input is effected by electron or photon bombardment.

In the following paragraphs the techniques used to measure thermal diffusivity at high temperature, namely the laser-flash and electron bombardment methods, will be discussed. The laser flash method, being the technique used in this work, will be discussed in more detail in the next chapter.

The flash method

The flash method is presently the most used method to measure the thermal diffusivity. Since the original paper of Parker *et al.*[10] in 1961, the method has been gradually improved, the precision has been enhanced, and the field of application greatly enlarged. Now, the laser pulse method is generally recognised as the preferred method for measuring the thermal diffusivity of solid materials (metals, ceramics, polymers) from room temperature to high temperatures[xii] and has been successfully applied to measure the thermal diffusivity of particular novel solid materials (*e.g.* multilayered composites[150], highly porous materials[151,152,153] and foams[154]) as well as liquid[155,156]. The pulse technique is based on the analysis of the temperature–time history of the rear face of a disk-shaped specimen whose front face has been exposed to a burst of radiant energy. A furnace controls the ambient temperature and as a source of energy pulses the laser is nowadays most commonly used, flash lamps being an alternative. The resulting temperature rise of the rear

surface of the specimen is measured, and thermal diffusivity values are computed from temperature rise versus time data. In the original model for the flash method to measure thermal diffusivity[10] a mathematical solution of the pulse propagation equation (see *e.g.* Carslaw and Yaeger[11]) is reduced for the ideal conditions of sample homogeneity, one dimensional conduction, impulse input and adiabatic boundary to yield the simple algebraic relation:

$$a = 0.1388L^2 / t_{1/2} \tag{2.26}$$

where L is the thickness, $t_{1/2}$ is the time to half-maximum rise and 0.1388, called the Parker coefficient, is the constant for the ideal case (later identified as $t_{1/2}/t_c$).

With correct specimen positioning and holding, and fairly homogeneous laser flash beam that ensures unidirectional heat flow through the specimen, detection of the specimen rear face temperature is the main problem in this method of thermal diffusivity measurement. Thermocouples are usually used as detectors below 250 K. Above this temperature, photoconductive infrared detectors, represent a better solution since the contact temperature detector may easily distort the temperature-time record and introduce a large systematic error in the measured thermal diffusivity[12].

Due to

i. the ease with which initial and boundary conditions of the mathematical heat conduction model can be reproduced in a physical experiment,

ii. the small and simple specimens shape, which represent an advantage in the study of materials where specimen handling is not simple, *i.e.*, for rare substance, irradiated or radioactive materials,

iii. the wide range of materials, diffusivities, and temperatures to which the method is applicable,

---

[xii] An estimation made in 1975 reported that, already at that time, about 75% of thermal diffusivity measurements made in the western world were obtained by this technique (R.E. Taylor, *Appl. Phys. Lett.* **5** 212 (1975)).

the flash method has gained very high popularity in the past two decades, and the greatest part of more recent data on thermal diffusivity in the literature has been produced by this technique.

The electron bombardment modulated heat input method

The electron bombardment modulated heat input method is a high-temperature variant of the temperature wave method[13].

In the temperature wave method the specimen is brought to the desired measuring temperature and on one surface of the sample a periodic modulation signal is superimposed, with an amplitude that is small compared to the magnitude of the mean steady-state signal. The temperature of the bombarded surface varies according to this modulation but it is shifted in phase with respect to the beam modulation. The temperature of the other surface is modulated accordingly as a result of the energy transported through the sample, but this modulation is smaller in amplitude and its phase again lags with respect to the modulation at the bombarded surface. Both the temperature phase shift created between either side of the specimen, as well as the amplitude decrement, are unequivocally connected with the thermal diffusivity value of the specimen[14,15]. The variants of the temperature wave method differ basically on the symmetry of temperature waves (plane, quasiplane, radial and spherical). The sources of information are the mean temperature field, the amplitudes and phases of temperature waves. Thermal diffusivity is determined from information on (*i*) the amplitude and phase of temperature oscillations at one frequency[16], (*ii*) by measuring the amplitudes at two different frequencies[17], or (*iii*) from data on temperature oscillation phases at two different frequencies[18]. The amount of information attainable permit inner checking of the experiment when data received from one pair of measured quantities are compared with data received from another pair obtained in the same experiment. The same characteristic enables the simultaneous measurement of more than one thermophysical property in one experiment. "Multi-property variants", in which thermal conductivity, thermal diffusivity, and the specific heat of the investigated material are simultaneously

measured are mostly applicable to electron bombardment[19,20,21] and low-inertia resistive heaters [22,23].

Modulated electron beam input techniques or modulated light beam variants, cover a large proportion of the high–temperature thermal diffusivity measurements of metals and non-metals. Electron heating, in fact, has made it possible to shift the working temperature limitations upwards and to easier produce the desired boundary-value conditions imposed by the theory, though the measurements are restricted to vacuum conditions.

Chapter 3

3. LASER-FLASH METHOD

3A. CLASSICAL LASER-FLASH METHOD FOR THERMAL DIFFUSIVITY MEASUREMENTS

The laser-flash method (LAF) for the measurement of thermophysical properties is conceptually simple and presents advantages with respect to the other methods described in § 2.3.2. Under ideal conditions, LAF enables the thermal diffusivity to be evaluated from the measured temperature transient in a straightforward manner. In practice, several undesired factors affect the temperature transient. Among them the most significant are:

1. the radiative (axial and radial) and conductive thermal losses, mainly influenced by the design of the specimen holder, and by the size of the deposited energy spot relative to that of the sample,
2. the finite duration of the laser pulse,
3. the non-homogeneity of the spatial profile of the laser beam,
4. the presence of optical and electrical noise during transient temperature measurement,
5. the possible drift of the baseline sample temperature during the shot,
6. the axial temperature gradients produced in the sample by the shot itself,
7. the losses produced at the sample geometrical boundary in the form of vaporisation,
8. the possible chemical interaction of the sample with the holder.

When the flash method was first applied in 1960s it was soon recognised that, even under optimal experimental conditions, it was necessary to compensate for the major systematic errors which, in some cases, can led to an error of the measured diffusivity value of several tens of percent[24,25,26,149]. One of the early solutions was simply to correct the Parker coefficient of Eq.(2.26). In the last years, thanks to the new computer technology, more powerful data reduction methods, which consider the entire thermogram for the calculation of thermal diffusivity, were developed.

However because of the complexity of these methods, the classical data reduction technique is still more used especially for "ideal case experiments", and low temperature measurements.

3A.1 Principle of the method

The laser flash method is based on the comparison of the measured temperature with the temperature obtained from mathematical solution of the pertinent heat conduction problem.

The general heat diffusion equation for homogeneous and isotropic materials is given by:

$$\nabla^2 T(z,r,t) + \frac{q(z,r,t)}{\lambda} = \frac{1}{a}\frac{\partial T(z,r,t)}{\partial t} \qquad (3A.1)$$

assuming that the thermal conductivity, λ, is independent of temperature (that is true for small perturbations). Parker *et al.*[10] considered the ideal case of an adiabatically insulated infinite slab (initially at constant temperature) which is subjected to a spike of energy inferred on one side. Using the following assumptions

1. no heat loss from the slab surface ($q(z,r,t)=0$),
2. one dimensional heat flow,
3. uniform pulse absorption at the front surface,
4. very short pulse duration compared with the characteristic time of thermal diffusion,
5. absorption of the pulse energy in a very thin surface layer,

the solution of Eq.(3A.1) expressed as the temperature T at time t of the rear face, $z=L$, of the slab, is given by[10]:

$$T(L,t) = \frac{Q}{\rho c_p L}\left[1 + 2\sum_{n=1}^{\infty}(-1)^n \exp\left(-n^2\pi^2 at/L^2\right)\right] \qquad (3A.2)$$

where Q is the energy density absorbed by the sample, ρ the density of the sample and c_P its specific heat.

After infinite time the rear-face temperature will reach its maximum asymptotic value:

$$T_{L_{max}} = Q/\rho c_P L$$

For a slab initially at reference temperature T_0, the reduced temperature $V(L,t)$ in its rear-face is then given by:

$$V(L,t) = \frac{T(L,t) - T_0}{T_{L_{max}} - T_0} = 1 + 2\sum_{n=1}^{\infty}(-1)^n \exp\left(-n^2\pi^2 at/L^2\right) \qquad (3A.3)$$

Eq.(3A.3) establishes a relation between the fractional rise in the rear-face temperature and the material thermal diffusivity:

$$a = k_x L^2 / t_x \qquad (3A.4)$$

where k_x is a constant corresponding to x percent rise and t_x is the corresponding elapsed time. In the method originally proposed by Parker *et al.*[10] the elapsed time considered was the time needed for the rear side temperature to reach 50% of its maximum value and the equation given to calculate thermal diffusivity was:

$$a = 0.1388 L^2 / t_{1/2} \qquad (3A.5)$$

This is still the most used technique to calculate the thermal diffusivity. In fact, since any point on the thermogram can be used to obtain the thermal diffusivity from Eq.(3A.5), values of k_x corresponding to different times have been calculated[7]. They are listed in Table 3A.1.

Table 3A.1.

Values of k_x in Eq.(3A.4)

x (%)	k_x	x (%)	k_x
10	0.066108	60	0.162236
20	0.084251	66 (2/3)	0.181067
25 (1/4)	0.092725	70	0.191874
30	0.101213	75 (3/4)	0.210493
33 (1/3)	0.106976	80	0.233200
40	0.118960	90	0.303520
50 (1/2)	0.138785		

From Eq.(3A.4) a characteristic rise time $t_c = L^2/a$ can be defined. It represents the time necessary for a heat pulse to propagate through the unit length of the specimen. The characteristic rise time is used as a parameter to verify if the 4th condition, implied by Eq.(3A.2), is actually satisfied.

3A.2 Data reduction accounting for disturbing phenomena

The "$t_{1/2}$-method" proposed by Parker, is not valid if any of the five restrictions listed in Section 3A.1 is not satisfied. In practice, non-ideal boundary conditions are always faced; heat losses from the sample, finite pulse time and non-uniform heating effects must be taken into account. Theoretical models which incorporate these effects (individually or simultaneously), and mathematical expressions which properly account for them, may be worked out. Problems arise, however, in mathematically expressing the actual experimental conditions, *e.g.* in formulating quantitatively the degree of non-uniformity of heating, the exact heat loss from each surface, etc. It must be remarked that in most cases these effects represent distinct deviations from the ideal situation, and thus can not be properly classified as sources of random errors.

3A.2.1 *Heat losses*

The 1st hypothesis under which Eq.(3A.2) was derived states that no heat loss from the slab surfaces occur. But heat transfer between the sample and the environment is unavoidable, at least via thermal radiation and the effect can not be neglected, especially at high temperature (above ~1500 K) or in measurements of high conductivity materials (such as metals). Corrections to Eq.(3A.5) are then necessary for the calculation of the real thermal diffusivity.

Experimentally, the occurrence of heat losses produces in the experimental thermogram

i. a lag of the experimental curve compared to the ideal case from 5% to 50% rise of ΔT_{max} (Fig. 3A.1),

ii. a lead of the experimental curve compared to the ideal case from 50% to 100% of ΔT_{max},

iii. a relatively short maximum followed by a pronounced decline.

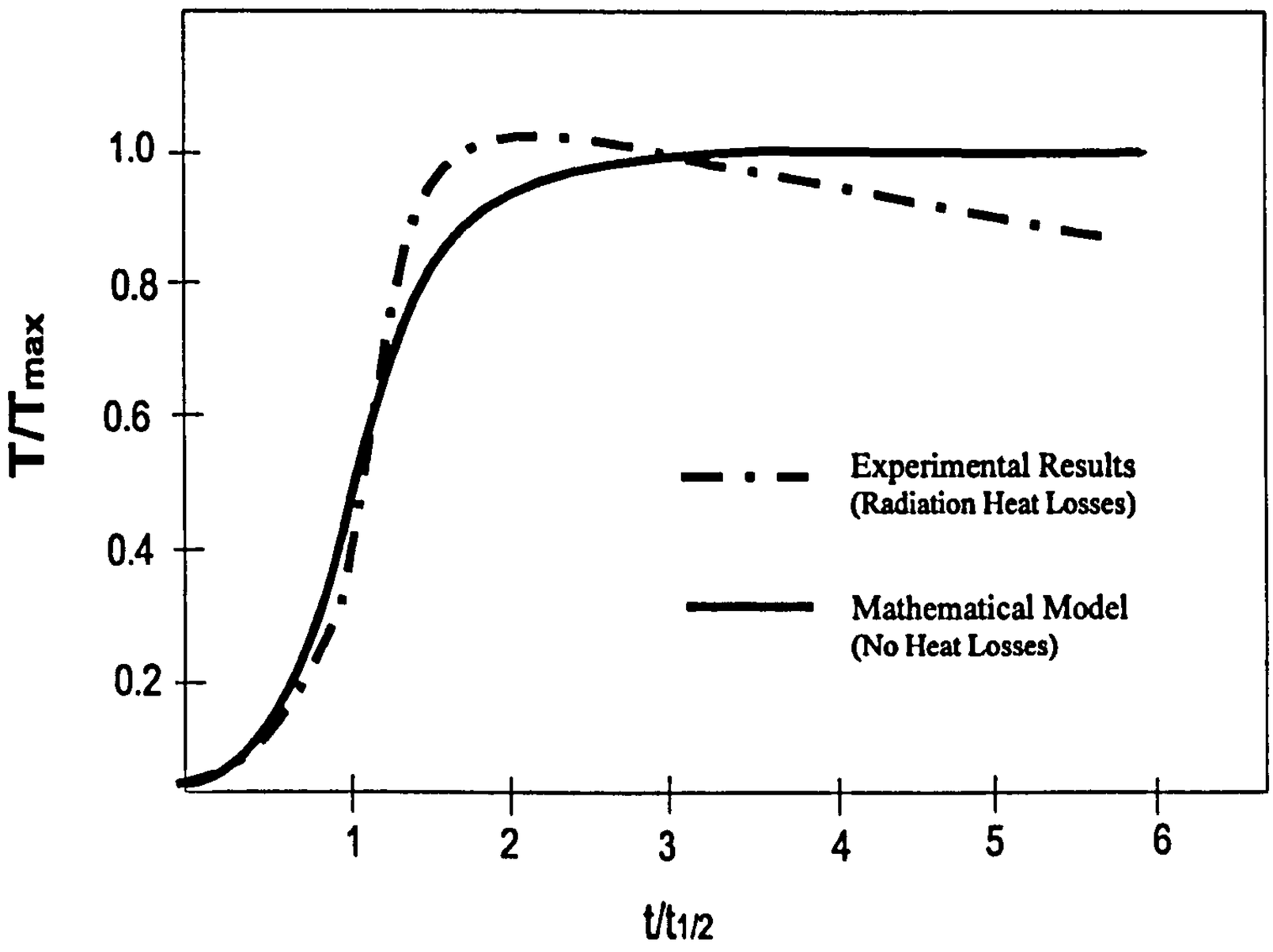

Fig. 3A.1. Rear face temperature rise: comparison of experimental thermogram effected by radiation heat losses with the mathematical ideal model.

The radiative heat loss may be expressed by non-dimensional parameters, so called Biot numbers. Since radiative heat losses, of different magnitudes, may occur from all the surfaces of the sample, three Biot numbers, Y_1, Y_2 and Y_r referring respectively to the front, rear and lateral surfaces must be defined for a cylindrical sample. They are defined as follows:

$$Y_1 = h_1 L/\lambda, \qquad Y_2 = h_2 L/\lambda \qquad Y_r = h_r R/\lambda \tag{3A.6}$$

where L, R and λ represent, respectively, the thickness, the radius and the thermal conductivity of the sample; h_1, h_2, and h_r are the corresponding heat transfer coefficients, which for the front and rear surfaces can be expressed by:

$$h_{1,2} = 4\varepsilon_{1,2}\sigma_S T_{1,2}^3 \tag{3A.7}$$

where ε is the total hemispherical emissivity of the specimen surface, T is the temperature, σ_S is the Stefan-Boltzmann constant. The suffix 1 and 2 refer, respectively, to the front and rear surface.

For the lateral surface the transfer coefficient, h_r, is expressed as:

$$h_r = 4\sigma_S T_r^3 \varepsilon_s \varepsilon_h / [1-(1-\varepsilon_s)(1-\varepsilon_h)] \tag{3A.8}$$

where ε_s and ε_h are, respectively the total hemispherical emissivity of the specimen and of the specimen holder, and T_r is the temperature of the lateral surface. h_r is corrected with a term that takes the reflected radiative heat from the surrounding isothermal container into account. Therefore, the net heat loss from the lateral surface is normally smaller than that from the front and the back surfaces.

Theoretical treatments regarding radiation loss corrections have been given by Parker[27], Mendelsohn[28], Cowan[26], Cape and Lehman[25], Watt[29], Donaldson[30], Clark and Taylor[31] and Degiovanni[32].

Parker[24,27] first considered the problem of heat losses in a pulse experiment utilising an analytical solution[33] satisfying appropriate boundary conditions. He studied, however, only the case of radiation energy loss from the front surface of the specimen. Mendelsohn[28] proposed a solution for the heat conduction equation for energy loss from the front surface, assuming a convective boundary. Cowan[26], Donaldson[30], and Clark and Taylor[31] also studied the case of one-dimensional heat flow and considered in this case both front and rear losses. General solutions of the heat conduction equation for radiative exchange from the two faces as well as the edge of the sample were proposed by Cape and Lehman[25], Watt[29] and Donaldson[30]. The two-dimensional heat conduction analysis, occurring simultaneously with surface heat losses, was in these cases based on a separate discussion of the radial and axial components. The equation presented by Cape and Lehman[25] and by Watt[29] considered also the finite pulse time effect.

Methods to correct the apparent thermal diffusivity for heat radiation losses have been given by Parker[24], Cowan[26], Donaldson[30], Clark and Taylor[31], and Heckman[34,35]. Basically in these procedures the theoretical temperature curve is compared with the experimental one, and simple relationships between particular points of the thermogram are established to correct the diffusivity value calculated by Eq.(3A.5). Alternative approaches are given by James[36], Balageas[37], Degiovanni[32], Gembarovic *et al.*[38] and Shaw *et al.*[39].

The most commonly used methods are the procedure proposed by Cowan, and by Clark and Taylor. These are separately discussed in the following sections.

<u>Procedures for heat loss correction</u>

Because in the case of heat losses the maximum temperature of the experimental curve occurs earlier in time, Parker[24] suggested that the constant in Eq.(3A.5) decreases as radiation loss increases. A non-linear correction curve for this parameter is therefore proposed.

Donaldson[30] compared the half-time rise obtained in the presence of two-dimensional heat flow with what is obtained when radial conduction is neglected,

and tabulated the correction factor for k_x for various ratios of the laser shot radius to the slab thickness.

Heckman[34,35] used Watt and Green's functions to formulate a one-dimensional solution by which he generated correction constants for front heat losses. Heckman's solution is similar to Cowan's, but has the advantage of being expressed in term of dimensionless times for both the heating and the cooling segments of the thermogram.

James[36] proposed a method based on the fact that a plot of $\ln\left(Tt^{1/2}\right)$ against t^{-1} for small values of t approaches a straight line which slope m, is a function of the thermal diffusivity: $m = -L^2/4a$.

Balageas[37] remarked that the effect of the heat losses is at a minimum near the time origin and suggested a method to obtained the diffusivity by extrapolating from the origin the apparent variation with time.

Degiovanni[32] proposed a new method using partial time moments. The method is based on the evolution in time of the normalised temperature T/T_{max}, which depends in a first approximation only on the Biot numbers and on the characteristic time, i.e. $a = f(t_c, h_i)$. In his procedure, Degiovanni introduced a reduced time to calculate the partial time moments, and from these (eliminating the Biot numbers) was able to determine t_c. The thermal diffusivity is then calculated from the relation $t_c = L^2/a$.

Gembarovic and Taylor[38] presented a new way to reduce the data. Experimental temperature versus time are first periodised, then transformed using the discrete Fourier transformation, and the real part of the second term of the transformed temperature is then fitted with a theoretical formula.

Shaw and Ellis[39] proposed a version of the logarithmic analysis technique (developed by James), to calculate the thermal diffusivity of samples deviating from the ideal geometry, allowing a standard analysis technique to be applied.

Cowan's procedure for heat loss correction

Cowan[26] analysed the problem of heat loss by examining the behaviour of the cooling segment of the thermogram. He considered one-dimensional conduction with linearized radiation loss for a finite square impulse of energy to the front face of the sample. A relationship was then established between the behaviour of the cooling curve and the heat losses in a dimensionless form. For the description the ratios of the dimensionless temperature at times when the sample is cooling are used. The dimensionless parameter $at_{1/2}/L^2$ versus the ratios of $V_{5t_{1/2}}/V_{t_{1/2}}$ or $V_{10t_{1/2}}/V_{t_{1/2}}$ where and $V_{5t_{1/2}}$ and $V_{10t_{1/2}}$ refer to the dimensionless temperature taken at times of five and ten times the half time, are shown for different heat losses.

Thus the thermal diffusivity in Cowan's method is calculated as $a_{1/2}$ corrected with a factor K_C, depending on the cooling part of the curve:

$$a_{C\,corr} = a_{1/2}K_C / 0.1388 \qquad (3A.9)$$

Defining $\Delta V = V_{5t_{1/2}}/V_{t_{1/2}}$ (or $V_{10t_{1/2}}/V_{t_{1/2}}$), K_C is given by:

$$K_C = \sum_{1}^{8} A_i (\Delta V)^{(i-1)} \qquad (3A.10)$$

where the coefficients A_i are given in Table 3A.2.

Clark and Taylor's procedure for heat loss correction

Clark and Taylor's[31] heat loss correction is based on the analysis of the rise part of the curve and, like Cowan's correction, employs the ratio technique. In this case the ratio between the time needed to reach 75% of the maximum temperature and the time needed to reach 25% of the maximum temperature is considered. Defining $\Delta t = t_{0.75}/t_{0.25}$, the correction factor K_{CT}, is calculated from the equation:

$$K_{CT} = -0.3461467 + 0.361578(t_{0.75}/t_{0.25}) - 0.06520543(t_{0.75}/t_{0.25})^2 \qquad (3A.11)$$

and the corrected value of thermal diffusivity at half time is calculated by:

$$a_{CT\,corr} = a_{1/2} K_{CT} / 0.1388 \tag{3A.12}$$

Since rise curve data are especially affected by non-uniform heating effects, Clark and Taylor's correction can be applied only in cases of uniform energy pulse.

Table 3A.2.

Coefficients for Cowan corrections, Eq.(3A.10)

	5 Half-times	10 Half-times
A_1	-0.1037162	0.054825246
A_2	1.239040	0.16697761
A_3	3.974433	-0.28603437
A_4	6.888738	0.28356337
A_5	-6.804883	-0.13403286
A_6	3.856663	0.024077586
A_7	-1.167799	0.0
A_8	0.1465332	0.0

3A.2.2 *Shape and duration of the pulse heating*

The relation expressed by Eq.(3A.5) is valid when the pulse-duration time τ is sufficiently short compared with the time needed for the temperature of the rear face to reach 50% of its maximum value. However in some applications of the flash heating technique (thin or very conductive samples[25], long pulses-experiments), the duration of the energy pulse τ, is comparable to the characteristic thermal diffusion time t_c, and the 4th hypothesis under which Eq.(3A.2) was derived, is not satisfied.

The finite pulse time effect, in the absence of other effects is shown in Fig. 3A.2. The following characteristics can be observed:

i. a lag of the experimental curve compared to the ideal case from 5% to 50% rise of ΔT_{max},

ii. a lead of the experimental curve compared to the ideal case from 60% to 98% of ΔT_{max},

iii. a long flat maximum.

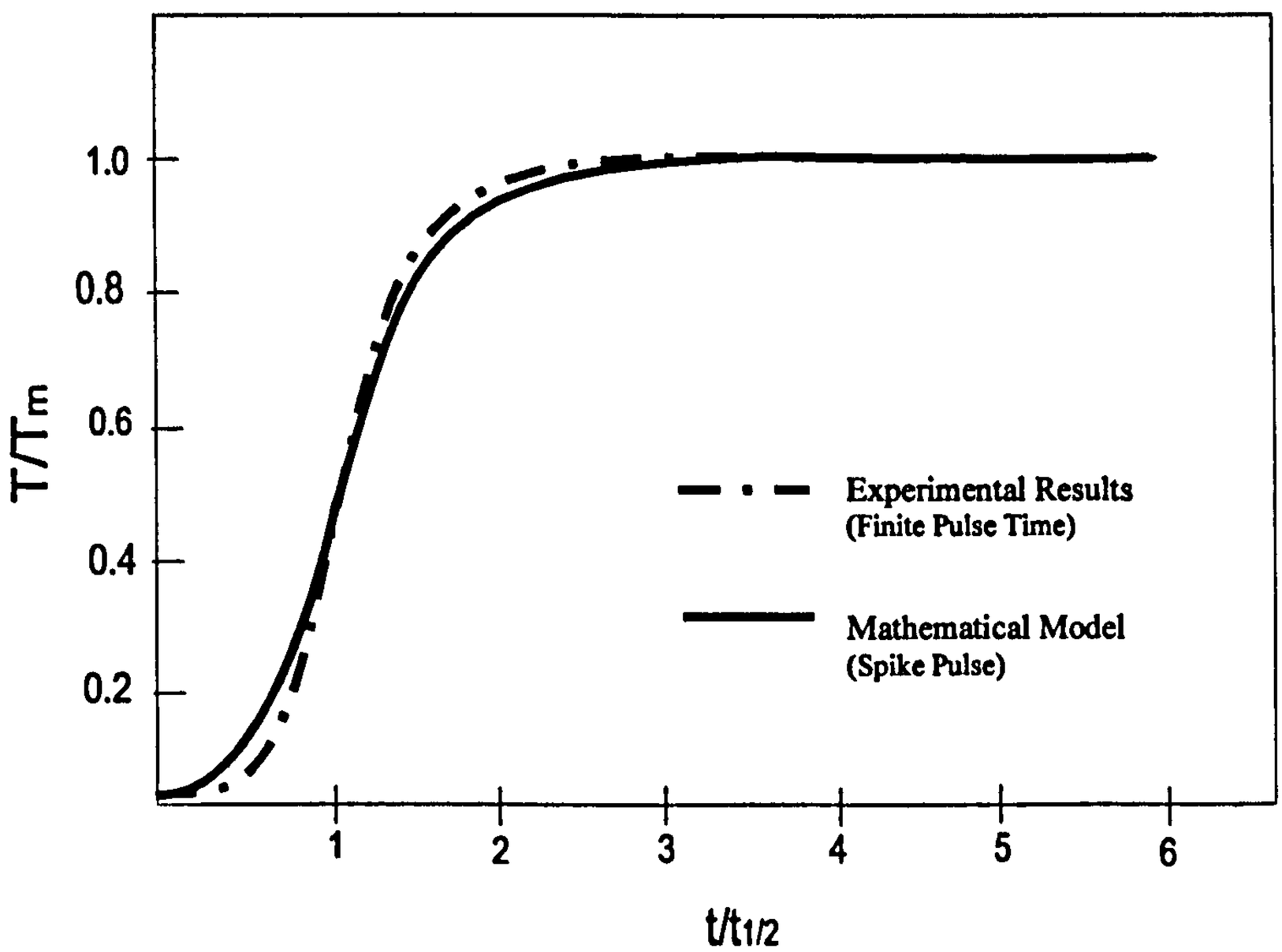

Fig. 3A.2. Rear temperature rise: comparison of the mathematical model (no finite pulse time effect) to experimental values with finite pulse time.

In order to avoid a need for the finite-pulse effect correction the duration of the pulse should be approximately one hundredth of $t_{1/2}$ [40]. When the effect of the finite pulse time cannot be reduced, *e.g.* by increasing sample thickness[xiii], corrections to Eq.(3A.5) must be applied.

[xiii] From the definition of the Biot numbers it can be seen that a reduction of the sample thickness reduce the radiative losses. Therefore the thinner is the sample, the higher is the temperature that can be reached without applying any correction for heat losses to Eq.(3A.5).

Procedures for finite pulse time correction

Parker[24] suggested accounting for finite pulse time effects by measuring $t_{1/2}$ not from the onset of the pulse, but from the time at which half the energy of the pulse is deposited in the sample. More complex general mathematical expressions for including pulse time effects in the solution of the heat diffusion equation have been developed by Cape and Lehman[25] and Watt[29].

In general, the reduced temperature rise of the rear surface of the sample $\theta(L,t)$, when $t \geq \tau$, can be expressed by:

$$\theta(L,t) = \frac{\int_0^t V\left(L,(t-t')/t_c\right) f(t')dt'}{\int_0^\tau f(t')dt'} \qquad (3A.13)$$

where $f(t')$ represents the shape of the pulse as a function of time, counted from the initial time of the pulse duration and $V\left(L,(t-t')/t_c\right)$ is the reduced temperature rise of the rear surface of the sample.

Solving Eq.(3A.13) the thermal diffusivity may be calculated from the equation:

$$a = K_0 L^2 / t_{1/2} \qquad (3A.14)$$

where $K_0 = t_{1/2}/t_0$ and t_0 is a parameter which depends on the values of τ and t_c.

In the case of no heat loss from the sample, the values of K_0 can be evaluated as a function of τ/t_c by resolving analytically the thermal diffusion equation.

Cape and Lehman[25], Taylor and Cape[40], Larson and Koyama[41] and Heckman[35] represented K_0 as $K_0 \approx 0.1388 + b\tau/t_c$, and, by specifying the shape of the pulse, a relation between K_0 and τ/t_c was deduced. Cape and Lehman computed τ/t_c as a function of $t_{1/2}/t_c$ for finite square and saw-tooth pulses, Taylor and Cape for triangular and rectangular waves and Larson and Koyama for particular exponential

pulses. If the energy pulse can be approximated by one of these shapes, an iterative calculation procedure can be executed to determine t_c, and hence a, starting from the experimental values of τ and $t_{1/2}$.

Taylor and Clark[42] proposed a similar method to correct the data at percent rises other than 50% of ΔT_{max}, so that the diffusivity values can be calculated over the entire experimental curve rather than from one single point. The thermal diffusivity can be calculated in case of triangular pulse from the relation:

$$a = \frac{c_1}{c_2 t_x - \tau} L^2 \qquad (3A.15)$$

where c_1 and c_2 are constants depending on the pulse intensity.

A different procedure for correcting the finite pulse time effects was elaborated by Azumi and Takahashi[43]. Their method consisted of two steps; *i*) adjustment for an "effective" irradiation time by using the center of gravity of the pulse and *ii*) correction for the deviation in the parameter K from the ideal value of 0.1388. The thermal diffusivity can be evaluated from:

$$a = K_g L^2 / (t_{1/2} - t_g) \qquad (3A.16)$$

where t_g is the time corresponding to the centre of gravity of the laser pulse, $t_g = \int_0^\tau t' f(t') dt' \Big/ \int_0^\tau f(t') dt'$ and $K_g = (t_{1/2} - t_g)/t_c$.

These authors however, demonstrated also that in general, after adjustment for the "effective" irradiation time, no further correction is needed for whatever the shape of the pulse, even at very short $t_{1/2}$ such as $t_{1/2} = 2\tau$. Thus $K_g = f(\tau/t_c) \approx 0.1388$.

Finally, Vining *et al.*[44] solved analytically the one-dimensional heat diffusion equation given by Watt for the case of a pulse with an exponential shape including the effects of heat losses from the front and rear surface.

3A.2.3 *Non-uniform heating*

Non-uniform heating of the sample may arise both from the nature of the energy pulse and from a non-uniform absorption on the specimen surface[45]. In these cases, respectively the 1st and the 3rd hypotheses under which Eq.(3A.2) was derived are not satisfied and a correction for Eq.(3A.5) is needed.

Contrary to the heat losses and finite pulse time effects, non-uniform heating is often a characteristic of the specific experimental set-up and may lead to systematic errors which are difficult to recognise[46]. For instance, in fact, while cold-centre cases result in a rear-face temperature continuing to rise significantly after $4t_{1/2}$, hot-centre cases approximate the radiation heat losses effect, and can remain undetermined.

Due to the variety of possible non-uniform heating conditions, only a few general features of this kind of perturbations were studied and little was published about the effect on the measured diffusivity. Beedham and Dalrymple[47], Schriempf [48,49], Taylor[45], Mackay and Schriempf[50], and Baba *et al.*[51] have described the sometimes-dramatic effects due to the spatial heterogeneity of the laser beam in LAF thermal diffusivity measurement.

<u>Procedures for non-uniform heating correction</u>

Beedham and Dalrymple[47] carried out a computational investigation of errors resulting from a measured non-uniformity in the laser profile (two humps symmetrically located about half way between the centre and edges, with the central region of the sample receiving 75% and the edges 40% of the intensity of humps). Their calculated error in the resulting thermal diffusivity ranged from 4 to 8%.
Schriempf[48,49] observed experimentally the effects of non uniform heating. Although no quantitative assessments of the error effecting the measured thermal diffusivity is given, it is indicated that a non-uniformity less than 4% yields satisfactory results.

Taylor[45] determined the effects of radially symmetrical non-uniform laser beams for several cases (including circular hot and cold spot). He found that the effect of an off-axis non-uniformity is much less than an on-axis non-uniformity. He also saw that a central hot spot causes diffusivity values in excess for all parts of the response curve. On the other hand, a central cold spot causes too low diffusivity

values with the error also increasing along the response curve. He estimated that errors due to laser-beam non-uniformity were, in general practice, of the order of several percents.

Mackay and Schriempf[50] investigated theoretically and experimentally the effects of non-uniform heating, and gave an expression for the temperature response of the specimen. Evaluation showed that 30% non-uniformity resulted in diffusivity errors of 2-7%, depending on the method of data reduction used.

Baba *et al.*[51] observed an error ranging from 5 to 10% in thermal diffusivity results for irradiation by an irregular beam, and suggested a new technique to convert irregular direct beams into spatially uniform beams by using a step index optical fiber of large core diameter. The non-uniform heating error was reduced to the order of 1% when this uniform beam irradiated the specimen.

3A.2.4 *New data reduction methods*

Contrary to the conventional data analysis methods, which consider only one point of the thermogram for calculating thermal diffusivity, data reduction methods introduced in the last years in the analysis consider the influence of all the points on the thermogram. In these methods the entire experimental temperature history of the rear face of the specimen is fitted with the theoretical curve. Since the theoretical equation may be derived under appropriate boundary conditions, thermal diffusivity calculated by these methods does not require any further correction for disturbing effects. The different methods proposed differ from each other primarily by the theoretical equation used to fit the experimental curve.

Cezairlyian *et al.*[46] proposed a method, which implements the equation given by Cape and Lehman[25] with the option to neglect or consider the radiative heat losses in the radial direction.

Finally, an advanced method was developed in this work, based on a comprehensive two-dimensional heat flow analysis.

3B. LASER FLASH CALORIMETRY

Heat capacity at high temperature (above 1100 K) is generally measured by the "drop" method or by direct pulse heating calorimetry. However, as already discussed in Section 2.1.3, none of them can be applied to insulators. In 1961 Parker[10], in his original paper, proposed the laser-flash technique as a method to solve the problem. The formula makes it possible, at least in principle, to calculate the specific heat, directly derived from the definition of heat capacity:

$$c_P = \frac{\overline{Q}\varepsilon}{\rho L \Delta T} \tag{3B.1}$$

where $\overline{Q}$ is the energy density delivered by the laser, ε is the front surface emissivity ($(\overline{Q}\varepsilon) = Q$ is then the energy absorbed by the sample per unit area) and ΔT is the maximum increase of the rear temperature of the specimen. While this technique is theoretically simple, the measurement of Q is in practice very difficult and the method was initially considered as merely hypothetical. The difficulties in the measurement of energy absorbed by the specimen arise from the fact that it depends both on the energy delivered by the laser pulse, that usually is not uniform over the spatial laser beam profile, and the absorption coefficient of the material investigated, which is temperature dependent. Over the years new techniques to adapt the flash technique to measure specific heat were implemented. The various methods proposed, however, have inherent limitations[52] since:

1. coating of the specimen and/or use of standard reference materials (except in the cavity method[53]) are always required,
2. they can not be applied to measure specific heat at temperatures above ~1300 K,
3. and, except in the case of the "cavity" variant (tested however, only at room temperature), do not allow the simultaneous and direct measurement of both the specific heat and the thermal diffusivity. The technique proposed by Agary[54] applied the method to measure at the

same time the specific heat and diffusivity of polymeric films, but a correction procedure to obtain the thermal diffusivity values is needed, due to the errors induced by the graphite coating.

Coating method

In the coating technique proposed by Parker *et al.*[10], and successfully applied by Vandersande *et al.*[55] in 1989, the energy density absorbed by the sample is estimated in a *separate* experiment, from the temperature rise of a standard specimen having known heat capacity. Indexing an apostrophe for the reference sample the valid expression for the absorbed energy density is:

$$\overline{Q}\varepsilon' = \rho' L' c_p' \Delta T' \tag{3B.2}$$

The specific heat of the measured specimen is then measured in a second experiment:

$$\overline{Q}\varepsilon = \rho L c_p \Delta T \tag{3B.3}$$

Under the assumption of equal absorbed energy density:

$$\overline{Q}\varepsilon = \overline{Q}\varepsilon' \tag{3B.4}$$

Eq.(3B.2) and Eq.(3B.3) give the specific heat of the unknown sample:

$$c_p = \frac{\rho' L' c_p' \Delta T'}{\rho L \Delta T} \tag{3B.5}$$

Assuming that the energy density delivered by the probe source is the same in the two experiments, (Eq.3B.4) is valid only if the emissivities of the reference and unknown samples are the same. To assure this, equal coatings have to be applied on the two specimens.

It is clear that since this technique based on two *different* and *consequent* experiments, to obtain accurate results the following features are necessary:

i. reproducibility of the laser pulse,

ii. reliable uniformity of the laser beam,

iii. adiabatic conditions,

iv. integrity of the coatings over the whole temperature range of the experiment.

Absorbing disk method

Takahashi[56,57], to overcome the difficulties in satisfying the conditions of the Parker's technique, proposed a method in which

- the total energy, E, absorbed by the sample, rather than the energy density is measured
- ΔT is determined after correction for heat losses, and
- an absorbing disk, instead of a coating is placed on the front surface of the two specimens.

The specific heat is calculated by:

$$c_P = \frac{\left(E/\Delta T - C_P^*\right)}{m} \tag{3B.6}$$

where m is the mass of the unknown sample and C_P^* represents the sum of the heat capacity of the absorbing disk and of the adhesive materials. As in the coating method, the energy absorbed by the sample is determined in a *separate* experiment; thus this technique again relies critically on the assumption of the reproducibility of the laser pulse. In addition, it is of fundamental importance the accuracy of the calculated heat capacity value of the absorbing disk and the adhesive material. The method, tested on aluminium dioxide samples, showed a precision of 0.5% over the temperature range from 300 to 800 K[56,58] and 1% from 800 to 1100 K[58]. It was used by Takahashi[58] to measure the specific heat of uranium-zirconium alloys from 300 to 1100 K.

Agary *et al.*[54] applied the technique (using a graphite coating instead of an absorbing disk) to measure both the thermal diffusivity and specific heat of polymers film. The specific heat was exactly measured at room temperature (a comparison with result obtained by differential scanning calorimetry was made). The thermal diffusivity values, however, needed a correction procedure because of error induced by the effects of the coated graphite layer.

Differential laser-flash calorimetry

To solve the problem of non-reproducibility of the laser pulse, Baba[59] proposed a comparative method in which the standard specimen and the measured specimen are closely placed and shot at the same time with a spatially homogeneous laser beam. In this technique the ratio of the temperature rise of the measured sample, ΔT, to the standard specimen, ΔT_s is observed. The front and the rear surfaces of the standard and the measured specimen, to assure the same energy absorption and temperature measurements, must be covered with the same black coating. The heat capacity of the measured specimen, C_P, is obtained from the ratio of the two temperature maxima and from the certified value of heat capacity of the standard specimen, C_P' in the following equation:

$$C_P = \frac{\Delta T_s'}{\Delta T'} C_P' \tag{3B.7}$$

where $\Delta T_s' = \varepsilon_s \Delta T_s$ and $\Delta T' = \varepsilon \Delta T$.

In this method the ratio of the temperature is considered rather than the absolute value and the adiabatic condition of the experiment is thus of fundamental importance. The reliability of a uniform laser spatial beam profile and the correct estimation of the energy absorbed by the coatings are also needed for an accurate measurement.

Pulse heating and cooling

Pulse heating and cooling[60,61] method requires a reference material having the same emissivity of the unknown sample. Again, a coating of the two specimens is necessary. The method is based on a separate analysis of the heating and cooling parts of the experimental thermogram. Assuming that after the irradiation by a laser pulse, the sample cooling is governed only by radiative exchange with the surrounding, the following formula is satisfied:

$$\frac{c_P}{\varepsilon_n} = F(t_2 - t_1)T_0^3\left[\ln\frac{T_1 - T_0}{T_1 - T_0} - \ln\frac{T_1 + T_0}{T_1 + T_0} + 2\left(\arctan\frac{T_2}{T_0} - \arctan\frac{T_1}{T_0}\right)\right] \qquad (3B.8)$$

where ε_n is the effective emissivity, $F = 4A\sigma_S/m$ with A the total surface area of the sample $\left(=\pi D^2/2 + \pi DL\right)$, σ_S Stefan-Boltzmann constant, T_0 the ambient temperature and T_1 and T_2 the temperature corresponding to the times t_1 and t_2 on the cooling part of the thermogram.

The method does not require the measurement of Q but relies on the exact value of the effective emissivity of the sample. This is supposed to be measured on a reference sample of known specific heat and emissivity. To assure the same emissivity of the two samples, a coating is applied on both specimens. The effective emissivity, however, depends not only on the thermal emissivity of the sample and sample holder but also on the position of the sample within the furnace.

Double-specimen method

In the double-specimen method proposed by Qinqzhao and Likun[62] two reference samples of the same material and known specific heat are used. In a first experiment, one reference sample is placed over the unknown sample and shot by the laser of energy $\overline{E}$. The impulse raises the temperature of both the materials by an amount ΔT_1 and:

$$\overline{E}\varepsilon' = \left(c_P' m_1' + c_P m\right)\Delta T_1 \qquad (3B.9)$$

where ε', m_1', and c_P' are respectively the absorption, the mass and the specific heat of the first sample of reference material. The reference sample is then replaced by the second one, of mass m_2', and the experiment repeated. The temperature rise ΔT_2 is recorded and a relation similar to Eq.(3B.9) is obtained:

$$\overline{E}\varepsilon' = \left(c_P' m_2' + c_P m\right)\Delta T_2 \tag{3B.10}$$

The specific heat of the unknown sample is then calculated by combining Eq.(3B.9) and Eq.(3B.10):

$$c_P = \frac{c_P'\left(m_2'\Delta T_1 - m_2'\Delta T_2\right)}{m\left(\Delta T_1 - \Delta T_2\right)} \tag{3B.11}$$

The drawbacks of this method are that nor neither the heat losses of sample, nor the effects of interfacial contact resistance between unknown and reference specimen are taken into consideration.

Cavity method

The cavity method[53] consists of placing a hollow cone over the surface of the specimen, with the cone and the sample thermally isolated from each other. The laser pulse of known energy is focused on the small hole at the apex of the hollow cone so that it can reach the interior of the cavity and be absorbed by the cone and the sample. Neglecting the amount of energy passing out of the hole, the specific heat of the sample is given by:

$$c_s = \frac{\overline{E} - c_h m_h \Delta T_h}{m_s \Delta T_s} \tag{3B.12}$$

where $\overline{E}$ is the energy delivered by the focused laser pulse, c is the specific heat, m is the mass, ΔT is the temperature rise, with the subscripts s and h referring to the sample and the hollow cone, respectively. This technique is based on the blackbody properties of the cavities, thus the sample does not require any surface treatment and

the use of a reference material is nor needed. It necessitates, however, the estimation of the heat capacity of the material comprising the cone.

Xue[53] tested the technique at room temperature on different metals, obtaining results for specific heat and thermal diffusivity with a precision, respectively within 1.5% and 3%.

Chapter 4

4. THE METHOD

4A. EXPERIMENTAL SET-UP

The laser-flash apparatus consists of: *i*) a chamber with a specimen holder, *ii*) a continuous-wave (CW) laser for conditioning heating *iii*) a pulsed laser probe source, *iv*) a system for measuring the transient and reference temperature, *v*) a system for the measurement of the power pulse laser and its time evolution, *vi*) a system for the measurement of the spatial profile of the pulse laser beam.

In the chamber the specimen is heated to the measurement temperature by the CW laser and, when steady state conditions are reached, is submitted to a probe pulse. Measurements of the energy and of the spatial profile of the probe-beam are made by splitting the laser beam and directing a small portion to a *Si*-photodiode and to the array of a CCD camera. The transient temperatures on the front and rear surfaces of the sample are monitored by two high-speed micro-pyrometers. The pyrometer signals, the pulsed laser time profile and its power are recorded by a *14-bit* transient digitiser (Nicolet Pro44) and transferred to a computer for subsequent data analysis. A picture of the instrument and the corresponding schematic diagram are given in Figs. 4A.1 and 4A.2, respectively.

The instrument consists of:

- a laser probe beam delivery system based on a high quality fibre optics, allowing a random mixing of the laser light and thus ensuring an excellent power homogeneity over the focal spot,
- a CW laser heating system, also provided with a fibre optics system, allowing an excellent stability of the operating temperature to be obtained,
- high precision fast pyrometers used for measuring the transient temperature on both the front and the rear surfaces of the sample,
- a small dimensions and a high degree of flexibility.

Thanks to these features the following improvements are obtained in respect to the conventional laser-flash set-up:

1. Both the thermal diffusivity, a, and the specific heat c_P can be measured directly and simultaneously. This enables the thermal conductivity λ to be calculated from a and c_P values obtained under strictly identical experimental conditions. Cross checking of data and errors on a, c_P and λ become therefore, possible, considerably increasing the degree of confidence in the measurement.
2. High accuracy of the thermal diffusivity measurements. This is obtained because the excellent power homogeneity of the laser beam eliminates "hot spots" on the heated specimen surface. Problems caused by laser beam heterogeneity (a typical defect of all multi-mode solid-state lasers), in fact, always lead to large and almost unpredictable errors in thermal diffusivity measurements (see § 3A.2.3). Furthermore, the "flatness" of the laser energy distribution over the focal spot provides an accurate determination of the *energy density* impinging the sample. Therefore, the evaluation of c_P, becomes effectively independent of the shape of the sample surface contour.
3. Most of the problems usually encountered with conventional heating systems[xiv] are eliminated. Measurements can, in fact, be carried out up to very high temperatures (the limit being the melting point of the material) in a very short time, and no restrictions are posed on the possible use of chemically active gas or any gaseous atmosphere even at elevated pressures.
4. Finally, the absolute calibration of the two pyrometers, in conjunction with the high-resolution transient digitiser, enables measurement of the *absolute temperature increase* on both the front and rear surface whence a precise and reliable measurement of the heat capacity and of the thermal diffusivity are obtained.

The new developed Continuous-wave Laser Surface Heating apparatus will be referred in Chapters 5 and 6 as CLASH.

[xiv] Problems typically encountered in furnace heating are due to the upper limit of the operating temperature, the drift in the temperature baseline, the background radiation, and the inert atmosphere used.

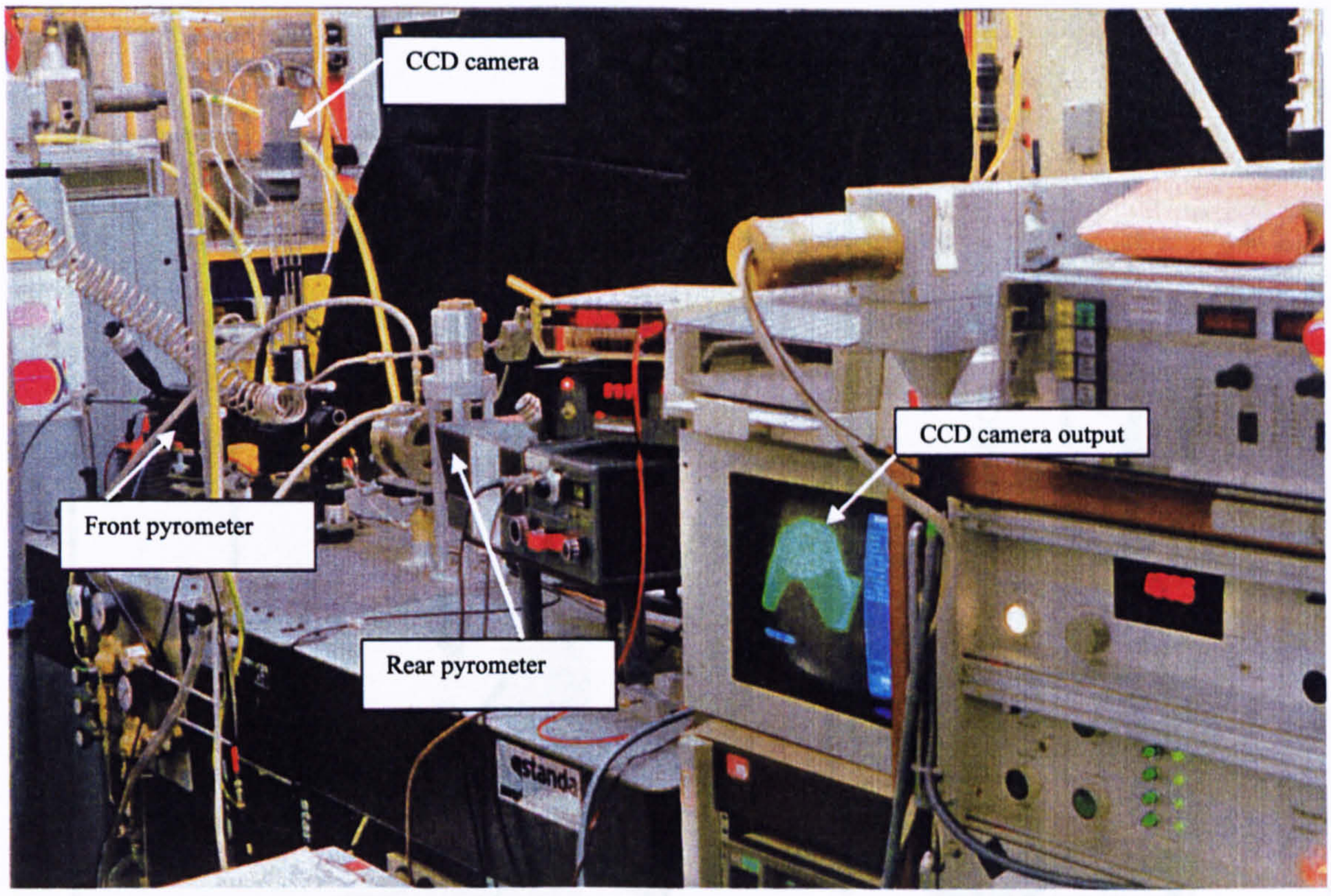

Fig. 4A.1 Picture of the CLASH set-up.

4A.1 Experimental chamber

The chamber, shown in Fig. 4A.3, consists of a vessel with a specimen holder. The vessel, fixed on a moving support and containing the support of the specimen holder, is a horizontal stainless-steel cylinder with two optical windows on its bases. The chamber is connected either to a rotary vacuum pump (10^{-3} Torr) or to a gas inlet system enabling the vessel to be filled with different gases (up to 5 bars). The specimen is mounted perpendicularly to the cylinder axis of the chamber. The sample holder consists of a graphite disk with a central cylindrical cavity where three adjustable zirconia pins are screwed in order to position the specimen. The use of zirconia pins avoids chemical reactions with the sample and the three-point mounting allows the sample to be suspended, minimising the surface of contact with the conductive support.

The laser beams and the pyrometers are focused on the sample through the optical windows.

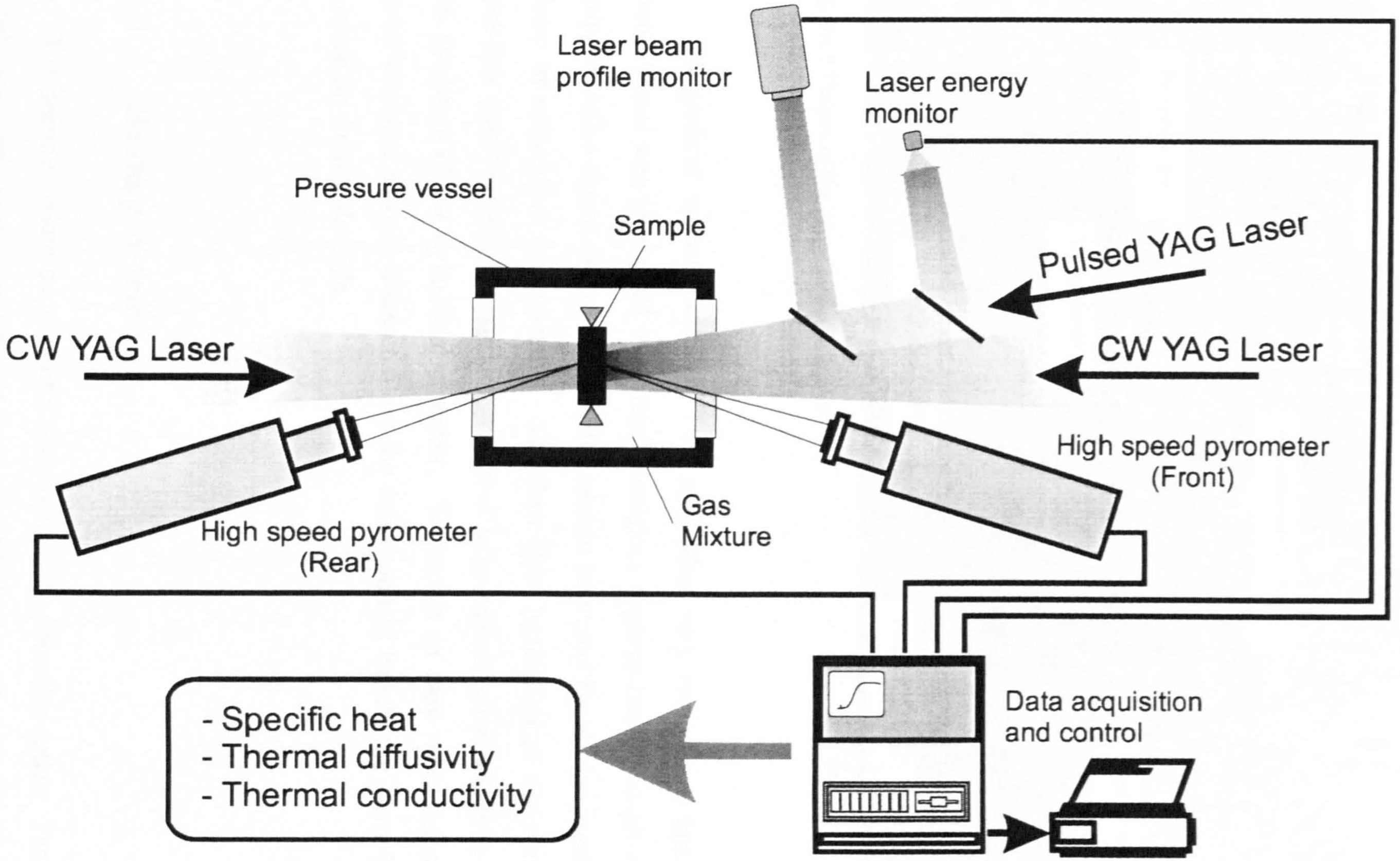

Fig. 4A.2. Schematic picture of the CLASH set up.

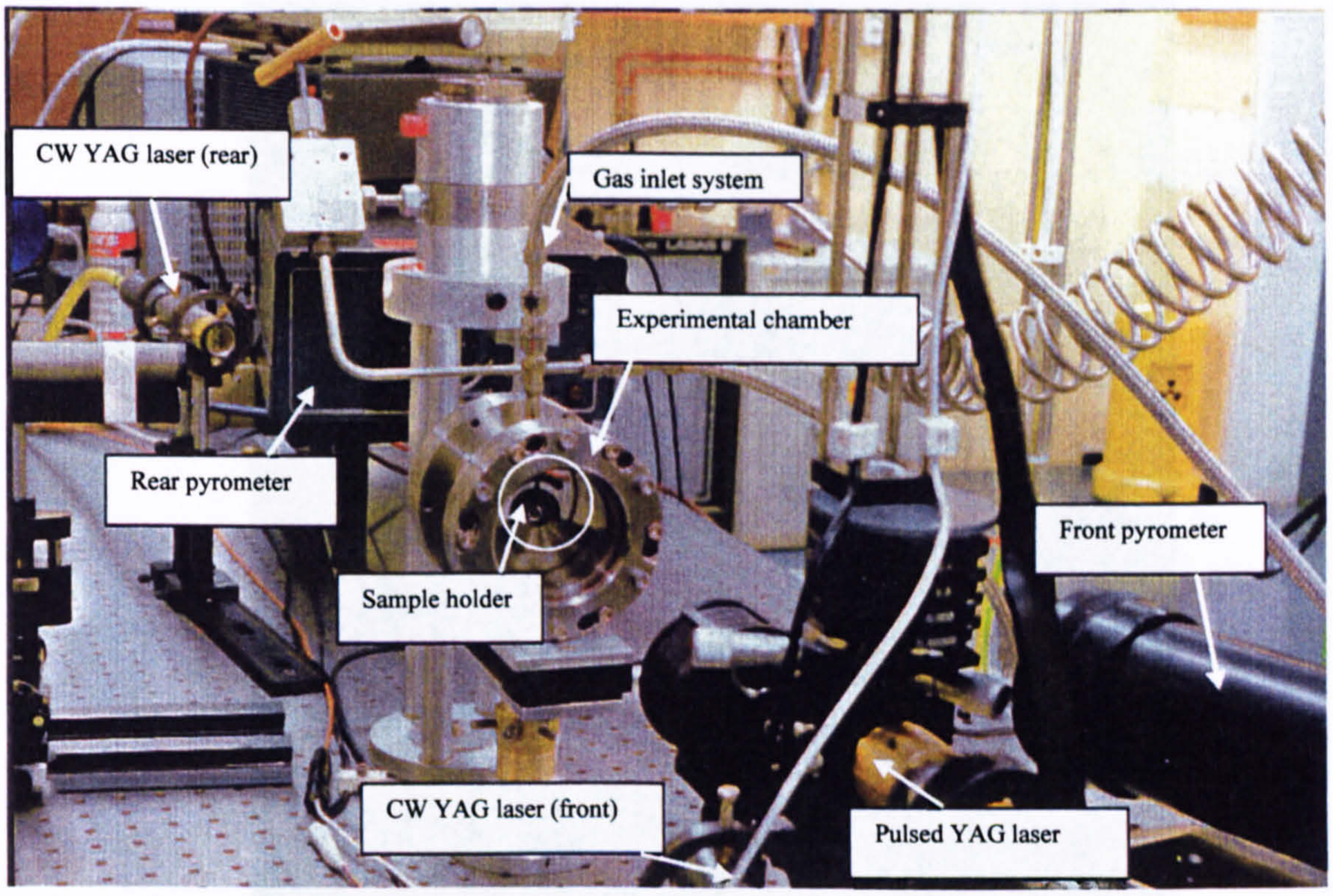

Fig. 4A.3 Picture of the experimental chamber.

To perform measurements on UO_2 and other very radioactive materials, a second vessel was assembled in a small plexiglass α-glove-box. The glove-box is equipped with a closed nitrogen circulation system to protect the environment against release of radioactive contaminants. To allow laser irradiation of the sample, the glove-box (see Fig. 4A.4) was built with two large optical glass windows aligned with the bases of the cylindrical chamber. To permit an easy replacement of the normal chamber without disassembling the entire optical bench, the glove-box was mounted on a movable table.

4A.2 Heating system

The heating system consists of a laser head and a focusing optics. The laser is a solid state continuous wave Nd-YAG laser (λ= 1060 nm) with a maximum power

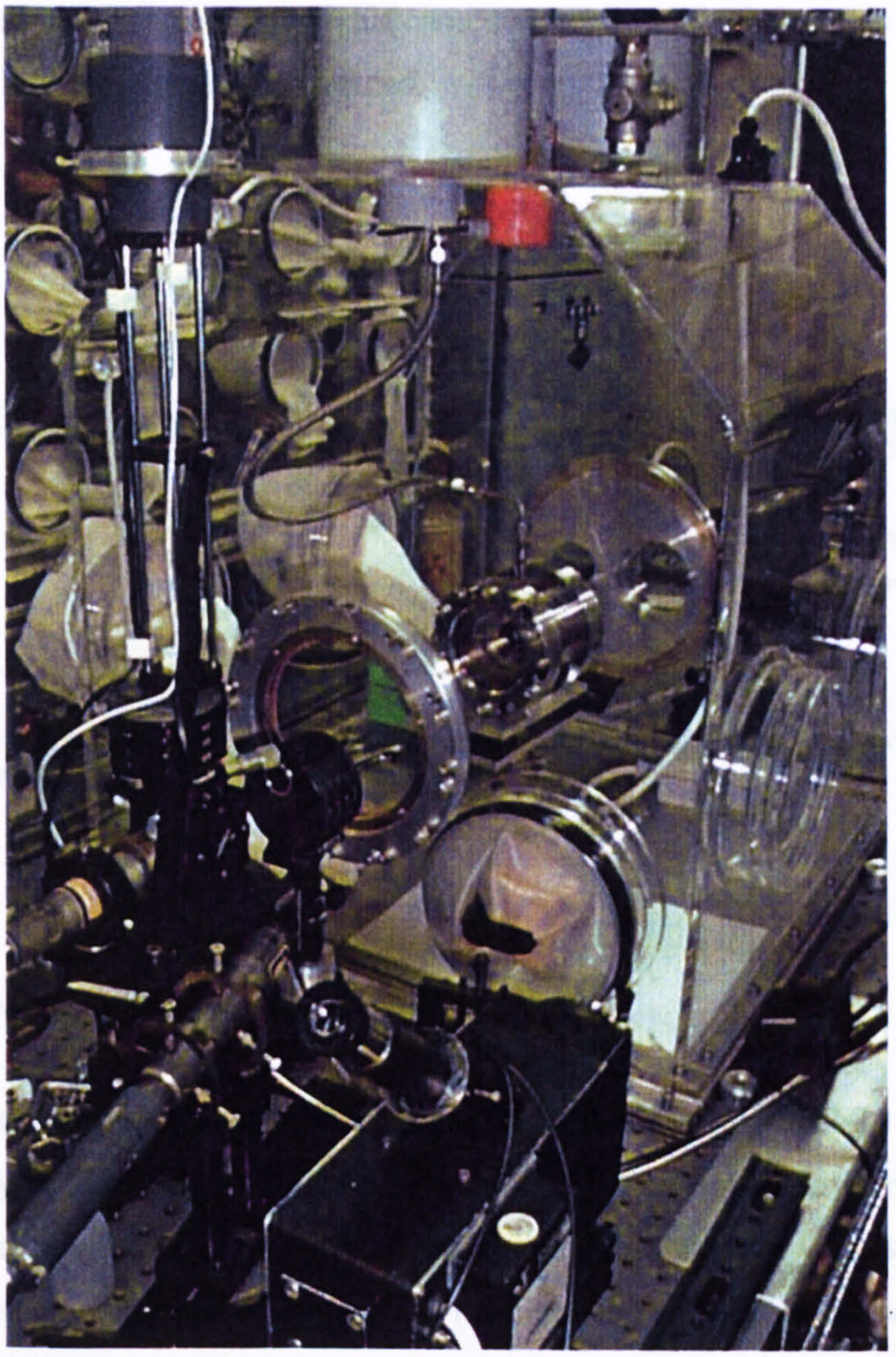

Fig. 4A.4. Glove-box used for the measurements of radioactive materials

of 300 W (HAAS VY 0302). The laser beam is split in two, and transmitted to two focusing systems via optical fibres (of 1mm core diameter). The magnified images (of 5 mm in diameter) of the core of the fibres are focused on the front and back surfaces of the sample. A schematic of the focusing system is shown in Fig.4A.5.

Due to the spatial homogeneity and stability in time of the two laser beams, a homogeneous and constant surface temperature can be rapidly achieved within the

illuminated surface spot, so that significant evaporation or changes in chemical composition of the samples can be avoided.

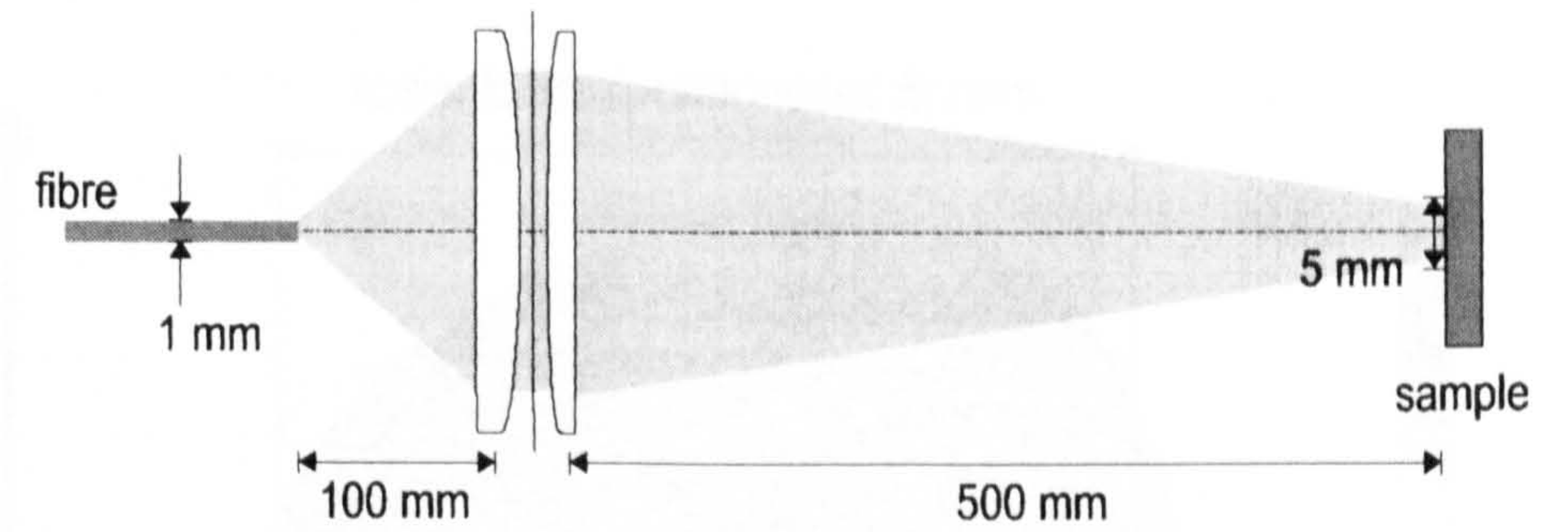

Fig. 4A.5. Focusing system of the laser beams. A focused laser beam spot of 5mm diameter impinges the sample.

4A.3 Probe pulse system

The pulse heat source is a solid state Nd-YAG laser (λ= 1060 nm) which supplies energy in the range of 1-65 J with a pulse duration from 1 to 10 ms (HAAS LAG 20). The laser beam is transmitted via optical fibre to a focusing system and from this to the front surface of the sample (the laser beam spot on the sample is 5 mm in diameter). The radial power profile of the laser beam is recorded during every shot by a CCD camera. The space power profile of the probe beam is shown in Fig. 4A.6.

The power of the pulse beam is suitably chosen in order to produce the least sample temperature perturbations necessary for the pulse propagation analysis. Usually, an energy between 0.5-1 J was delivered producing an increase of the rear temperature ranging from ~5 K, at low temperatures, to ~10 K, at high temperatures. Given the delivered energy, the increase in temperature of the front surface of the sample is *inversely* proportional to the duration of the pulse. To reduce the axial temperature gradient in the specimen and to avoid melting of the front surface of the

sample long pulses are therefore required. In the ceramic disks studied, however, pulse times longer than 1 ms are comparable with the characteristic time of thermal diffusion and, consequently, a correction for "finite pulse time" is necessary.

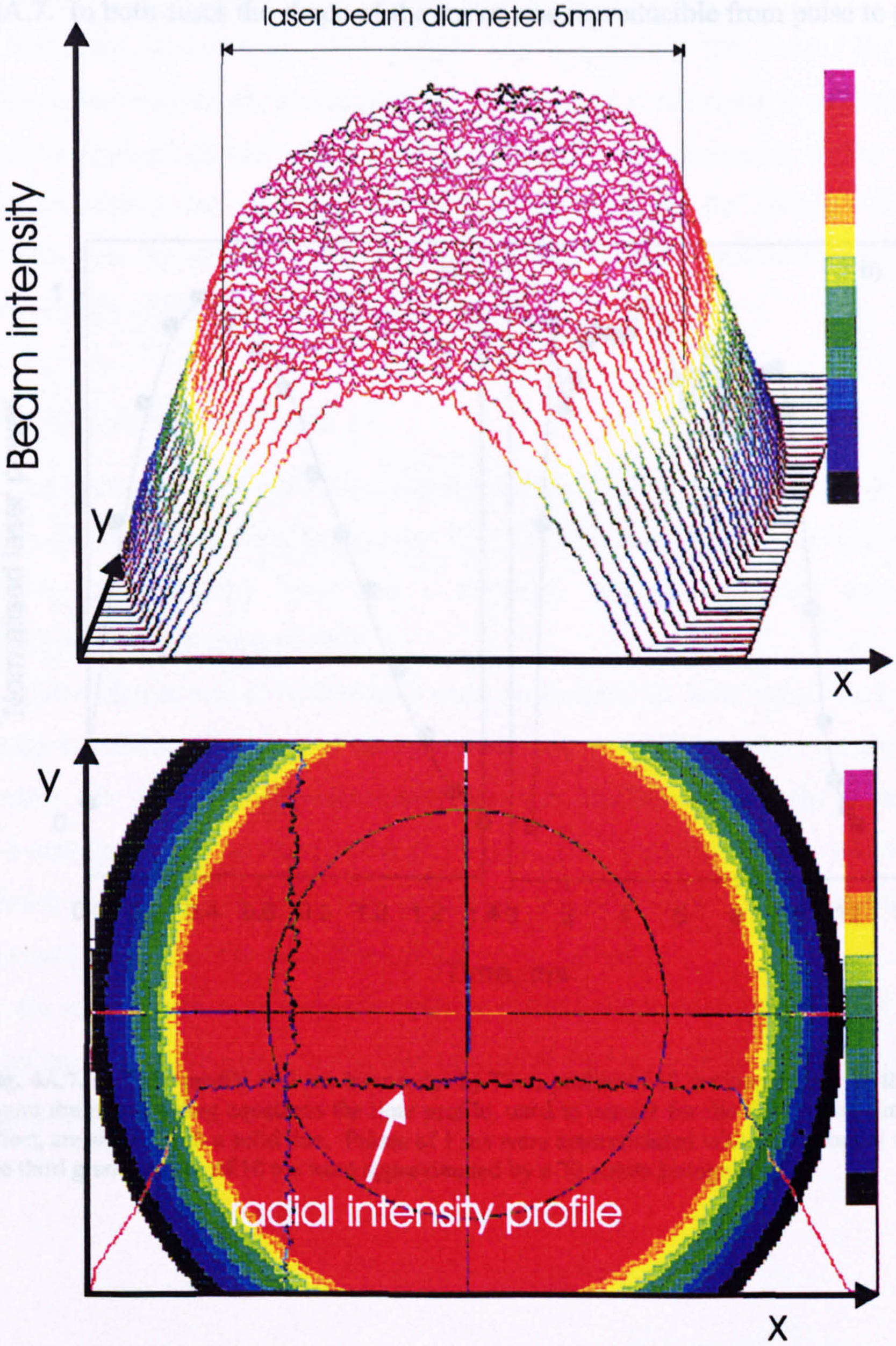

Fig. 4A.6. Laser space profile of the probe pulse beam.

Hence the duration of the pulse used usually corresponds to a compromise dictated by the necessity to keep as low as possible the temperature increase of the front surface of the sample, and by the possibility to fit the experimental thermogram with the simplest mathematical model.

The time profiles of the laser beam for 1 ms and 10 ms pulses are shown in Fig.4A.7. In both cases the shape of the curve was reproducible from pulse to pulse.

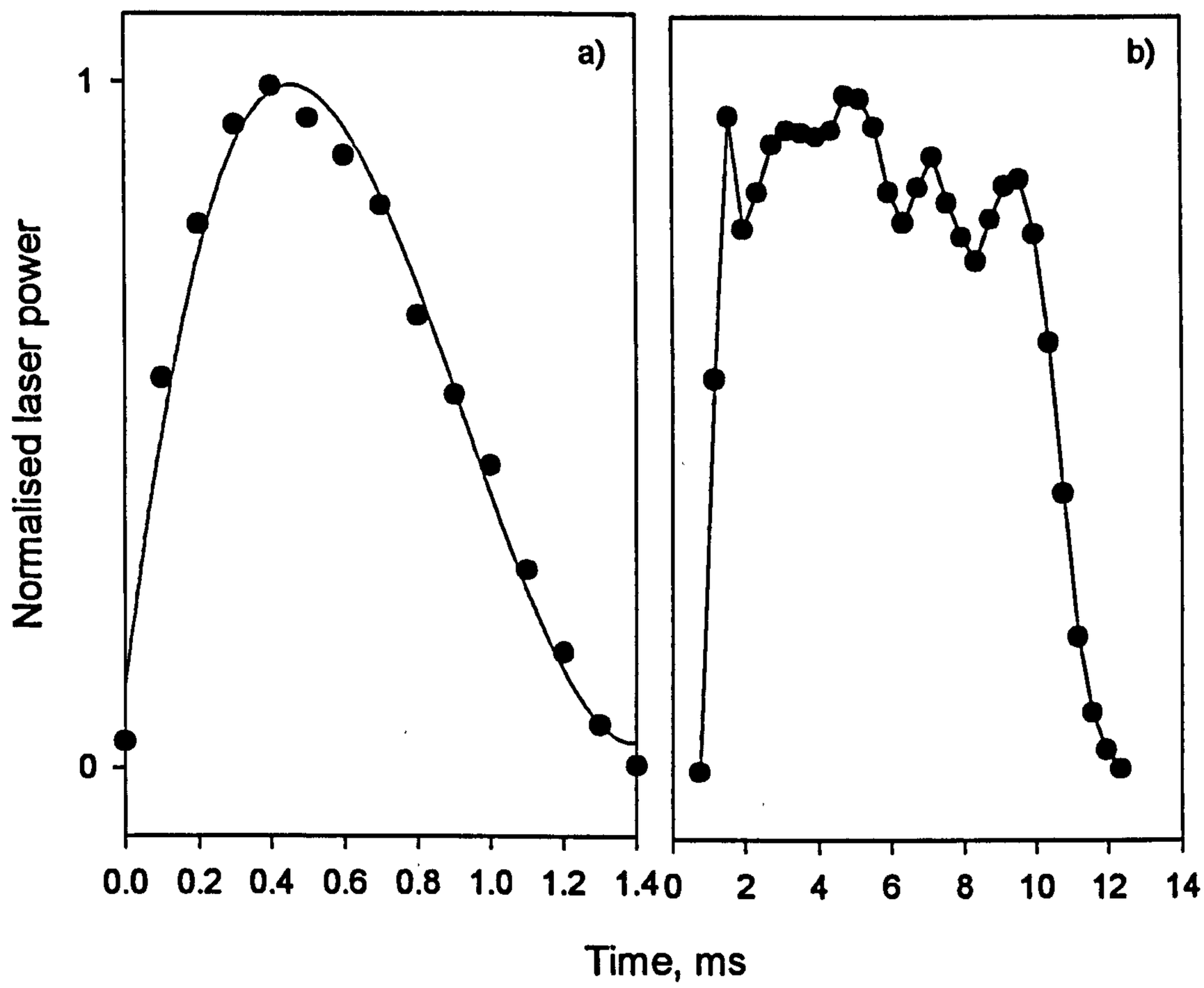

Fig. 4A.7. a) Time profile of 1 ms laser pulse **b)** Time profile of 10 ms laser pulse. In the figure the interpolating equations the time profile, used to correct for the finite pulse time effect, are shown with a solid line. Pulses of 1 ms were approximated with a polynomial of the third grade; pulses of 10 ms were approximated by a 30 points histogram.

4A.4 Energy density measurement

The integrated power of the pulse was recorded as a function of time in each experiment. This was accomplished by means of a partially reflecting mirror: a fraction of the laser pulse beam was sent to a *Si*-photodiode, and then to an integrating amplifier, where the integrated power was measured.

Since the spatial laser beam profile was sufficiently flat around the beam centreline (see Fig. 4A.6), it was possible to carry out a calorimetric calibration of the laser integrated power, which enabled an *absolute measurement* of the *energy density* impinging the sample. The energy absorbed by the sample was then calculated from the product of the measured energy and the sample absorptivity at the wavelength of the Nd-YAG laser (λ=1060 nm).

Energy density calibration

The energy density calibration was performed by substituting the sample with a graphite diaphragm of diameter smaller than the diameter of the laser spot and by impinging the resulting beam on a standard volume absorbing calorimeter (SCIENTECH Co.; accuracy: 3%).

Two different sets of calibrations were performed: for laser pulses of 1 and 10 ms under normal conditions, and for laser pulses of 1 and 10 ms when the glove-box was used. In the latter case the calibration was performed with the calorimeter placed outside the rear window of the glove box. The absorption of this window was previously measured and taken into account in the calibration. A schematic of the set-up used for the energy calibration is shown in Fig. 4A.8.

An example of a calibration curve, *i.e.* the energy density measured by the calorimeter versus the integrated power measured by the *Si*-photodiode, is presented in Fig. 4A.9.

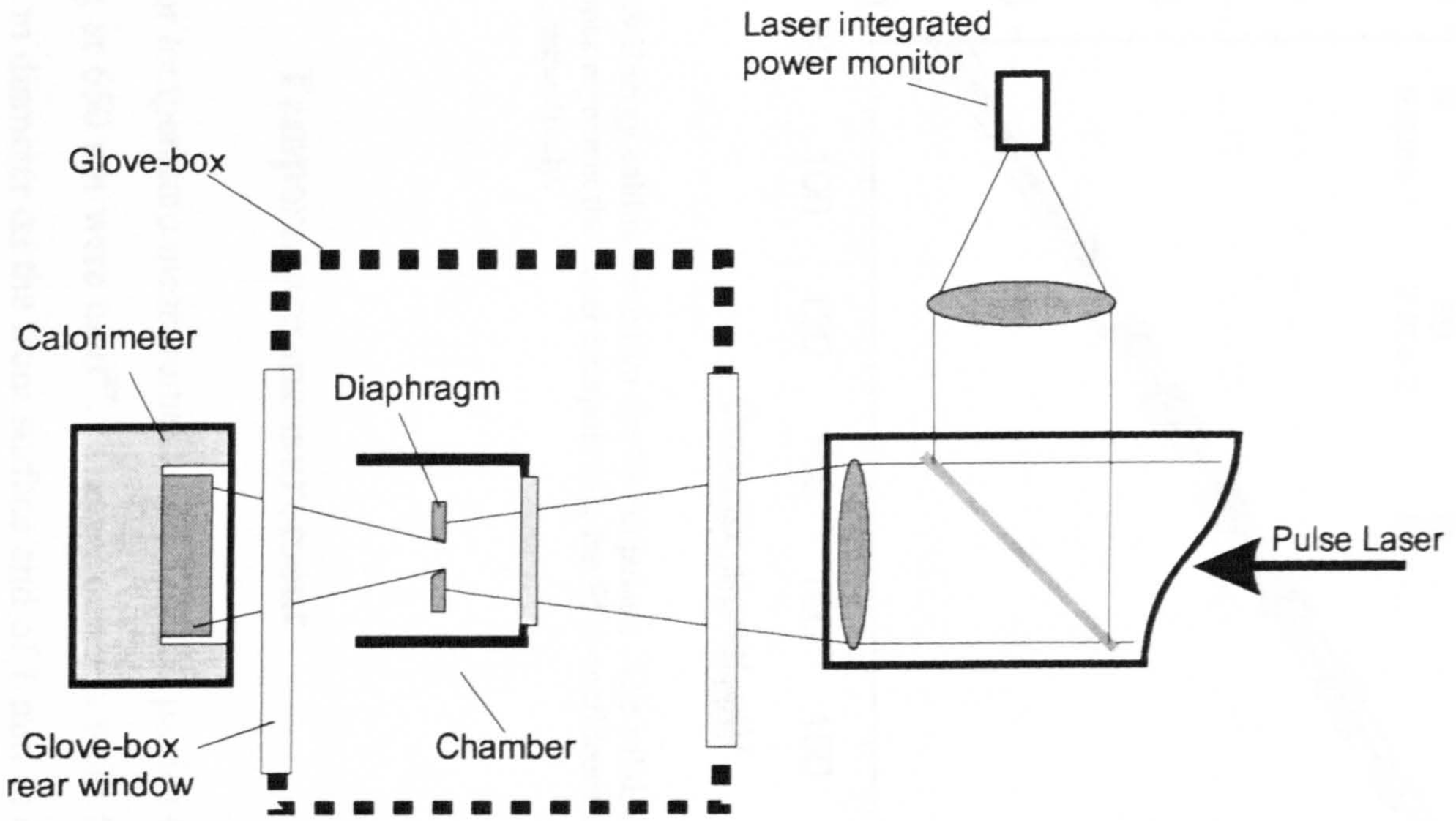

Fig. 4A.8 Schematic of the set-up used for the energy calibration with the use of the glove box. In a "normal" energy calibration the glove-box is removed.

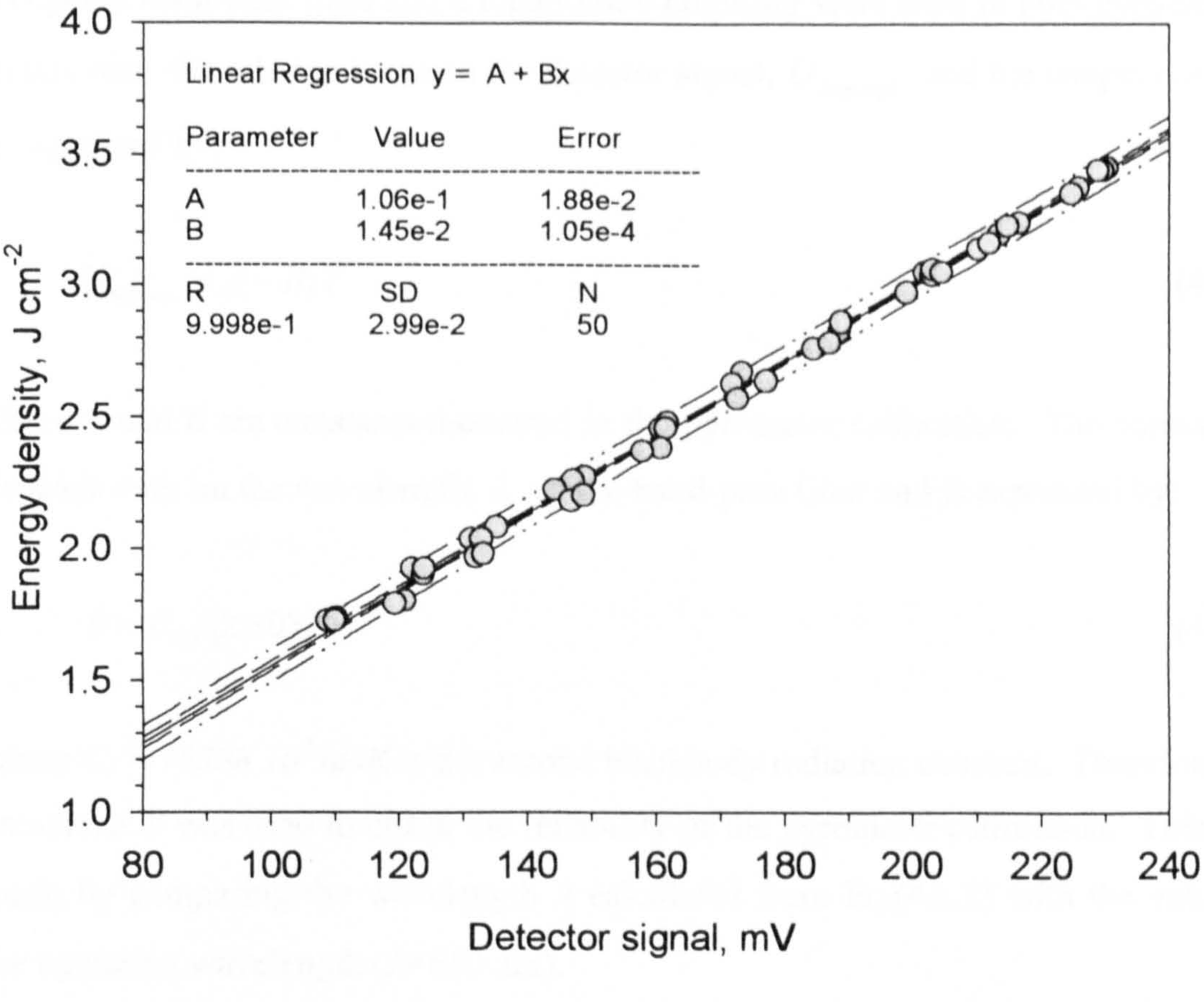

Fig. 4A.9 Energy calibration curve for 10 ms pulses. The solid, dashed and dashed-dotted-dotted lines represent the linear interpolation, the 95% confidence interval, and the prediction interval, respectively.

4A.5 Temperature measurement

For temperature measurements two fast (10 μs rise-time) brightness pyrometers working at 650 nm were used[xv]. The pyrometers were focused on a central area of 1.5 mm in diameter on the front surface and of 1 mm in diameter on the rear surface of the sample.

In order to deduce the temperature in Kelvin, needed for the specific heat calculation, a calibration of both pyrometers was performed. To obtain a simple

[xv] The pyrometer response time was tested with a special set-up to ensure that the most rapid temperature variations expected during the pulses could be correctly measured.

linear relationship between the detector signal and the inverse of the temperature[xvi], an optical band-pass filter and a logarithmic amplifier were used in both pyrometers. In this case, the relation between the detector signal, $U_{Logampl}$, and the temperature, T, is expressed by:

$$U_{logamp} = A - B/T \tag{4A.1}$$

where A and B are constants measured in the pyrometer calibration. The constant B depends only on the wavelength, λ, of the band-pass filter and is expressed by:

$$B = C_2/(2.303\lambda) \tag{4A.2}$$

where $C_2 = 14388\ 10^3\ nmK$ is the second blackbody radiation constant. Therefore the parameter B was used to check the reliability of the pyrometer calibration. This was made by comparing the wavelength λ calculated from Eq.(4A.2) with the value of the operating wavelength (λ=650 nm).

The sensitivity factor[xvii], n, of the pyrometer is expressed by:

$$n = |dU_{Logamp}/dT| = B/T^2 \tag{4A.3}$$

and hence the precision of the absolute values of the temperature increase, ΔT, is a function of both the parameter B and of the steady-state temperature.

Since the precision of the measured parameter B is by far better than the high frequency fluctuations of the thermal radiation, these fluctuations determine the accuracy of the recorded transient temperature curve. For instance, at 1800 K the noise was typically of the order of 0.2 K, but at 2500 K it increased up to 0.5 K. To

---

[xvi] According to Wien'a approximation, the light intensity, J, emitted by the surface of a material of emissivity ε, is expressed as $J(\lambda,T) = \varepsilon(\lambda,T)C_1\lambda^{-5}\exp(-C_2/\lambda T)$ where λ is the wavelength and C_1 and C_2 are constants.

compensate for the higher noise-to-signal ratio, at very high temperatures a higher energy pulse (yielding a higher temperature increase) had to be used.

Pyrometer calibration

To obtain an absolute measurement of the temperature increase of the front and rear surfaces of the specimen a calibration of the two pyrometers with two certified lamps (Polaron, 22/V Nr. P224c and 22/G Nr. P212c) was performed. The two tungsten band lamps were certified in the temperature range of 1100K - 1800 K and 1800 K - 2500 K, respectively. An example of the calibration curve for the rear pyrometer is given in Fig. 4A.10.

In this case the wavelength λ calculated from Eq.(4A.2) with the parameter B obtained in the calibration, presented a difference of 0.6% with respect to the nominal value of the wavelength filter used.

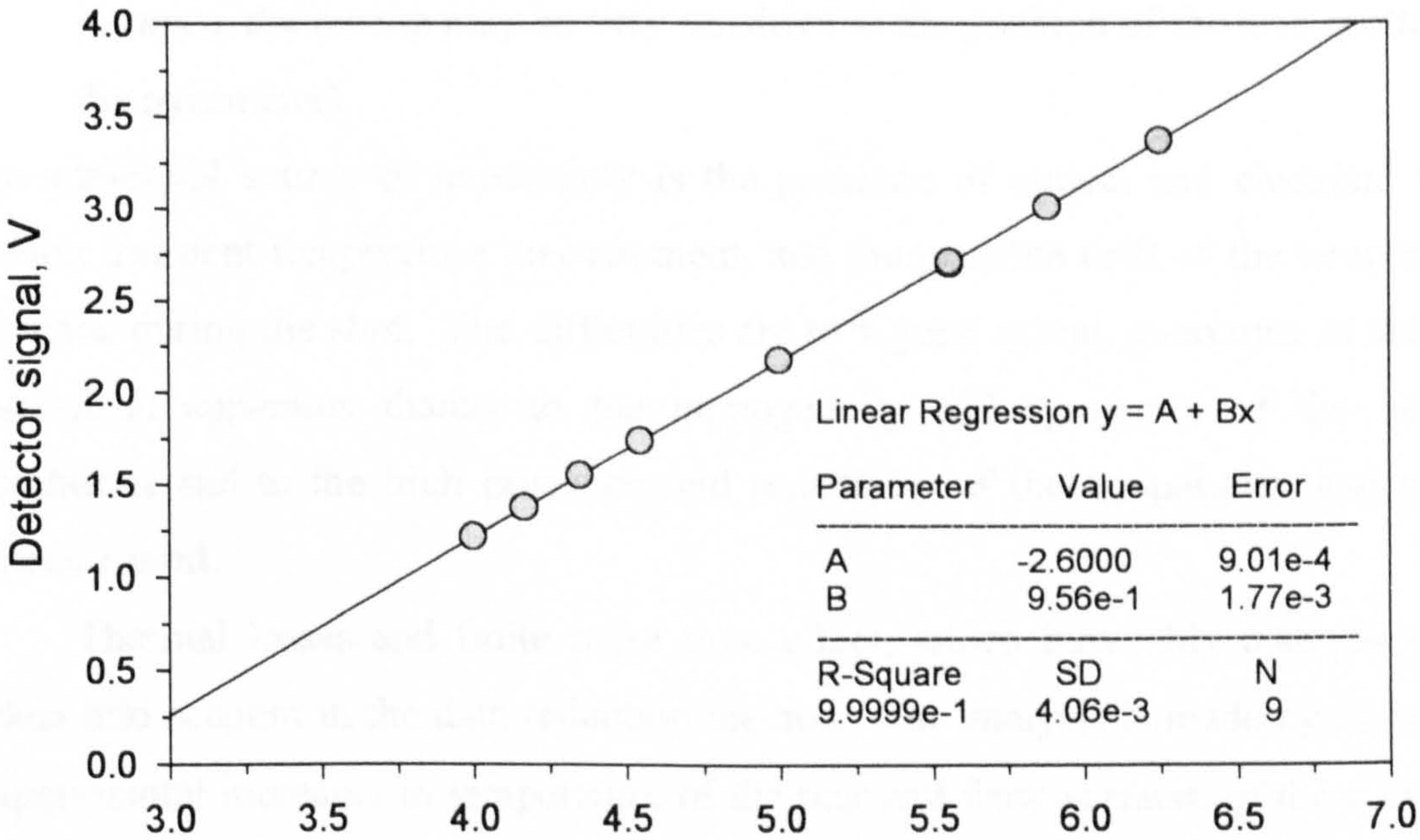

Fig. 4A.10 Pyrometer calibration curve based on band lamps references of certified temperatures.

[xvii] The sensitivity factor of the pyrometer, n, is defined as the derivative of the detector signal U, with respect to temperature T: $n = |dU/dT|$.

4B. DATA ANALYSIS

The evaluation method of the thermal diffusivity and specific heat depends on the possibility of obtaining an analytical integral of the pulse-heat transport equation, in the presence of sufficiently realistic boundary conditions. Thus, an essential requirement is to produce experimental conditions that are closer to selected ideal cases, for which the heat transport equation can be integrated analytically. As discussed in Section 3A, the difficulties are mainly due to three factors:

1. the radiative (axial and radial) as well as conductive thermal losses during and after the applied pulse,
2. the finite pulse time effect,
3. the possible spatial and temporal variations in the deposited pulse power density. This effect, in particular, entails drastic restrictions in the possibility of correlating experimental measurements with theoretical predictions (for instance, the results may be very sensitive to the position of the area spotted by the pyrometer).

An additional source of uncertainty is the presence of optical and electrical noise during transient temperature measurement, and the possible drift of the temperature baseline during the shot. The difficulties are to a great extent, overcome in the new laser-flash apparatus thanks to the homogeneity and symmetry of the heating conditions and to the high precision and sensitivity of the temperature and power detector used.

Thermal losses and finite pulse time effect, which inevitably take place, are taken into account in the data reduction method. The analysis is made by fitting the experimental increases in temperature of the rear and front surfaces of the specimen with the integral of the heat transport equation, solved for three different sets of boundary conditions (see Table 4B.1).

- The first solution (**Model 1**) considers radial heat losses from the front and rear surfaces of the sample, and conductive heat losses from the lateral surfaces; this corresponds to the case when the *sample diameter* is *larger* than the *laser beam diameter*.

- The second solution (**Model 2**), considers radial heat losses from all the surfaces (front, rear and lateral) of the sample and corresponds to the case where the laser beam spot covers the whole sample. In Model 1 and Model 2 the theoretical solutions allow the applied heat pulse to vary with time, and to display an arbitrary radial intensity profile.
- The third solution (**Model 3**) is a simplified case of the second one, where the radial thermal losses from the front and rear surface are assumed equal. This provides an easier fitting procedure (*e.g.* in measurements at low temperature and in cases where the quality of the experimental data does not allow a very precise analysis).

Table 4B.1

Boundary conditions used in the heat transport equation

	Parameters of **Model 1**	Parameters of **Model 2**	Parameters of **Model 3**
Front face losses	Radiative	Radiative	Radiative
Parameter	*Biot Number,* Y_1	*Biot Number,* Y_1	*Biot Number,* Y_z
Rear face losses	Radiative	Radiative	Radiative
Parameter	*Biot Number,* Y_2	*Biot Number,* Y_2	*Biot Number,* Y_z
Radial losses	Conductive into a cooler medium	Radiative	Radiative
Parameter	*Effective beam radius,* R^*	*Biot Number,* Y_r	*Biot Number,* Y_r

4B.1 Theoretical models

The heat diffusion equation for a cylindrical system of co-ordinates around the z axis, expressed by Eq.(3A.1), was solved for the general case of a surface pulse propagation into a circular platelet, assuming axial symmetry of the laser profile and spatially symmetrical energy deposition on the sample. The integral $T(z,r,t)$,

describing the transient temperature in the sample as a function of the axial and radial co-ordinates and of time, was obtained under the simplification of variable separation:

$$T(z,r,t) = T_1(z,t)\psi(r,t) \tag{4B.1}$$

where $T_1(z,t)$ and $\psi(r,t)$ are the axial and radial temperature evolution functions, respectively.

4B.1.1 *Axial temperature evolution function*

The axial heat diffusion is described by the classical solution for an infinite slab of thickness L and a surface source at $z = 0$. If the source is symmetric-cylindrical, the time dependence of the axial temperature is given by[63]:

$$T_1 = T_0 \sum_{n=1}^{\infty} A_n(z) \int_0^t \frac{Q}{\tau} \varphi(t') \exp\left(\frac{-\alpha_n^2}{L^2} a t'\right) dt' \tag{4B.2}$$

where T_0 is a scaling factor inversely proportional to the effective specific heat of the sample, c_P

$$c_P = \frac{Q}{L\rho T_0} \tag{4B.3}$$

where Q is the energy density (per unit of area) absorbed by the sample, ρ is the density and L the thickness. The coefficients A_n are expressed as:

$$A_n(z) = \frac{2\alpha_n\left(\alpha_n^2 + Y_2^2\right)\left(\alpha_n \cos\alpha_n z + Y_1 \sin\alpha_n z\right)}{\left(\alpha_n^2 + Y_1^2\right)\left(\alpha_n^2 + Y_2^2 + Y_2\right) + Y_1\left(\alpha_n^2 + Y_2^2\right)} \tag{4B.4}$$

α_n ($n = 1 \ldots \infty$) are the roots of the equation:

$$\left(\alpha^2 + Y_1 Y_2\right) tg(\alpha) = \alpha\left(Y_1 + Y_2\right) \tag{4B.5}$$

where Y_1, Y_2 are the values of the Biot numbers at the *front*, ($z = 0$) and at the *rear* ($z = L$) surface of the sample, respectively. The function $\varphi(t)$ represents the time-variable part of the fractional surface power, which is expressed as:

$$P_s = \frac{Q}{\tau}\varphi(t) f(r) \tag{4B.6}$$

with:

$$\int_0^{\tau} \varphi(t')dt' = 1; \quad \int_0^{R} f(r')2\pi r' dr' = 1 \tag{4B.7}$$

where τ is the laser pulse time and R the laser spot radius impinging the sample.

4B.1.2 *Radial temperature evolution function*

In the approximation of the variable separation, the effect of radial losses is independently calculated from the solution of the radial flow equation in a cylinder at initial zero temperature with an instantaneous cylindrical source centred on its axis. The source is assumed to be of strength $2\pi r' f(r')dr'$ at r', so that any symmetrical profile of laser power deposited onto the disk surface of radius R can be taken into account.

Two solutions, describing the experimental conditions, are available for the radial transport equation[63].

The first one (see Model 1, Table 4B.1), corresponds to *conductive radial losses at the boundary, $T(r) = 0$* at $r = R$ (the laser beam does not impinge the outer

edge of the sample disk and the lateral surface remains almost unperturbed during the shot):

$$\psi(r,t)=\frac{2}{R^2}\sum_{j=1}^{\infty}\exp(-a\lambda_j^2 t)\frac{J_0(r\lambda_j)}{J_1^2(R\lambda_j)}\int_0^R r' f(r')J_0(r'\lambda_j)dr' \qquad (4B.8)$$

where J_n indicates the Bessel functions of the first kind and λ_j are the zero's of $J_0(R\lambda)$.

The second solution (see Model 2, Table 4B.1), corresponds to *radiation boundary conditions* at $r = R$:

$$\psi(r,t)=\frac{2}{R^2}\sum_{j=1}^{\infty}\exp(-a\lambda_j^2 t)\frac{J_0(r\lambda_j)}{J_0^2(R\lambda_j)+J_1^2(R\lambda_j)}\int_0^R r' f(r')J_0(r'\lambda_j)dr' \qquad (4B.9)$$

where here λ_j are the zero's of the equation $\lambda J_1(R\lambda_j)=Y_r J_0(R\lambda_j)$, and Y_r represents the radial Biot number.

4B.1.3 *Assumed integral of the heat transport equation*

In the presence of the three independent heat losses, *i.e.* radiation from the front surface, radiation from the rear surface (both accounted for in Eq.(4B.2)), and conductive (Eq.(4B.8)) or radiative (Eq.(4B.9)) radial losses, the transient temperature can be expressed by Eq.(4B.1) where the axial temperature evolution function $T_1(z,t)$, is expressed by Eq.(4B.2), and the radial temperature evolution $\psi(r,t)$, is given by Eqs.(4B.8) and (4B.9) for Model 1 and Model 2, respectively.

If the laser specific power profile is constant ($f(r) \cong 1$) over the "effective" laser beam radius R^*, and $R^* < R$, the integral at the right-hand side of Eqs.(4B.8) and (4B.9) is:

$$\int_0^R rf(r)J_0(r\lambda_j)dr \cong \int_0^{R^*} rJ_0(r\lambda_j)dr = \frac{R^*}{\lambda_j}J_1(R^*\lambda_j) \qquad (4B.10)$$

which is a simple function of R^*.

The "effective" laser beam radius, R^* is approximately equal to the impacting laser beam diameter measured at 50% of its flank. However, its experimental measurement is often not very precise, and R^* may also be considered as a fitting parameter (Model 2), which, of course, is allowed to vary only within its experimental uncertainty range.

Thus Eq.(4B.1) presents *five* parameters; a, T_0, Y_1, Y_2, R^* (or Y_r) which may be, effectively or by definition, unknown. In addition, it depends on the dimensions R and L of the sample, and on the laser pulse features Q and τ, quantities that are all supposed to be independently measurable with adequate accuracy.

4B.1.4 *Simplified integral of the heat transport equation*

The simplified solution of the heat diffusion equation given by Cape and Lehman[25] was also considered in the case of laser pulse spot covering the whole face of the sample (see Model 3, Table 4B.1). The approximate solution for a cylindrical plate subject to equal radiation heat losses from both the base surfaces, and to radial heat losses is given by:

$$T(t) = T_0 \sum_{j=0}^{\infty} A_j(z) \int_0^t \frac{Q}{\tau}\varphi(t')\exp\left(-M_j a\frac{t}{L^2}\right)dt' \qquad (4B.11)$$

where L is the thickness of the sample, R its radius, a the thermal diffusivity, T_0 is expressed by Eq.(4B.2), $\varphi(t)$ represents the time-variable part of the fractional power surface expressed by Eq.(4B.6), and

$$A_j = \frac{(-1)^j 2X_j^2}{\left(X_j^2 + 2Y_z + Y_z^2\right)} \tag{4B.12}$$

$$M_j = X_j^2 + \left(\frac{L}{R} z_0\right)^2 \tag{4B.13}$$

$$z_0 = \sqrt{2Y_r}\left(1 - \frac{Y_r}{8}\right) \tag{4B.14}$$

$$X_0 = \sqrt{2Y_r}\left(1 - \frac{Y_z}{12} + \frac{7Y_z^2}{288}\right) \tag{4B.15}$$

$$X_j = j\pi + 2\frac{Y_z}{j\pi} - 4\frac{Y_z^2}{(j\pi)^2} - 2\frac{Y_z^3}{(j\pi)^3} - 16\frac{Y_z^4}{(j\pi)^4} \text{ with } j \geq 1 \tag{4B.16}$$

where Y_z and Y_r represent the axial and radial Biot numbers, respectively. Though this solution is less accurate than those of Model 1 and 2 for sufficiently flat power profiles it can be applied to obtain thermal diffusivity precision of up to 1%.

4B.2 Data fitting

The adopted method consists of fitting the experimental transient thermogram, $T_{exp}(t)$, with one of the theoretical solutions to obtain the *thermal diffusivity, a*, the pre-exponential factor, T_0, (inversely proportional to the *specific heat*), as well as the governing heat-loss parameters. Altogether, up to *five* unknowns must be determined. The type of pulse applied determines the most convenient theoretical model to be used. The Mean-SQuares (MSQ) difference between the theoretical and experimental temperatures is minimised by varying the above unknowns. Usually, several hundreds of experimental points, (T_i, t_i), are available to enable a non-linear multi-parameter Least-SQuares (LSQ) method to be efficiently applied. The technique employed is a combination of Newton-Raphson, Marquardt, and steepest-descent methods[64] to find the minimum of the sum:

$$F = \sum_{m=1}^{M} f_m^2 \tag{4B.17}$$

where

$$f_m = \frac{\delta T(t_m)}{T_{\exp}(t_m)} = \left[1 - \frac{T(z,r,t_m,\vec{x})}{T_{\exp}(t_m)}\right] \tag{4B.18}$$

with $m = 1,.....,M$ = total number of measurements, t_m = time at which T_{exp} is measured, z = axial position of the measurement, r = radial position of the measurement; $\vec{x}$, represents the vector of the above mentioned $N \leq 5$ fitting parameters, depending on the model used, *i.e.* (Table 4B.1):

- for Model 1 $\vec{x} = (x_1, x_2, x_3, x_4, x_5) = (a, T_0, Y_1, Y_2, R^*)$
- for Model 2 $\vec{x} = (x_1, x_2, x_3, x_4, x_5) = (a, T_0, Y_1, Y_2, Y_r)$
- for Model 3 $\vec{x} = (x_1, x_2, x_3, x_4) = (a, T_0, Y_z, Y_r)$.

Since in the computer program a large number of double or triple precision evaluations[xviii] of the rather complex theoretical temperature functions are required in the recursive procedure, a powerful processor had to be used for the on-line fitting calculations.

Solutions of Eq.(4B.17) are always found, provided that the number of measurements, M, is not less than the number of unknown parameters, N ($M \geq N$). However, the confidence limits (in the sense of stability against variations in the experimental data) of the solutions may be unacceptable, and can not be appraised *a priori* since they depend in a very complex manner on:

- the number of experimental data, M,
- the total measurement time of the pulse,
- the temperature variation during the time of the measurement,
- the experimental temperature errors.

This issue will be discussed below in order to judge the performance of the adopted method.

4B.2.1 *Evaluation of the result uncertainty*

The main question in a multiparameter nonlinear regression –"How stable is a Least-Squares solution against input perturbation?"- involves a number of complex statistical and algebraic problems, which cannot be discussed in this context. In our case, the question of interest is to which extent do experimental errors in the temperature measurements affect the fitting parameters of Eq.(4B.1) [or Eq.(4B.11)]?

An answer can be found if function δT in Eq.(4B.18) in the vicinity of the true temperature is approximately linear in $\vec{x}$, or, at least, if it is sufficiently regular with respect to continuity and derivability, to allow a linear series expansion around the *true* value, in the linear truncated form:

$$\delta T_m = \sum_{n=1}^{N} \frac{\partial T_m}{\partial x_n}\left(x_n - x_n^{true}\right) = const + \sum_{n=1}^{N} \frac{\partial T_m}{\partial x_n} x_n \qquad (4B.19)$$

where $T_m = T(t_m)$ with $m = 1,\ldots\ldots,M$.

If the *formulation* of the theoretical temperature is considered as *correct*, the initial definition of δT_m can be reversed, this difference being seen as the error by which the measurement T_{exp} is affected. Therefore according to the maximum likelihood method, the unknown x_n should be chosen so as to minimise the weighted sum, F, of the square errors of Eq.(4B.17). To minimise F, its partial derivatives have to be taken with respect to each x_n, and equated to zero. This leads to the definition of a normal equation system, with the $N \times N$ coefficient matrix of $\vec{x}$ given by:

[xviii] For cases where large radial losses are present, triple numerical precision (real*16) must be used in the subroutine where f_m is evaluated.

$$b_{rs} = \sum_{m=1}^{M} \frac{\partial T_m}{\partial x_r} \frac{\partial T_m}{\partial x_s} \tag{4B.20}$$

If the partial derivatives are constant, this formula can be considered as a straightforward application of the multivariable linear regression problem, with $\|b\|$ representing the covariance matrix. In reality, these derivatives are dependent on $\vec{x}$, and, as such, are they treated in the F-minimisation procedure mentioned in the preceding section- so that this analogy is strictly applicable only within an infinitesimal interval around the true value of $\vec{x}$, that is to say only under sufficiently good fitting conditions. The most important restriction regards the statistical distribution of the values of f_m, calculated from Eq.(4B.17). This must be reasonably interpretable as the observed values of a *normally distributed* random variable[xix]; only under this condition it can be demonstrated that the value of x_n that minimises F is an unbiased estimate of the unknown true value, whereby the variance of x_n is expressed as:

$$\sigma_n = \sigma' \sqrt{\frac{M}{M-N} \frac{B_{ii}}{B}}, \tag{4B.21}$$

where B is the determinant of $\|b\|$, B_{ii} the cofactor corresponding to the element b_{ii}, and

$$\sigma' = \sqrt{\frac{1}{M} \sum_{m=1}^{M} f_m^2} \tag{4B.22}$$

is the final MSQ fitting error.

[xix] This implies that the assumed theoretical temperature function does correctly represent, within the experimental error, the measured pulse, and that no systematic errors are made in the measurements of the pairs (T_i, t_i).

In conclusion, it can be seen that the goodness of fitting, described by Eq.(4B.22), does not generally imply that the obtained results are reliable, for the ratio of the determinants in Eq.(4B.21) may be strongly dependent on the rank, *i.e.* on the number, N, of fitted parameters. Therefore, only Eq.(4B.21) provides an objective criterion for evaluating the confidence limit of the fitted variable, x_n, and must, therefore, be used to accept or reject the solution.

4B.2.2 *Adopted fitting strategy*

A computer program was written with the aim to perform the fitting procedure with the best attainable exploitation of the information provided by the available input. The schematic relations between the input and the output parameters in the fitting of a transient pulse, and the step sequence of the program are summarised in Tables 4B.2 and 4B.3, respectively.

Fig. 4B.1 shows the analysis results for a shot on uranium dioxide at 900 K. The chosen measurement corresponds to a probe beam smaller (5 mm) than the sample diameter (10 mm). By using Model 1 a fitting precision of 1.27% was obtained by the program. It was possible, in this case, to increase the rank of the unknown vector up to 5, finding all the parameters, a, T_0, Y_1, Y_2, and R^*, with good confidence limits.

For less precise measurements the analysis might be more problematic. Even if fitting results are viable *only* with three or four parameters, and, therefore, additional assumptions must be introduced on the values of the three Biot numbers or on their mutual relationships, an acceptable evaluation of diffusivity and specific heat (with however, lower accuracy) can still be obtained.

If accuracies *not* better than *5%* are required for *thermal diffusivity*, it is normally enough that the resulting *total* heat loss is fairly evaluated by the program, no matter how this is partitioned in the different directions. However, some important restrictions are worth mentioning:

Table 4B.2

Input/output data of the overall-fitting model

	Sample and laser shot input	Transient input		Program output
1)	Laser specific power		1)	Thermal diffusivity
2)	Laser beam spatial profile	Transient	2)	T_0 (inversely proportional to the specific heat)
3)	Laser beam time evolution	time/temperature	3)	Radiation losses from the specimen front surface
4)	Specimen thickness	measurements	4)	Radiation losses from the specimen rear surface
5)	Specimen diameter	(up to 500 points)	5)	Radial losses (radiative or conductive)
6)	Specimen laser light absorbivity		6)	Expected accuracy of the above quantities
7)	Specimen density			

1. There is a strict implicit connection between the average experimental error and the maximum permissible number of fitting parameters. Once a value of σ' equal to the random experimental error of $T_{exp}(t)$ is obtained, by using N fitting parameters, any attempt to improve the accuracy of the results by increasing N is essentially erroneous. This is not obvious, since increasing the number of fitting parameters generally leads to a decrease of σ', with an apparent, but in fact illusory, precision improvement. The failure of the procedure is normally revealed by a decrease of one (or more) of the $\sigma_{n=1,\ldots,N}$, accompanied, by a dramatic increase of others.
2. σ_n represents the probable errors of x_n only if the local residuals $f_{m=1,\ldots,M}$ are *normally* distributed. Therefore, in the presence of *systematic* deviations the calculated errors may become meaningless. The danger of losing statistical

Table 4B.3

Schematic instruction system of the used program

1) Read sample and shot parameters, and values of M temperature/time pairs from the measurement file.

⇓

2) Assess the most suitable model for the given experiment [i.e., Eq.(4B.2)/Eq.(4B.8), Eq.(4B.2)/Eq.(4B.9), or Eq.(4B.11)].

⇓

3) Fit data with parameters a, c_P, Y_1 ($N=3$), assuming, e.g. $Y_2=Y_1$ and no radial losses, or other *ad-hoc* hypotheses on Y_2 and Y_r (or R^*)

⇓

4) Evaluate confidence limits of a, c_P, Y_1 from Eq.(4B.21).

⇓

5) Increase the number of fitting parameters: a, c_P, Y_1, Y_2 ($N=4$).

⇓

6) Compare new confidence limits of a, c_P, Y_1, Y_2 with the previous.

⇓

7) If check is positive go to 8), otherwise take previous results and stop.

⇓

8) Increase the number of fitting parameters: a, c_P, Y_1, Y_2, Y_r (or R^*) ($N=5$).

⇓

9) Compare the confidence limits of a, c_P, Y_1, Y_2, Y_r (or R^*) with the previous.

⇓

10) If check is positive stop, otherwise take previous results and stop.

significance in the errors, and hence in the confidence limits of the results, is often faced when a high experimental accuracy of $T_{exp}(t)$ is encountered, and consequently, high fitting precision are pursued by using the maximum number of fitting parameters ($N = 5$). In these cases it is advisable to determine the extent and the location of possible systematic errors in the fitted curve, due to non-perfect adequacy of the theoretical model to the experiment. This can be made by a variance analysis of different segments of the curve $f_i=f_i(t)$ as described by Fisher[65]. For instance, a suitable method is to compare the residuals in the ascending flank of the rear-face temperature pulse, in the zone

of its maximum, and in the tail. If the resulting systematic error is larger than the experimental temperature accuracy, the sum of squared residuals of Eq.(4B.21) must be replaced by $\sigma'_{systematic} > \sigma'$, and the attainable limit of the fitting precision is correspondingly lowered. This substitution leads to a stronger dependence of the confidence limits of the fitting results on the correlation factors B and B_{ii}, and as a result, more restrictive conditions for the acceptance of fitting results are imposed.

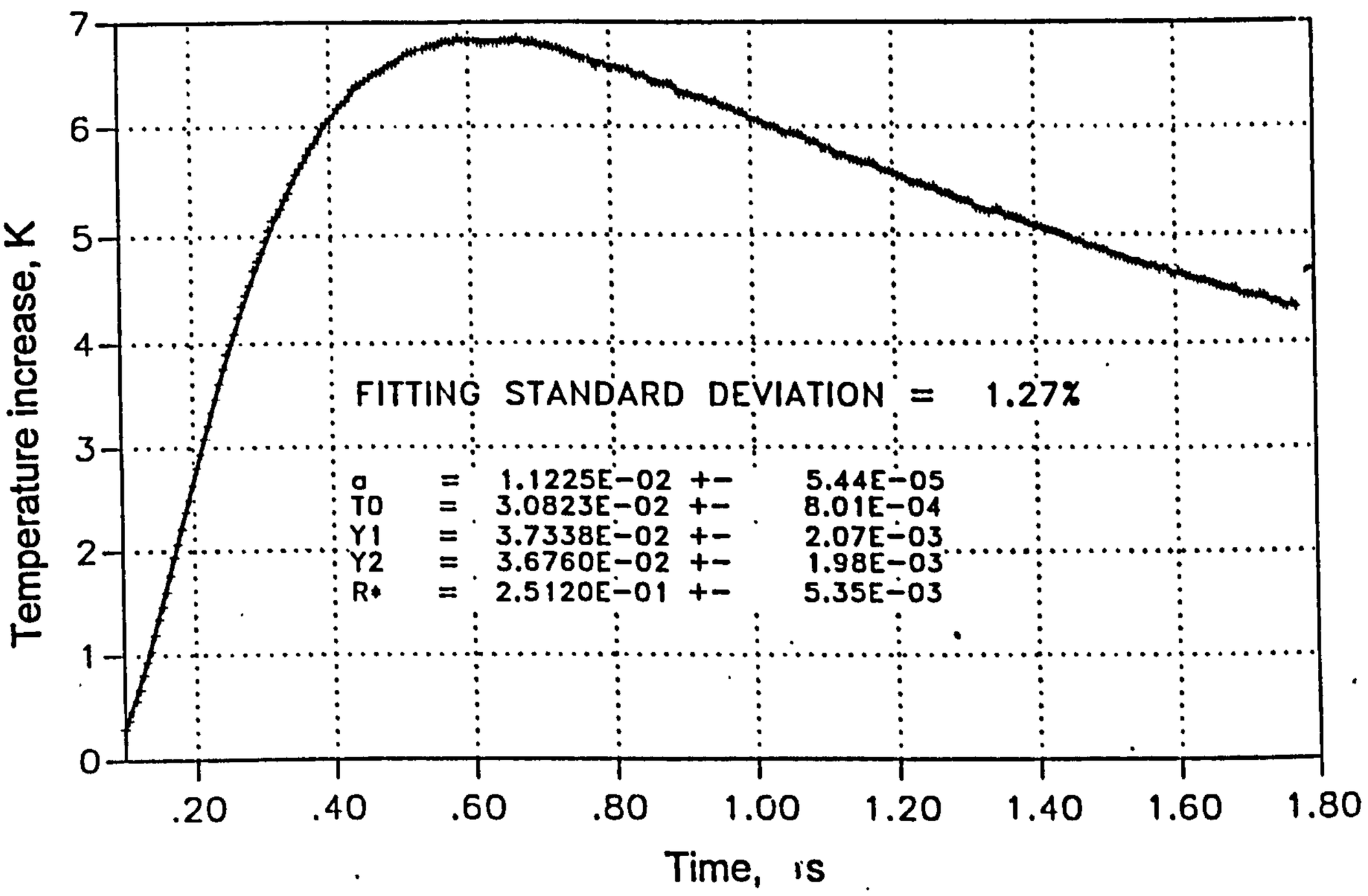

Fig. 4B.1 Fitting of the measured transient temperature curve with the five-parameter function of Eqs.(4B.2)/(4B.8). The sample is uranium dioxide at 900 K. The full line represents the predicted theoretical curve. The original experimental thermogram consisted of several thousands of temperature measurements, however, for the fitting procedure these have been compressed to 300 points, each of which was assigned a local error.

The problem of over-fitting is illustrated in the following example. A sample, a UO_2 disk of 12 mm diameter, and 1.5 mm thickness, was submitted to a pulse with a homogeneous laser beam of 5 mm diameter. The radial heat losses were, therefore, expected to be relevant. As in the preceding case, the program could fit 300 experimental points with five parameters. The fitting result was excellent, giving a residual MSQ deviation of less than 1%. The obtained values are reported in the first column of Table 4B.4. The order in which they appear from the top to the bottom reflects their hierarchical rank (in the sense of sensitivity on fitting) as it was recognised by the fitting algorithm. It can be seen that, after a and T_0, follows the effective laser beam radius R^*, whose resulting value is very close to the empirical measurement.

A calculation experiment was then carried out. These parameters were used to calculate a set of 300 points on the temperature curve represented by Eqs.(4B.2) and (4B.8); these were subsequently perturbed by applying to the calculated values, using a random-number generator, an error of the order of 0 - 5% (*i.e.* with an upper limit five times greater than the initial experimental error). The perturbed data set was then refitted with three, four, and five parameters, respectively, in the same order as in Table 4B.4. The results are shown in Fig. 4B.2 and are reported, with the respective uncertainties, in the other three columns of Table 4B.4. It can be seen that the fitting precision of the perturbed points increases weakly by increasing the numbers of parameters, indicating a permanent large uncertainty in the Biot numbers $Y_{1,2}$. While the uncertainties decreased when *four* parameters were used instead of *three*, a further attempt to improve the results by using *five* parameters failed, resulting in a better fitting, but with a larger uncertainty in a and R^* (two parameters of higher rank). Evidently, the resulting improvement in the precision of Y_1, together with the specification of Y_2, cannot be seen as a compensation for the loss in precision of R^*, confirming that in this experiment the radiation losses play a minor role compared to radial losses. In conclusion, the four-parameter fitting is predicted to provide here the best results (in the sense of statistical likelihood), and this is indeed confirmed by the values obtained, which are closest to the "true" ones reported in the first column.

Finally, it should be remarked that this calculation experiment shows that by substantially increasing the *random* experimental temperature error, the thermal diffusivity can still be evaluated with a reasonable precision, confirming the power and robustness of the adopted method.

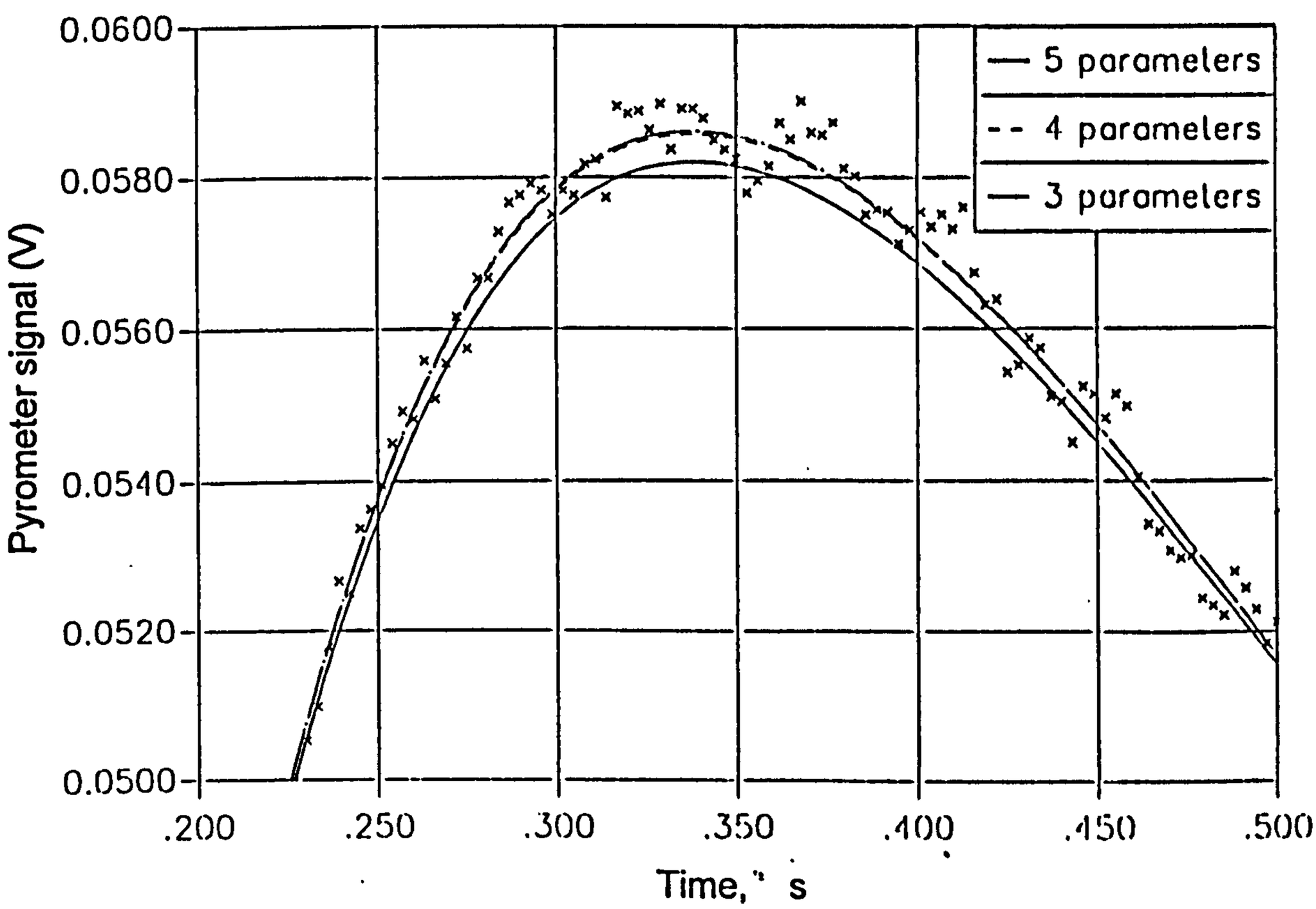

Fig. 4B.2 Fitting results with different number of parameters. The curves represent only a small segment of the total curve. The sample is uranium dioxide at 900 K.

This method is essentially heuristic as far as the resulting precision is concerned. However, it is possible to establish in advance an approximate relation between the experimental noise-to-signal ratio and the attainable precision of a and T_0. For instance, by starting with 500 experimental points of the function $T = T(t)$, homogeneously distributed over a time interval corresponding to approximately $5t_{1/2}$, the conditions described in Table 4B.5 are normally met.

Table 4B.4

Fitted parameters obtained with Model 1 from data plotted in Fig. 4B.2. The asterisk denotes an uncertainty of more than 100%. The non-fitted parameters are taken equal to zero.

		Three-parameter fitting Prec. 2.98%		Four-parameter fitting Prec. 2.97%		Five-parameter fitting Prec. 2.96%	
	True values	Values	±%	Values	±%	Values	±%
a ($10^{-6}m^2s^{-1}$)	1.500	1.544	3.668	1.521	2.396	1.551	2.479
T_0 (mV)	3.240	3.322	2.592	3.260	1.748	3.197	1.417
R^*	0.250	0.252	5.620	0.250	5.160	0.259	5.516
Y_1	0.010	0.000	*	0.018	*	0.013	40.000
Y_2	0.010	0.000	*	0.000	*	0.131	*

Table 4B.5

Relation between temperature accuracy and resulting precision of diffusivity.

Noise-to-signal ratio of temperature, T	Number of usable parameters	Achievable precision of thermal diffusivity, a
<1%	5-4	0.1%-0.5%
1%-2%	4-3	0.5%-1%
2%-5%	3	1%-5%

An example of the fitting performed with three parameters is reported in Fig. 4B.3, for POCO AXM-5Q graphite. The measurement corresponds to a probe beam equal to the sample diameter (5 mm) and Model 2 was used for the analysis. In this case the transient curve, recorded at 2292 K, did not allow an analysis to be performed with more than three parameters. Hence the rear and radial Biot numbers, Y_2 and Y_r (fourth and fifth parameter, respectively) were calculated by the formula:

$$Y_2 = Y_1\left(T_2/T_1\right)^3 \tag{4B.23}$$

$$Y_r = Y_2\varepsilon_r(R/L)\left[1-(1-\varepsilon_r)(1-\varepsilon_h)\right] \tag{4B.24}$$

where T is the temperature, L, R and ε are the thickness, the radius, and the total hemispherical emissivity of the sample. The suffix 1, 2, and r, refer to the front, rear, and lateral surface of the sample, and h refers to the sample holder. The program, with good confidence limits for all the three parameters, obtained a fitting precision of 2.02% (see Fig. 4B.3).

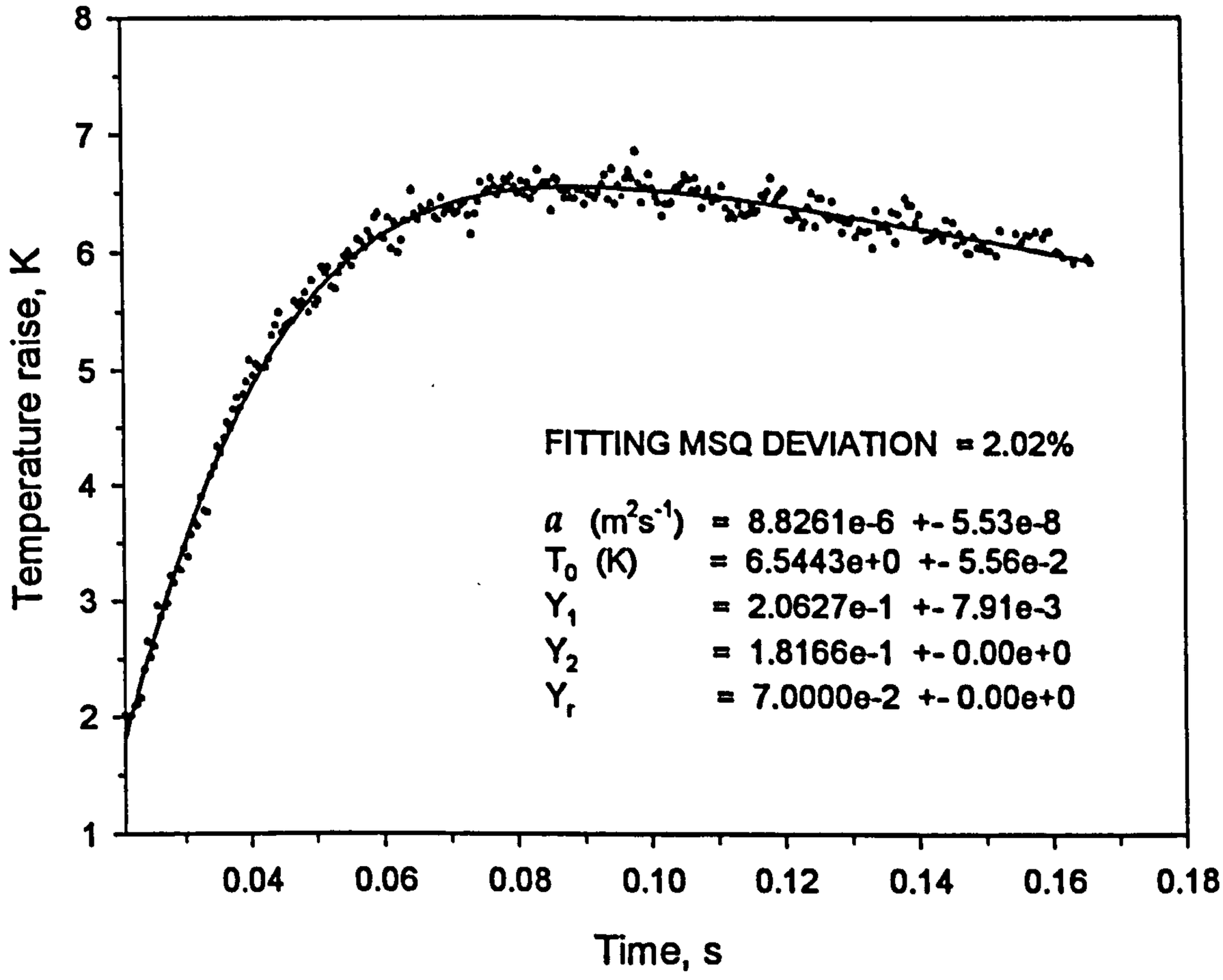

Fig. 4B.3 Fitting of the measured transient temperature curve with Model 2 using three-parameters. The sample is POCO AXM-5Q graphite at 2292 K. The full line represents the predicted theoretical curve. The original experimental thermogram consisted of several thousands of temperature measurements, however, for the fitting procedure these have been compressed to 300 points, each of which was assigned a local error.

4B.2.3 *Simultaneous rear- and front-temperature fitting*

In the experiments both front and rear face temperature are measured, and hence both can be fitted with the theoretical function. However, for the front-face temperature the procedure is less accurate, due to the analytical properties of the front-temperature curve. At short times the shape of this curve is strongly dependent on the time evolution of the input power, and becomes less and less sensitive to the variation of the physical parameters for longer times.

Nevertheless, while a *separate* analysis of the front-temperature and rear-temperature pulse does *not* lead to a significant improvement of the results, a *simultaneous* fitting of back- and front-temperature offers three important advantages:

1. it confirms that the front-surface temperature evolves in agreement with the values of a and c_p calculated for the body of the sample,
2. the numerical range where the LSQ variables are searched is much better individuated around the *physically true* values because the correlation among the variables is strengthened, and this contributes to exclude pseudo-solutions,
3. the convergence of the numerical fitting is substantially enhanced.

From the computational point of view the evaluation of Eq.(4B.1) was done with all measured experimental points, attaching a flag to each point, indicating whether the calculation of Eq.(4B.2) has to be performed at $z=0$ (front) or at $z=L$ (rear).

The simultaneous fitting of both rear- and front- temperature was adopted for the calculation of the thermal diffusivity and the specific heat of zirconium dioxide. In this case, where the correct measurement of a and c_P is relying on the expected decrease in transparency of the sample at high temperatures, the consistency of the analysis of the rear and front surface thermograms is, in fact, of great significance.

For POCO AXM-5Q graphite and uranium dioxide, fitting of both rear- and front- temperature curves was used in a first step of the data analysis to confirm the stability of the surface of the sample under laser irradiation. In a second step, to enhance the precision of the calculated parameters, rear fitting only was carried out. In Table 4B.6 the parameters, and their precision, obtained by a simultaneous fitting of rear- and front- temperature are compared with the parameters obtained from only

rear fitting. The example refers to a thermogram obtained on a POCO AXM-5Q graphite sample at temperature of 2643 K, where the probe beam was equal to the sample diameter. The fitting was performed by using Model 2 with three parameters, by applying the conditions expressed by Eqs.(4B.23) and (4B.24) for the fourth and fifth parameters, respectively.

Table 4B.6

Comparison of parameters obtained for simultaneous front/rear and rear fitting for POCO AXM-5Q graphite at 2643 K.

	Front and rear fitting Prec. 2.99%		Rear fitting Prec. 2.02%	
	Values	±%	Values	±%
a ($10^{-5}m^2s^{-1}$)	9.129	1.010	9.116	0.620
T_0 (K)	2.139	0.438	2.165	0.355
Y_1	1.182	2.47	1.172	1.940
Y_2	1.0185	...	1.010	...
Y_r	0.829	...	0.829	...

4B.2.4 *Independent check of the Biot numbers*

The measurement of the front- and rear-temperature, T, makes it possible to carry out an independent verification of the resulting specific heat. In fact, if the sample total emissivity, ε, and the density, ρ, are known, a simple formula, derived from Eq.(3A.6), relating the basal and radial Biot numbers to the specific heat, can be obtained:

$$Y_{1,2} = \frac{4\varepsilon\sigma_S T_{1,2}^{\ 3} L}{a\rho c_P} \tag{4B.25}$$

$$Y_r = \frac{4\sigma_S T_r^3\, \varepsilon_s\varepsilon_h / [1-(1-\varepsilon_s)(1-\varepsilon_h)]R}{a\rho c_P} \tag{4B.26}$$

Thus, the fitted value of Y_k can be compared with that calculated from the respective formula: since the obtained thermal diffusivity, a, is normally very accurate, a good agreement of the two values is an important confirmation of the correctness of c_P. Though the dependence of Y_k on the third power of temperature entails significant error amplification, the difference between fitted and calculated Biot numbers, in the reported measurements, was of the order of 10%, never exceeding 20%.

4B.3 Comparison with classical correction methods

In the adopted overall-fitting procedure, the heat losses are *directly correlated* with the thermal diffusivity and specific heat. In the customary methods, an "uncorrected" diffusivity is first evaluated, to which the heat loss corrections are *subsequently* and *separately* calculated from distinct features of the thermogram; therefore, the effect of the heat losses is implicitly assumed to be a linear perturbation. As already discussed in Section 3A, the simplest and mostly used radiative heat-loss compensation methods are those proposed by Clark and Taylor, and by Cowan. From the quality and type of experimental data, it is usually possible to establish which method specifically provides more reliable results. Under favourable experimental conditions the applied corrections are, in general in the order of 5%-10% of the uncorrected value of a, however, they markedly increase with the measurement temperature.

In the overall-fitting model of this work, the obtained thermal diffusivity has a predicted uncertainty by one order of magnitude smaller than Clark and Taylor's and Cowan's corrections (see *e.g.* the data of Fig. 4B.2). Calculation experiments have shown that in cases where the heat losses are low and the specimen surface is completely covered by the probe beam, the three methods lead to diffusivity values whose difference are within the measurement precision. However, when larger losses are caused by radial heat transport, the above mentioned corrections become

significantly less accurate. A comparison of diffusivity measurements on UO_2 is presented in Table 4B.7.

Table 4B.7

Thermal diffusivity of UO_2 at 1100 K (in 10^{-6} m^2s^{-1})

Uncorrected	Corrected (Taylor) by taking 25% and 75% T_{max}	Corrected (Cowan) by taking $t_{end} = 5\ t_{1/2}$	Overall fitting by taking 300 points within $0 < t \leq 10\ t_{1/2}$
1.1077 ± 0.010	1.0424 ± 0.015	1.0385 ± 0.010	1.0370 ± 0.0026

From Table 4B.7 it can be seen that Cowan's correction is very near to the fitting prediction, while Taylor's correction leads to a somewhat higher value, but the difference is only 0.5%. When, however, larger losses are caused (for instance by radial transport) the difference increases. An example is presented in Fig. 4B.4. The UO_2 sample was of 5.6 mm diameter, while the diameter of the probe laser beam was only 3 mm. In this context, the examined data represent a temperature pulse measurement of mediocre quality; the existing high-frequency signal noise is here much higher (2%) than in the case of Fig. 4B.2, in addition, marked heat losses are present with a non-negligible conductive component in the radial direction.

The diagram of Fig. 4B.4 shows the uncorrected values of a, calculated from $t_{1/2}$, and those obtained after applying Cowan's and Taylor's corrections, respectively. In Fig. 4B.4 the values obtained from the overall-fitting model (using 300 experimental points) are indicated by lines marked with diamonds, whose vertical lengths correspond to the expected uncertainty calculated from Eq.(4B.21), which is of the order of 1-2%. From inspection of Fig. 4B.4, it can be seen that that Cowan's and Taylor's corrections present reciprocal deviations of ± 3%. On the other hand, the values of a obtained by the overall-fitting model are systematically higher than the corresponding "corrected" values by 3-5%. This difference is essentially due to the diverse functional dependence of temperature on the conductive and radiative heat losses in Eqs.(4B.8) and (4B.9) than in the simpler Taylor and Cowan models.

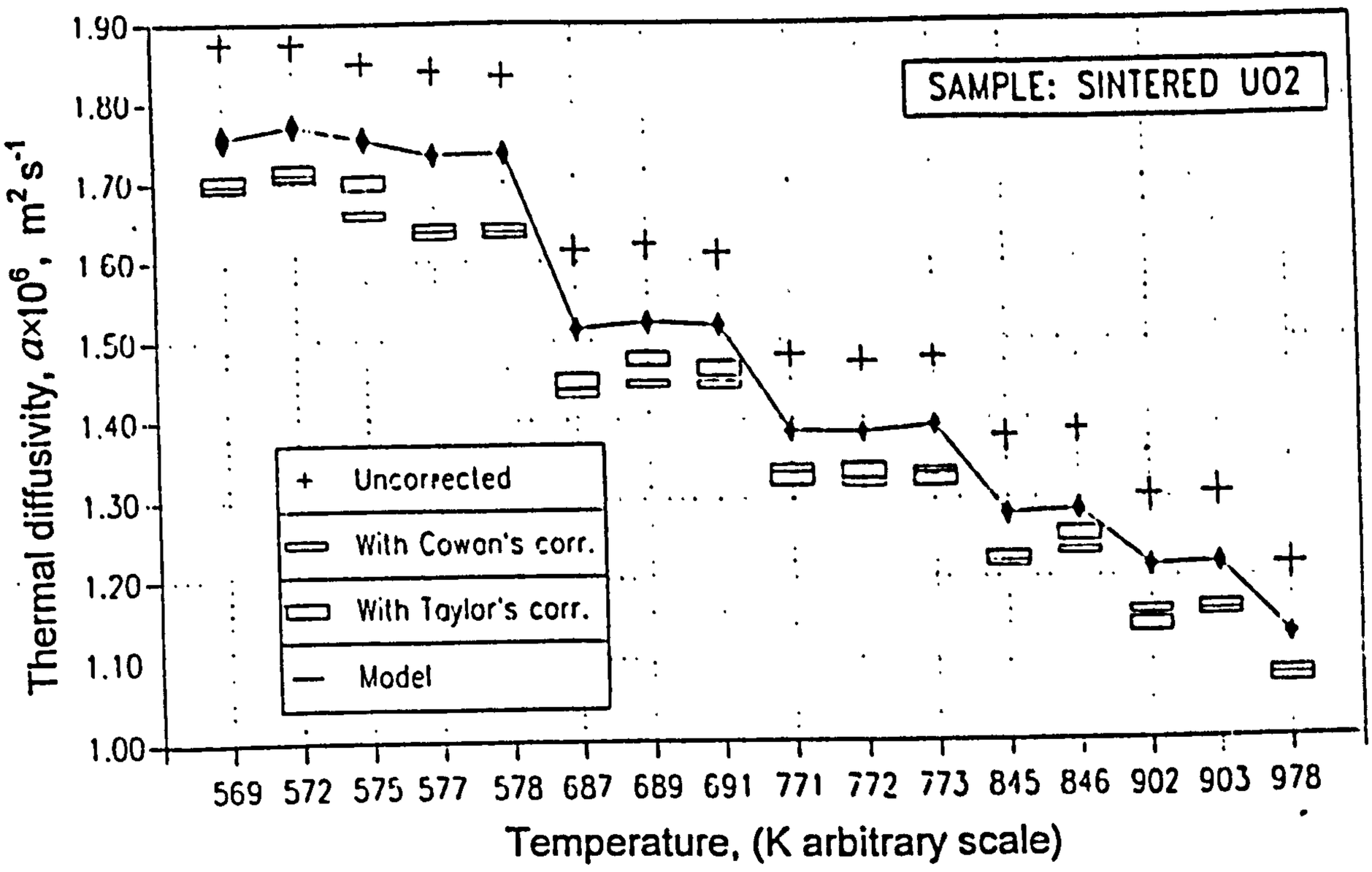

Fig. 4B.4 Comparison of uranium dioxide thermal diffusivities from measurements at different temperatures obtained by using standard corrections and the overall-fitting method.

A comparison of the thermal diffusivity values calculated by the overall-fitting model, and by applying Taylor's and Cowan's corrections is shown in Fig. 4B.5 for measurements on UO_2 at very high temperatures (T>1800 K). The experiments correspond to a probe beam equal to the sample diameter (5 mm) and Model 2 was used for the analysis. The fitting was performed with three parameters, by applying the conditions expressed by Eqs.(4B.23) and (4B.24) for the fourth and fifth parameters, respectively. It can be seen that the difference between the calculated values is of the order of 5%.

This confirms the reliability of the overall-fitting method, which can be thus applied for the calculation of thermal diffusivity when the experiment is performed with long laser pulses and arbitrary variations of the laser power with time.

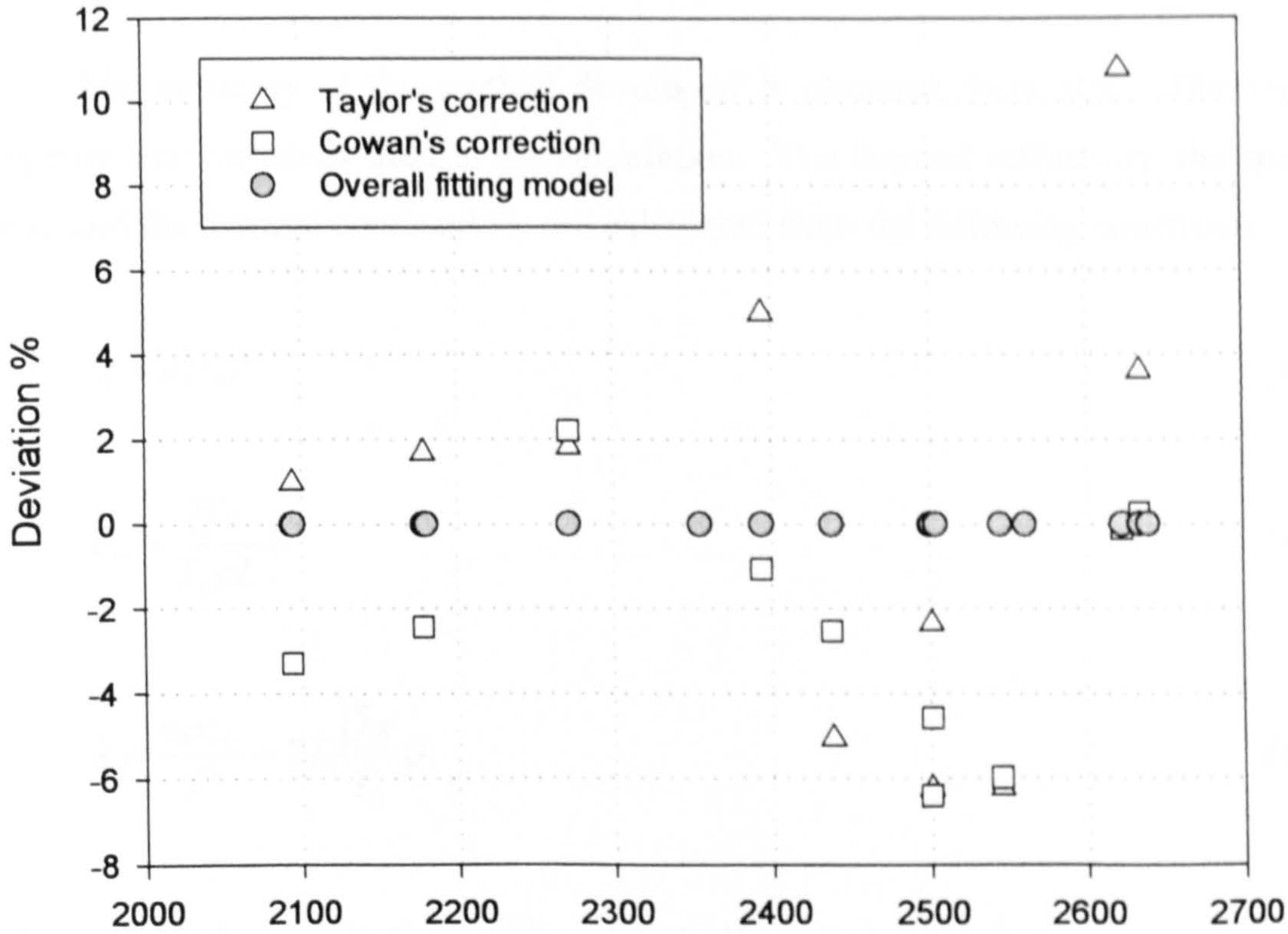

Fig. 4B.5 Comparison of thermal diffusivity values of UO_2 calculated by the overall-fitting model respect to the values calculated applying the Clark and Taylor's and Cowan's corrections.

4C. ERROR ANALYSIS

The accuracy of the method developed is obtained from error affecting the experimental variables used in the calculation. The thermal diffusivity, the specific heat, and the thermal conductivity are calculated from the following equations:

$$a = \bar{a} L^2 \vartheta^2 \tag{4C.1}$$

$$c_P = \frac{\overline{Q}\varepsilon}{T_0 \rho L} \vartheta^2 \tag{4C.2}$$

$$\lambda = \frac{a \rho c_P}{\vartheta^3} = \bar{a} L \frac{\overline{Q}\varepsilon}{T_0} \vartheta \tag{4C.3}$$

where $\bar{a}$, having dimension of s^{-1}, and T_0 in K, represent the fitting parameters, $\overline{Q}$ is the energy density delivered by the laser probe, ε is the emissivity of the front surface of the specimen; L and ρ are the thickness and the density of the sample at room temperature, respectively, and $\vartheta = (1+\alpha)$ represents the correction factor due to thermal expansion $\alpha(T)$.

In Eqs.(4C.1) (4C.2) (4C.3) three different types of variables may be distinguished:

1. the fitting parameters,
2. the variables depending on the laser pulse features,
3. the variables depending on the specimen characteristics (geometry and material properties).

The fitting parameters $\bar{a}$ and T_0, depend on the analysis of the experimental thermogram. Their precision, expressed by $\sigma_{\bar{a}}$ and σ_{T_0} (Eq.(4B.21)), was discussed in Section 4B.2. The error affecting the other variables depends on the precision of their measurement. The fractional fitting errors $\sigma_{\bar{a}}$ and σ_{T_0} are of complex nature as they possibly contain bias components due to deviation from ideality of the

experiment with respect to the model. It shall however assumed that these systematic error components are *not* affected by the experimental variables ε, L, ρ and $\overline{Q}$, so that their errors are not correlated with $\sigma_{\bar{a}}$ and σ_{T_0}.

The final fractional accuracy of a, c_P and λ can be simply expressed as:

$$\frac{\delta a}{a} = \sqrt{\sigma_{\bar{a}}^{\,2} + 4\left(\frac{\delta L}{L}\right)^2 + 4\left(\frac{\delta \vartheta}{\vartheta}\right)^2} \tag{4C.4}$$

$$\frac{\delta c_P}{c_P} = \sqrt{\left(\frac{\delta \overline{Q}}{\overline{Q}}\right)^2 + \left(\frac{\delta \varepsilon}{\varepsilon}\right)^2 + \sigma_{T_0}^{\,2} + \left(\frac{\delta \rho}{\rho}\right)^2 + \left(\frac{\delta L}{L}\right)^2 + 4\left(\frac{\delta \vartheta}{\vartheta}\right)^2} \tag{4C.5}$$

$$\frac{\delta \lambda}{\lambda} = \sqrt{\sigma_{\bar{a}}^{\,2} + \sigma_{T_0}^{\,2} + \left(\frac{\delta L}{L}\right)^2 + \left(\frac{\delta \overline{Q}}{Q}\right)^2 + \left(\frac{\delta \varepsilon}{\varepsilon}\right)^2 + \left(\frac{\delta \vartheta}{\vartheta}\right)^2} \tag{4C.6}$$

Each contribution affecting the error of the values of the thermal diffusivity, the specific heat and the thermal conductivity for the different materials studied was determined and reported in the respective sections.

Chapter 5

5. EXPERIMENTAL RESULTS

5A. GRAPHITE

The selection of a suitable standard reference material for thermophysical measurements at high temperatures is a difficult problem. As defined in AGARD Advisory Report 31[66] and 38[67] and in the AGARD Report 606[68], the suitability of the choice is judged by the degree to which the following requirements are satisfied:

- the sample must be representative of the material,
- the material must not change as a consequence of prolonged or repeated exposure to elevated temperatures during the measurements,
- the material should be isotropic and opaque,
- the samples used must be reproducibly and easily manufactured,
- the thermal conductivity must be well correlated with other more easily measured physical properties.

Up to now there is no standard reference material for thermophysical properties at very high temperatures. In the 70's, POCO AXM-5Q(1) graphite[xx], a homogeneous, isotropic material, stable at high temperatures, and very low reflecting, was considered as a candidate. Round Robin measurements[69,66,67,68] and several co-operative projects[70] were conducted to measure its thermophysical properties. Unfortunately, from this work and from following investigations[71,72], no general conclusions on the behaviour of this material at very high temperatures could be drawn. Good agreement in the measured properties was obtained up to ~2400 K, but at higher temperatures too large differences were observed. Difficulties in the data interpretation at very high temperatures were attributed to the error sources in the measurements and the high equilibrium vapour pressure, the latter possibly reducing the thickness and altering the emissivity of the samples. Therefore, whilst POCO

[xx] Product of POCO Graphite, Inc., Garland, Texas. Grade designation labels: *AXM* = medium grain fuel cell grade; *5Q = 2500 °C* graphitization temperature; *1* = purified.

AXM-5Q graphite is well suited as a standard reference material up to ~2400 K further investigations are required to study the limits of its applicability at higher temperatures.

POCO AXM-5Q graphite was investigated with the newly developed apparatus. The thermal diffusivity, the specific heat, and thermal conductivity were measured up to 2400 K, the results found to be in excellent agreement with the reported values in literature. Based on this important validation, measurements up to 3200 K were carried out with the aim of reducing the uncertainty of the literature data.

5A.1 Measurement conditions and data analysis

5A.1.1 *The material*

The specimens having density of 1.715 ± 0.02 gcm^{-3}, were cut from a rod of 5mm diameter, as disks of thickness between 0.8 and 1.5 mm. The thickness values, measured at the centre of the sample with an uncertainty of 2μm, are listed in Table 5A.1.

Table 5A.1

POCO AXM-5Q graphite samples

Specimen	Thickness (mm)
POCOM01	1.421
POCOM02	0.928
POCOM03	1.222
POCOM04	1.161
POCOM05	1.469
POCOM06	1.150
POCOM07	0.780
POCOM08	0.801
POCOM09	0.799
POCOM10	0.802

5A.1.2 *Experimental conditions*

The experimental parameters, *e.g.* sample thickness, deposited power, gaseous atmosphere, were optimised, based on some preliminary measurements at very high temperatures. A first set of experiments was carried out in vacuum. This condition was thought to be the best solution to limit the heat losses during the measurement. After the analysis, however, a systematic error occurred both in the thermal diffusivity and in the specific heat at $T > 2400$ K. The thermal diffusivity values indicated an over-estimation of about 4% and the specific heat values were systematically under-estimated of approximately 2% (this error being within the uncertainty of the measurement was difficult to estimate). The analysis by optical microscope of the samples after the test revealed that sublimation of material had occurred during the experiment, and the thickness, measured after several shots using a micrometer, had decreased between 1 to 2% with respect to the starting value. A second set of experiments was carried out in inert atmosphere at low pressure, to suppress graphite sublimation. In this case, the thermal diffusivity did not show any remarkable deviation, however a systematic error in the specific heat values at lower temperature was observed. The specific heat was now over-estimated of about 5% with respect to the recommended value. The error was attributed to the data analysis: in fact, the conductive heat losses during the test (comparable at $T < 2000$ K with the radiative losses) had been underestimated. The two sets of preliminary tests revealed that at very high temperature graphite tends to sublimate, and therefore the gas pressure, as well as the total experimental time may affect the results. After careful considerations of these phenomena it was decided to work in vacuum at temperatures between 1800 and 2000 K (to limit conductive heat losses), and in argon at pressures from 0.1 to 1 bar at higher temperature (to limit the sublimation of the sample). To be sure of the effective thickness of the sample, only one pulse was applied on each sample at each temperature, with the exception of temperatures between 1800-2000 K where in a few cases two shots were applied. Furthermore, to limit sublimation of material, the heating time of the specimen at the conditioning temperature and the cooling time to room temperature were reduced as much as possible (to the order of a few minutes).

Probe pulses of 1 ms were applied with a laser beam energy of 0.3-0.6 J, producing an instantaneous front temperature increase of approximately 100 K, while the corresponding maximum rear-temperature increase was more than one order of magnitude lower (5 K).

After the experiments each sample was analysed by optical microscopy to check the conditions of the surfaces, and the thickness was measured again to evaluate the entity of the possible sublimation. Thanks to the fast measurements, the sublimation was practically suppressed, and no changes of the thickness were found.

A second set of diffusivity measurements was carried out in the temperature range 600-1900 K by the laser-flash method with the device described in Ref.[73]. These measurements are used in § 5A.2 for analytical purposes. In the chapter this device will be referred as LAF.

5A.1.3 *Data analysis*

The transient temperature measurements of the rear-surface of the graphite disks were satisfactory both with respect to the quality of the signals and to reproducibility. A typical measured transient temperature curve of the back and front surfaces of a POCO AXM-5Q specimen is shown in Fig. 5A.1.

According to the set-up chosen (*i.e.* the laser spot size equal to the sample diameter), the analysis was carried out by using Model 2. The analysis was carried out firstly by a simultaneous fitting of both front and rear temperature, and then by using only the rear temperature data. A three-parameter fitting was performed, in which the conditions expressed by Eqs.(4B.23) and (4B.24) were used. A representative fitted curve is shown in Fig. 4B.3, Section 4B.2. The quality of fitting of the experimental thermogram can be estimated from the resulting errors of the parameters involved, summarised in Table 5A.2.

From the values reported in Table 5A.2 it can be seen that the experiments are more accurate and reproducible at low temperatures than at high temperatures. It must be noted, however, that the errors in the calculated parameters corresponding to the thermal diffusivity and to the specific heat are in any case within 1%.

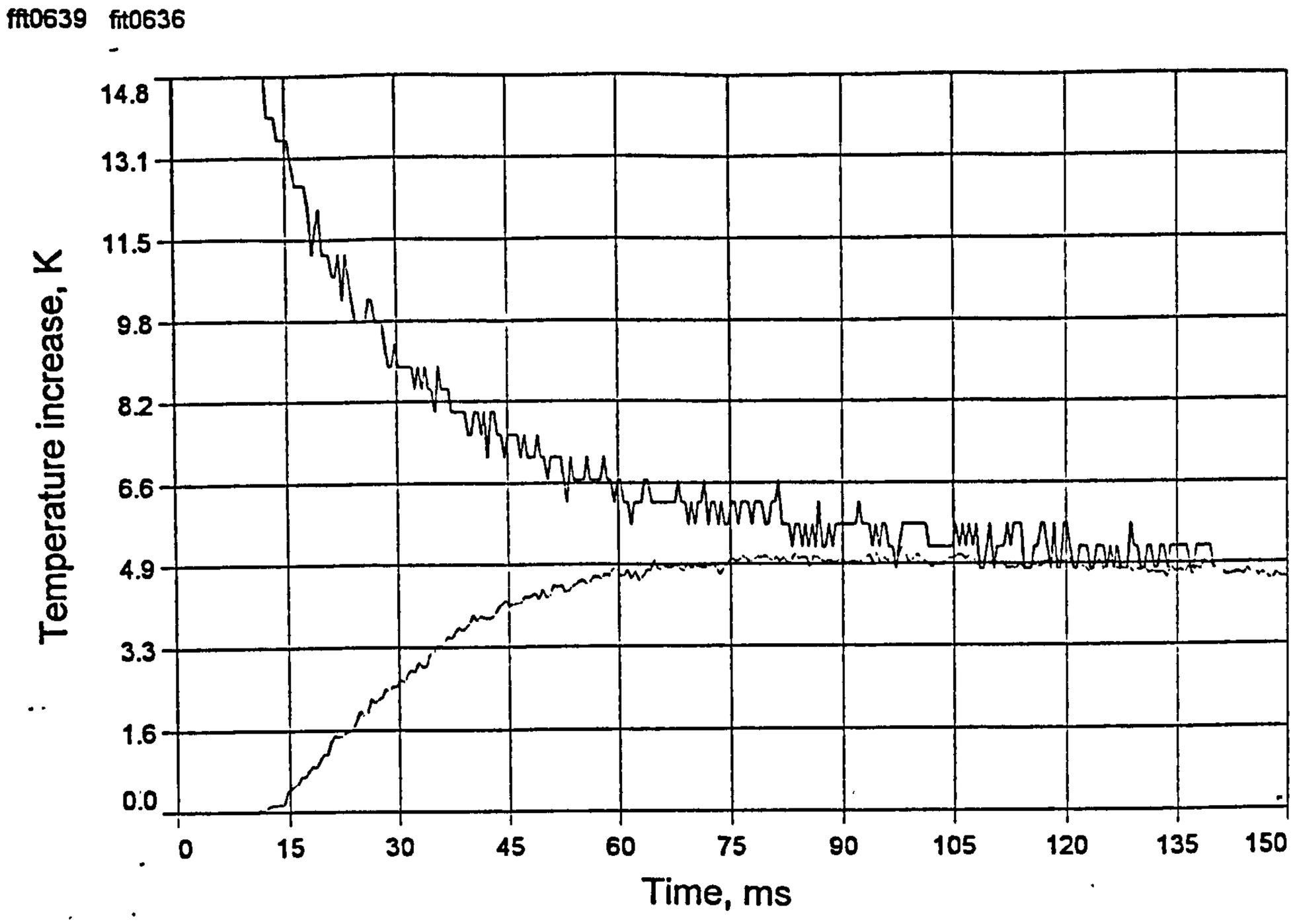

Fig. 5A.1 Experimental thermogram of the rear and front surfaces of a POCO AXM-5Q graphite specimen at 2292 K. The sample, a disk of 5 mm in diameter 1.421 mm thickness (sample POCOM01) was shot with a pulse time of 1 ms delivering an energy density of 3.734 Jcm^{-2}.

Table 5A.2
Error analysis in the fitting procedure. The parameters error is calculated from Eq.(4B.21)

Parameter	**Average Error %**	
	1800 K	3200 K
Thermal diffusivity: $\overline{a}$ (s^{-1})	0.2	0.3
Specific heat : T_0 (K)	0.5	1
Biot numbers : Y_1, Y_2, Y_r	5	15
Fitting MSQ deviation	1.5	5

To compute the energy absorbed by the sample the spectral normal emissivity values listed in Table 5A.3[74] were assumed. The error in the emissivity values was estimated to be of the order of 3%.

Table 5A.3

Normal spectral emissivity of graphite at λ=1060 nm

Temperature	Absorption
1800	0.88
1900	0.88
2000	0.87
2100	0.87
2200	0.87
2300	0.86
2400	0.86
2500	0.85
2600	0.85
2700	0.85
2800	0.84
2900	0.84
3000	0.84
3100	0.83
3200	0.83

The calculated thermal diffusivity, specific heat and thermal conductivity values were corrected for thermal expansion with the use of the equation proposed by Taylor and Groot[71]:

$$\alpha = 1.8613\cdot10^{-2} + 6.78970\cdot10^{-4}\,T + 1.63081\cdot10^{-8}\,T^2 + \\ + 1.10737\cdot10^{-10}\,T^3 - 5.03268\cdot10^{-14}\,T^4 + 8.04718\cdot10^{-18}\,T^5 \qquad (5A.1)$$

where $\alpha = \frac{\Delta L}{L_0}$ is the linear thermal expansion, with L a linear dimension of the sample and L_0 is its initial value at room temperature, and T is in ℃. In the frame of the AGARD Round Robin's program[67] several experiments have been performed to measure the thermal expansion of POCO AXM-5Q graphite. Eq.(5A.1), calculated with an error of 1%, was chosen since it well represents the recommended values proposed by AGARD. A comparison of the thermal expansion data reported by Taylor and Groot and by different Participants at the AGARD project is given in Fig.5A.2.

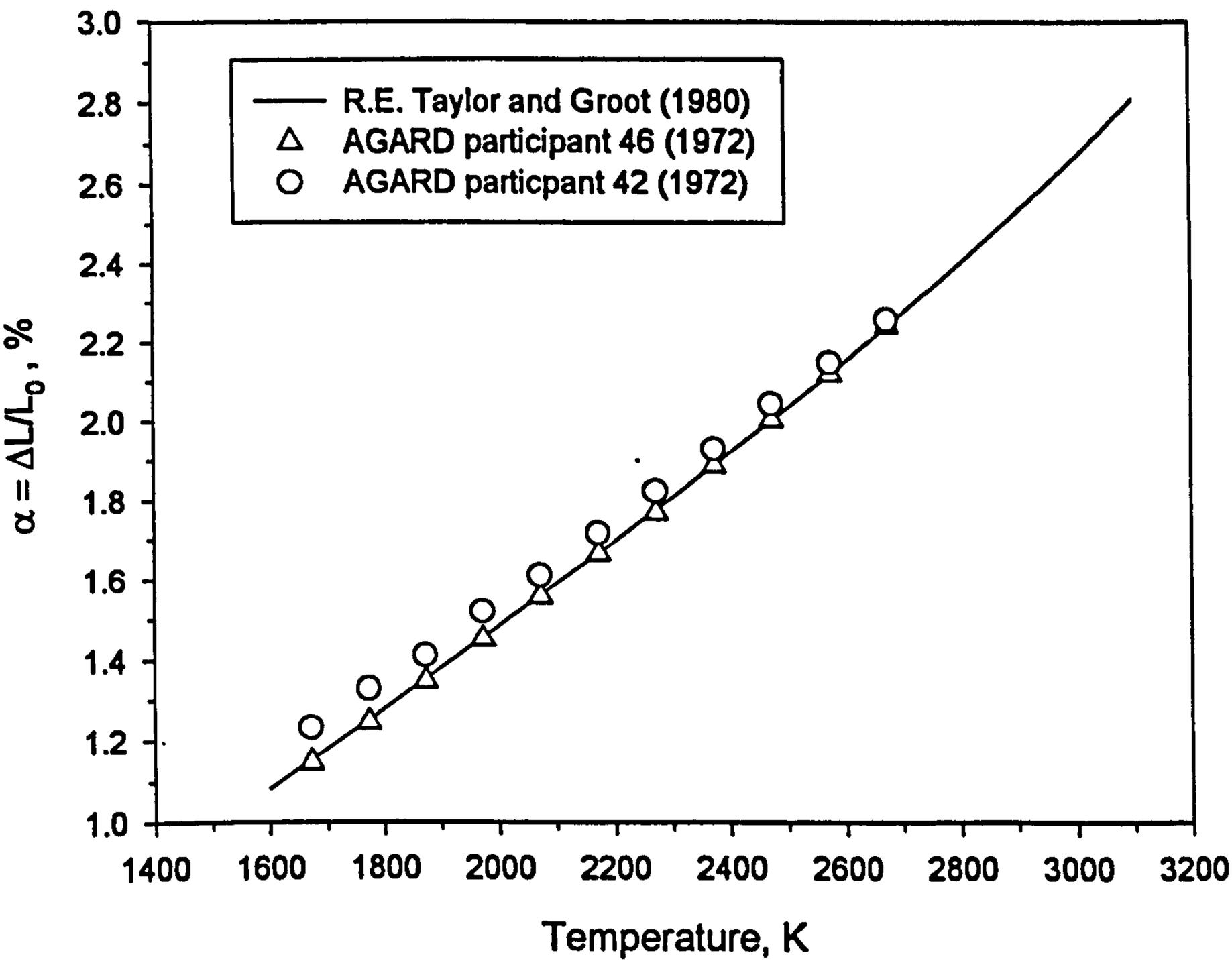

Fig. 5A.2 Comparison of thermal expansion data for POCO AXM-5Q graphite.

The agreement between the results obtain by Taylor and Groot and the recommended AGARD values (Participant No. 46) is within 0.4% at T = 2000 K and 0.03% at 2700 K.

The deviation of the values obtained by the Participant No. 42 is less than 4% at T = 2000 K and 0.7% at 2700 K.

The curve obtained by Taylor and Groot, corresponding to measurements for 293 K < T < 2523 K, was extrapolated to calculate the thermal expansion up to 3200 K.

The thermal conductivity values measured will be compared in § 5A.3.3 with literature values. Since some of the data reported are calculated from diffusivity measurements using equation $\lambda = a\rho c_p$, the temperature dependencies of ρ used by the authors in literature are compared with the values used in this work (proposed by Taylor and Groot and calculated according to Eq.(5A.1)) in Fig. 5A.3.

The values used by R. Taylor[72] differ from those used by Taylor and Groot less than 0.2%.

To compute the density as a function of temperature the AGARD Participant used the equation $\rho = \rho_0[1 - 3\alpha_m(T - T_0)]$, where α_m is the mean linear thermal expansion coefficient between a given temperature T and room temperature T_0. The difference between the Taylor and Groot values is less than 0.5% at low temperature and 0.2% at high temperature, respectively.

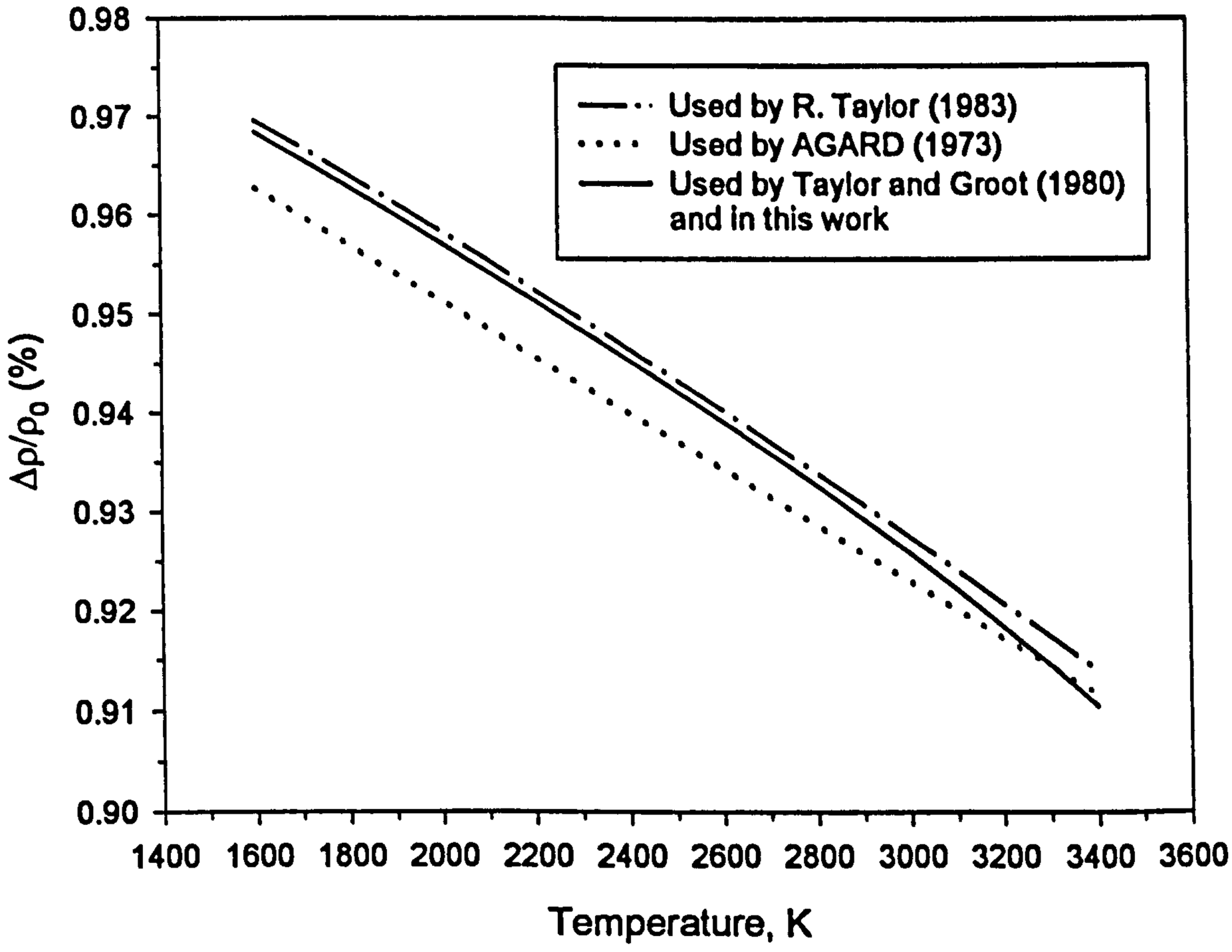

Fig. 5A.3 Comparison of equations for the density temperature dependence of POCO AXM-5Q graphite.

The errors in the measured values of thermal diffusivity, specific heat and thermal conductivity, calculated according to Eqs.(4C.4), (4C.5) and (4C.6) are, respectively: $\frac{\delta a}{a} = 2.08\%$, $\frac{\delta c_p}{c_p} = 4.9\%$, $\frac{\delta \lambda}{\lambda} = 4.8\%$.

5A.2 Results

5A.2.1 *Specific heat*

The results of the specific heat measurements as a function of temperature are shown in Fig. 5A.4. The measured values increase with temperature from 1800 K to 2400 K, and remain essentially constant from 2400 K to 3200 K.

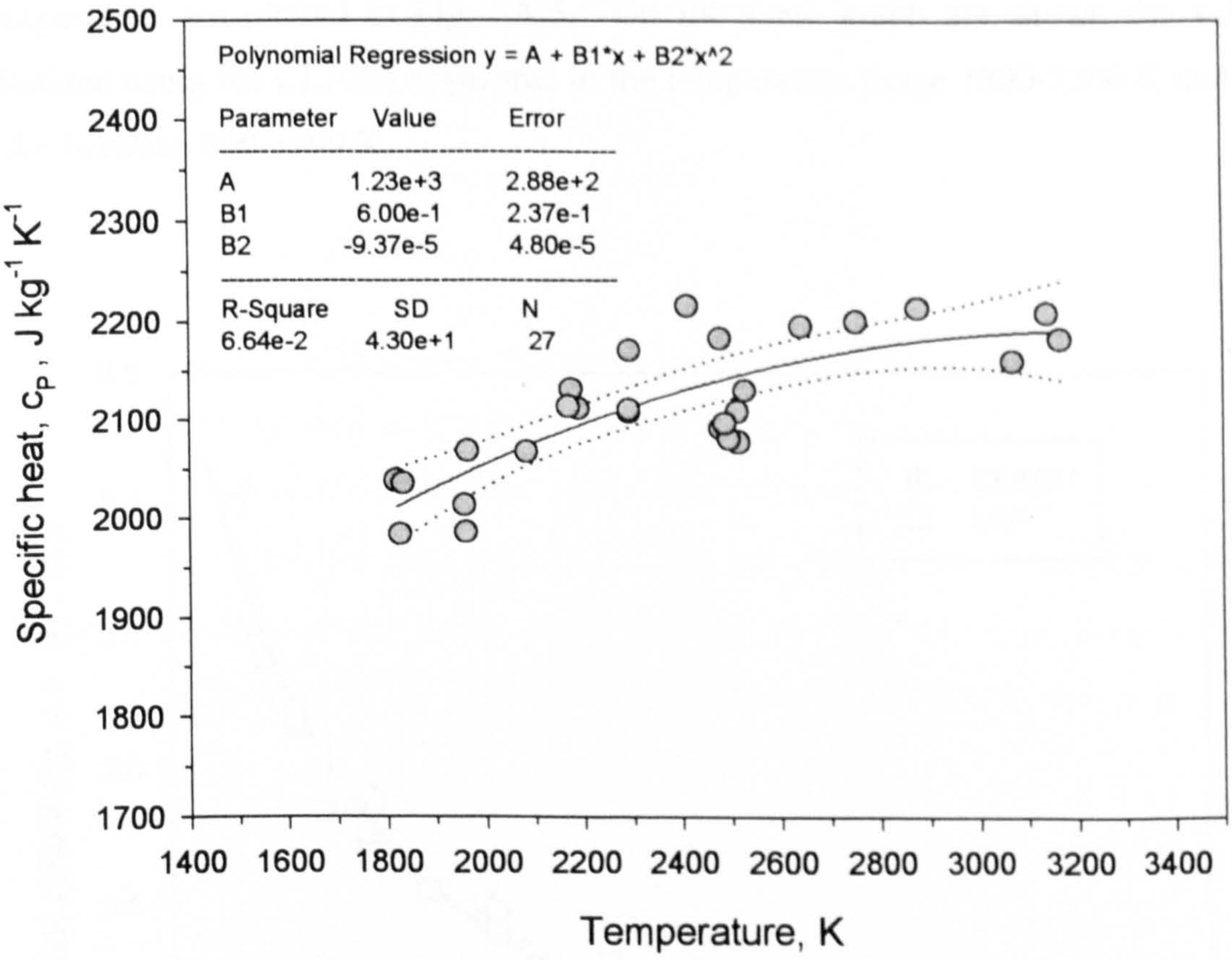

Fig. 5A.4 Specific heat of POCO AXM-5Q graphite as a function of temperature. The solid line represents the data interpolation (Eq.(5A.2), the dotted lines define the 95% confidence interval.

The values of the specific heat, c_P from 1800 to 3200 K were fitted to the function:

$$c_P = 1230 + 0.600T - 9.37 \cdot 10^{-5} T^2 \quad (\mathrm{Jkg^{-1}K^{-1}}) \tag{5A.2}$$

The experimental data and their fitting are shown in Fig. 5A.4, where the solid line represents Eq.(5A.2) and the dotted lines indicate the 95% confidence interval. The deviations of specific heat values from the fitted function expressed by Eq.(5A.2) are of the order of 1%, never exceeding 3%.

5A.2.2 *Thermal diffusivity*

The results of the thermal diffusivity measurements as a function of temperature are plotted in Fig. 5A.5. On the same graph are shown the values obtained using the CLASH apparatus in the temperature range 1800-3200 K and the LAF between 600-1900 K.

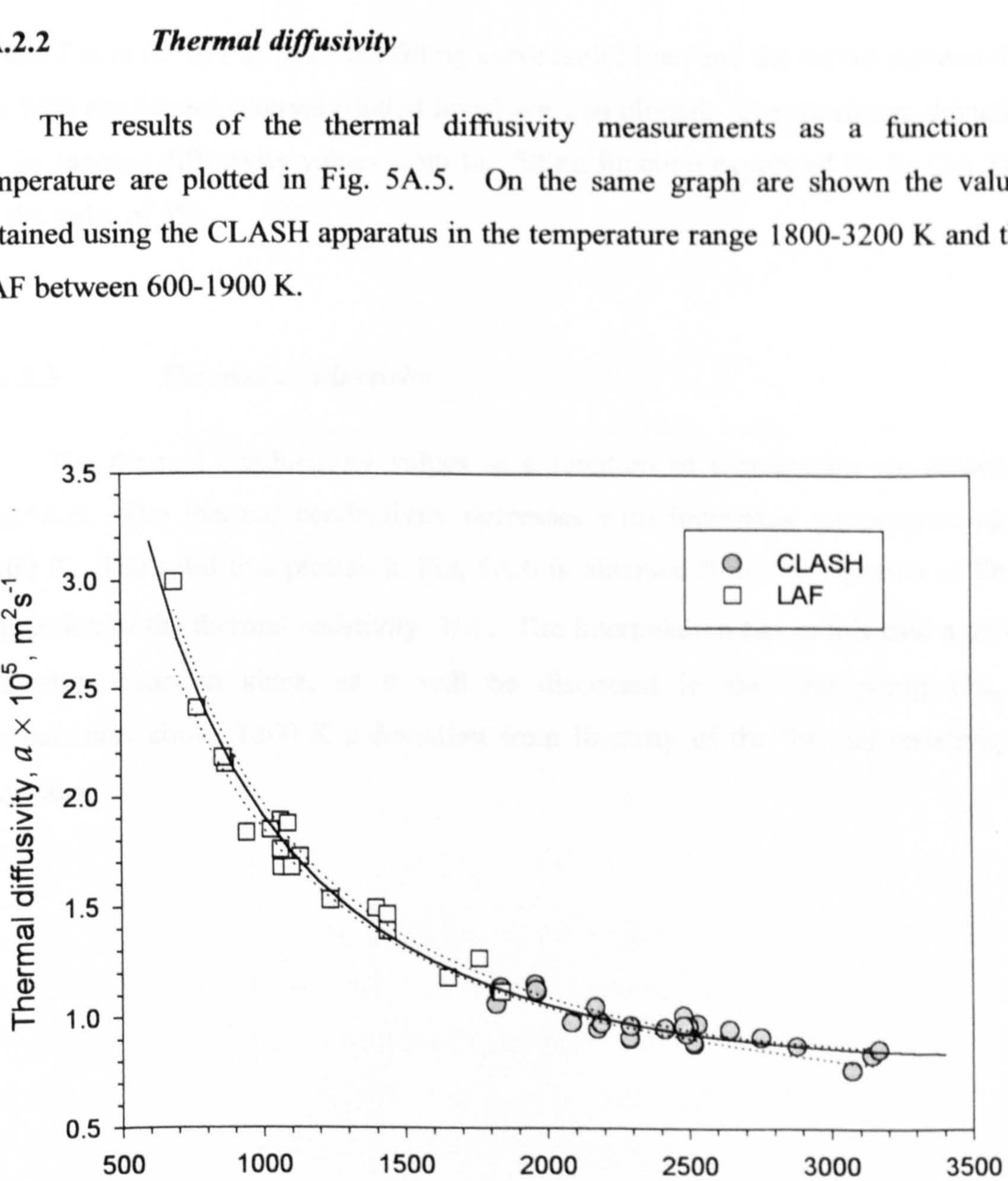

Fig. 5A.5 Thermal diffusivity of POCO AXM-5Q graphite as a function of temperature. The low temperature data-set was obtained with the LAF apparatus, while CLASH was used for T >1800 K. The solid line represents the data interpolation (Eq.(5A.3)), the dotted lines define the 95% confidence interval.

Since the diffusivity values measured at low temperature by LAF smoothly join the values obtained at higher temperature by CLASH, all the data were merged and fitted, in the temperature range 600-3200 K, by a single equation:

$$a = -1.946 \cdot 10^{-6} + 1.338 \cdot 10^{-9} T + 0.0198 / T \ (\mathrm{m^2 s^{-1}}) \qquad (5A.3)$$

where T is in K. In Fig. 5A.5 the fitting curve (solid line) and the curves representing the 95% confidence interval (dotted lines) are also plotted. The maximum deviation of the thermal diffusivity values from the fitting function expressed by Eq.(5A.3) is of the order of 5%.

5A.2.3 *Thermal conductivity*

The thermal conductivity values as a function of temperature are shown in Fig.5A.6. The thermal conductivity decreases with increasing temperature up to 3200 K. The solid line plotted in Fig. 5A.6 is obtained from the equation of linear regression of the thermal resistivity, $1/\lambda$. The interpolation has in this case a purely indicative function since, as it will be discussed in the next paragraphs, at temperatures above 1800 K a deviation from linearity of the thermal resistivity is expected.

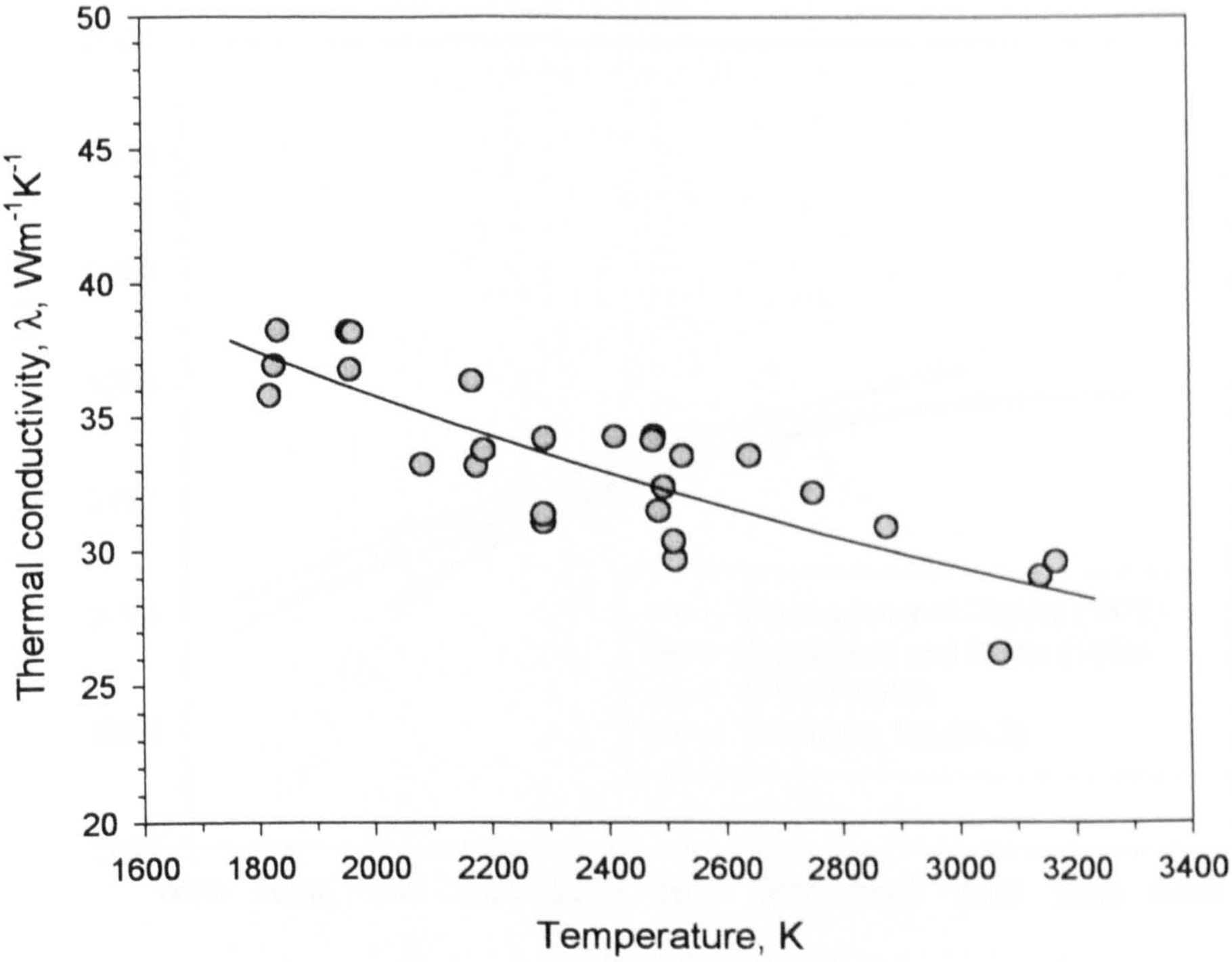

Fig.5A.6 Thermal conductivity of POCO AXM-5Q graphite as a function of temperature.

5A.3 Discussion

5A.3.1 *Specific heat*

The specific heat results of the present work are compared with literature data in Fig. 5A.7. These measurements agree up to 3000 K best with the data reported by Cezairliyan and Righini[75] and Cazairliyan and Miiller[76], obtained by a subsecond pulse-heating technique. They are also in good agreement with the values recommended by IVTAN[77], except for the increase in the specific heat at temperature above 3000 K, which is not confirmed by these results.

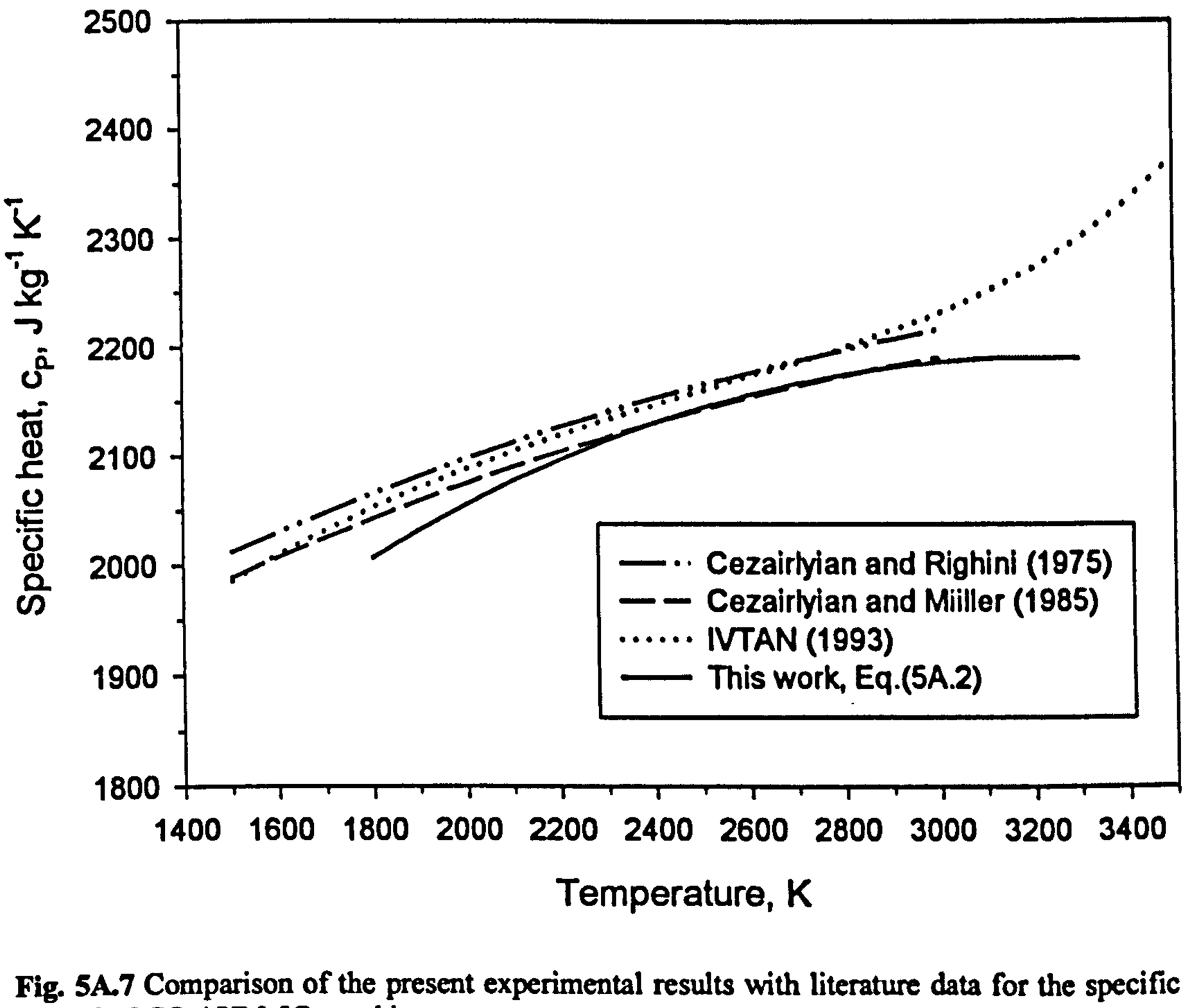

Fig. 5A.7 Comparison of the present experimental results with literature data for the specific heat of POCO AXM-5Q graphite.

The results for specific heat of POCO AXM-5Q graphite are compared in Fig.5A.8 with values obtained at low temperature by AGARD[68], Lucks *et al.*[78] and West *et al.*[79] by ice calorimeter. Since the values reported by these authors smoothly join the values obtained in this work at high temperature, all the points can be merged and fitted by the following polynomial of the 5th order:

$$c_P = 3.0605T - 1.63376\cdot10^{-3}T^2 + 2.79280\cdot10^{-7}T^3 + 4.08065\cdot10^{-11}T^4 - 1.28780\cdot10^{-14}T^5 \quad (\mathrm{Jkg^{-1}K^{-1}}) \qquad (5A.4)$$

where T is in K. In the same figure a comparison with the specific heat values recommended by Taylor and Groot[71] is given. Their curve refers to the interpolation of the heat capacity values measured by the authors from 330 to 1000 K and by

Cezairliyan and Righini[75] from 1500 to 3000 K. The difference between the curve proposed by Taylor and Groot with the present suggestion, Eq.5A.4, is ≤ 4%.

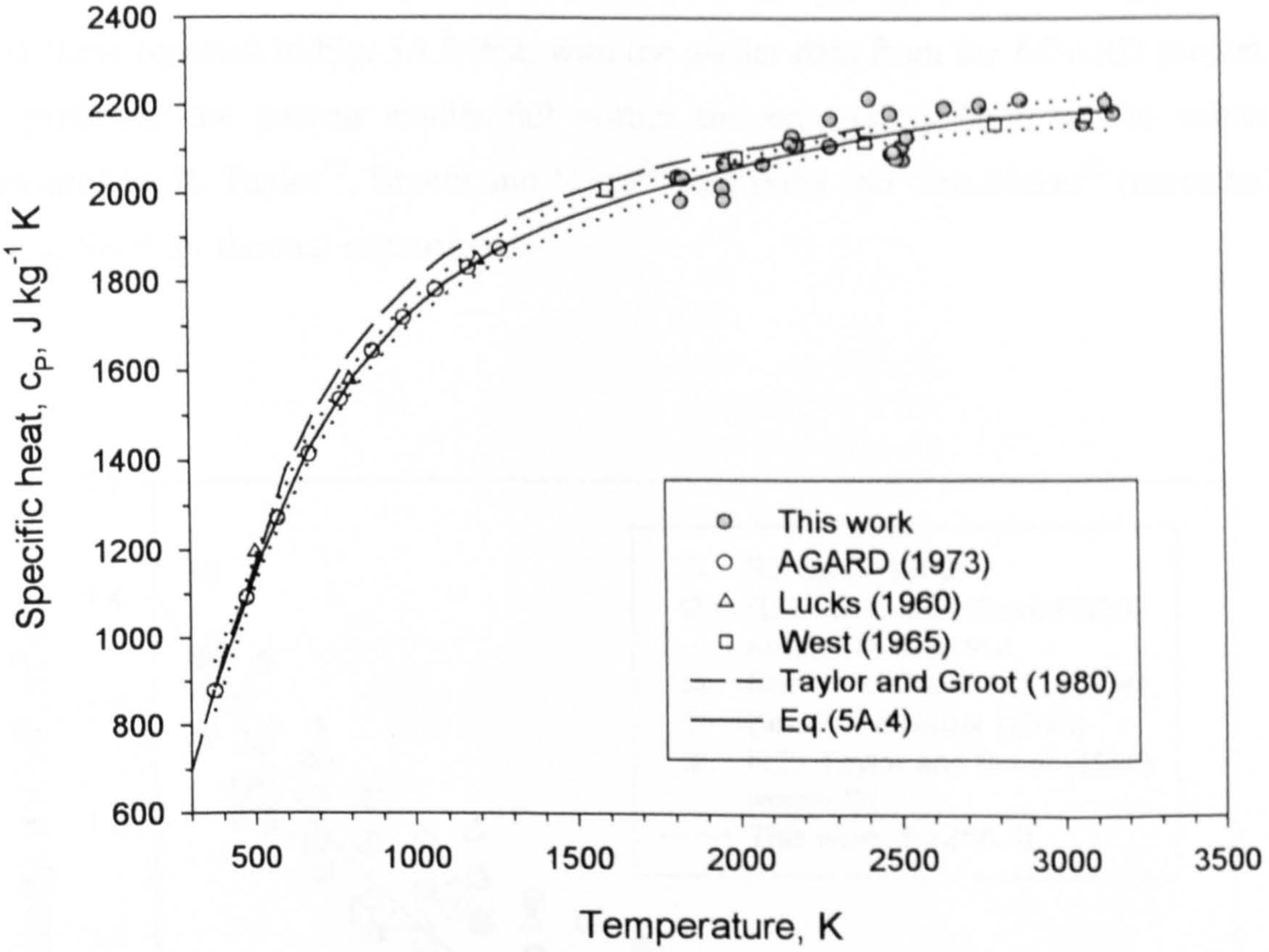

Fig. 5A.8 Comparison of the experimental results with literature data for the specific heat of POCO AXM-5Q graphite. The solid line represent the interpolation of all the data by Eq.(5A.4). The dotted lines define the 95% confidence intervals.

This equation is used in § 5A.3.3 to compute the specific heat of POCO AXM-5Q graphite in the temperature range 600-1900 K, for the calculation of the thermal conductivity from the diffusivity values measured by LAF.

5A.3.2 *Thermal diffusivity*

A comparison of the present results with literature data on POCO AXM-5Q graphite is presented in Figs. 5A.9 and 5A.10. The most recent data, reported in

Fig.5A.9, were measured by laser-flash[71,72,80,] and xenon-lamp modulated-beam methods[81]. The data shown in Fig. 5A.10, referring to the AGARD Round Robin program[68], were measured by modulated electron beam (Participants No. 1, 15), modulated light beam (Participant No. 13), and laser-flash (Participants No. 20, 30).

The thermal diffusivity values of this work are generally in better agreement with those reported in Fig. 5A.9 than with the earlier data from the AGARD project. In particular the present results fall within the uncertainty band of the values measured by R. Taylor[72], Brandt and Neuer[81] and Baba and Cezairlyian[80] (corrected in Fig. 5A.9 for thermal expansion).

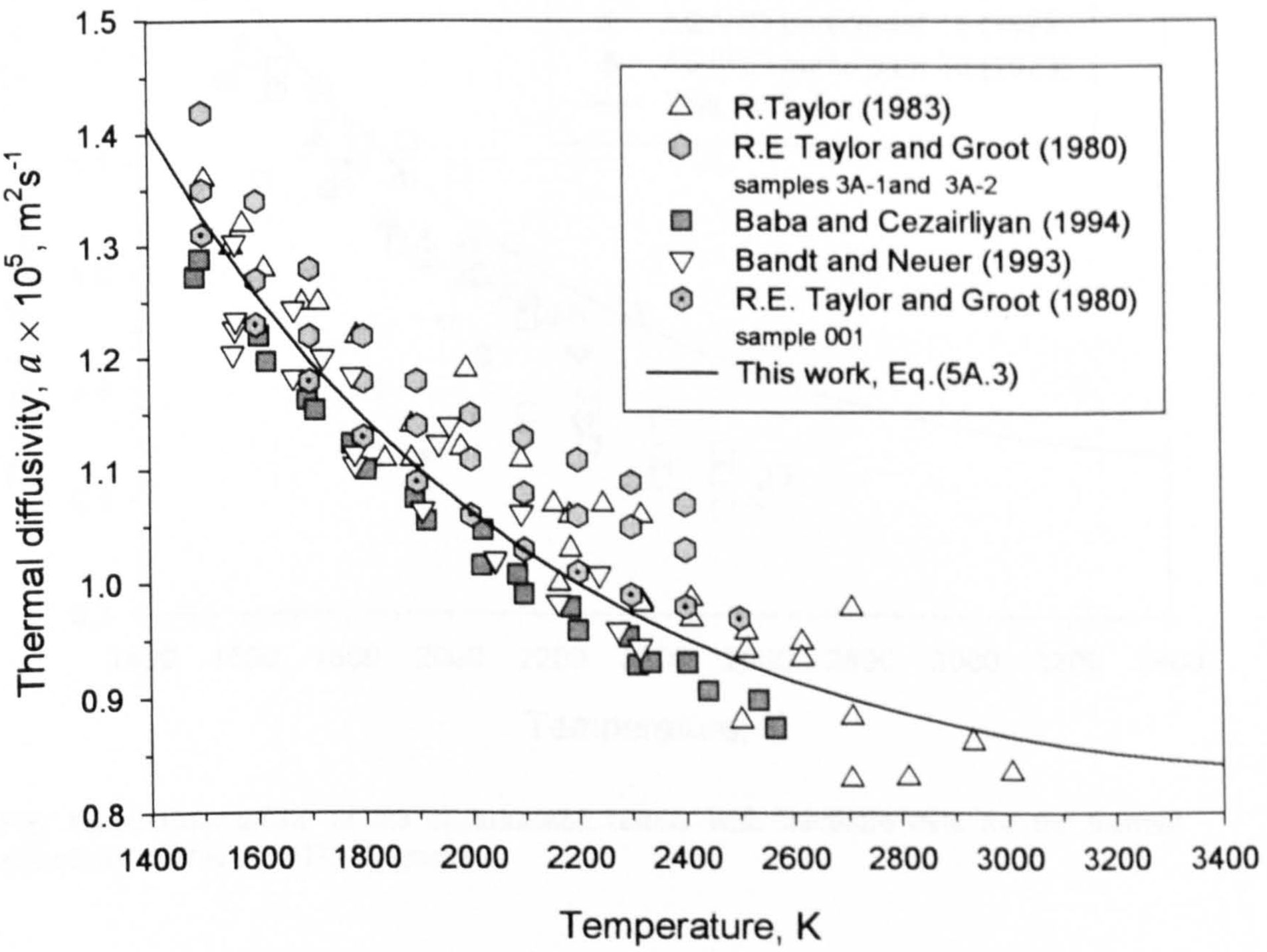

Fig. 5A.9 Comparison of the experimental results with literature data for the thermal diffusivity of POCO AXM-5Q graphite.

The data reported by R.E. Taylor and Groot[71] refer to three different samples: the thermal diffusivity of the sample # 001 was directly measured while the *thermal*

diffusivity values of the samples 3A-1 and 3A-2 were *calculated* from the measured thermal conductivity. It can be seen that the values reported for the sample 001 (directly measured) are in excellent agreement with the present results while the values calculated from the thermal conductivity lie systematically higher. The difference between these last values and the present results is of the order of 7% at 1800 K and 10% at 3000 K.

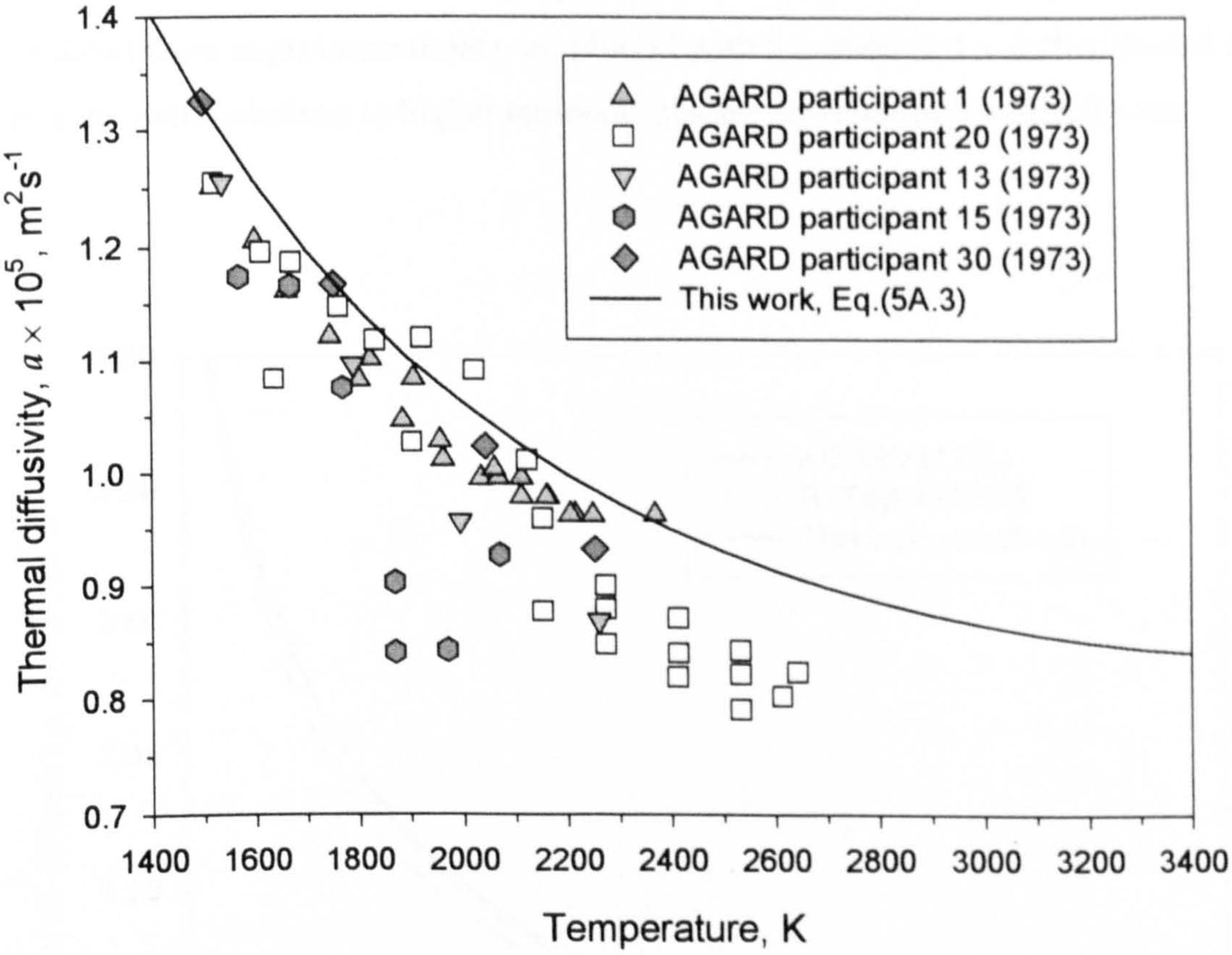

Fig. 5A.10 Comparison of the experimental results with literature data for the thermal diffusivity of POCO AMX-5Q graphite.

The results of this work are compared with the Round Robin results in Fig. 5A.10. The present results are in good agreement with those of the AGARD Participants for $T < 1900$. For higher temperatures the results remain in good agreement with the results of the AGARD Participants No. 1 and 30, while are approximately 10% higher than the values reported by the AGARD Participants No. 13, 15, and 20. A

critical analysis of these results, however show that a systematic error affects the measurement at very high temperature and the data, especially that of the Participant No. 15, were considered not reliable.

It must be noted that none of the literature data sets cover the whole temperature range studied in this work, and only the results reported by R. Taylor extended up to 3000 K.

Fig. 5A.11 shows a comparison of the interpolated thermal diffusivity curve (Eq.(5A.3)) with reference curves given in literature. In the figure the curves calculated from experimental data are plotted with a dashed and a dashed/dotted line, while the extrapolations to higher temperatures are represented by dotted lines.

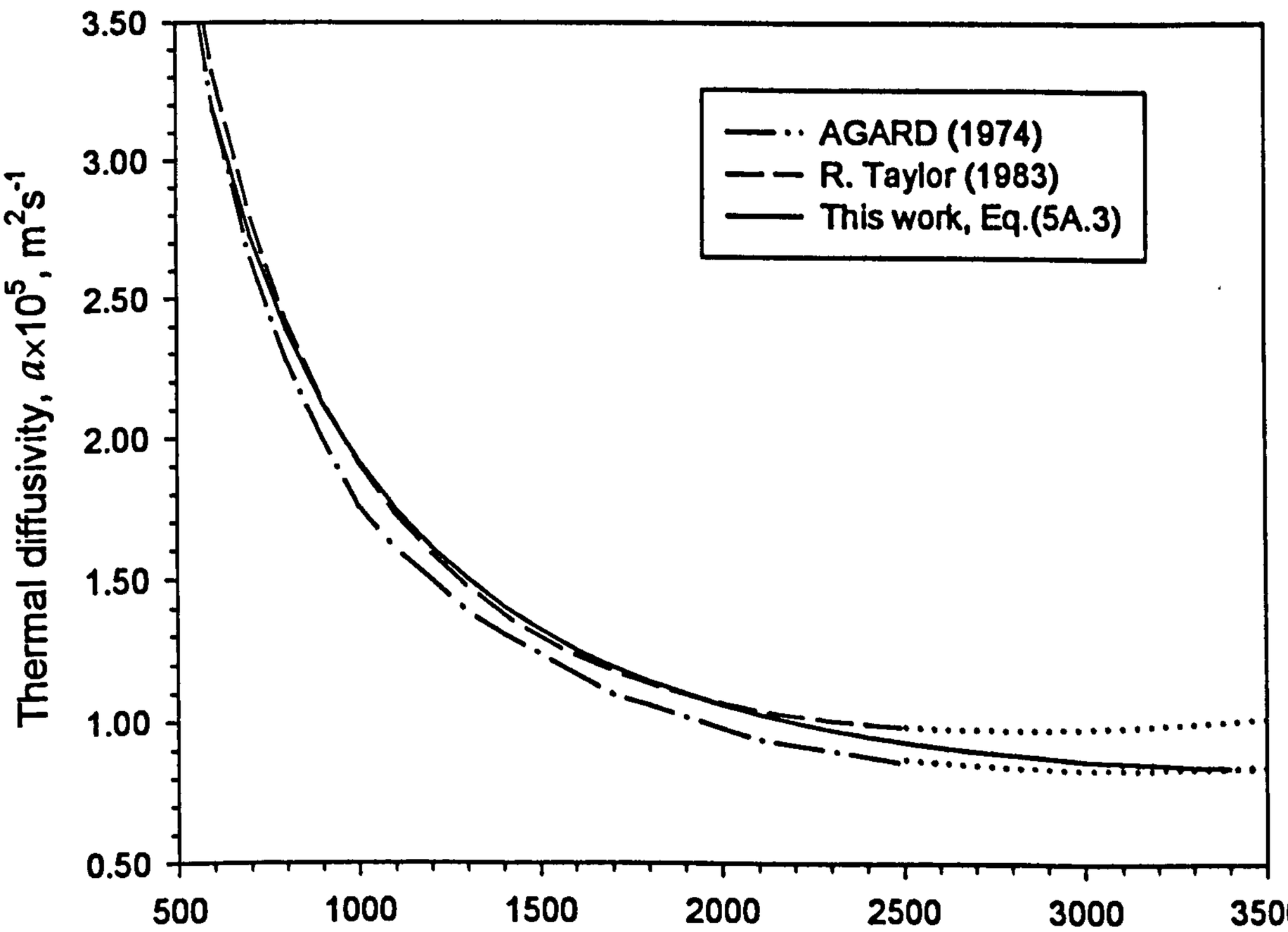

Fig. 5A.11 Comparison of the experimental results and the recommended curves for the thermal diffusivity of POCO AXM-5Q graphite.

The present results lie systematically above (of about 9%) the AGARD recommended curve[82] in the temperature range investigated by the Round Robin Project, *i.e.* up 2500 K. Nevertheless AGARD's curve, if extrapolated at higher temperature, fits the results of this work with a difference of less than 2%. Taylor's recommended curve fits these values with a difference of 2% up to 2200 K, but it predicts too high diffusivity values above 2500 K. It must be remarked, however, that, as pointed out by Taylor, the recommended curve also slightly over-estimates his experimental results.

5A.3.3 *Thermal conductivity*

A comparison of the thermal conductivity results with other literature data on POCO AXM-5Q graphite is presented in Fig. 5A.12. The data reported by R.E Taylor and Groot[71] were measured by direct electrical heating, while the others were calculated from diffusivity values. To convert thermal diffusivity into thermal conductivity, R. Taylor[72] used the density values as a function of temperature reported in Fig. 5A.3, and the c_p values suggested by Cezairliyan and Righini[75]. The Participants in the AGARD's Round Robin Project[69] used the density variation with temperature as reported in Fig. 5A.3 and the c_p values measured by West *et al.*[79].

The present results lie below those of Taylor[72] up to 2400 K while are in excellent agreement for temperature above 2500 K.

The results of Taylor and Groot[71], as already mentioned, refer to three different samples, whereby each data set was separately smoothed. Therefore, the dispersion of these points represents the effective accuracy of the data. The present results are in good agreement with the data reported for the sample 001 and fall in general, in the uncertainty band of the measurements.

The data reported by the Participants at the AGARD' s Round Robin Project[69] are in good agreement with the present results up 1900 K but lie approximately 10% lower for higher temperatures, reproducing the results obtained for thermal diffusivity.

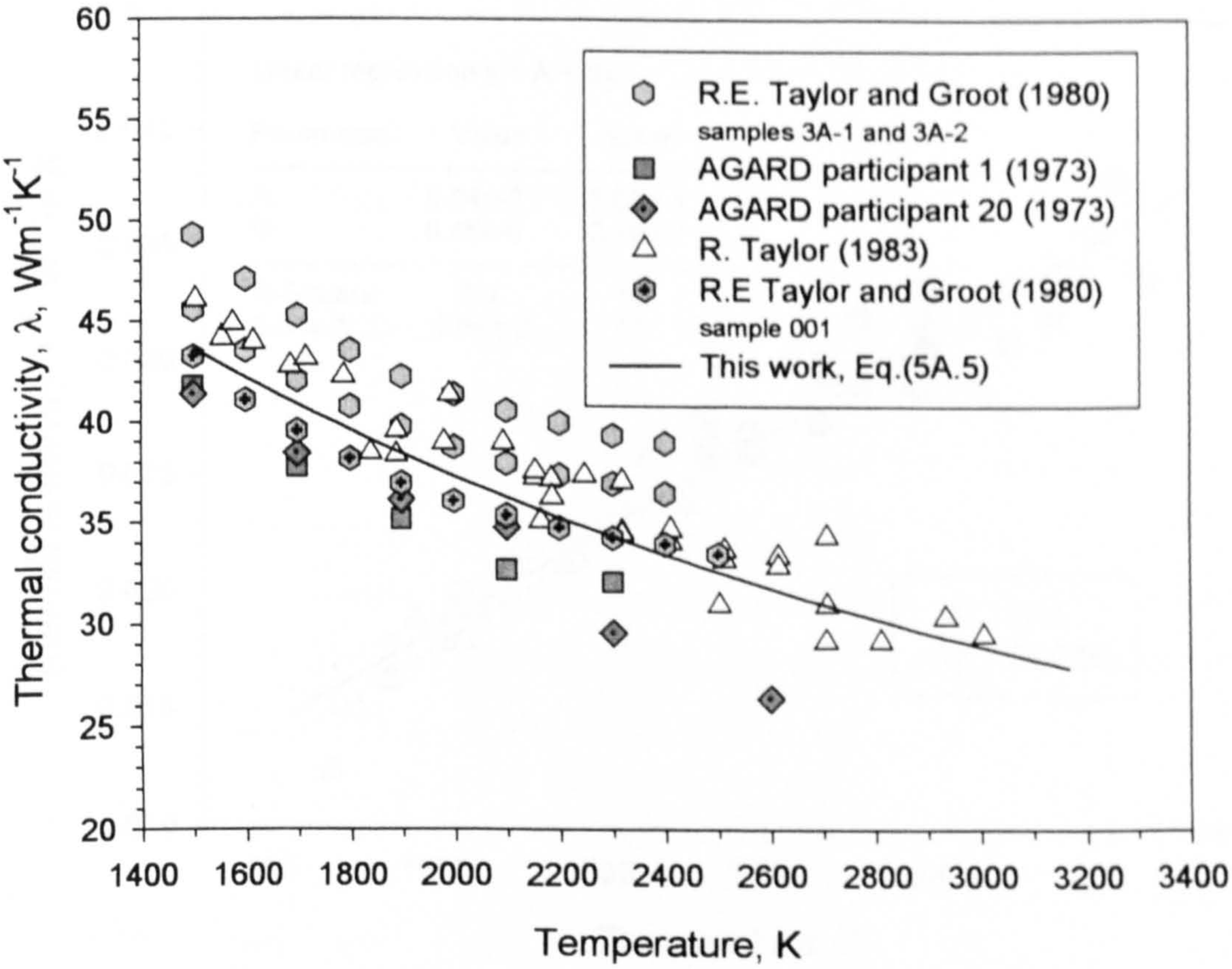

Fig. 5A.12 Comparison of the experimental results with literature data for the thermal conductivity of POCO AXM-5Q graphite.

The thermal resistivity, $1/\lambda$, obtained for POCO AXM-5Q graphite as a function of temperature, is plotted in Fig. 5A.13. The specific heat values calculated with Eq.(5A.4) were used to calculate the thermal conductivity at low temperature (T<1800 K). All the thermal conductivity data were merged and fitted with the equation:

$$1/\lambda = 9.94 \cdot 10^{-3} + 8.46 \cdot 10^{-6} T \quad (\mathrm{W^{-1}mK}) \tag{5A.5}$$

The resulting thermal resistivity is compared in Fig. 5A.14 with the thermal resistivity derived by Minges[83], fitting different data sets obtained using a variety of measurement techniques, together with the results obtained by Taylor[72].

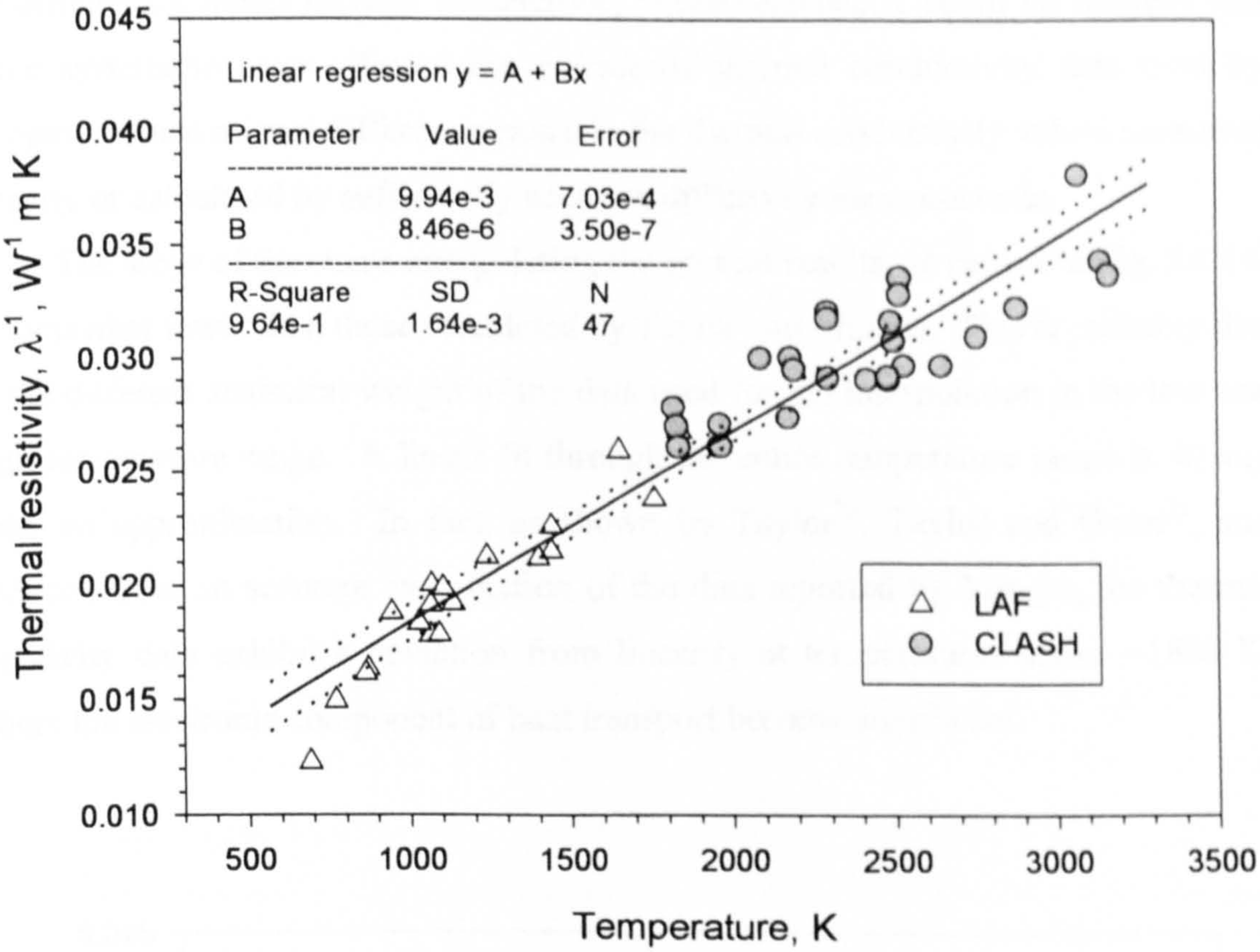

Fig. 5A.13 Thermal resistivity of POCO AXM-5Q graphite as a function of temperature. The solid line represents the linear regression, the dotted lines define the 95% confidence interval.

Minges[83] gives two linear thermal resistivity equations:

$$1/\lambda = 8.058 \cdot 10^{-3} + 9.136 \cdot 10^{-6} T \quad (\mathrm{W^{-1}mK}) \tag{5A.6}$$

$$1/\lambda = 7.546 \cdot 10^{-3} + 10.730 \cdot 10^{-6} T \quad (\mathrm{W^{-1}mK}) \tag{5A.7}$$

Eq(5A.6) describes the interpolation of directly measured thermal conductivity while Eq(5A.7) describes the conductivity derived from measured diffusivity. An attempt to justify the difference between the two equations obtained by Minges, was made by Taylor[72], but no definitive explanation was found. Thus the question whether the difference in the results obtained is real or is due to some fundamental discrepancy between diffusivity and conductivity measurements is still open. Since both the present results and those of Taylor are in good agreement with the equation derived

by Minges for *direct* thermal conductivity measurements, it could be inferred that some systematic error affected the *calculated* thermal conductivity data used by Minges. Hence no real difference exists in the thermal conductivity values measured directly or calculated by sufficiently accurate diffusivity measurements.

The slope of the curve interpolating the present results, as shown in Fig. 5A.14, is somewhat lower than those calculated by Taylor and Minges. This is probably due to the different statistical weight of the data used for the interpolation in the low and high temperature range. A linear fit through the entire temperature range is, in any case, an approximation. In fact, as shown by Taylor[72], Taylor and Groot[71], and deduced from an accurate examination of the data reported by Minges, the thermal resistivity data exhibit a deviation from linearity at temperatures above ~1800 K, where the electronic component of heat transport become significant.

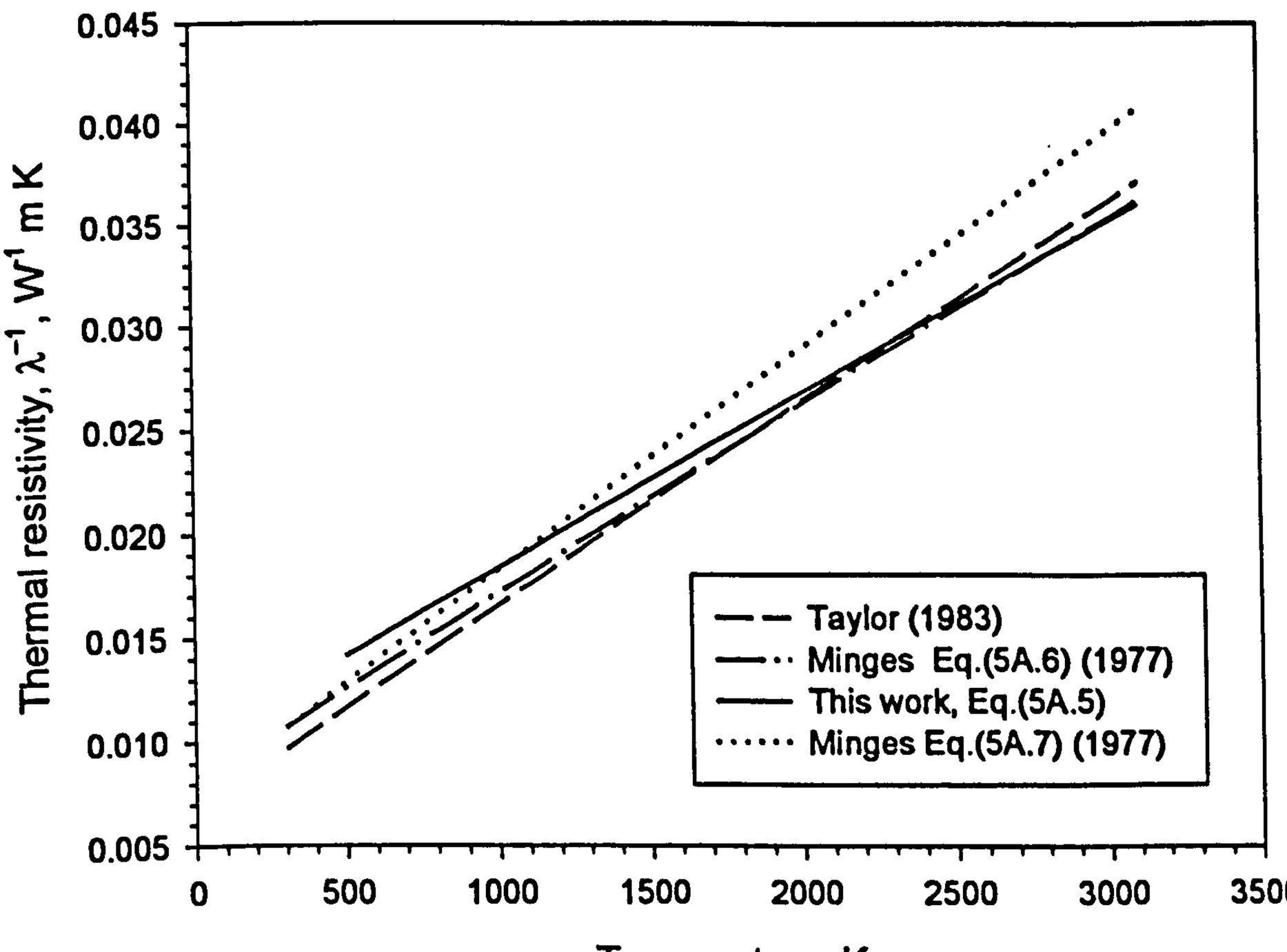

Fig. 5A.14 Comparison of the experimental results with literature data for the thermal resistivity of POCO AXM-5Q graphite.

5A.4 Conclusions

The thermal diffusivity, the specific heat and the thermal conductivity of POCO AXM-5Q graphite were measured by CLASH from 1800 to 3200 K with a precision of about 2% for thermal diffusivity and 5% for specific heat and thermal conductivity, respectively. The temperatures studied encompassed a temperature range larger than those previously reported.

The thermal diffusivity and specific heat values measured were found to be in excellent agreement -the difference being within the uncertainty of the measurements- with respect to the recommended values reported (and measured up to 3000 K).

The thermal conductivity, derived from the measured diffusivity and specific heat measured values, was found to be in good agreement in the common temperature range studied with respect both to the data reported by Taylor[72], calculated from diffusivity experiments, and to the data reported by Taylor and Groot[71], derived from electrical conductivity measurements.

From the results obtained it can be concluded that the new laser-flash device can be used for *simultaneous* and *consistent* measurements of thermal diffusivity and specific heat, and thus for conductivity measurements, with good precision and accuracy.

The specific heat values measured from 1800 to 3200 K were compared with literature data reported for lower temperatures (300-1600K); the values were found to smoothly join the values reported, and the following equation fitted the c_P data from 300 to 3200 K:

$$c_P = 3.0605T - 1.63376\cdot10^{-3}T^2 + 2.79280\cdot10^{-7}T^3 + 4.08065\cdot10^{-11}T^4 - 1.28780\cdot10^{-14}T^5 \quad (\mathrm{Jkg^{-1}K^{-1}})$$

The thermal diffusivity values measured at high temperature smoothly join the values measured from 600 to 1900 K using the laser-flash device LAF. Hence, all

the experimental values were merged and fitted in the temperature range 700-3200 K by the function:

$$a = -1.946 \cdot 10^{-6} + 1.338 \cdot 10^{-9} T + 0.0198 / T \ (\mathrm{m^2 s^{-1}})$$

The thermal resistivity, calculated over the temperature range 600-3200 K, was compared with recommended values obtained both by direct conductivity measurements and from diffusivity values. The agreement of the present results with the directly measured conductivity values shows that no systematic errors affect the present measurements. However, probably due to the low number of experimental points at low temperature, as well as to the expected deviation from the linear behaviour of the thermal resistivity at high temperature, the slope of the present linear interpolation is somewhat lower then that recommended in literature.

Since no real difference exists in the thermal conductivity values measured directly or calculated from sufficiently accurate diffusivity measurements, POCO AXM-5Q graphite is thought to be suitable as a standard reference material. However, further work is necessary to describe and understand the thermal resistivity at very high temperatures.

5B. ZIRCONIUM DIOXIDE

One of the major difficulties encountered in applications of the laser-flash technique for thermal property measurements is related to the energy deposition mechanism. In fact, the analysis of the pulse experiment is practicable only if the photon energy is deposited within a surface layer, which is very thin compared with the thickness of the sample. Consequently, transparent materials are not suitable for this kind of measurements. Unfortunately, most ceramics exhibit, to different extents, this property. Yet, many of these ceramics, which have a low optical absorption at room temperature, become much more opaque at higher temperatures. Laser heating of these materials is nevertheless problematic, since the heating rate at constant power tends to diverge as the temperature increases; moreover, the low fraction of power absorbed at room temperature requires an ignition power, which may greatly exceed the effective power-to melt-threshold. The question faced is therefore whether laser heating can still be successfully applied to obtain stable conditioning temperatures; this is even more important since during the initial heating stage, part of the laser power is absorbed in a relatively thick surface layer.

In order to test the performance limits of the CLASH apparatus, as well as the sensitivity of the pulse propagation analysis to these effects, a ZrO_2 - based ceramic, widely employed in nuclear technology, was investigated. On account of the difficulties mentioned, only a few studies on the high temperature thermal properties of this material are available: these show large discrepancies, which entail serious drawbacks to the use of this material at high temperatures.

5B.1 Measurement conditions and data analysis

5B.1.1 *The material*

The studied material, labelled 20YSZ, was zirconium dioxide stabilised with 20% wt Y_2O_3, and fabricated by plasma spraying. The employed specimens, of 5.17

$\pm$ 0.06 gcm^{-3} density, were disks of 5 mm diameter and thickness between 0.34 and 0.38 mm, cut from platelets of 10 mm diameter and 2 mm thickness. The disks were cut as thin as possible, to reduce heat losses during the laser-flash measurements, the thickness should not, however, be reduced below 0.33 mm since at this thickness the material is translucent[84]. The two faces of the disks were ground parallel, and the thickness, measured in the central area of the sample with an uncertainty of 2 μm, is listed in Table 5B.1.

Table 5B.1

Thickness of 20YSZ specimens

Specimen	Thickness (mm)
20YSZ01	0.370
20YSZ02	0.382
20YSZ03	0.367
20YSZ04	0.341

The ceramographs of the fresh material (Fig. 5B.1a) show a coarse structure with heterogeneous sintering. The grain structure in both cases is very heterogeneous, both in size and shape. Most of the large grains have irregular shapes, and the grain boundaries are only partially developed since inter-granular voids strongly reduce the area of contact between adjacent grains. The porosity is markedly textured in the plane perpendicular to the disk axis, so that, macroscopically, the material exhibits a pronounced stratified aspect (Fig. 5B.1b). The ceramic exhibits a very good resistance against thermal shock in the investigated temperature range. However, during the thermal treatment a pronounced restructuring process, leading to a dense (Fig. 5B.1c) and more brittle structure, occurred. The starting materials, of a light grey colour, appeared completely white after the measurements.

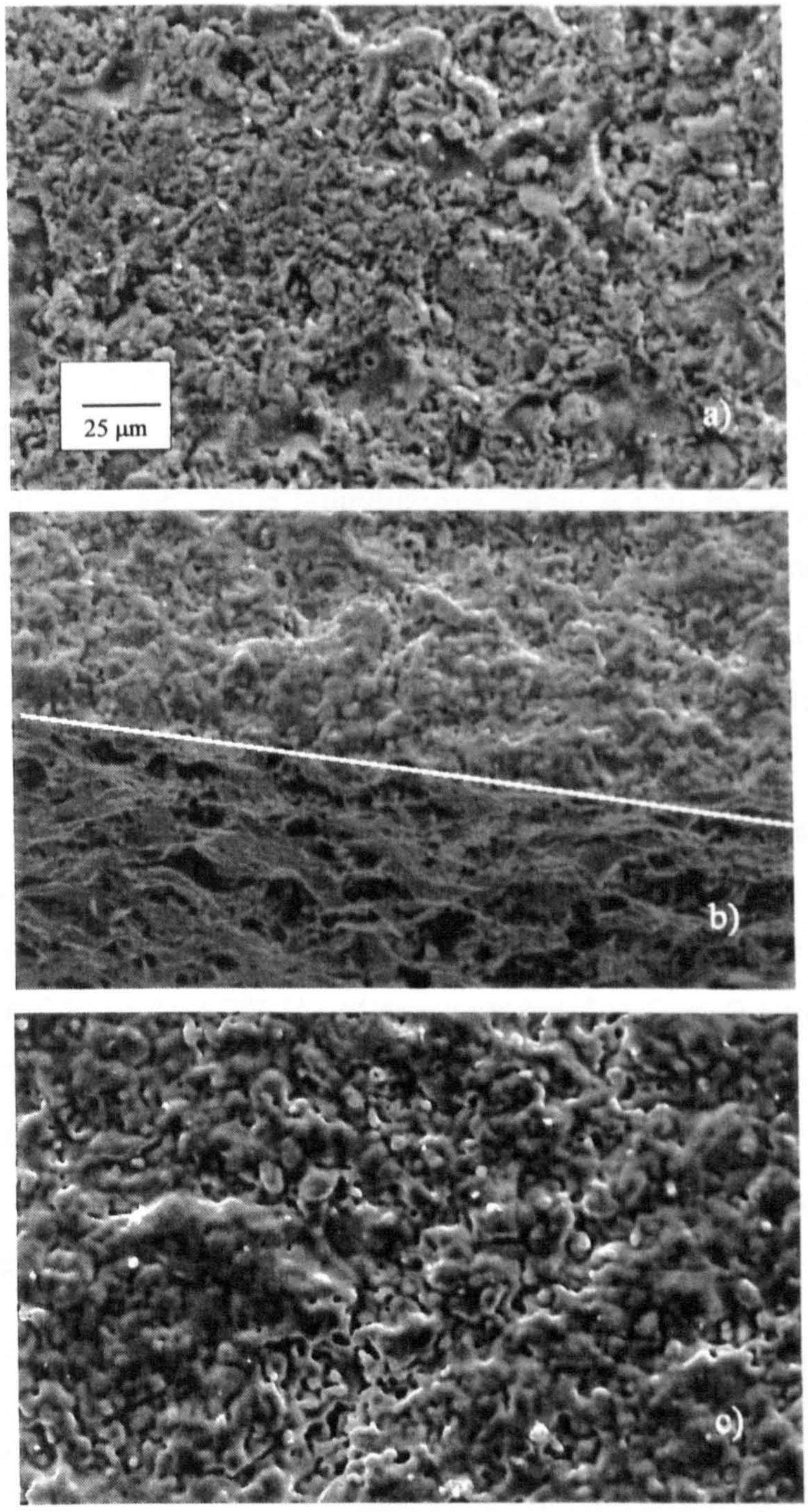

Fig. 5B.1 Structure of the samples used: **a)** Scanning electron micrograph (SEM) of the surface of a fresh 20YSZ sample. **b)** Transversal section of a 20YSZ sample after a measurement at 2500K. The sample has been cut for SEM observation: the brighter area above the white line corresponds to the platelet surface, whilst the brighter area below the white line corresponds to the cut surface perpendicular to the disk basis. **c)** View of the disk surface (SEM) after a measurement at 2500 K. The magnification is the same in all the pictures.

5B.1.2 *Experimental conditions*

A number of explorative measurements were preliminary carried out to optimise the experimental parameters. In particular, the heating rate of the samples had a crucial importance, since the starting material was semi-transparent at the wavelength of the laser (λ =1060 nm). The absorbivity of ZrO_2 at 1060 nm is in fact very small at room temperatures (of the order of 0.1), though it increases to more than 0.65 at 1800 K [147]. This created some problems in laser-power control during the heat-up stage; however, once temperatures above approximately 1800 K were attained, a good brightness temperature stability (±1 K) was obtained during time intervals of several minutes, indicating that the radiative properties of the specimen surface remained constant. The temperature stability, however, slightly decreased with increasing temperature and at 2800 K was of the order of 2 K.

The experiments were made after a short thermal conditioning by heating the front face of the disk with a continuous CW Nd-YAG laser. The measurements were carried out during heating steps of one minute duration at temperature intervals of approximately 100 K, in Ar + 2% H_2, at pressures ranging from 0.1 to 2 bars. A 1ms probe pulse was applied with a laser beam energy of the order of 0.5 J, producing an instantaneous front temperature increases of approximately 100 K, while the corresponding maximum rear-temperature increase was more than one order of magnitude lower (5 K).

5B.1.3 *Data analysis*

Fig. 5B.2 shows a typical pulse thermogram and its fitting curve, respectively. According to the chosen set-up (laser spot size equal to the sample diameter) Model 2 was used for the analysis. A combined rear/front temperature fitting was performed using three-parameters (with the conditions expressed by Eqs.(4B.23) and (4B.24)). The quality of fitting can be estimated from the resulting errors of the parameters involved, summarised in Table 5B.2.

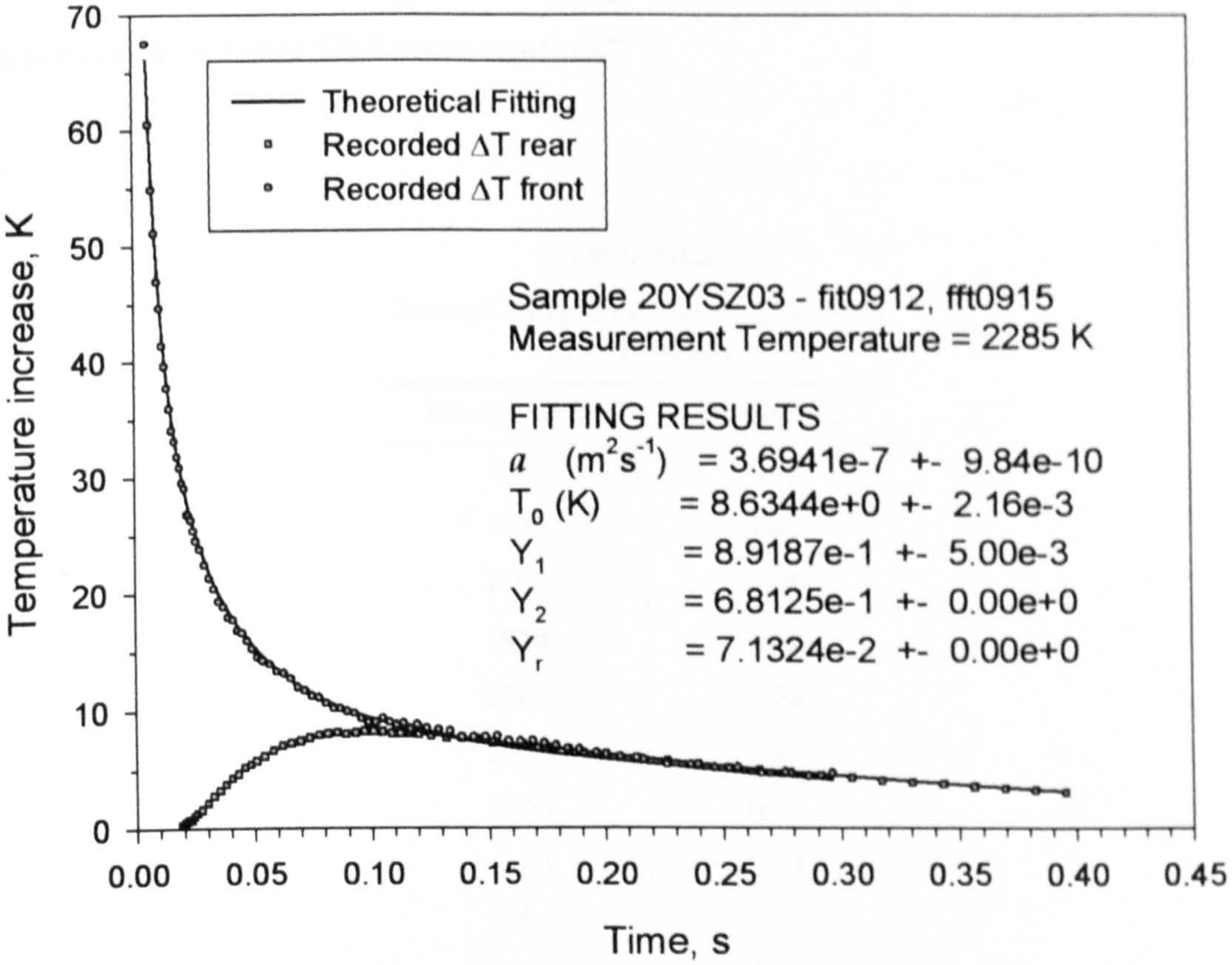

Fig. 5B.2 Recorded front and rear-surface thermogram and fitted theoretical curve for 20YSZ. The sample, a disk of 0.367 mm thickness (sample 20YSZ03) was shot with a pulse time of 1 ms and 2.552 J/cm^2 energy density. The original experimental thermogram consisted of several thousands of temperature measurements, however, for the fitting procedure these have been compressed to 300 points, each of which was assigned a local error.

Table 5B.2
Error analysis in the fitting procedure. The parameters error is calculated from Eq.(5B.21).

Parameter	**Average error %**	
	2000 K	2700 K
Thermal diffusivity: $\overline{a}$ (s^{-1})	0.2	0.3
*S*pecific heat: T_0 (K)	0.5	1
Biot numbers: Y_1, Y_2, Y_r	5	20
Fitting MSQ deviation	1.5	5

To compute the energy absorbed by the sample, the spectral normal emissivity values listed in Table 5B.3 were assumed[xxi].

Table 5B.3

Normal spectral emissivity of 20YSZ
at λ=1060 nm

Temperature	Emissivity
1800	0.65
1850	0.67
1900	0.68
1950	0.69
2000	0.70
2050	0.72
2100	0.74
2150	0.75
2200	0.76
2250	0.78
2300	0.80
2350	0.83
2400	0.85
2500	0.85
2600	0.85
2700	0.85

The error in the measured values of thermal diffusivity, specific heat and thermal conductivity, calculated according to Eqs.(4C.4), (4C.5) and (4C.6) were, respectively:

$$\frac{\delta a}{a}=1\%,\ \frac{\delta c_P}{c_P}=6\%,\frac{\delta \lambda}{\lambda}=5.9\%.$$

[xxi] Emissivity measurements were previously performed (see ITU Report HT-493) on the same material with the six-wavelength pyrometer method. The explored range was between 500 and 960 nm, and the accuracy of ε_λ was better than 5%. The emissivity values at 1060 nm were obtained by linearly extrapolating the spectral emissivity curve.

5B.2 Results

The measured specific heat is plotted as a function of temperature in Fig. 5B.4. The specific heat weakly increases with temperature, in the interval between 2000 and 2700 K, from 620 to 700 $Jkg^{-1}K^{-1}$. The results have been interpolated with a linear function, represented in the figure by the solid line.

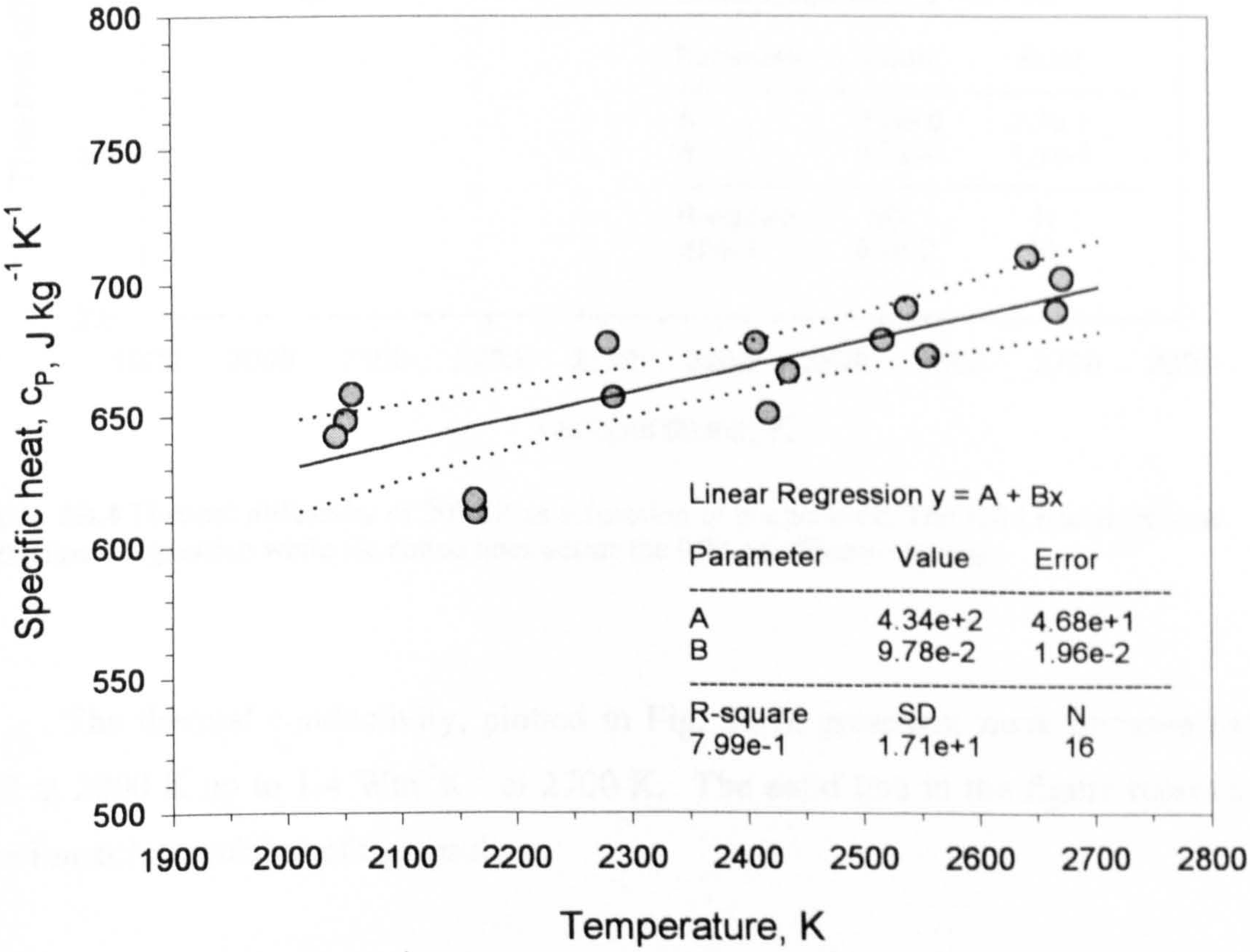

Fig. 5B.3 Specific heat of 20YSZ as a function of temperature. The solid line represent the linear regression, the dotted lines define the 95% confidence interval.

The measured thermal diffusivity is plotted as a function of temperature in Fig.5B.4. The values show a slight increase, from 3.5 10^{-6} m^2s^{-1} to 4.0 10^{-6} m^2s^{-1}, in the temperature range studied. The results are interpolated with a linear function, represented in the figure by the solid line.

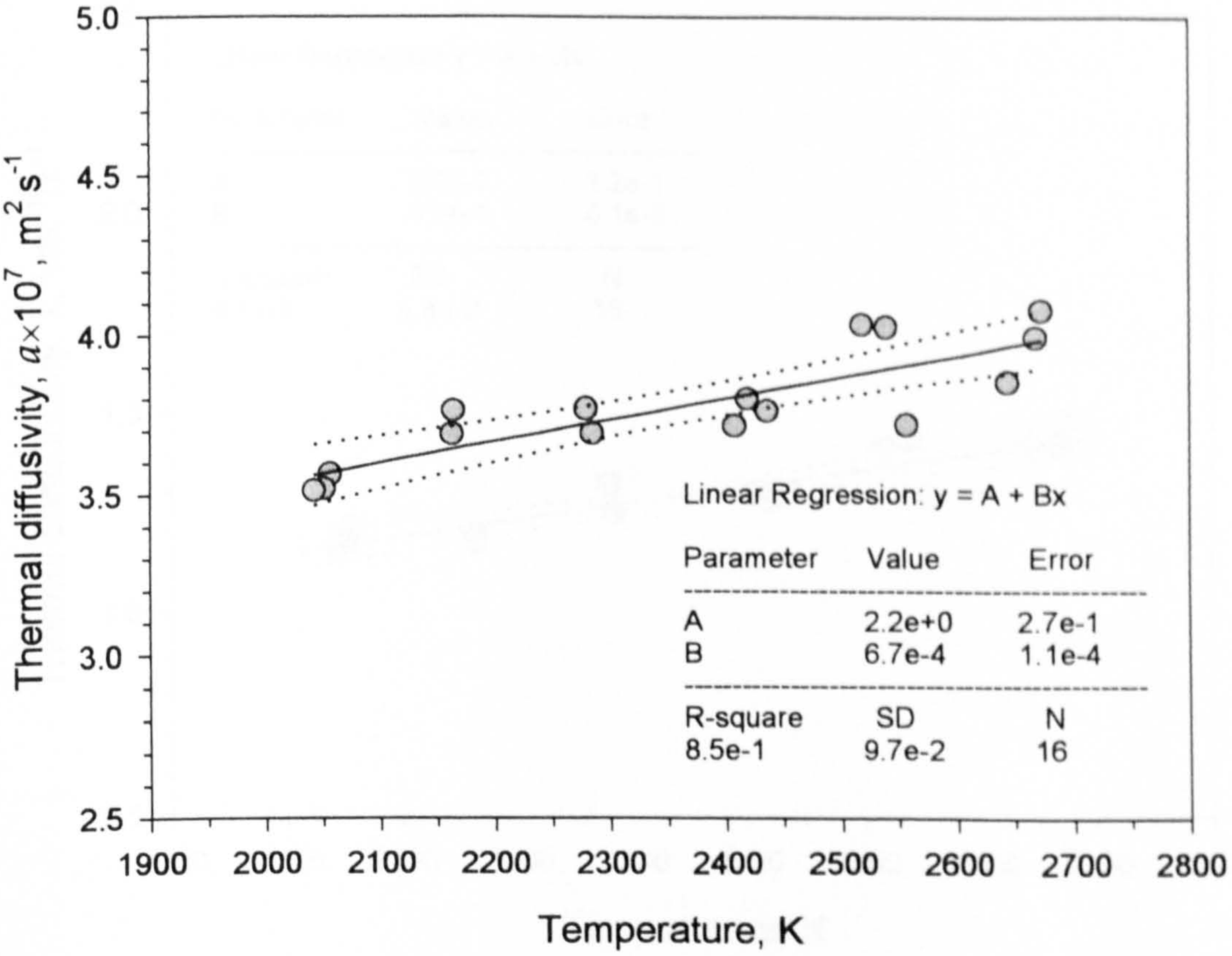

Fig. 5B.4 Thermal diffusivity of 20YSZ as a function of temperature. The solid line represents the linear regression while the dotted lines define the 95% confidence interval.

The thermal conductivity, plotted in Fig. 5B.5, present a weak increase from 1.2 at 2000 K up to 1.4 $Wm^{-1}K^{-1}$ at 2700 K. The solid line in the figure represents the linear interpolated of the results.

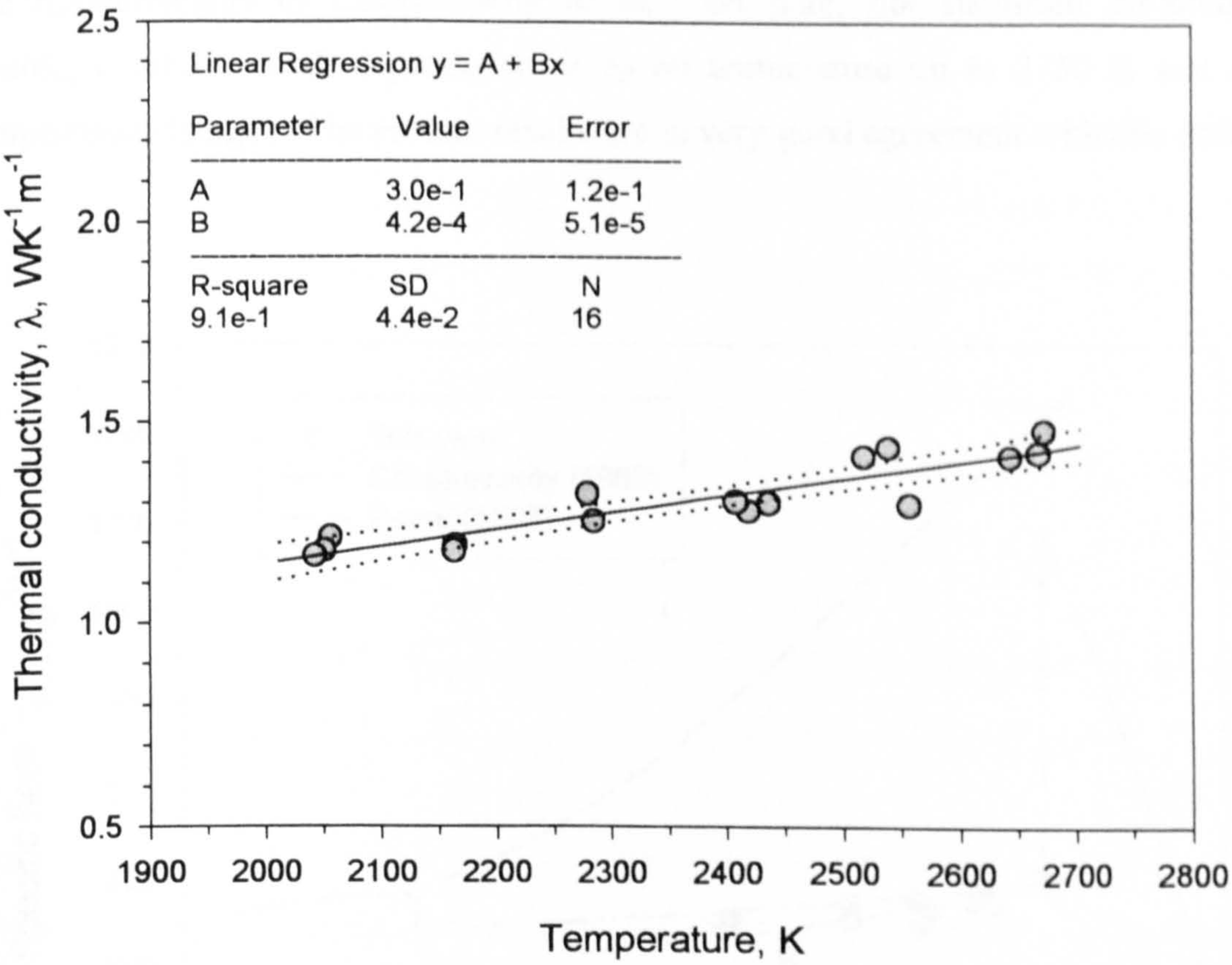

Fig. 5B.5 Thermal conductivity of 20YSZ as a function of temperature. The solid line represent the linear regression, the dotted lines define the 95% confidence interval.

5B.3 Discussion

Specific heat

The measured specific heat values are compared with literature data in Fig. 5B.6. The values reported by Chekhovskoy *et al.*[85] and Pears[86] have been obtained by drop calorimetry technique. From Fig. 5B.6 it can be seen that the existing literature data are in disagreement with each other.

The measurements by Pears[86], indicate a marked upswing of c_P above 1600 K, the material used by the author was 1% CaO-stabilised, and chemical analysis after exposure at high temperature indicated a net decrease of the oxygen-to-metal ratio and of calcium content.

The measurements of Chekhovskoy *et al.*[85] on pure, non-stabilised zirconium dioxide, exhibit a weak dependence of c_P on temperature up to 2750 K and no composition changes. The present results are in very good agreement with this data.

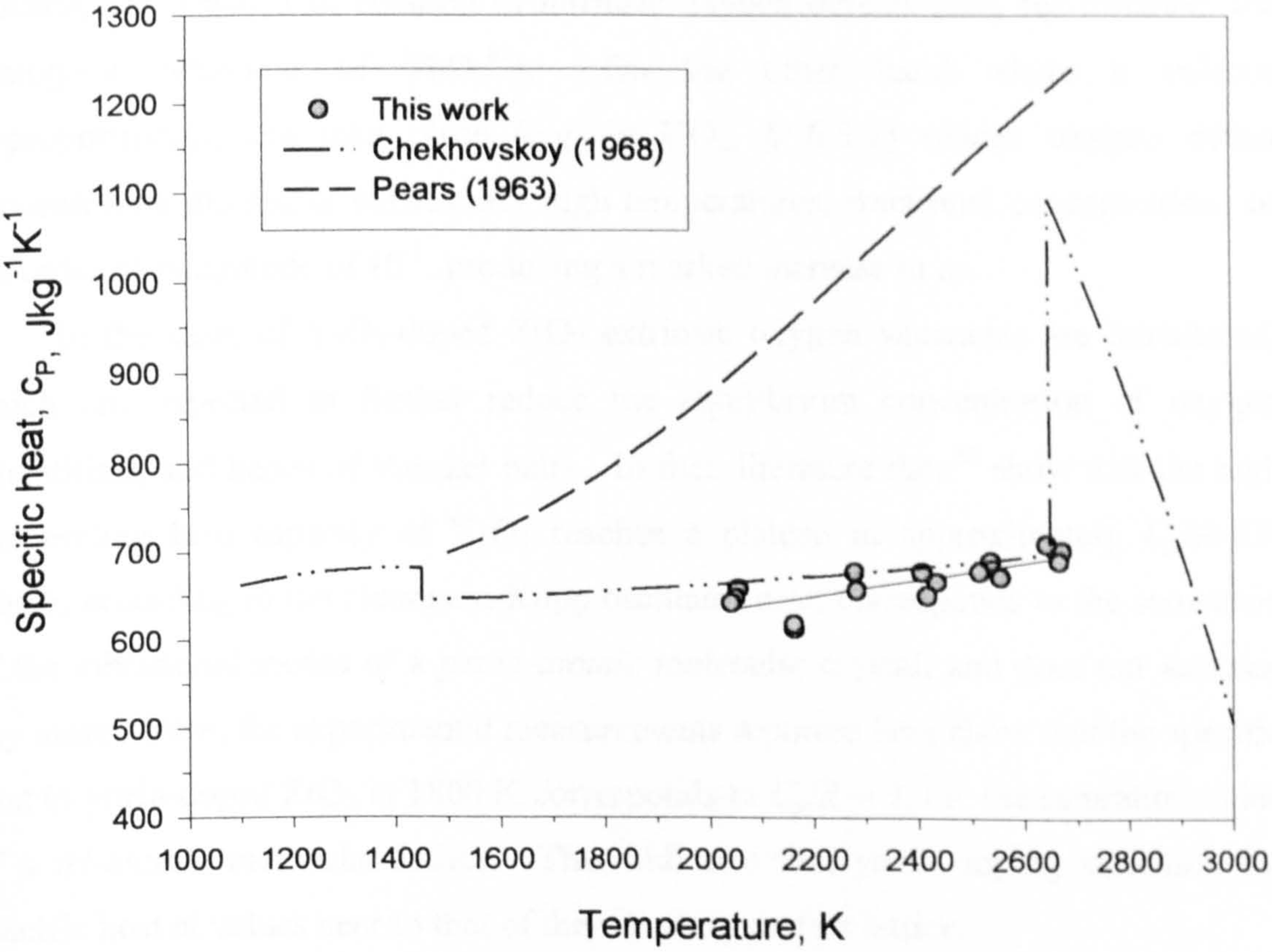

Fig. 5B.6 Comparison of the experimental results with literature data for the specific heat of ZrO_2. The zirconia used by Chekhovskoy was *not* stabilised, and consequently a discontinuity in c_P is found at the monoclinic-tetragonal and tetragonal-cubic phase transitions at the temperature of ≅1450 K and ≅2640 K, respectively.

The observed behaviour of c_P has an important physical implication. In f.c.c ionic dioxides, a marked increase of heat capacity at high temperatures can be expected, due to formation of oxygen vacancy/interstitial Frenkel pairs, a thermal process in which a substantial energy is spent. Normally, an increase in concentration of these lattice defects up to a few percents within a temperature interval of the order of 500 K, results into an extra contribution to c_P equal or larger than that of all the possibly activated phonon modes of the defect free lattice.

If this observation is associated with the modest measured variation of c_P with temperature it may be inferred that in ZrO_2 intrinsic defect formation is not very effective in the explored temperature range. This is understandable since creation of one oxygen vacancy/interstitial pair requires a charge re-arrangement in the surrounding cations. Thus, compounds like pure ZrO_2, where all cations have a fixed valence, are resistant to creation of intrinsic oxygen defects (see, for instance, the analogous behaviour of ThO_2[87]). On the other hand where a valence disproportioning can take place (*e.g.* in UO_2, § 6.3.1) oxides oxygen defect concentration attains, at sufficiently high temperatures, fractional concentrations of the order of magnitude of 10^{-1}, producing a marked increase in c_P.

In the case, of Y_2O_3-doped ZrO_2 extrinsic oxygen vacancies are introduced, which are expected to further reduce the equilibrium concentration of oxygen interstitials, and hence of Frenkel pairs. In fact, literature data[88] show that the high temperature heat capacity of Y_2O_3 reaches a plateau at approximately C_p/R=15, which, according to the Neumann-Kopp oscillator rule, corresponds to the saturation of the vibrational modes of a *penta-atomic* molecular crystal, and does not increase any more. Now, the experimental measurements reported here show that the specific heat in yttria-doped ZrO_2 at 1800 K corresponds to $C_p/R = 9$, *i.e.* the saturation value of a *tri-atomic* molecular lattice. This indicates that yttria doping stabilises the specific heat at values near to that of the vibrating perfect lattice.

Though perfectly plausible, these conclusions, which may be important for the refractory properties of the various types of sintered zirconium dioxide, leave out of consideration the underlying dependence on doping of the effective free energy and entropy of formation of defects in the considered real lattice, an aspect which may entail unexpected dramatic changes in the temperature dependence of c_P[89].
Therefore, extrapolations of these results to other types of stabilized zirconium dioxide must be considered with care.

Thermal diffusivity

The thermal diffusivity values obtained are in fairly good agreement with the data reported by Faucher *et al.*[90] on sintered ZrO_2 stabilised with 20% wt Y_2O_3 (as

can be seen from Fig.(5B.7)). Thermal diffusivity of "plasma spray zirconium dioxide", stabilised with 8% wt yttria have been measured from 400 to 1500 K by Schwingel *et al*[158]. The results reported by the authors (obtained on different samples for three temperatures) show averages value of approximately $3 \cdot 10^{-7}$ m^2s^{-1} at 373 K, $2.4 \cdot 10^{-7}$ m^2s^{-1} at 923 K, and $2.7\ 10^{-7}$ m^2s^{-1} at 1473 K. In all the samples the thermal diffusivity show a weak dependence on temperature: slightly decreasing between 400 and 1000 K and slightly increasing above this temperature. In all the cases the values of thermal diffusivity measured during heating are lower than the values measured during cooling.

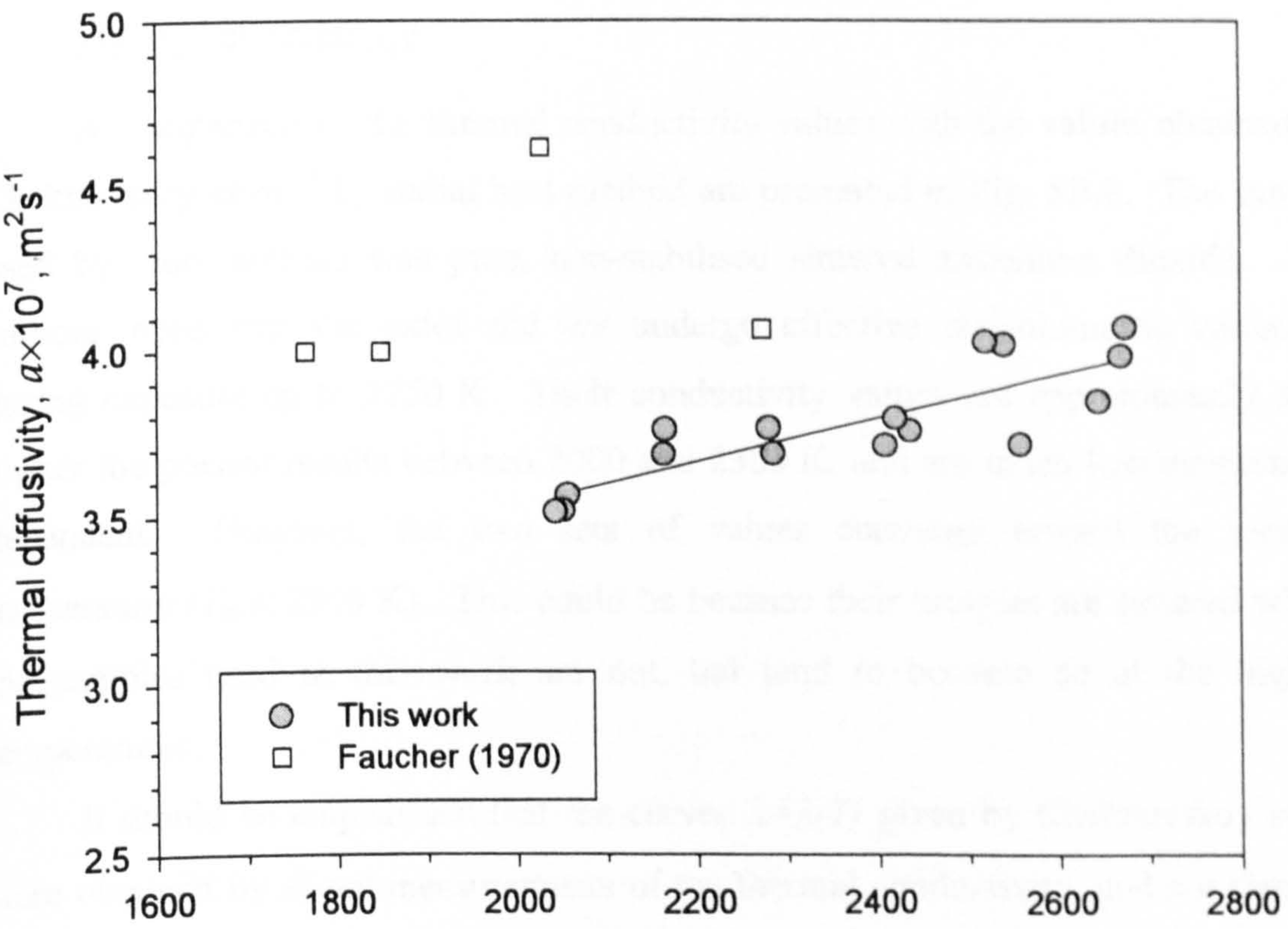

Fig. 5B.7 Comparison of the experimental results with literature data for the thermal diffusivity of 20YSZ.

The same features were observed in the thermal diffusivity measurements made between 400 and 1500 K by Morrell and Taylor[91] on plasma sprayed zirconium

dioxide stabilised with different percent of yttria. The values reported are in this case of $2{\cdot}10^{-7}$-$5{\cdot}10^{-7}$ m^2s^{-1}. Schwingel *et al* and Morrell and Taylor attributed the above mentioned features of their data to a sintering process that takes place at temperatures above 1000 K. A linear extrapolation of the present data to lower temperatures suggests a value of $3.2{\cdot}10^{-7}$ m^2s^{-1} at 1500 K, value which is in good agreement with the literature ones.

Apart from the difference in the materials (differently stabilised) and temperature range studied, direct comparison of data is difficult since the thermal diffusivity of this material, at least at low temperature, depends on the fabrication properties[91] (porosity, composition, shape of the grain) as well as on the spray parameters[92,158,159].

Thermal conductivity

A comparison of the thermal conductivity values with the values obtained by Chekhovskoy *et al.*[93] by radial heat method are presented in Fig. 5B.8. The sample used by these authors was pure, non-stabilised sintered zirconium dioxide. The authors report that the oxide did *not* undergo effective stoichiometric variations during exposure up to 2750 K. Their conductivity values are approximately 30% higher the present results between 2000 and 2300 K, and are much less temperature dependent. However, the two sets of values converge toward the melting temperature ($T_m \cong 2950$ K). This could be because their samples are sintered whilst the samples used in this work are not, but tend to become so at the highest temperatures.

It should be emphasised that the curves $\lambda=\lambda(T)$ given by Chekhovskoy *et al.* were obtained by *direct* measurements of the thermal conductivity, and not through the product of a and c_P. The agreement with the present measurements is therefore *not* a mere corollary of that found for the heat capacity.

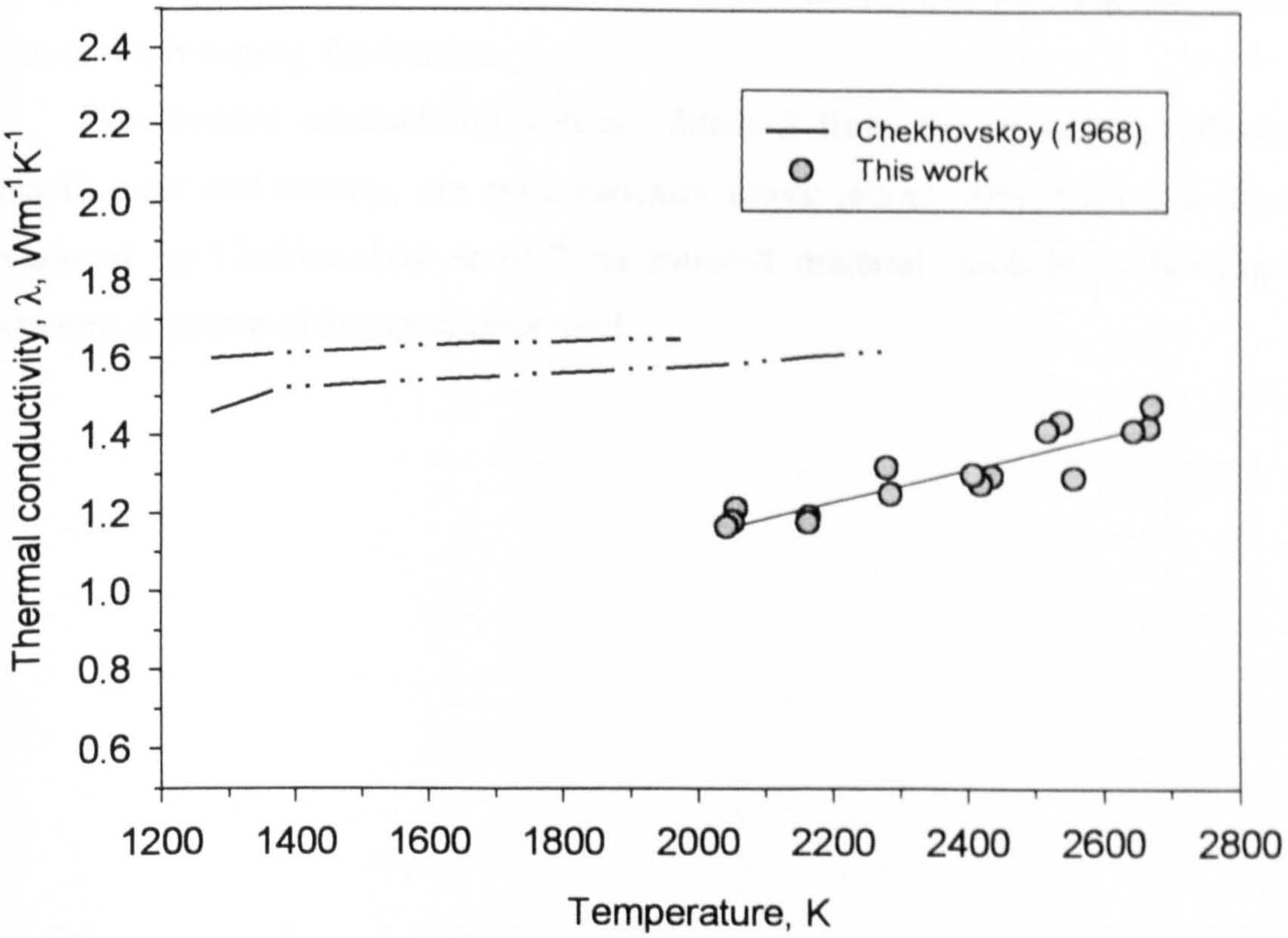

Fig. 5B.8 Comparison of the experimental results with literature data for the thermal conductivity of ZrO_2.

5B.4 Conclusions

The newly developed method proved to be successful for the measurements of thermophysical properties of zirconium dioxide at high temperature. The thermal diffusivity, the specific heat and the thermal conductivity were measured by CLASH with good precision (about 1% for thermal diffusivity and 6% for specific heat and thermal conductivity) from 1800 to 2700 K.

The results for c_P show good agreement with the data of Chekhovskoy *et al.*[85], but not with that of Pears[86]; this discrepancy could be attributable to the different material used by the author (CaO stabilised) and to the changes in the composition of the specimens reported.

The thermal diffusivity values shown a fairly good agreement with the data reported in literature at lower temperatures, but direct comparison is difficult since

the diffusivity is very dependent on the structure of the material, especially in the case of plasma-spray fabrication.

The thermal conductivity values, obtained from the measured diffusivity, specific heat and density, are systematically lower (about 30%) than that directly measured by Chekhovskoy *et al.*[93] on sintered material, probably reflecting the different structure of the specimens used.

Chapter 6

6. URANIUM DIOXIDE

The investigation of the thermophysical properties of uranium dioxide is the principal part of this Thesis.

Since the very beginning of the nuclear reactor history, sintered UO_2 proved to be a most reliable fuel. In fact, in addition to good refractory properties (melting point at 3150 K, sufficient plasticity at high temperatures, stable thermal conductivity, and good thermochemical stability), this compound exhibits an excellent behaviour under the heavy radiation damage conditions produced in pile. Low-stress configurations around lattice point defects, high capability of absorbing substitutional impurities, little tendency for splitting Frenkel pairs to form vacancy clusters and voids, ensure low swelling and dimensional stability of uranium dioxide fuel rods. In the thermal reactors of the last generation, the in-pile performance of UO_2 made it possible, through exploitation of concomitant nuclear fertilisation processes, to reach burnups of up to 10% of the total original uranium atoms (instead of the usual 3-4%). Now, since one fission creates two atomic fragments, at these high burnups approximately one out of five uranium atoms is replaced in the lattice by a substitutional, interstitial or segregated guest atom; nevertheless, the material still exhibits distinct thermophysical properties.

Since the function of the fuel is to produce heat and transfer it to the coolant, its thermal conductivity is a key parameter both for fuel element design and reactor operation conditions. Therefore, each reactor user takes particular care in characterising the thermal conductivity of his specific fuel, in the foreseen temperature range of operation, which, for water-cooled reactors, extends approximately from 500 K to 2000 K. Higher temperatures are, in fact, only involved in abnormal or accident conditions. At these temperatures, the thermal conductivity is much less dependent on fabrication properties, and, therefore, is normally determined on the basis of the full set of literature data. Unfortunately, due to experimental difficulties, high temperature measurements are scanty and imprecise. On the other hand, a more accurate determination of the thermophysical

properties up to temperatures near the melting point, is important not only for reactor safety calculations, but also for the understanding of the intrinsic defect properties of the uranium dioxide lattice.

6.1 Measurements conditions and data analysis

6.1.1 *The material*

The UO_2 samples were disks of 5 mm diameter and thickness less than 0.5 mm, cut from the middle of standard light-water reactor fuel pellets of 9.9 mm diameter and sintered density of 95% the theoretical density (th.d.). The thickness of the specimens, listed in Table 6.1 was measured at the centre of the sample with an uncertainty of 2 μm. The characterisation data of the samples are shown in Table 6.2.

Table 6.1

Thickness and experimental conditions of UO_2 specimens

Specimen	Thickness (mm)	Treatment
UO201	0.501	A
UO202	0.512	A
UO203	0.449	A
UO204	0.368	A
UO205	0.450	B
UO206	0.351	B
UO207	0.322	B
UO208	0.500	C
UO209	0.301	C

A = 1 ms pulse; B = 10 ms pulse; C = 10 ms pulse heated from both sides

Table 6.2

Data analysis of the UO_2 samples

Sintering	1750 ^{0}C in Ar:3% H_2 Sintered density = 95% of theoretical density (th.d.) Mean grain size = 10 μm	
Stoichiometry	O/U = 2.002±0.002	
Chemical analysis	Total impurities	~1000 ppm

The samples, after cutting, were treated at 1123 K for 24 hours in a carbon dioxide/carbon monoxide atmosphere (CO/CO_2=10) to anneal the internal stresses and bring the samples to stoichiometry. In fact, cutting and drilling of the material introduced internal stresses that during the fast heating made the specimen break. Annealed samples on the other hand, displayed a better resistance to thermal shocks.

The oxide stoichiometry, determined by thermogravimetric analysis from the weight increase after total oxidation to U_3O_8 in air at 900 ^{0}C, corresponds to O/U=2.002 ± 0.002.

The samples were analysed by scanning electron microscopy before and after the measurements. Grain size (≈ 10 μm), porosity -mostly intergranular- as well as grain boundary morphology indicate that the "as fabricated" pellets were well sintered (Fig. 6.1a), though zones of higher porosity and smaller grain size are occasionally observed. After the high temperature measurements, the front surface of the sample (Fig. 6.1b), which is subjected to the highest temperature peak, is thermally etched (Fig. 6.1c), showing very clearly the grain structure. The average grain size is about twice the initial one, but the dispersion of the statistical grain-size distribution remains broad. Locally, almost total densification is observed, the average porosity being approximately 2% lower than in the "as-fabricated" structure. Most of the pores are still in intergranular positions. Occasionally, coalescence effects leading to channel-like structures are observed; it is evident, however, that coalescence occurred only on sub-granular scale, since several small pores are still present at inter-distances of only a few microns.

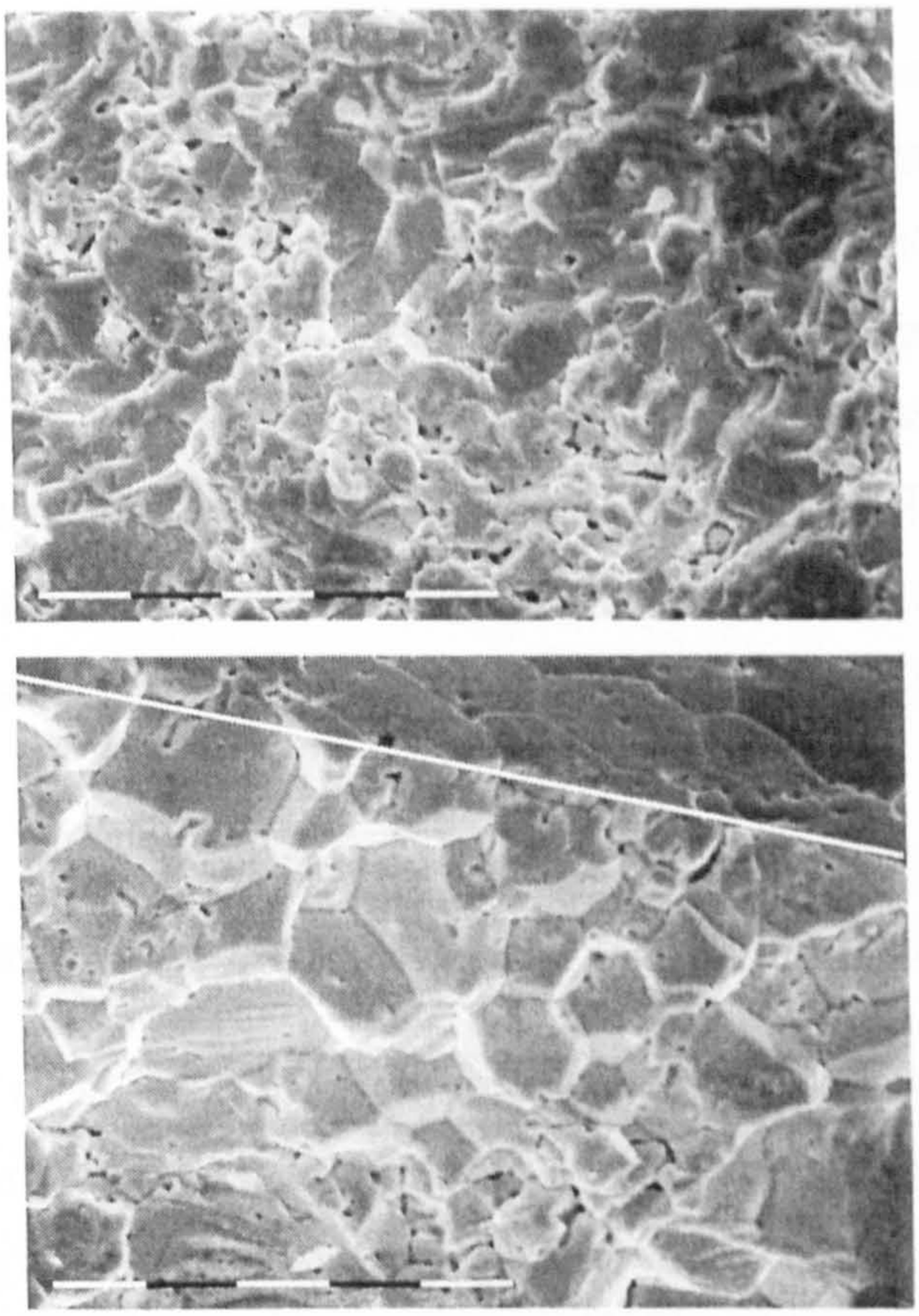

Fig. 6.1 Structure of the sample used: **a)** Scanning electron micrograph (SEM) of a fracture surface of an as-fabricated UO_2 sample. The sintering density is 95% of the theoretical density. The magnification is the same as in Fig. 6.1b, where the white bar corresponds to 10 µm. **b)** The material after a measurement at 2800 K. The sample has been fractured for SEM observation: the darker zone above the white line corresponds to the platelet surface, whilst the brighter area below the white line corresponds to the fracture surface approximately perpendicular to the disk basis. **c)** View of the disk surface (SEM) after a measurement at 2800 K.

In conclusion, thermal restructuring during measurements at the highest temperatures did not dramatically change the ceramographic structure of the sample; in particular, despite the presence of a thermal gradient, columnar grains with textured lenticular pores were *not* formed during the reported experiments[xxii].

After the measurements the stoichiometry of the oxide was measured. Each specimen was separately analysed and an average O/U ratio of 1.994 ± 0.008 was found. The large error in the stoichiometry measurement is due to the small quantity of mass available for each sample (a few hundreds of milligrams).

6.1.2 *Experimental conditions*

A number of explorative measurements have been preliminary carried out to study the property of the material at high temperature and optimise the experimental parameters. During these tests it was found that 1) the thickness of the sample, 2) the type and pressure of the gaseous atmosphere, 3) the heating conditions, and 4) the pulse time and deposited power on the sample were of fundamental importance to keep the material under stable conditions and reduce the experimental errors.

Thickness of the sample

A first batch of samples was cut in the form of disks of thickness between 0.5 and 1.0 mm. Preliminary experiments made on these specimens showed that, in order to reduce the thermal gradient and limit heat losses, a thickness of less than 0.5 mm was needed. Furthermore, the thinner the sample, the lower was the time needed to bring the sample to the conditioning temperature. In this contest, a second batch of samples of thickness between 0.3 and 0.4 mm was prepared. The thinner specimens were used for measurements at very high temperatures.

[xxii] In pellets which are well sintered at densities above 95% th.d. and with grain sizes larger than 5 μm, the conductivity is effectively proportional to the fractional density. A densification of the present samples to 100% th.d. would therefore produce an increase in conductivity of no more than

Gaseous atmosphere and pressure

Since UO_2 at high temperature can exist over a broad composition range of oxygen excess or deficiency, the control of a given stoichiometric composition at elevated temperatures requires control of the atmosphere surrounding the specimen. To avoid composition changes during the experiments it was chosen to work in inert atmosphere at a slight over-pressure to suppress material sublimation. The experiments were performed basically in argon at 2 bar. Depending on the heating conditions, small amounts of H_2O/H_2 mixtures were added in order to obtain suitable oxygen partial pressures in the buffer gas. In fact, from one side it was necessary to prevent oxidation of UO_2 (its sublimation rate increases dramatically at O/U >2.00); from the other side, a substantial reduction below 2.00 was also to be avoided. Since under the experimental conditions thermodynamic equilibrium could not be ensured, the oxygen concentration in the gas was controlled through the $2H_2O \leftrightharpoons 2H_2+O_2$ reaction to obtain above 2000 K a tentative value of $\Delta G(O_2)$ of approximately -70 kcal/mole. Post measurement analyses of the sample reveal that these conditions produced an oxygen content decrease of approximately 0.3%. At lower measurement temperatures the oxygen partial pressure was fixed at approximately the equilibrium values of the stoichiometric oxide, and the variation of the initial O/U ratio was below the detection limit.

Heating conditions

In the preliminary tests it was observed that, despite the good quality of the sintered samples, random high-frequency temperature fluctuations, increasing with temperature, occurred on the rear-surface during steady state laser heating. These fluctuations were significantly damped if an axial thermal gradient was produced across the sample[xxiii]. To generate a small thermal gradient across the sample, one-side laser heating was used. For this reason, all the experiments, except two at very

---

5%. Larger "porosity corrections" have been introduced by other authors to compensate for more substantial differences in conductivity observed in different samples.

[xxiii] The reason is that the surface temperature variations, δT_s, due to input power fluctuations are proportional to the *difference* of the derivative with respect to T_s of the thermal radiation rate, and the

high temperature (see Table 6.1) were carried out by heating only the front face of the specimen. Both sides heating was, however, necessary to bring the sample to the highest temperature, by avoiding melting of the front face.

Pulse time and deposited power

To minimise perturbations of the sample properties due to thermal restructuring, heating was produced within approximately one minute. The samples were, in the main, resistant to thermal shocks: in only 10% of the experiments micro-crack formation was observed *during* the measurements. Since this always resulted into a drastic deviation from the expected course of the thermogram, such events could be visually recognised from the recorded pyrometer signal. As expected[xxiv], cracking of the sample occurred more frequently during cool down *after* the measurements, unless this was made at a very low rate.

Two types of shots were applied, of 1 and 10 ms duration, respectively. In the second case the probe-laser power, and hence the temperature increase on the front face of the sample, was much lower, so that the sample conditioning temperature was only slightly perturbed by the pulse. Once the finite pulse-time effect is correctly taken into account in the analysis, the low power experiments are more accurate and better reproducible than those at higher power (see Table 6.2). It should be noted that all the measurements above 2700 K have been made with 10 ms pulses, to avoid risk of surface melting.

Finally, a set of diffusivity measurements was carried out in the temperature range 550-1100 K by LAF[73]. These measurements are of particularly high precision and are used in Section 6.5 for analytical purposes.

---

heat flux through the bulk. In fact, more stable conditions could be produced in the sample by slightly decreasing the power of the laser beam impinging *on the rear surface*.

[xxiv] The outer annulus of the sample disk is cooler than the central part, which undergoes significant plastic deformations at high temperature. By rapid sample cool-down large *tensile* stresses are therefore created in the central zone, and in most cases cracking occurs. On the other hand, during the measurement, as long as the external annulus remains intact, a *compressive* stress field is present in the high temperature zone, preventing microcracking of the sample, while when the external annulus fails the sample undergoes severe cracking. Therefore two well-separated states of the sample are

6.1.3 *Data analysis*

Fig. 6.2 shows a typical example of the measured transient temperature of the rear surface of a UO_2 sample and its fitting.

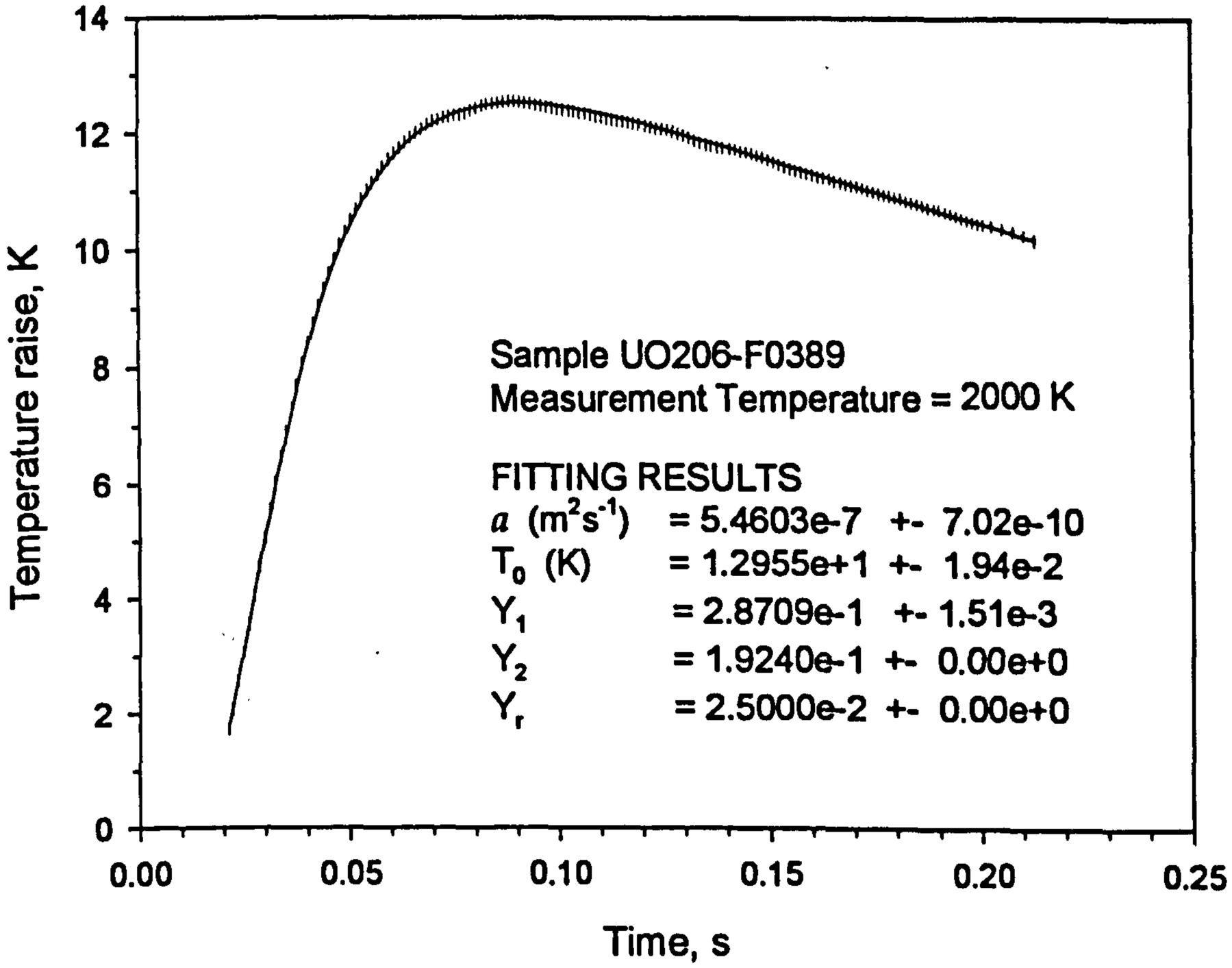

Fig 6.2 Recorded rear-surface thermogram and fitted theoretical curve for UO_2. The sample a disk of 0.351 mm thickness, was heated with a pulse time of 12.3 ms and 2.76 Jcm^{-2} energy density. The original experimental thermogram consists of several thousands points of temperature measurements, but for the fitting procedure they have been compressed to 300 points, each assigned with a local error.

According to the chosen set-up, with a laser spot size equal to the sample diameter, the analysis was carried out by using Model 2, firstly by a simultaneous fitting of both front and rear temperature, and then by using only the rear temperature

---

expected: one in which heat conduction is measured in a compressed, sound structure, and one in which the measurements are completely invalidated by macroscopic cracking.

data. A three-parameter fitting was performed, in which the conditions expressed by Eqs.(4B.23) and (4B.24) were used. The quality of fitting can be seen from the resulting parameter errors, summarised in Table 6.3.

Table 6.3
Error analysis in the fitting procedure. The parameter errors are calculated from Eq.(4B.21).

Parameter	Error %			
	τ = 1 ms		τ = 10 ms	
	2000 K	2600 K	2000 K	2800 K
Thermal diffusivity: $\bar{a}$ (s^{-1})	0.2	0.3	0.1	0.6
Specific heat:T_0 (K)	0.2	0.5	0.15	1
Biot numbers (Y_1, Y_2, Y_r)	2	5	1.5	6
Fitting MSQ deviation	1.5	3	1	2

To compute the energy absorbed by the sample, the normal spectral emissivity values according to Bober *et al.*[94] and listed in Table 6.4 were considered. The error in the emissivity values was estimated to be of the order of 5%.

Table 6.4
Normal spectral emissivity of uranium dioxide at λ=1060 nm

Temperature	Emissivity
1800	0.91
2600	0.90
2800	0.89
2900	0.88
3000	0.87

The thermal expansion values to correct the thermal diffusivity, the specific heat and the thermal conductivity were calculated by interpolating the joint macroscopic measurements of Conway *et al.*[95] and Christensen[96] with the equation:

$$\alpha = 6.5238 \cdot 10^{-2} + 5.4005 \cdot 10^{-4} T + 2.7553 \cdot 10^{-7} T^2 - 6.6650 \cdot 10^{-12} T^3 \qquad (6.1)$$

where $\alpha = \frac{\Delta L}{L_0}$ is the linear thermal expansion in percent between 1500 and 3100 K, with L a linear dimension of the sample and L_0 its initial value at room temperature, and T is temperature in K.

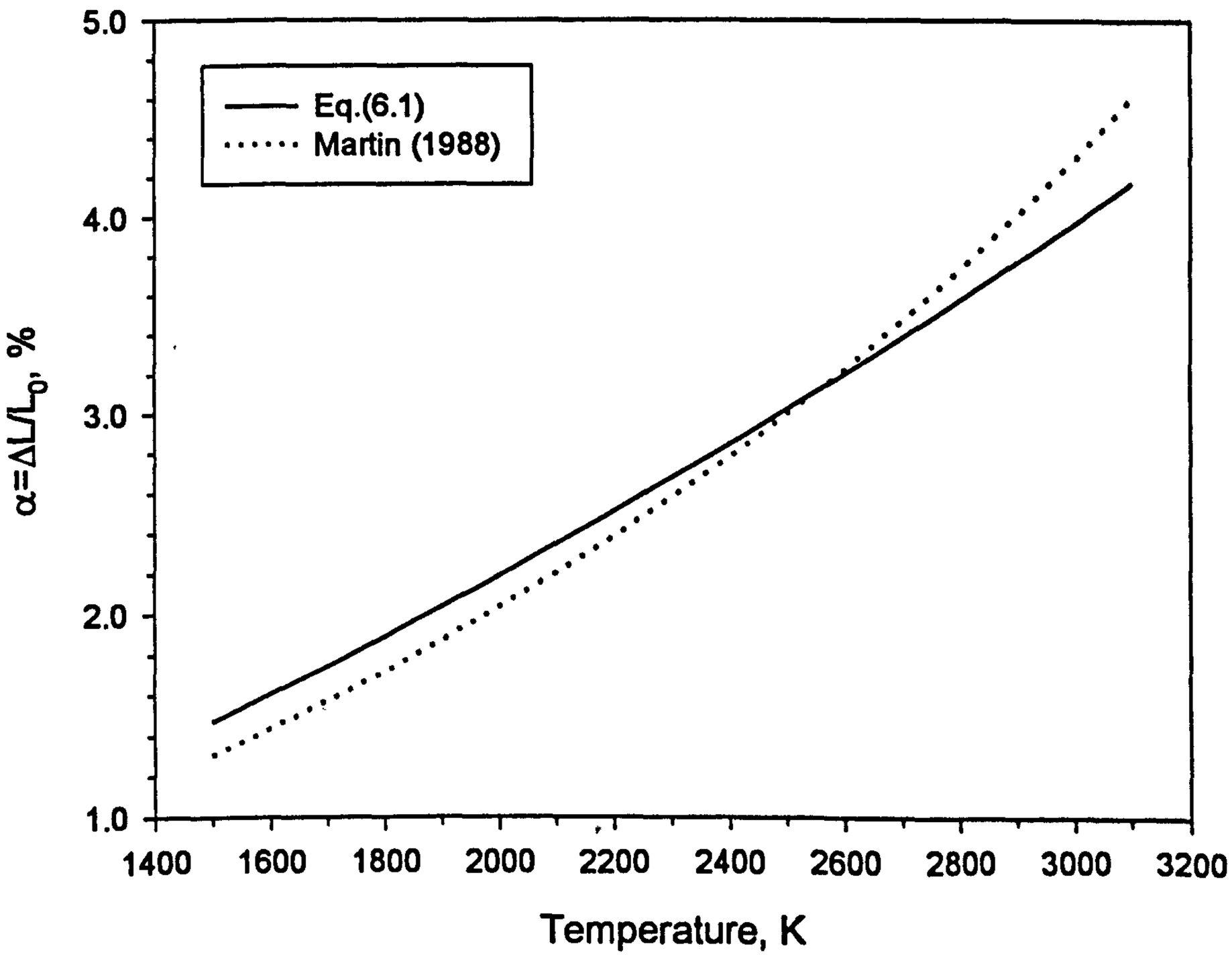

Fig. 6.3 Comparison of interpolating functions for the thermal expansion of UO_2.

The thermal expansivity values provided by this formula with a precision of ~1%, effectively coincide with those used by the authors in the past to correct their

diffusivity and conductivity measurements. In the comprehensive review of the UO_2 thermal expansion data by Martin[97] a somewhat different interpolating polynomial was obtained by completely omitting the Christensen data, and using above 2500 K only the set of Hutchings' *indirect* expansivity measurements from neutron scattering experiments[98]. Though the differences of Martin's polynomial values from those obtained from Eq.(6.1) (being of the order of 4%, at 2900 K) are in this context negligible (see Fig. 6.3), the high temperature Christensen data should be taken into account. In fact, the curve representing data obtained by Eq.(6.1) lies between these latter and those of Hutchings.

The errors in the measured values of thermal diffusivity, specific heat and thermal conductivity, calculated according to Eqs.(4C.4), (4C.5) and (4C.6) are, respectively:

$$\frac{\delta a}{a} = 2.4\%, \frac{\delta c_P}{c_P} = 6.3\%, \frac{\delta \lambda}{\lambda} = 6\%.$$

6.2 Results

6.2.1 *Specific heat*

The results of the specific heat measurements as a function of temperature are shown in Fig. 6.4. The measured values increase with temperature from 350 $Jkg^{-1}K^{-1}$ at 1800 K to 700 $Jkg^{-1}K^{-1}$ at 2900 K.

The two types of measurements obtained by applying laser pulses of 1 and 10ms, are marked with squares and circles, respectively. The obtained thermograms are, in the two cases, very different, their shape depending on the different thermal losses occurring during the two different pulse times applied. Nevertheless, the agreement between the two sets of measurements is good, confirming the reliability of the analytical solution adopted for each case.

Owing to the presence of a temperature gradient in the sample, in these experiments it was not possible to detect the thermal arrest produced by the lambda

transition[xxv] [99]; above this transition, indicated by the dashed zone in Fig. 6.4, the measurements indicate a further increase of c_P from 600 to 700 J/kgK between 2700 and 2900 K.

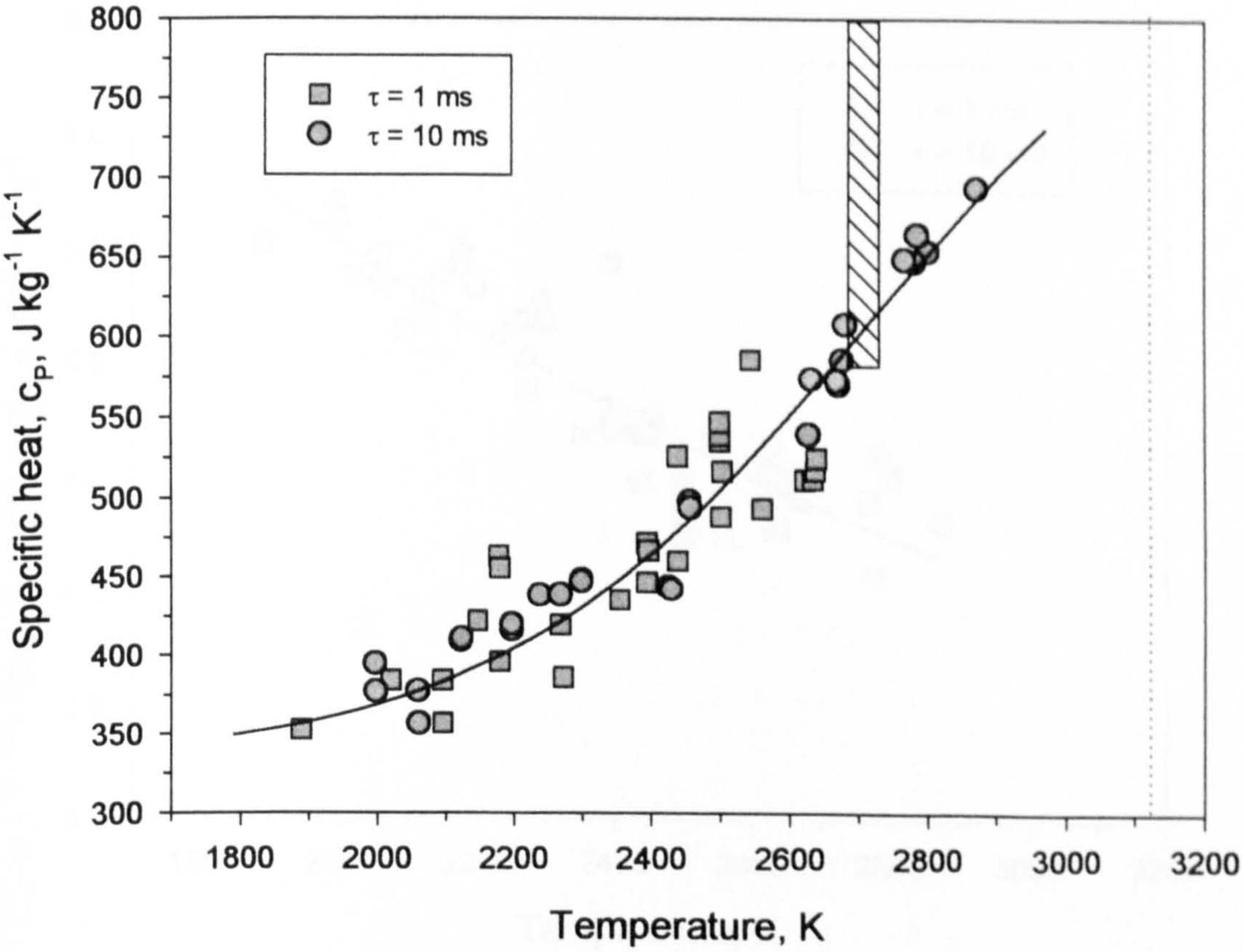

Fig. 6.4 Specific heat of UO_2 as a function of temperature. All the values are interpolated with a polynomial of the third order (solid line). The lambda-transition temperature[99], $T_B = 2670 \pm 30$ K, and the melting temperature, $T_m = 3120 \pm 20$ K, are shown on the graph with a dashed zone and a dotted vertical line, respectively.

6.2.2 *Thermal diffusivity*

The measured thermal diffusivity is plotted as a function of temperature in Fig.6.5. The values exhibit a continuous, net decrease with temperature up to 2600 K

[xxv] The Bredig-transition (also called lambda-transition) is a pre-melting transition that occurs near $0.85T_m$, where T_m is the melting temperature, in fluorite compounds (M.A. Bredig, Report 4437, Oak Ridge National Laboratory (1969), p.103).

but above this temperature the decrease is less pronounced and the curve seems to flatten out.

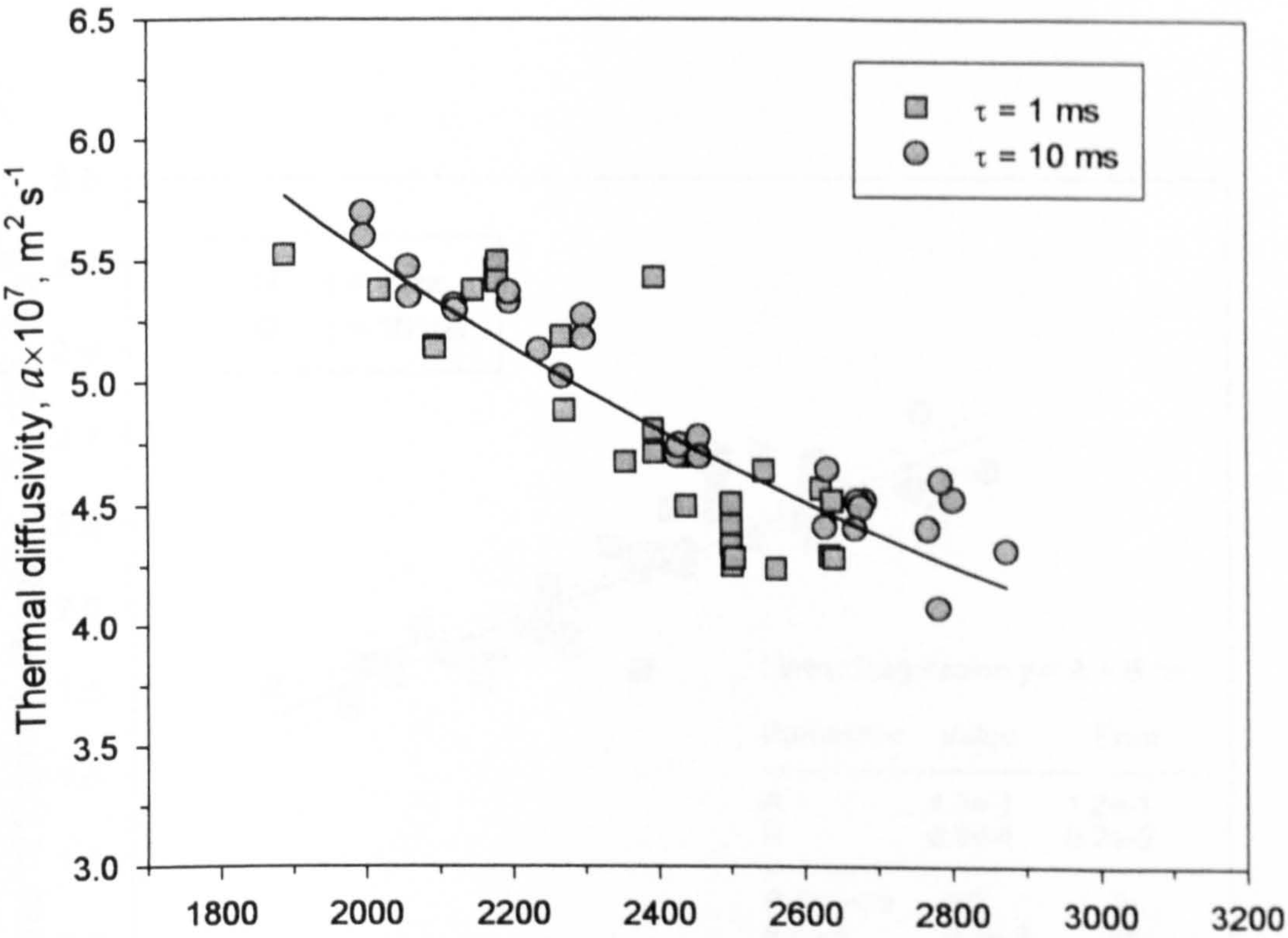

Fig. 6.5 Thermal diffusivity of UO_2 as a function of temperature. The solid line is obtained from the linear regression of the inverse of the thermal diffusivity values. For the interpolation both the values measured with 1 and 10 ms were considered.

Plotting *1/a* versus *T,* Fig 6.6, reveals a linear trend in *T* up to 2600 K, above which temperature the slope decreases. However, the accuracy limit of the measurements and the narrow temperature range explored above 2700 K did not allow detecting a possible change in *sign* of the slope.

In the specific heat measurements the observed scatter is of the same order of magnitude of the measurement precision, but in the case of thermal diffusivity the measurements precision is almost one order of magnitude better than the experimental scatter. It is therefore very likely that the scatter observed in Fig. 6.5

and Fig. 6.6 is caused by small restructuring effects in the samples during the measurements. Although the experimental scatter is bigger than expected, it is much lower than the observed deviation from the recommended literature values (see § 6.3.2).

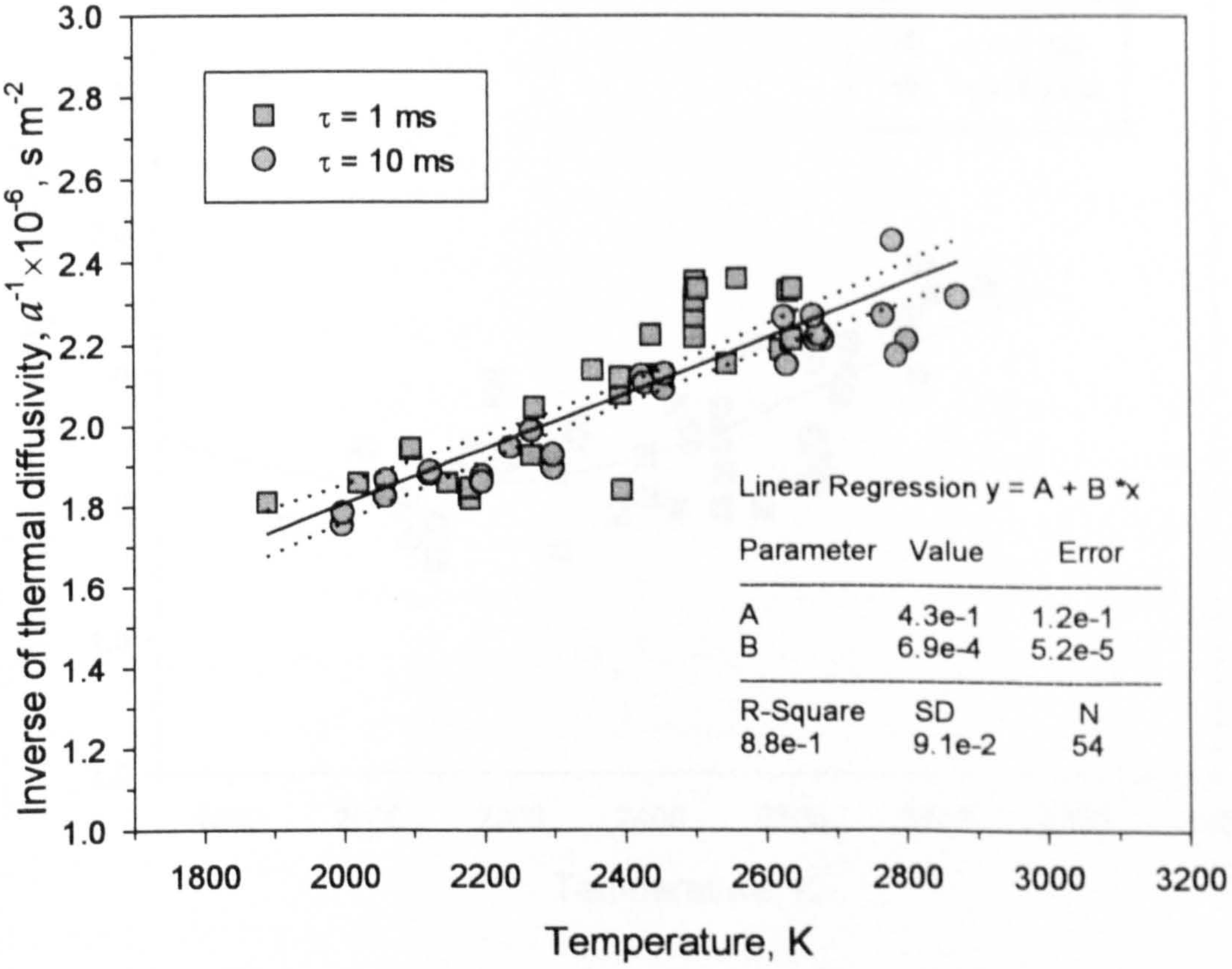

Fig. 6.6 Inverse of the UO_2 thermal diffusivity as a function of temperature. The solid line represents the linear regression of all the points on the graph, the dotted lines represent the 95% confidence interval.

6.2.3 *Thermal Conductivity*

The obtained thermal conductivity, λ, as a function of temperature is plotted in Fig.6.7. In the investigated temperature range, from 2000 to 2900 K, the values of λ exhibit a slight but unambiguous increase with temperature.

Since the thermal conductivity, is calculated from the equation $\lambda = a\rho c_P$, the upswing is caused by the continuous increase of c_P with temperature up to 2900 K, that slightly predominates over the decreases in both a and ρ.

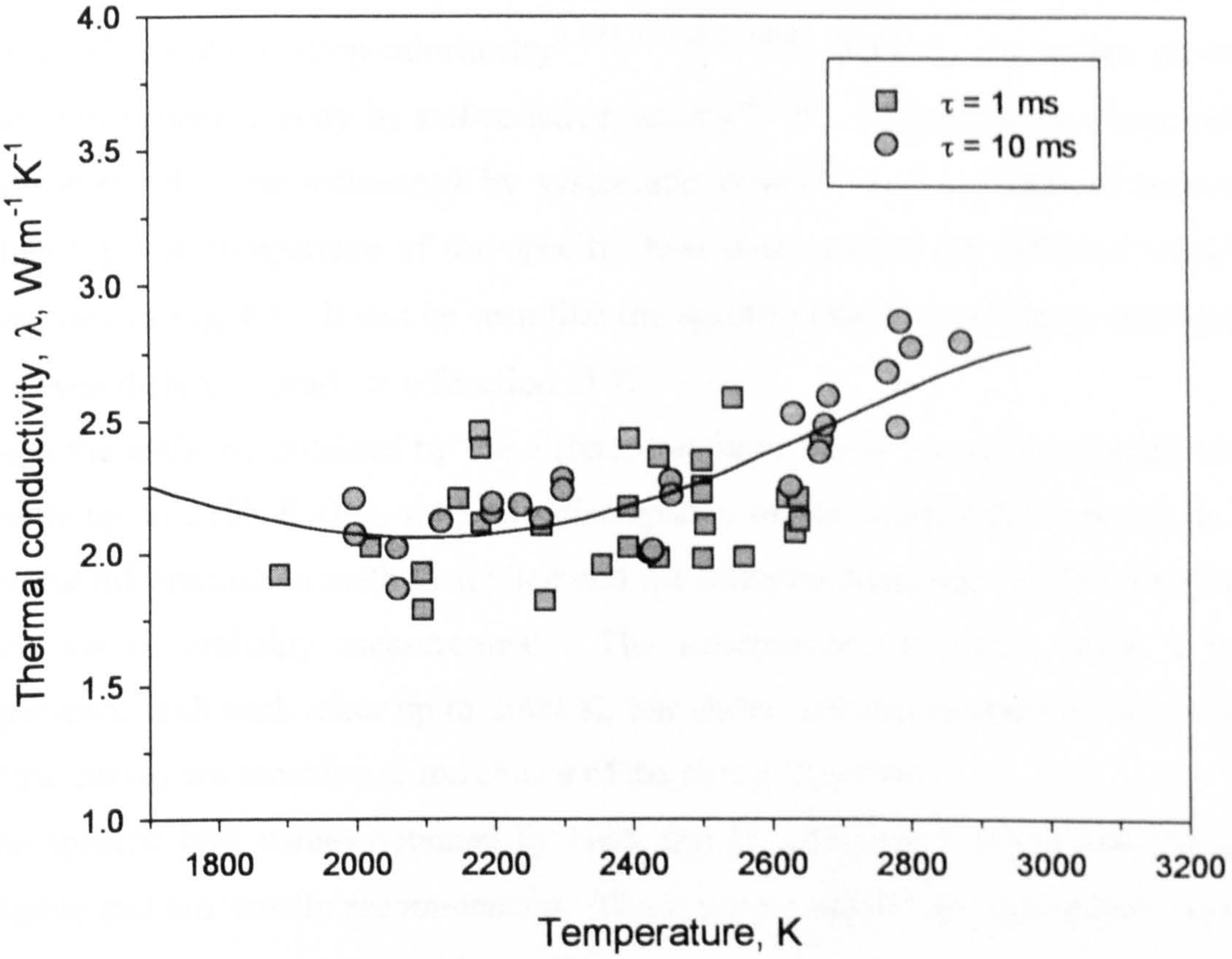

Fig. 6.7 Thermal conductivity of UO_2 as a function of temperature. The solid line represents the data interpolation of measurements made by CLASH ($1800 \leq T \leq 2900$ K) and by LAF ($550 \leq T \leq 1100$ K) by Eq.(6.4). The discussion is reported in § 6.5.

6.3 Discussion

6.3.1 *Specific heat*

A large number of investigations have been carried out to determine the specific heat of uranium dioxide at high temperatures, but the results above 1800 K show a large scatter. The specific heat at temperature above 1500 K has been measured mainly by drop calorimetry[2,3,95,100,101,102,103], and only one author reported values measured directly by self-resistive heating[104,105]. Unfortunately, those values are suspected to be influenced by systematic errors[106] and are thus of unknown reliability. A comparison of the specific heat measured in the different works is presented in Fig. 6.9. It can be seen that the specific heat shows a large uncertainty and even different trends as a function of *T*.

Since the enthalpy obtained by the different authors shows a good agreement in the results up to 3100 K (Fig. 6.8), the discrepancy in the specific heat, is due to the diverse differentiation method applied and the different functions used to interpolate each set of enthalpy measurement. The interpolating functions show a good agreement with each other up to 2000 K, but above this temperature the local slope of the curves are sensitive to the choice of the spline function[107].

The specific heat values obtained by Hein and Flagella[3] were considered the most reliable and are usually recommended. These values exhibit an exponential increase with temperature up to the melting point.

The specific heat calculated by Godfrey *et al.*[108] from the enthalpy data of Conway and Hein[101] are in good agreement with the results of Hein and Fagella, being the difference at 3000 K less than 4%.

The specific heat results proposed by Moore and Kelley[102] show a steady increase of c_P with temperature with a deviation of the order of 43% with respect to the Hein and Flagella's results. The values of Moore and Kelley at high temperatures are in error due to the fact that they measured the heat content only up to 1500 K and linearly extrapolated the heat capacity at higher temperatures.

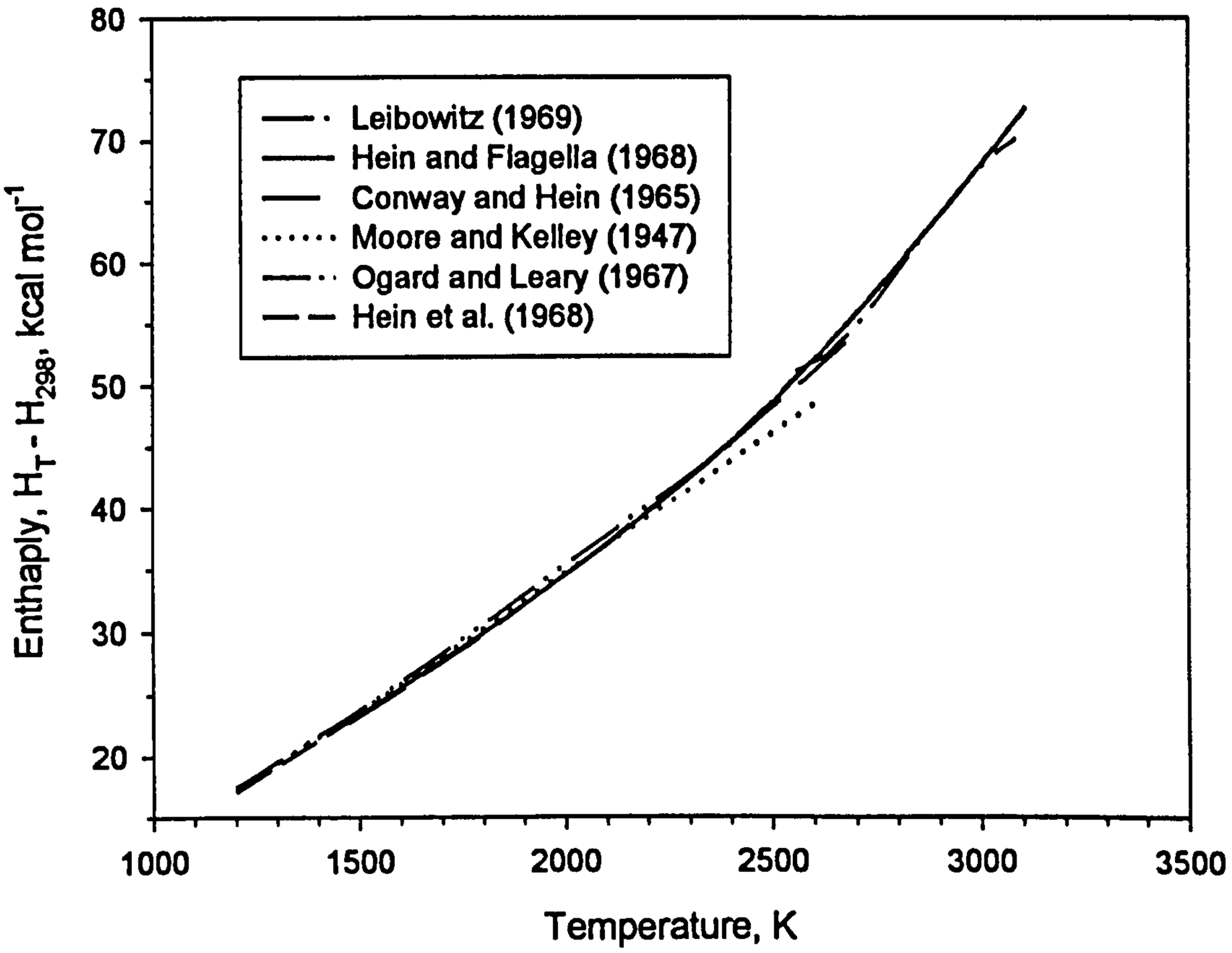

Fig. 6.8 Comparison of equations for the enthalpy of UO_2.

The mean specific heat data calculated by Hein *et al.*[2] with the formula $(H_T - H_{298.2})/(T - 298.2)$ compared with the results of Hein and Flagella, show an error of 7% at 1500 K which increases up to 40% at 3100 K.

The results obtained by Ogard and Leary[103] lie above the Hein and Flagella's specific heat values for T < 2000 K, and are lower at higher temperatures, with a discrepancy of the order of 18% at 2600 K.

Even re-fitting, globally or locally, the different enthalpy data, using different formulae, either empirical or physical, a great uncertainty remains in the specific heat values above 2000 K[109].

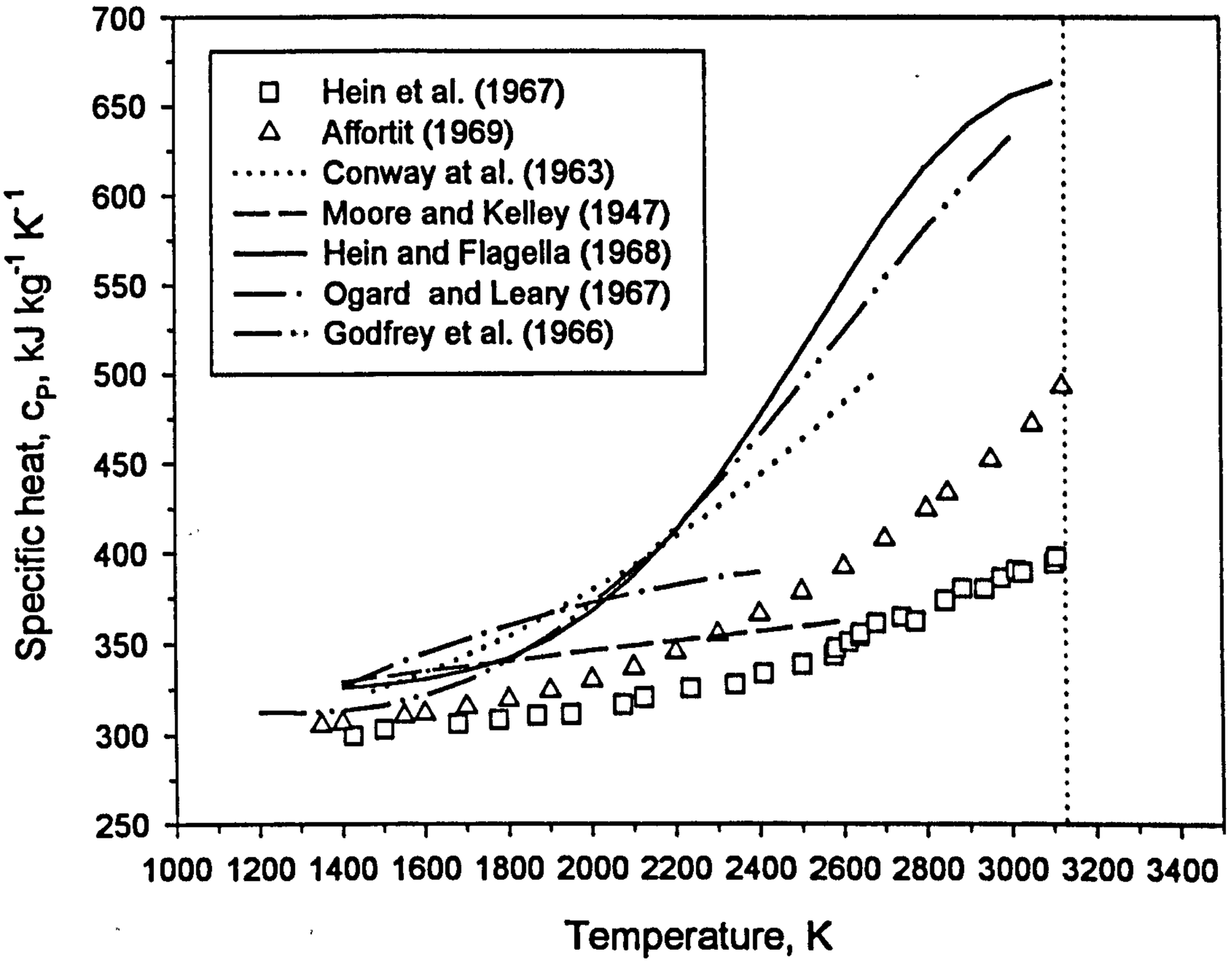

Fig. 6.9 Comparison of literature data for the specific heat of UO_2. The melting temperature of UO_2, $T_m = 3120 \pm 20$ K, is shown on the graph with a dotted vertical line.

Affortit was the only author to measure heat capacity directly, his values however, differ greatly from those of other workers, being much lower even in the low temperature range, where, generally the other literature data show a good agreement. The errors in the Affortit's measurements may be due to *i*) non-uniform temperature in the specimens, and *ii*) incongruent evaporation of the materials. The former is due to the difficulty of obtaining a uniform temperature distribution in the radial direction in refractory samples. In this kind of specimen in fact, because of the low thermal diffusivity of the material, a large temperature gradient exists in the radial direction whenever heat flows from the surface of the sample to its surroundings. Furthermore, vaporisation can dramatically affect the heat capacity measurements: actually, these authors recognise themselves that excessive sublimation occurred in the samples during fast heating.

In the last years, reviews[110,111] and critics[109] of the different works have been made, and a recommended curve has been proposed for the heat capacity up to the melting temperature[110]. Different assessments have been made, and theoretical equations have been developed to describe the observed increment of specific heat at high temperatures. However, due to the lack of experimental values above 2700 K, the question whether at temperatures above the Bredig-transition the specific heat of uranium dioxide is constant or continues to increase was still open[107].

In Fig. 6.10 the results for specific heat are compared with the recommended curve given by Fink[112] and by the JANAF database[113].

From the analysis[89] of the empirical c_P data at T > 2000 K (temperatures at which the lattice harmonic vibrational modes are certainly saturated), the increase of the heat capacity of stoichiometric UO_2 is interpreted as principally due to synergistic Frenkel-pair formation, which, between 2600 K and 2700 K, culminates in an order-disorder lambda-transition in the anion sub-lattice. Above this transition, in a temperature range where experimental measurements of c_P are less precise, it was until now uncertain whether other thermally activated mechanisms (*e.g.* small polaron formation, anharmonic vibrations, Schottky-trios formation) might sustain a further increase in the specific heat. For instance, in the above-mentioned review by Fink, a *constant* specific heat (620 $Jkg^{-1}K^{-1}$) is proposed between 2700 K and the melting point. Actually, since before the present measurements the specific heat at high temperature could only be calculated from the temperature-derivative of the enthalpy, any parametrical fitting of the few available measurements of *H(T)* above 2700K by functions other than linear was statistically meaningless.

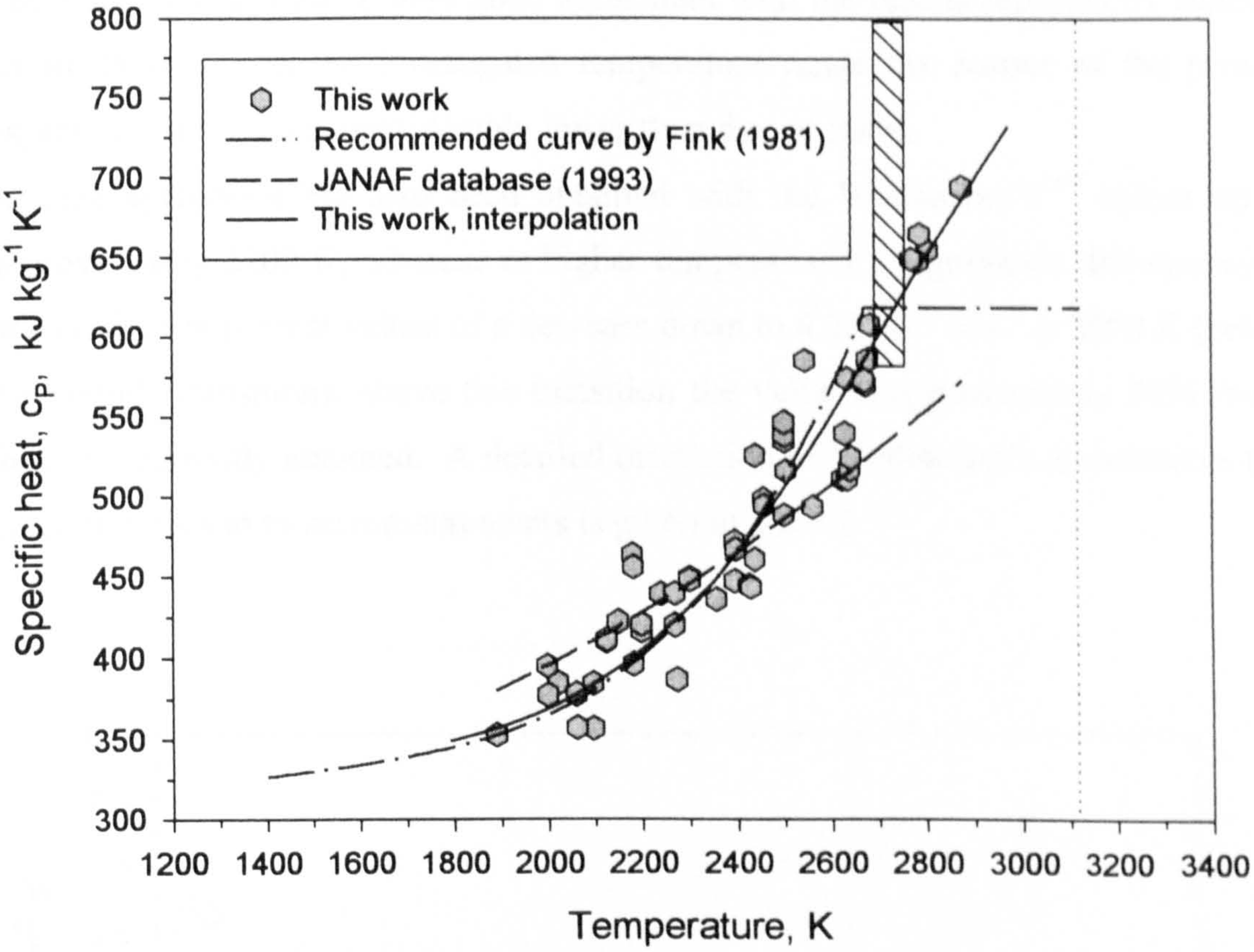

Fig. 6.10 Comparison of the experimental results with recommended curves for the specific heat of UO_2. The lambda-transition temperature, T_B = 2670 ± 30 K, and the melting temperature, T_m = 3120 ± 20 K, are shown on the graph with a dashed zone and a dotted vertical line, respectively.

The present measurements, above the lambda-transition and in the temperature range between 2700 K and 2900 K, indicate a further increase of c_P from 600 to 700 Jkg^{-1}K^{-1}. The value at 2800 K is slightly *above* the value given by the derivative of the empirical enthalpy *vs* temperature curve of Hein and Flagella[3] (630 Jkg^{-1}K^{-1}), and *below* a recent theoretical prediction[89] (740 Jkg^{-1}K^{-1}).

6.3.2 *Thermal diffusivity*

A comparison of the thermal diffusivity results at high temperatures with literature data obtained using the laser pulse technique[114,115] is presented in Fig. 6.11.

The measured data are in very good agreement with the results reported by Bates[115] up to 2800 K. In the investigated temperature range the scatter of the present experimental results is considerably lower than that of Bates.

A good agreement has also been obtained with the Weilbacher's[114] values up to approximately 2200 K, whereas at higher temperatures a significant discrepancy is observed. The present values of *a* decrease down to 4.25 10^{-7} m^2s^{-1} at 2600 K (below the lambda transition); above this transition the value is approximately 30% *lower* than that currently assumed. A detailed discussion of Weilbacher's experiments and possible errors in those measurements is given in § 6.4.2.

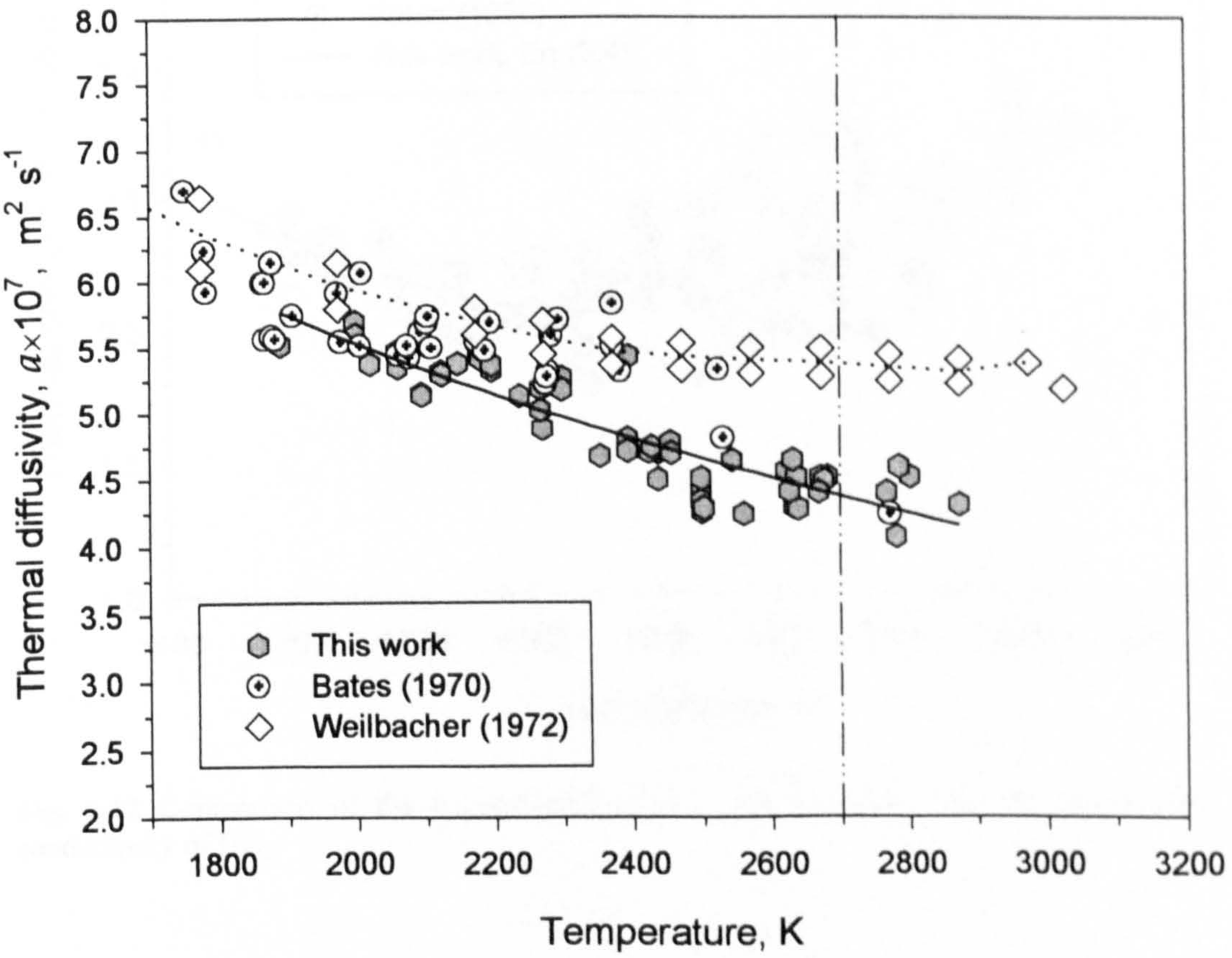

Fig. 6.11 Comparison of the experimental results with literature data for the thermal diffusivity of UO_2. The interpolation of the present experimental results is shown with a solid line, the interpolation of the Weilbacher's data with a dotted line. The lambda-transition temperature, $T_B = 2670 \pm 30$ K, is shown on the graph with a dashed–dotted-dotted vertical line.

6.3.3 *Thermal conductivity*

The thermal conductivity values at high temperature are compared with the recommended literature data in Fig. 6.12. The reported values in literature have been directly measured by radial heat flow method (Stora *et al.*[116] and Kolyadin *et al.*[117]) and calculated from measured thermal diffusivity values (Bates[115]).

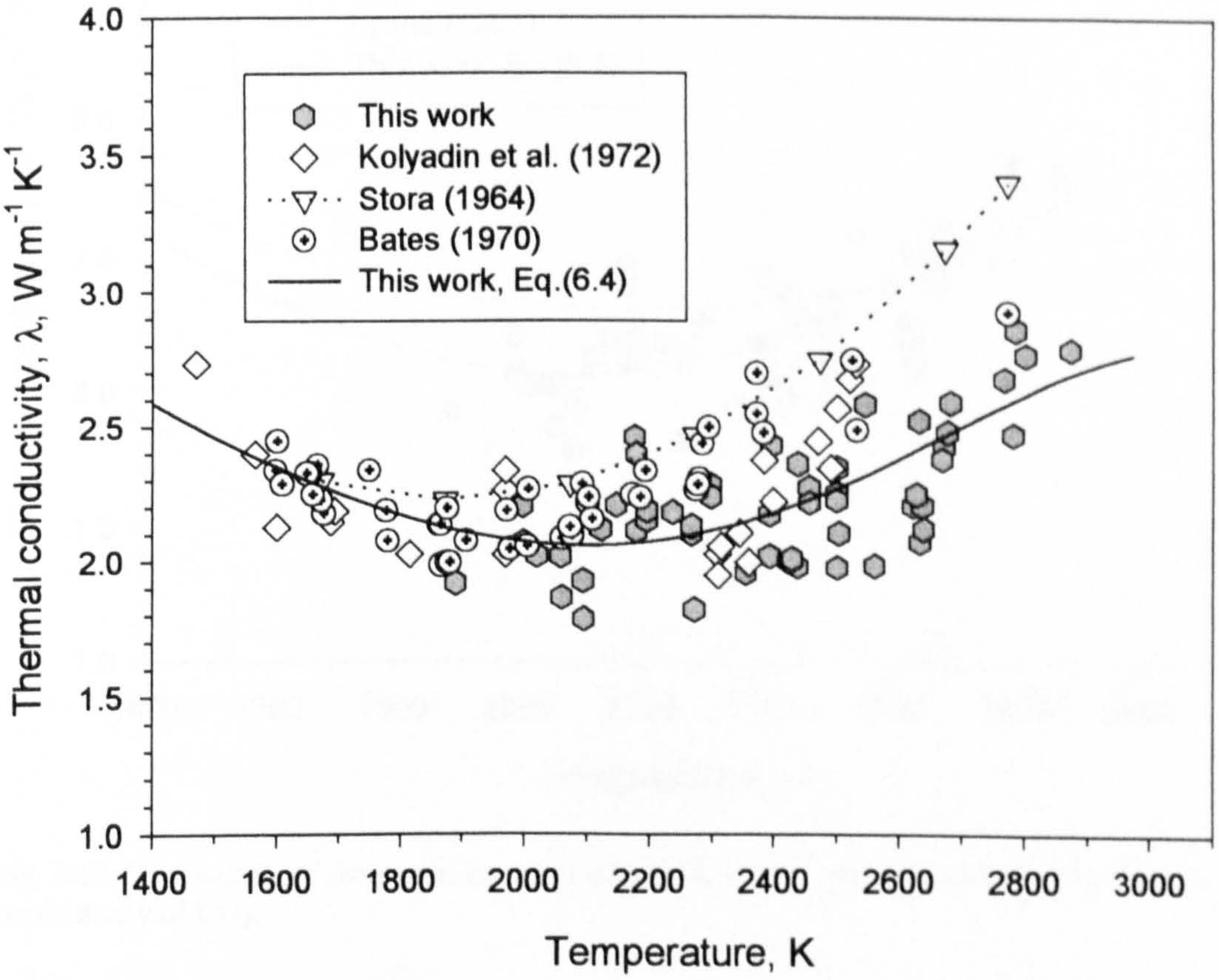

Fig. 6.12 Comparison of the experimental results with literature data for the thermal conductivity of UO_2.

The results are in good agreement with the values reported by Kolyadin[117] and Bates[115] over the whole temperature range studied, and with the values reported by Stora *et al.*[116] (presently recommended) up to 2200 K. The resulting conductivity above 2200 K is *lower* than that recommended.

The thermal conductivity values are in agreement (Fig 6.13) with those calculated by Gyllander[118] and slightly above those obtained by Lyons *et al.*[119] in their in-pile measurements.

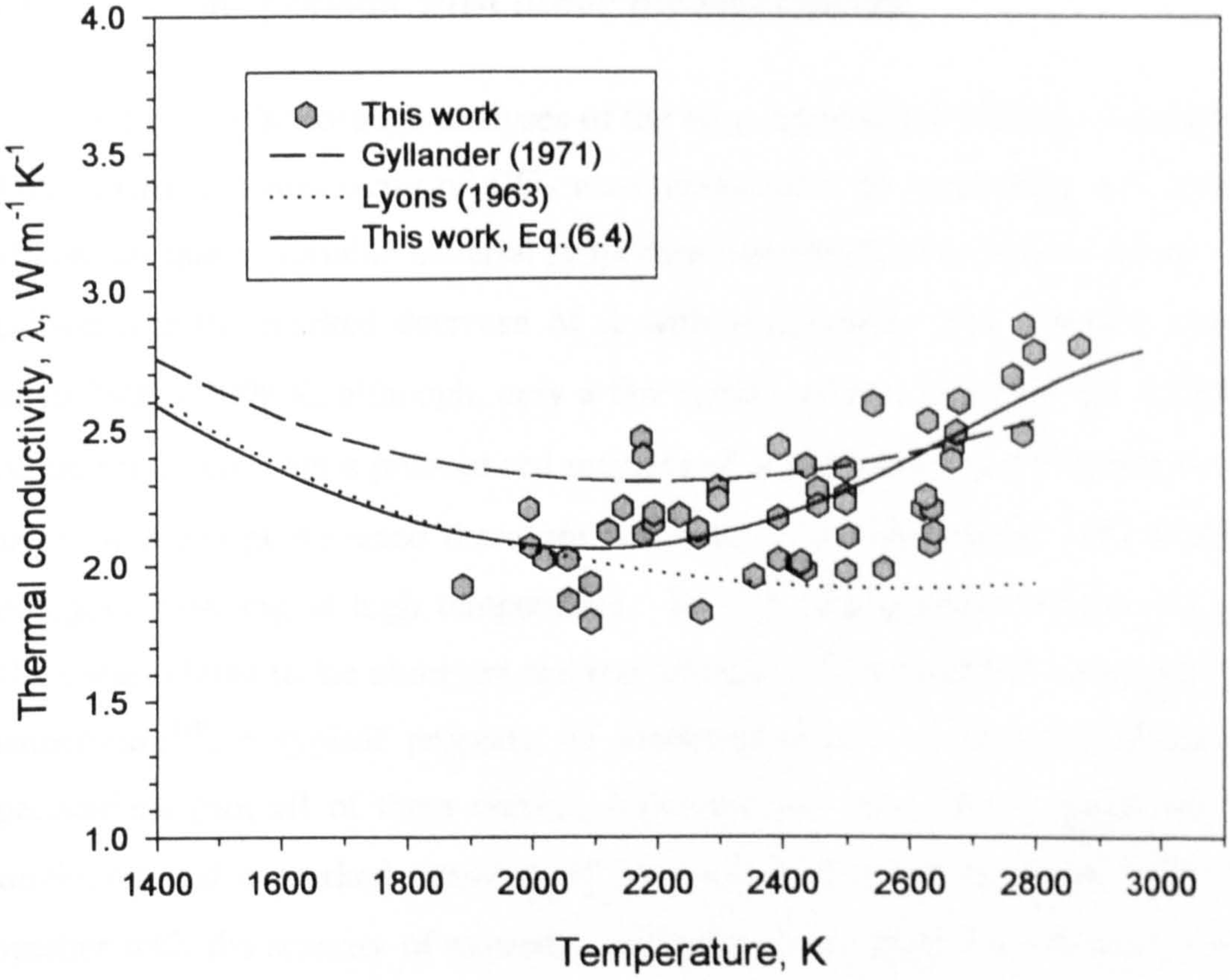

Fig. 6.13 Comparison of the experimental results with in-pile measurements for the thermal conductivity of UO_2.

From a critical analysis of a, and c_P, and considering the variation of the density with temperature, is it possible to extrapolate the value of λ at the melting point (3120 ± 20K). Between 2700 K and 2900 K the measured values of a are stationary within the error band, and - as it will be discussed in Section 6.5- a drastic increase between 2900 K and 3120 K is improbable. Considering the uncertainties[107] in the differentiation of the available enthalpy data by Hein and Flagella[3], a fractional increase of c_P of no more than 10% is expected in the same interval. Finally, between 2900 K and 3120 K the extrapolated solid density decrease calculated with

Eq.(6.1) is less than 2%. Therefore, it can be concluded that the value of the solid conductivity at the melting point should *not exceed* 3.5 $Wm^{-1}K^{-1}$.

6.4 Comparison with other measurements

In the 1970's thorough analyses of the large number of available measurements of the thermal conductivity of UO_2 were undertaken by separating out systematic differences due to variable material properties from those of a random nature. It was realised that the marked decrease of λ with temperature was strongly attenuated above 1800 - 2000 K; although, only a few measurements indicated the existence of a clear minimum with a pronounced increase of λ at higher solid temperatures. The matter was intriguing since there are not many materials whose $\lambda(T)$ exhibits an analogous upswing at high temperature. In UO_2, the possible occurrence of this effect was related to the observed marked increase of the electrical conductivity with temperature[120], a typical property of semiconductors. A number of theoretical speculations (not all of them correct, however) led most of the specialists to the conviction that a marked upswing of λ was indeed to be expected. This belief, together with the scarcity of experimental data at very high temperatures, led some theoreticians, as well as the authors of certain review papers, to give more weight to measurements, which appeared to confirm this trend. Two sets of measurements, which corroborated each other, did eventually play a key role in the development of world-wide recommended λ databases and associated interpolating functions: the first was that of Stora *et al.*[116], and the second that of Weilbacher[114]. Both measurements were carried out with different standard methods, so that there was no reason to doubt either their correctness, or the reported errors. To add credit to these high-temperature measurements, there was also the fact that results obtained at lower temperatures by the same authors using the same equipment were in perfect agreement with other data obtained in different laboratories.

Yet, after examining the present results and the experimental conditions under which they have been obtained, and after considering the most conservative limits of their

errors, it may be concluded that some uncontrolled effects must have perturbed the measurements of Stora *et al.* and Weilbacher at very high temperatures.

The experiment of Stora *et al.*

Up to now, direct thermal *conductivity measurements of ceramic materials at temperatures higher than 2000 K* could only be realised by using the radial heat flow method, whose merits and limits have been discussed in § 2.2.3. The apparatus of Stora *et al.*[116] was based on this principle. In the case of UO_2, sublimation and mechanical deformations make it virtually impossible to maintain this material at temperatures near the melting point for sufficiently long times: thus, the highest temperature attainable by the radial method was found to be approximately 2500 K[117,121]. Since the temperature of the inner surface of the cylindrical sample cannot be very close to the melting temperature, the highest achievable reference temperature is usually significantly lower than the melting point. The measurements of Stora *et al.* above 2500 K on pellet stacks should, therefore, be treated with caution. In fact, in these experiments the highest conditioning temperatures were obtained only by means of the central heater - with no effective thermal screens - so that, when the highest temperature on the inner surface reached ≈ 2800 K, the temperature on the outer surface was only 600 K. Finally, the measurement point closest to the inner surface of the sample was at a radial distance of 2.5 mm, corresponding to a temperature 1000 K lower than the nominal highest reference temperature. Since the temperature of the inner pellet hole could not be measured directly, this was deduced by performing a complicated temperature calibration and extrapolation procedure. Consequently, the measurements of λ were actually obtained by an *indirect* method.

The greatest source of systematic error in the λ measurements of Stora *et al.* was almost certainly the evaluation of the local gradient. This is confirmed by other similar experiments. For instance, in 1967 Susnik and Runfors[122] carried out thermal conductivity measurements using the same method, in the Studsvik Laboratory. In this case, the temperature was measured pyrometrically through small radial holes of

different depths. One of the original reports on this work is particularly interesting since it contains a detailed ceramographic analysis of the sample after the experiment, which shows the important effects of thermal restructuring on the temperature profile in the sample. In this report it was recognised that a substantial correction was necessary to account for the real position of the temperature measurement points after restructuring. In the absence of this correction, the conductivity is greatly *overestimated*. According to the Studsvik experiments, λ in the temperature interval 2200-2800 K should be in the range 2 ± 0.4 $Wm^{-1}K^{-1}$.

The experiment of Weilbacher

Weilbacher, using a laser-flash method[114], measured the thermal diffusivity of UO_2 up to 3000 K, obtaining values approximately 30% higher than the present results. His device was constructed according to the conventional laser-flash standards. The diffusivity was evaluated from the pulse rise-time formula, to which the customary "Cowan correction" was applied (see Section 3A.2.1). This correction takes into account radiation losses, and is expected to be less sensitive to laser-power heterogeneity than the alternative "Taylor's correction". The paper of Weilbacher on this subject[114] is very concise and does not present any original high-temperature thermogram however, from a somewhat more detailed description of these experiments[123] two criticisms can be made:

1) As shown above, in laser-flash diffusivity measurements the front-surface layer is subjected to a rapid temperature rise of, usually, a few hundreds of degrees above the reference temperature. For this reason, even in this method, the sample reference temperature has to be kept significantly lower than the melting temperature. Weilbacher claimed to have carried out thermal diffusivity measurements up to near 3000 K. Unfortunately, this important aspect is not discussed in his papers. From the parameter values reported by this author (rear-surface temperature rise =10 K, laser time-pulse =150 μs, specimen thickness =0.5 mm, energy =10 J) however, is it possible to calculate the amplitude of the front-surface temperature rise in his experiments. The

expected temperature rise of the front surface is *at least 300 K*. It must, therefore, conclude that, at the highest temperatures reported by Weilbacher, the instantaneous temperature rise of the *front* surface of the sample actually *exceeded* the melting point. If this were indeed the case, the *rear* temperature response, used for evaluation of thermal diffusivity, would have been considerably perturbed by liquid formation.

2) The sample disk was positioned vertically on the axis of a relatively short tube heated by high frequency induction. It is well known that such a set-up entails, at high temperatures, a marked imbalance between the large radiation losses from the base surfaces of the disk and the small lateral surface facing the heater, causing a negative temperature gradient both in the radial and axial directions. An observation reported by Weilbacher himself seems to confirm this conjecture: he tried to measure the sample emissivity (which at that time was unknown) by measuring the brightness temperature of a thick (15 mm) sample, first inside a 10 mm deep hole and then on the adjacent external base surface. Assuming that the two real temperatures were equal, he deduced an emissivity of 0.6 for an 800 nm wavelength - and used this value for further temperature measurements. Furthermore, he found that the apparent emissivity slightly *decreased* with temperature. Meanwhile, the emissivity of UO_2 has been measured with good accuracy up to above the melting point[94,124], and its value at T >2000 K is approximately 40% higher than that deduced by Weilbacher, and actually *increases* with temperature. In other words, during Weilbacher's experiment, the temperature in the hole was more than 100 K higher than on the surface. In the given set-up, the existence of an axial gradient entails that in each cross-section the surface is hotter than the centre. During the pulse, this positive radial heat flux attenuates the cooling slope of the thermogram, and hence reduces the extent of the (negative) Cowan correction, leading to *over* evaluations of the diffusivity[xxvi]. Actually, it is

[xxvi] In fact, in cases where substantial radial heat losses are present, the Cowan correction is too large, and produces under-evaluation of the thermal diffusivity. The failure of the Cowan method is characterised by a marked discrepancy from the Taylor correction, which in these cases produces better results. This effect can be also verified by applying the corrections on theoretical thermograms

worth noting that the few diffusivity measurements of Bates between 2400 and 2800 K (carried out in the course of the "Round-Robin" programme of 1969) are nearer to those presented in this work. Although Bates used the same method as Weilbacher, his long resistance furnace provided a *much more uniform* temperature distribution in the sample.

In the absence of the original thermograms, it is difficult to estimate the systematic errors of these old measurements. It is, however, probable that they were due to the inadequacy of the analysis to the pulse experimental conditions, which could be realised at that time.

6.5 Result overview

In order to obtain a full overview of the thermal properties of UO_2, in this section the new high temperature measurements are connected and compared to the measurements at lower temperatures and to the measurements related to the lambda transition.

Specific heat

It was mentioned above that the new measurements of the specific heat up to ~2600-2700 K are in good agreement with present recommendations, but diverge at higher temperatures, necessitating a revision of the current views on the physical heat absorption mechanisms. Actually, at temperatures above 2700 K the effects of the lambda-transition should be negligible[125] (its peak is only 20-30 K wide); therefore the further increase of c_P must be connected to the creation of a different type of defects, very likely small polarons or Schottky defects. The value of c_P measured at 2850 K is only 10% higher than that previously measured just below the melting point, using a more sophisticated laser heating technique, requiring a more

---

accounting for both axial and radial heat losses. The opposite effect occurs when, instead of a radial heat loss, a gain is present.

complicated analysis[126]. Therefore, the high value of c_P in the vicinity of the solidus confirms the existence of a pronounced fall of the heat capacity across melting.

Thermal diffusivity

Thermal diffusivity measurement of UO_2 were carried out in the temperature range 550-1100 K using a different device (LAF), enabling a very high accuracy to be obtained. These measurements are plotted in Fig. 6.14 together with the results obtained at high temperatures with the CLASH apparatus. It can be seen that the values measured at high temperatures appear to join smoothly with the thermal diffusivity values obtained at lower temperature. All the data obtained were thus merged and fitted by an inverse function of temperature by means of the least square method. The best fit was given by the equation:

$$a = \frac{1}{1.30 \cdot 10^5 + 8.099 \cdot 10^2 T} \quad (m^2 s^{-1}) \tag{6.3}$$

where T is in K.

In Fig. 6.15 the inverse of the thermal diffusivity and the linear interpolation of the obtained data are plotted. The deviations of the thermal diffusivity values from the fitted function expressed by the inverse of Eq.(6.3) are generally less than 2% and 5% at low and high temperature, respectively. From the graph it can be seen that for T<2600 K the high temperature measurements are reasonably well aligned with the extrapolation of the straight line defined by the low temperature points. Above the lambda-transition, however, the measured $1/a$ values fall below this line. Unfortunately, the scatter of the experimental points above 2700 K does not enable a deduction of a clear trend, so that it can only be assumed that between 2700 and 2900 K the variation of $1/a$ is less than 10%.

For comparison, Fig. 6.16 shows the inverse diffusivity data of Bates and of Weilbacher. The full line indicates the best fit given by Bates for of all his measurements up to approximately 1800 K, performed in the frame of the "Round Robin" programme[115]. It can be seen that at high temperatures the values are more

scattered, displaying a negative deviation with respect to the straight line defined by the low temperature measurements - although at the highest temperatures this deviation reduces somewhat. In the same figure are also shown the inverse diffusivity values obtained by Weilbacher, which are seen to lie well below the same straight line.

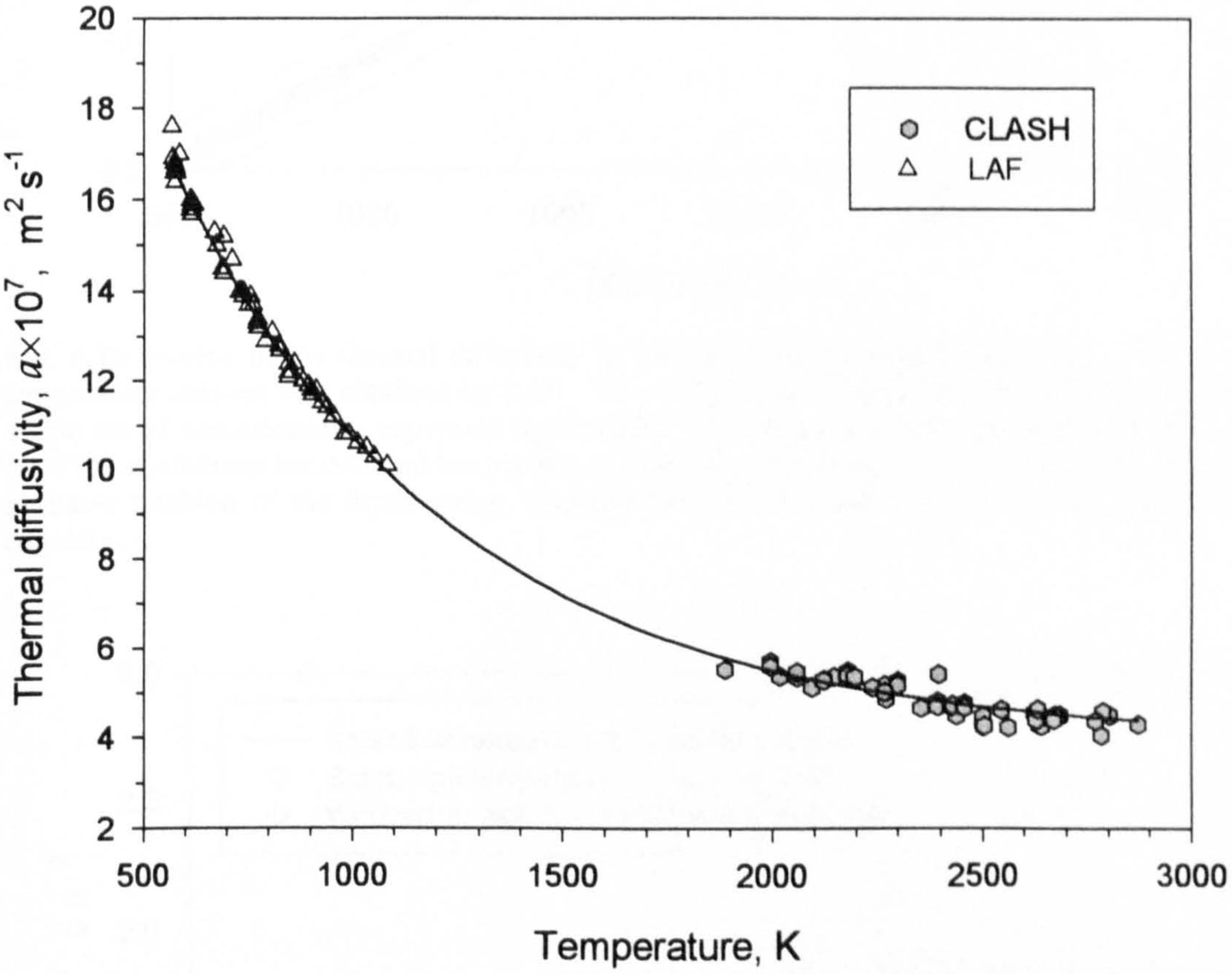

Fig. 6.14 Thermal diffusivity of UO_2 as a function of temperature. The low temperature data-set was obtained by LAF. The solid line represents the data interpolation to Eq.(6.3).

The linear dependence on temperature of the present *1/a* data over the whole measurement range is very interesting[xxvii], and will be examined in some more detail in Section 6.7.

[xxvii] The proportionality of *1/a* to temperature is a prediction of the anharmonic phonon scattering theory in simple lattices. The result holds only for temperatures above the Debye temperature, Θ_D, which in UO_2 is approximately 500 K.

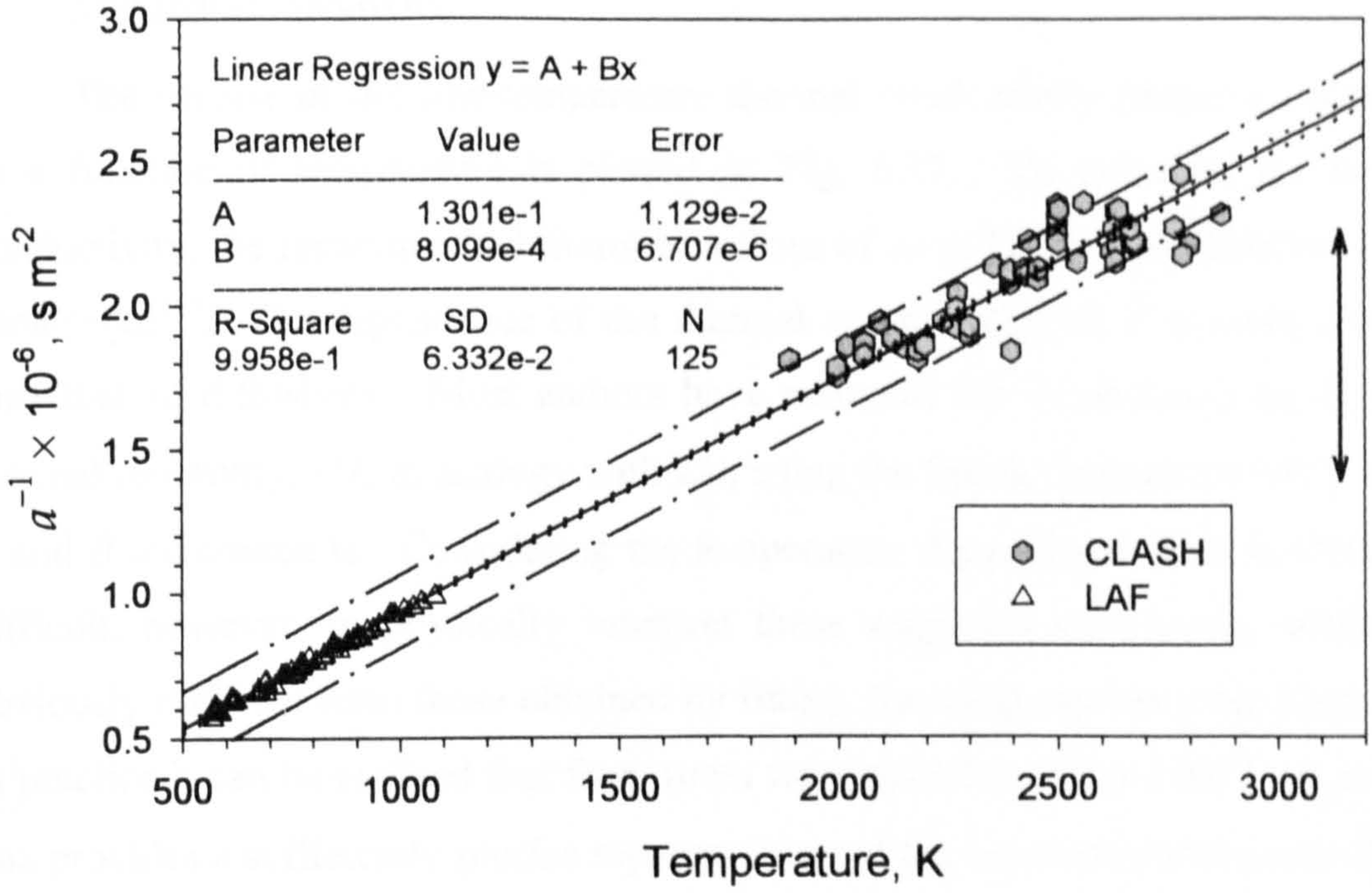

Fig. 6.15 Inverse of the thermal diffusivity of UO_2 as a function of temperature. The low temperature data-set was obtained by LAF. The solid lines represents the linear fitting of the whole set of measurements, expressed by Eq.(6.3). The dotted and dashed-dotted lines define the 95% confidence interval and the prediction interval, respectively. The arrow indicates the probable position of the liquid value, deduced from the thermal conductivity and the heat capacity.

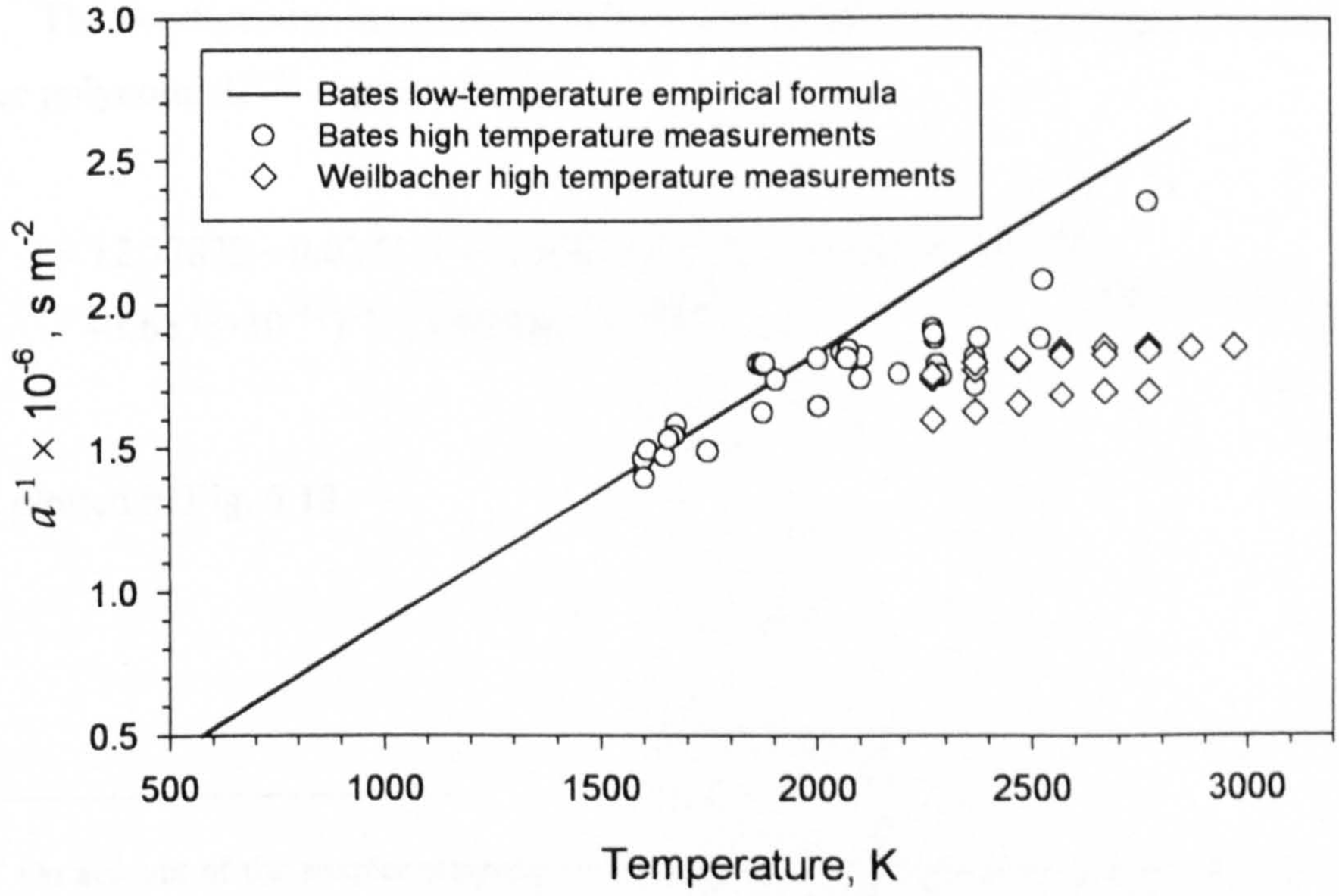

Fig. 6.16 Inverse of the thermal diffusivity values measured by Bates and by Weilbacher, as a function of temperature. The solid line represents the best fitting of the *low temperature* measurements of Bates.

Thermal conductivity

The inverse of the low-temperature thermal conductivity (thermal resistivity) as a function of temperature is plotted in Fig. 6.17. To calculate the thermal conductivity, the recommended literature values of c_P at low temperature have been considered[110]. The dependence of the thermal conductivity on T is more complex than that of diffusivity. Most authors have analysed the dependence on T of the thermal resistivity, $1/\lambda$, in analogy with $1/a$, using the fitting function $(A+BT)$, where A and B are constants. Considering the temperature dependence of c_P in UO_2, it is difficult, however, to physically interpret these empirical parameters, which are obviously different from those obtained by fitting $1/a$ using the same function. Yet, in practice it can be realised that from room temperature to 1500-1600 K, a straight line provides a sufficiently precise representation of the experimental data of $1/\lambda(T)$. This line is usually interpreted as the thermal resistivity due to phonon-phonon and phonon-impurity scattering.

The optimal interpolation and extrapolation of the empirical data at higher temperatures is, however, problematic, since the uncertainties of the heat capacity and of the diffusivity are of the same order of magnitude.

The conductivity measurements have been, therefore interpolated with a fifth-order polynomial[xxviii] expressed by:

$$\lambda = 12.57829 - 0.02311T + 2.36675\cdot10^{-5}T^2 - 1.30812\cdot10^{-8}T^3 + 3.6373\cdot10^{-12}T^4 - 3.90508\cdot10^{-16}T^5 \quad (\mathrm{Wm^{-1}K^{-1}}) \quad (6.4)$$

and plotted in Fig. 6.18.

[xxviii] On account of the simpler temperature dependence as well as of the discussed bounds of the quantities ρ, c_P and a, here the values of the conductivity obtained from the equation $\lambda=\rho\, c_P\, a$, are fitted, where the three quantities at the right hand side are given the respective empirical interpolating curves. An alternative interpolation of the individual, independent values $\lambda^k=\rho c_P{}^k a^k$, $k=1...N$, would introduce an irrealistic uncertainty in the extrapolation of the fitted polynomial at high temperatures.

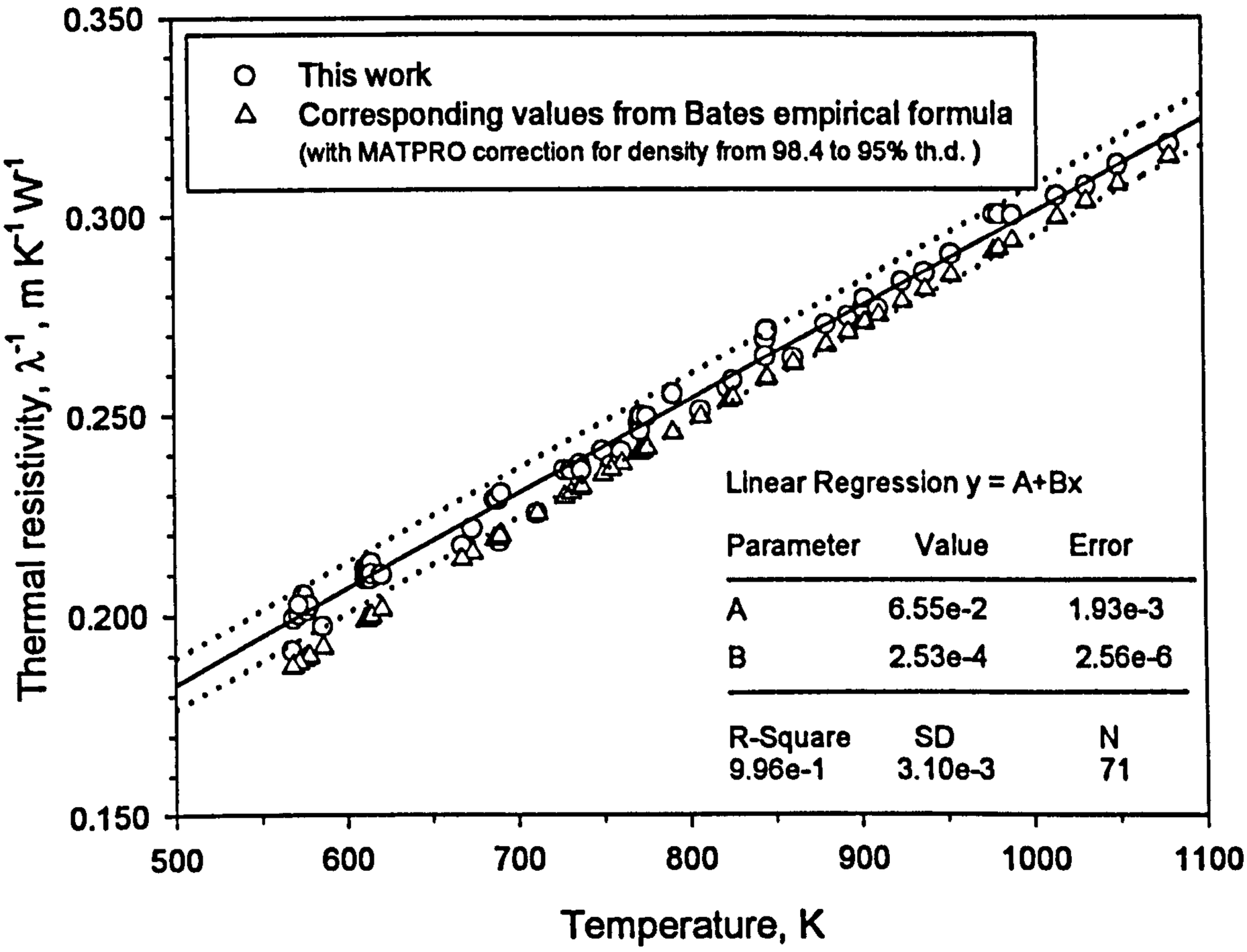

Fig. 6.17 Measured low temperature thermal resistivity as a function of temperature compared with the values calculated from the interpolating formula of Bates, and corrected for the difference in sample density. It can be seen that, between 500 K and 1100 K, there is a good agreement between the two data set. The dotted lines represent the 95% confidence interval.

The high order of polynomial (6.4) entails a large uncertainty band in the extrapolated range from 2900 K to the melting point. In fact two extremes can be reasonably calculated, between which the real value of λ should fall. The upper one is obtained (*i*) by assuming a linear extrapolation of c_P, which gives approximately 800 $Jkg^{-1}K^{-1}$ at 3120 K, and (*ii*) by a constant extrapolated value of the diffusivity ($4.5\ 10^{-7}\ m^2s^{-1}$): the resulting thermal conductivity is in this case 3.5 $W\ m^{-1}K^{-1}$. The lower limit is realised by a linear extrapolation of $1/a$, and a constant c_P (700 $Jkg^{-1}K^{-1}$) at temperatures above those reached in the present experiments: the corresponding conductivity is 2.4 $Wm^{-1}K^{-1}$. It can be thus concluded that:

$$2.4 \leq \lambda_{T_m} \leq 3.5 \qquad (Wm^{-1}K^{-1})$$

values which are not too far from that of liquid UO_2 measured by Tasman[127,157]. The conservative lower and upper limit for the conductivity at the melting point are plotted in Fig. 6.18 with two solid dots at 3120 K, the probable position of the conductivity of liquid UO_2 is indicated in figure with an arrow.

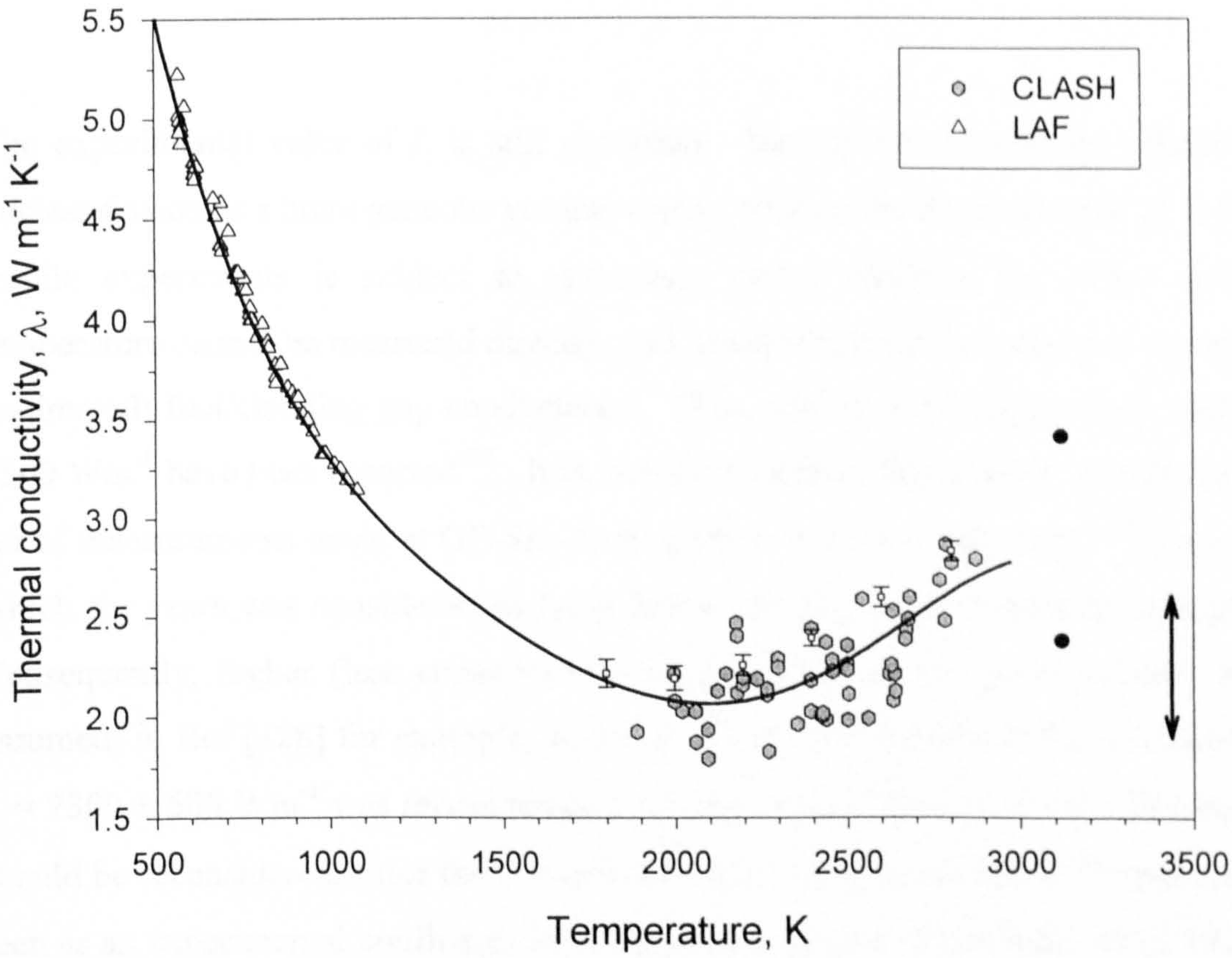

Fig. 6.18 Thermal conductivity deduced from the experimental measurements. The bars correspond to the theoretical calculations (see Section 6.7). The arrow indicates the probable position of the conductivity of liquid UO_2. The solid line represents the empirical interpolation curve given by Eq.(6.4). The two solid dots at 3120 K represent, respectively, the conservative lower and upper limit for the conductivity of the melting point.

Finally, some words are in order here on the conductivity integral

$$L = \int_{773K}^{T_m} \lambda(T)dT \tag{6.5}$$

which represents the reactor linear power at which melting starts on the centre line of a cylindrical fuel pellet whose outer surface is assumed to be at a reference temperature of 773 K. Using the polynomial fit (Eq.(6.4)) to the new thermal conductivity values, Eq.(6.5) gives:

$$L = 6080 \;{}^{+500}_{-300}\; Wm^{-1}.$$

The experimental value of L is still uncertain. Despite the advantages offered by nuclear fission as a homogeneous volume energy source, the determination of L from in-pile experiments is subject to systematic errors, because the pellet surface temperature cannot be measured directly, and, therefore, must be calculated using the (estimated) fuel/cladding gap conductance. Thus, values of L ranging from 5500 to 7500 Wm^{-1} have been reported[128]. It is, however, noteworthy that the most complete set of measurements made at GE-San Jose' gives $L = 6300 \pm 300$ Wm^{-1} [129] - a value which for years was considered as lying below the laboratory determinations of L; Consequently, higher (less conservative) in-pile values of the power-to-melt were assumed; in Ref [128] for example, based on AECL and Battelle NWL evaluations, $L = 7300 \pm 500$ Wm^{-1} was recommended. In the light of the new results this matter should be reconsidered, since the GE data now appears to be plausible[xxix], and can be seen as an experimental confirmation of the weak increase of conductivity of UO_2 at high temperatures under in-pile conditions.

[xxix] It should be reminded that an important source of discrepancy in the evaluation of L is the assumption by the various authors of essentially different metallographic features as markers for the melt boundary. The criterion adopted by the GE team is that complete densification observed after freezing is a sufficient indication for melting occurrence (a *more restrictive* claim that, under in-pile heating conditions, a necessary feature for inferring presence of melting in UO_2 pellets is the formation on freezing of radial basaltic textures).

6.6 Analysis of the underlying physical mechanisms

6.6.1 *Introduction and overview*

As already discussed in the earlier sections, a considerable work has been carried out in the last 40 years to analyse the different mechanisms of heat transport in UO_2, and to derive an expression that describes the temperature dependence of thermal conductivity of stoichiometric and non-stoichiometric material up to the melting point (solidus). Up to 1800 K, the data is well described by the *1/T* dependence, characteristic of *lattice* conduction. Above this temperature, however, the experimental curve flattens out, and even rises when the temperature is further increased above 2000 K. This increase was initially attributed to transport by *radiation*[130], but this could not be quantitatively confirmed with the data then available. Somewhat later, the increase was attributed[120,131] to the so-called *ambipolar* contribution associated with electron- hole pairs, which start to dominate the intrinsic electrical conductivity of the material above about 1200 K[132]. This, and all subsequent estimates (*e.g.* Refs.[133] and [134]) were based, however, on an expression that is valid for the thermal conductivity of a *conventional* semiconductor, in which electrons and holes moves in energy *bands*.

Subsequently, with the advent of more experimental data permitting the various contributions to be better quantified, several reviews on the topic appeared, together with recommended conductivity values up to the melting temperature (*e.g.* Refs.[107] and [135]).

In 1983, attention was drawn to the fact that the electrical charge carriers in UO_2 are *not* electrons and holes, but rather small polarons which move by hopping from cation to cation[136]. This necessitated a modification of the form of the ambipolar contribution, and, in turn, reconsideration of how well the sum of (independently evaluated) contributions described the then available data. It should be noted that the small polaron form of the ambipolar contribution was subsequently incorporated into various recommendations (*e.g.* Ref.[137]).

The above mentioned discrepancy (§ 5.3.3) between the up to now available data and that obtained in the course of the present work, necessitates now that the

analysis of Ref.[136] must be reconsidered.

Before doing this, however, it is appropriate to give a short overview of the various contributions to the thermal conductivity identified above - namely:

1) phonon or lattice conductivity, $\lambda_L(T)$,
2) small polaron conductivity, $\lambda_{AP}(T)$,which for T > 1500 K dominates that from extrinsic sources, *e.g.* to non-stoichiometry,
3) radiative or photon conductivity.

Lattice thermal conductivity

The lattice thermal conductivity $\lambda_L(T)$, of (stoichiometric) UO_2 is expressed by

$$\lambda_L = \frac{1}{A+BT}, \tag{6.6}$$

where the "extrinsic" term A incorporates the phonon scattering by lattice imperfection of various kind (impurities, isotopes, dislocations, vacancies and all kind of defects which affect the periodicity of the lattice by creating local density changes), whilst the term BT characterises the "intrinsic" contribution arising from anharmonic phonon-phonon interaction (three phonon model).

Small polaron thermal conductivity

In consequence of the *hopping* character of the small polarons in UO_2, their *ambipolar* contribution, $\lambda_{AP}(T)$, to the thermal conductivity of the material is given by[136]

$$\lambda_{AP}(T) = \frac{1}{4}\left(\frac{U}{e}\right)^2 \frac{\sigma(T)}{T} \tag{6.7}$$

where U is the activation energy for the formation of electron-hole pairs (out of the Mott insulating ground-state) which can be expressed as:

$$U \equiv 2(\varepsilon_i - \varepsilon_x) \tag{6.8}$$

where ε_i and ε_x are, respectively, the activation energy (in *eV*) of the intrinsic σ_i, and extrinsic σ_x, *d.c.* electrical conductivity.

Radiative thermal conductivity

The transfer of heat through a medium by radiation is given by

$$\lambda_R = \frac{16\sigma_S n^2 T^3}{3\alpha(\lambda,T)} \tag{6.9}$$

where , σ_S is the Stefan-Boltzmann constant, n is the index of refraction, and α is the absorption coefficient. As shown by Stoddard and McCormick[138], and Anderson[139], if the wavelength and temperature dependence of the refractive index are neglected, and $\alpha(\lambda, T)$, – where λ is the wavelength - is replaced by an appropriate average, $\alpha_R(T)$, over the Planck distribution of the radiation, Eq.(6.9) can be written as:

$$\lambda_R = \frac{0.003 n^2 T^3}{\alpha_R(T)} \tag{6.10}$$

Each of these contributions will now be considered more quantitatively, starting with the radiative.

6.6.2 *The radiative thermal conductivity*

Of the three thermal conductivity contributions considered in Ref.[136] the estimate of $\lambda_R(T)$ was the most uncertain, due to a lack of data (at the time) on the spectral absorption of polycrystalline UO_2 at the temperatures of interest

(T > 1000 K). Subsequently available absorption data[140] for *molten* UO_2 (measured for the first time in the same period) became available, permitting a first estimate of the radiative contribution in the liquid to be made. This was found to be much lower than that previously estimated for solid UO_2 - which were *already much smaller* than those of λ_L and λ_{AP}. Given the additional sources of scattering which are operative in polycrystalline, solid UO_2 - in particular, that due to grain boundaries - the values of $\lambda_R(T)$ must here be even smaller than in the liquid, and will - from now on - thus be *completely neglected* in comparison with λ_L and λ_{AP}.

6.6.3 *The small-polaron thermal conductivity*

The expression given for $\lambda_{AP}(T)$ in Ref.[136] and derived from Eq.(6.7) was based on the electrical conductivity expression given by Killeen[134], who fitted his own experimental data with the equation:

$$\sigma(T) = \sigma_o e^{-\varepsilon'/kT} \tag{6.11}$$

The T-dependence of $\sigma_1(T)$ used in Eq.(6.11) however, was actually *inconsistent* with the non-adiabatic nature of the hopping transport in which the small polarons participate. Theoretical work undertaken subsequent to the analysis of Ref.[136], revealed that the correct T-dependence of $\sigma_1(T)$, in both intrinsic and extrinsic regimes, is given by[141]:

$$\sigma(T) = \frac{\sigma_1}{T^{3/2}} e^{-\varepsilon/kT} \tag{6.12}$$

Refitting Killeen's electrical conductivity data on 98% dense, polycrystalline $UO_{2.0005}$ to Eq. (6.12) yields

$$\sigma_1^i = 5 \times 10^6 \ (\Omega m)^{-1} K^{3/2} ,$$

$$\varepsilon_i = 1.41\ eV \qquad (c.f.\ \varepsilon_i' = 1.07\ eV)$$

$$\sigma_1^x = 3.868\times10^2\ (\Omega m)^{-1}K^{3/2}\ ,$$

$$\varepsilon_x = 0.26\ eV \qquad (c.f.\ \varepsilon_x' = 0.14 eV),$$

whence Eq. (6.7) can be rewritten (with $t = T/1000\ K$) as:

$$\lambda_{AP}(t) = \frac{6600e^{-16.35/t}}{t^{5/2}} \quad Wm^{-1}K^{-1} \tag{6.13}$$

In consequence of the opposing T-trends of $T^{3/2}$ and $e^{-\varepsilon/kT}$, it follows that $\varepsilon > \varepsilon'$; accordingly, since λ_{AP} depends (*via* Eqs.(6.7) and (6.8)) on the *square* of the activation energy difference and $(\varepsilon_i - \varepsilon_x) > (\varepsilon_i' - \varepsilon_x')$, it is clear that, the λ_{AP} values calculated in Ref.[136] were erroneously *low*. This accounts for the necessity of having to assume, in the previous analysis, that the lattice thermal conductivity contribution, λ_L, attained a *minimum* value near 2000 K; which is then *maintained* up to melting - rather than continuing to follow the empirical $(A+BT)^{-1}$ dependence, established at temperatures sufficiently low ($T < 1500$ K) that $\lambda_L(T) \simeq \lambda(T)$. In fact, only in this way could the erroneously low values of λ_{AP} be compensated for, and the spuriously high values of $\lambda(T)$ reproduced. The converse situation holds now - *i.e.* it is required to reproduce the new *lower* $\lambda(T)$ values reported above, using the *higher* $\lambda_{AP}(T)$ values entailed by Eq.(6.13).

6.6.4 *The lattice thermal conductivity*

Given the above requirement, $\lambda_L(T)$ is now allowed[xxx] to *continue* to follow the

---

[xxx] In view of the objections [M. C. Roufosse and P.G. Klemens, *J. Geophysical Research*, **79**, 703 (1974)] which can be raised against a simplistic basis of a minimum λ_L involving a *single* phonon mean-free-path, $\bar{\ell}$, this must be considered rather satisfactory. In fact, consideration of the frequency dependence of $\bar{\ell}$ reveals that $\lambda_L(T)$ does *not* attain a temperature-*in*dependent minimum, but remains T-dependent, albeit with a slightly *weaker* T-dependence than $(A+BT)^{-1}$.

lower temperature $(A+BT)^{-1}$ dependence up to melting. The defining "low" temperature values of $1/\lambda$ obtained between 500 K and 1100 K - with the *same* 95% dense samples as used up to the highest temperatures - are shown in Fig. 6.17. A *linear* fitting yields a regression coefficient of 0.996, a standard deviation for $1/\lambda$ of 0.003, and the following parameterisation of $\lambda_L(t)$ (with $t \equiv T/1000\ K$)

$$\lambda_L(t) = \frac{10^2}{6.548 + 23.533t} \ (\mathrm{Wm^{-1}K^{-1}}) \tag{6.14}$$

For comparison, in Fig. 6.17 are also plotted the values of $1/\lambda$ deduced from Bates' diffusivity measurements[115] on 98% dense polycrystalline UO_2 which, although of lower precision than ours, span a much larger temperature interval. Linear fitting up to $T = 2000$ K yields a regression coefficient of 0.987 and a standard deviation of 0.02 - the associated parameterisation of λ^{Bates} being:

$$\lambda^{Bates} = \frac{10^2}{2.325 + 24.329t} \ (\mathrm{Wm^{-1}K^{-1}}) \tag{6.15}$$

Correcting[xxxi] the values given by Eq.(6.15) from 98% to 95% theoretical density, yields values essentially identical (to within 0.02 $\mathrm{Wm^{-1}K^{-1}}$) to those given by Eq.(6.14), which refer to 95% dense material.

6.6.5 *Synthesis and discussion*

Neglecting any radiative contribution, the total thermal conductivity of UO_2 is given by:

$$\lambda(T) = \lambda_L(T) + \lambda_{AP}(T) \tag{6.16}$$

[xxxi] To implement the correction, the Loeb expression was used - *i.e.* $\lambda^{100\%} = \lambda p(1-\alpha p)^{-1}$, where p is the fraction porosity, and $\alpha = 2.74\text{-}0.5t$ ($t=T/1000K$) [see R. Brandt *et al*, *"Thermal Conductivity and*

which, using Eqs.(6.13) and (6.14) , takes the form (with $t \equiv T/1000\,K$)

$$\lambda(t) = \left(\frac{10^2}{6.548 + 23.533t} + \frac{6400 e^{-\frac{16.35}{t}}}{t^{5/2}} \right) \quad (\mathrm{Wm^{-1}K^{-1}}) \tag{6.17}$$

where the difference in the value of the pre-exponential coefficient in the second term on the right hand side of Eq.(6.17) from that given in Eq.(6.13) arises from the reduction in sintered density from 98 to for 95%.

Theoretical values of $\lambda(T)$ - calculated (*via* Eq.6.17) at selected temperatures - are given in Table 6.5, where they are compared with the new values synthesised from the *experimental data* on thermal diffusivity and specific heat according to $\lambda = ac_P\rho$: the comparison is shown graphically in Fig.6.18.

It will be noted that the theoretical values of $\lambda(T)$ agree[xxxii] with the new experimental values to better than 0.2 $\mathrm{Wm^{-1}K^{-1}}$, the calculated $\lambda(T)$ values lying systematically *above* the experimental ones, but within the uncertainty band. Given this high degree of agreement, an upper limit on the value of the thermal conductivity of *solid* UO_2 (of 95% th.d.) at its melting point T_m can be rather confidently obtained *via* Eq.(6.17) as:

$$\lambda(T_m) \leq 3.1 \pm 0.3 \quad \mathrm{Wm^{-1}K^{-1}}$$

It must be noted that this calculated value falls in the centre of the band defined by the two extrapolations of the new "experimental" λ values, presented at the end of Section 6.5.

Emittance of Solid UO_2" CINDAS, Purdue University, Indiana, USA (1976) unpublished].

[xxxii] Despite this approximate agreement between the calculated and 'experimental' values of $\lambda(T)$, the situation with regards the total thermal diffusivity a ($=\lambda/c_P$ if c_P is in $\mathrm{Jm^{-3}K^{-1}}$) is *less* satisfactory, in consequence of the discrepancy between the calculated and experimental values of c_P (see Ref.[89]).

Table 6.5

Ambipolar and lattice contributions to the thermal conductivity in UO_2

T	λ_L Eq.(6.14)	λ_{AP} Eq.(6.13) (*)	$\lambda(T)$	$\lambda_{expt}(T)$
1.8	2.04	0.16	2.20	2.18 ± 0.1
2.0	1.87	0.31	2.18	2.07 ± 0.1
2.2	1.71	0.51	2.22	2.08 ± 0.1
2.4	1.59	0.77	2.36	2.18 ± 0.1
2.6	1.48	1.08	2.56	2.38 ± 0.1
2.8	1.38	1.40	2,78	2.63 ± 0.1
3.0	1.30	1.75	3.05	-
3.12	1.25	1.85	3.10	-

(*) The values of λ_{AP} given by Eq.(6.13) have been corrected (see Footnote xxxi)from 98% theoretical density (relevant to Killeen's $\sigma(T)$ data) to 95%, to which the λ_L values given by Eq.(6.14) refer.

Dr. G.J. Hyland[148] has suggested several reasons for the high-calculated thermal conductivity values:

1) The validity of the $(A+BT)^{-1}$ dependence of λ_L is restricted to 3-phonon scattering *U*-processes (including scattering of acoustic[xxxiii] phonons by optic phonons[142]) under constant *volume* conditions. Under constant pressure, however, thermal expansion introduces a contribution[xxxiv] to the thermal resistivity proportional to T^2 [143], which opposes the *T*-dependence arising from transforming the *T*-independent high temperature constant volume lattice heat capacity to constant pressure. Unfortunately, however, attempts to refit the thermal resistivity values shown in Fig. 6.17 to $A+BT+CT^2$ produced a larger error in the *B* coefficient - a typical overfitting-effect. A similar attempt on Bates' thermal resistivity values, which cover a much larger temperature

[xxxiii] Heat transport (as opposed to scattering) by optic phonons can be neglected in consequence of the very large *U/O* atomic mass ratio.

[xxxiv] The magnitude of this T^2 contribution is much larger than that due to 4-phonon processes (P.G. Klemens and D.J. Ecsedy, *'Phonon Scattering in Solids"*, ed. L.J. Challis *et al.*, p.367, Plenum Publ.,

range, produced an uncertainty in C of more than 100%, and increased the uncertainty in B from 1.2% to 6.5%. Accordingly, any departure from the constant volume $(A+BT)^{-1}$ dependence of λ_L could not be quantified from the data available.

2) The above considerations pertain to a *'perfect'* lattice, which UO_2 *ceases* to be once (oxygen) Frenkel disorder sets in at $T > 2000$ K. An additional contribution to the lattice thermal resistivity must then be anticipated proportional to $e^{-E/2kT}$, where E is the Frenkel pair formation enthalpy. A rough estimate of the magnitude of this contribution can be obtained by identifying x in the empirical expressions for the thermal resistivity, W, of $UO_{2\pm x}$ with the fractional concentration of Frenkel defects (which is, of course, T-dependent), and taking their contribution, W_F, to W to be given by:

$$W_F = \frac{1}{2}[W(UO_{2+x}) + W(UO_{2-x})] \qquad (6.18)$$

Although empirical expressions are available[144] for the enhanced thermal *resistivity* of UO_{2+x} (relative to $UO_{2.00}$) a function of x, the situation in the case of UO_{2-x} is much *less* clear - values of $\lambda(UO_{2-x})$ both higher *and* lower than those of UO_2 having been reported[145], depending both on the temperatures attained and the range of x values of the specimens used; it is, however, difficult to understand the occurrence of the elevated values unless a U-metal phase was present – which is usually the case unless $T >> 2000$ K. If the x-trends of $\lambda(UO_{2\pm x})$ are genuinely *opposite*, then to a first approximation, $W_F \approx 0$, *whence* the dominant effect of Frenkel disorder must be anticipated to be on the values of the lattice frequencies, on which the parameter B in $\lambda_L = (A+BT)^{-1}$ depends.

Assuming, however, that both hyper and hypo deviations from stoichiometry result in *lower* λ values, then it can be shown - if the oxygen interstitials and

---

New York, USA (1976)).

vacancies give *equal* contributions to W_F - that at the highest temperatures reached in the present experiments, the oxygen Frenkel induced decrease in λ_L actually *outweighs*[xxxv] the increase due to λ_{AP}. Only if W_F is assumed to be independent of oxygen vacancies and the empirical x-dependencies of both A *and* B are taken into account, can the empirical temperature trend of $\lambda(T)$ be reproduced. Evidence of enhanced phonon scattering due to oxygen Frenkel disorder may be provided by the thermal conductivity (diffusivity) of ThO_2 (which has no λ_{AP} contribution), where it would manifest itself in $\lambda(T)$ values *lower* than those given by extrapolation of the T-dependence of $\lambda(T)$ established at temperatures well below the onset of Frenkel disorder (including, of course, that due to thermal expansion).

6.6.6 *Cross-effects*

As emphasised in the Chapter 1, whilst it is valid to linearly superpose λ_L and λ_{AP}, it must be realised that the two components are *not* actually *independent*[xxxvi]; this is readily apparent in the case of λ_{AP}, where the effect of phonon scattering is automatically included *via* the electrical conductivity, $\sigma(T)$. In the case of λ_L, however, the reciprocal scattering of phonons by *small polarons* has not yet been considered in the case of UO_2. Assuming a contribution proportional to the number density of intrinsically produced small polarons, an *additional*, T-dependent

---

[xxxv] The increased phonon scattering due to oxygen interstitials present in high concentrations [see Ref. 89], consistent with high temperature neutron scattering data [Ref. 98] resulting in a decrease of λ_L by about 0.1 $Wm^{-1}K^{-1}$.

[xxxvi] The *inter*dependence of λ_L and λ_{AP} which arises essentially from that of the respective relaxation times, manifests itself more transparently in the following *non-additive* expression for the total thermal diffusivity, a (itself an 'effective' relaxation, of course) which can be obtained directly from the definition of a in terms of the total thermal conductivity λ and total heat capacity c_P (in $Jm^{-3}K^{-3}$) - namely $a=\lambda/c_P$ - using the *additivity* of the lattice and ambipolar contributions to λ and c_P:

$$a = \frac{a_1}{(1+C_2/C_1)} + \frac{a_2}{(1+C_1/C_2)} = a_1 + a_2 - \frac{1}{C}(a_1C_2 + a_2C_1)$$

Where $\alpha_i \equiv \lambda_i / C_i$, and index $1 \equiv L$ and $2 \equiv AP$, and C is the total heat capacity at constant pressure. The second form of the above equation clearly reveals the extrinsic *non*-additivity of the individual diffusivity contributions. However, the 'cross-effects' between the lattice and ambipolar

contribution to the *lattice* thermal resistivity $\propto e^{-U/2kT}$ must be anticipated, where U (which can be empirically evaluated from Eq.(6.9)) is the enthalpy required to produce U^{3+} and U^{5+} ions *via* $2U^{4+} \Leftrightarrow U^{3+} + U^{5+}$). If this contribution is of a magnitude comparable to the remaining *purely* lattice contributions, then the lattice thermal conductivity of UO_2 will be *lower* then, for instance, that of ThO_2 (where there are *no* intrinsic small polarons), so precluding the possibility of identifying $\lambda_L(UO_2)$ with $\lambda_{Total}(ThO_2)$.

A secondary effect of the existence of small polarons on the lattice conductivity is a modification in the value of the 3-phonon-scattering coefficient B through its dependence on the lattice frequencies. For, as shown in Ref.[146], the lattice frequencies are perturbed in the vicinity of the small polarons (the altered valent U^{5+} and U^{3+} cations), resulting in a *softening* of the lattice in the vicinity of the U^{3+} *i*ons and a (much stronger) *hardening* in the vicinity of the U^{5+} ions.

6.7 Conclusions

For the first time, values of the thermal diffusivity, a, and specific heat c_P, of uranium dioxide were experimentally obtained in the temperature range 1800 K-2900 K from simultaneous measurement of *on the same sample,* using precise instrumentation and sophisticated analysis.

Up to the highest temperature investigated the new specific heat data is in excellent agreement with the reported literature values obtained from enthalpy measurements[3]. It should be noted however, that in neither the present work or in that of Hein and Flagella[3] is there any indication of the Bredig transition - although this was revealed in a more sophisicated analysis of the data, subsequently developed[146]. In the present work, temperatures in the immediate vicinity of the transition were deliberately excluded because of the existence of significant temperature gradients in the sample, entailing a temperature difference of ~ 100 K between the front and the back surfaces of the sample.

---

contributions, mentioned in Chapter 1, may intrinsically affect both a and a_i, according to Eq.(1.1).

Above the temperature of the Bredig-transition, the new values of c_P continue to increase, but somewhat less strongly than below this temperature; the values are nevertheless higher than what can be accounted for theoretically[89], and, most interestingly, when extrapolated to the melting point are very close to the liquid values obtained directly using laser heating[126].

The measured thermal diffusivity is in good agreement with previous experiments[114,115] up 2200 K, above which the new values are close to those of Bates[115], but lie systematically below those of Weilbacher[114].

The thermal conductivity of UO_2 was derived from the equation $\lambda = a c_P \rho$, using the measured values of c_P, a and density at room temperature, corrected to the temperatures of the experiment using thermal expansion data from the literature.

The new values of λ confirm the existence of a minimum around 2000 K, but the upswing at higher temperature is less pronounced than previously reported - see Fig 6.12.

The thermal diffusivity of the *same* samples of UO_2 (as were studied at high temperatures) was measured (using a different laser-flash device) in the temperature range 550 to 1900 K. The values obtained are in excellent agreement with those in the literature (when corrected to the same porosity - 95% th.d.), and smoothly join the values measured at higher temperatures. Hence all the experimental measured values were merged and fitted in the temperature range 550-2900 K with the equation:

$$a = \frac{1}{1.30 \cdot 10^5 + 8.099 \cdot 10^2 T} \ (\mathrm{m^2 s^{-1}})$$

where T is in K.

The thermal conductivity values derived from all the experimental measurements (to calculate λ at low temperatures, the c_P values of Ref.[110] were used) have been fitted with the following equation:

$$\lambda = 12.57829 - 0.02311T + 2.36675 \cdot 10^{-5} T^2 - 1.30812 \cdot 10^{-8} T^3 + 3.6373 \cdot 10^{-12} T^4 - 3.90508 \cdot 10^{-16} T^5 \quad (\mathrm{Wm^{-1}K^{-1}}) \quad (6.4)$$

The thermal conductivity of stoichiometric UO_2, extrapolated to the melting point using Eq.(6.4), give $\lambda(T_m) \cong 3$ $\mathrm{Wm^{-1}K^{-1}}$, a value which is no longer inexplicably high compared to that of the liquid (2.5 ± 1 $\mathrm{Wm^{-1}K^{-1}}$)[127].

Using Eq.(6.4), much better agreement is now obtained with the experimental value of the conductivity integral to melting.

The new thermal conductivity values are reproducible with the following theoretical equation (valid between room temperature and the melting point, for 95% dense, stoichiometric material), derived from an analysis of the heat transport mechanisms UO_2

$$\lambda(t) = \left(\frac{10^2}{6.548 + 23.533t} + \frac{6400 e^{\frac{16.35}{t}}}{t^{5/2}} \right)^{-1} \quad (\mathrm{Wm^{-1}K^{-1}})$$

where the first term on the right hand side is the lattice conductivity and the second is the ambipolar contribution; $t = 10^{-3} T$

Chapter 7

7. SUMMARISED CONCLUSIONS

In this Thesis, a new technique is described by which *one single heat pulse*, deposited onto the surface of a sample under cylindrical symmetry conditions, enables both the thermal diffusivity and the specific heat to be *simultaneously* measured with an *absolute method*. The technique is based on the accurate record of the temperature perturbation produced on one or both faces of the sample platelet, and on the analysis of its propagation along the axial and radial directions.

This technique was successfully applied for high temperature measurements in three important refractory materials exhibiting diverse thermophysical properties.

- The method, which represents an extension of the classical laser-flash technique, was realised by an experimental set-up especially constructed for this purpose. Four design features resulted to be crucial for its successful application, *i.e.*:
  - *i.* the homogeneity and axial symmetry of the energy deposition on the sample surface by the probe laser,
  - *ii.* the use of a continuous-wave laser for the steady state temperature conditioning,
  - *iii.* the sensitivity, precision and rapidity of the (ad-hoc constructed) pyrometers,
  - *iv.* the development of a new analytical procedure, which utilises the entire experimental transient temperature curve, accounting for realistic laser-pulse shapes and heat losses.

  The first feature is essential for an *absolute measurement* of c_p, whilst *iii*) and *iv*) ensure a high accuracy of both c_p and a measurements. Flexible, appropriate and very clean heating and environmental conditions can be finally established thanks to *ii*).

The method was applied in a temperature range where it offers unique advantages:

a) with respect to traditional drop calorimetry, where c_p is calculated from the numerical temperature derivative of enthalpy. In our case c_p is measured:
   1. *directly,* from the energy input,
   2. with a better precision and accuracy, since at high temperatures the unavoidable heat losses are intrinsically accounted for, evaluated, and checked for self-consistency with other measured quantities,
   3. rapidly (within a few minutes), thus avoiding problems deriving from too long exposures of the sample to high temperatures.

b) with respect to preceding, similar calorimetric techniques based on laser-flash, since the new technique allows:
   1. an *absolute* measurement of the specific heat,
   2. a simultaneous measurement, through a *single* laser pulse, of *both* specific heat *and* thermal diffusivity.

   And, furthermore,
   3. the surface of the specimen does not require any blackening treatment.

- The technique was firstly tested on POCO AXM-5Q graphite, a recommended standard reference material for thermophysical measurements at high temperatures. The new measurements of thermal diffusivity and specific heat cover a range (1800 K - 3200 K) higher than that explored in published works; in the common temperature range, they are in good agreement with the recommended values, whilst above 3000 K they provide an extension of the previous database. The thermal conductivity, derived from the measured diffusivity and specific heat values, shows a good agreement with the published conductivity values calculated from the *electrical* resistivity.

- Y_2O_3-stabilised zirconia is a widely used refractory ceramic, whose optical transparency entails, however, serious difficulties in the application of the laser-flash method. The successful measurements of the thermal diffusivity and specific heat of this material at very high temperatures - where zirconia becomes *less* transparent - represents an important validation of the new method. The results obtained indicate that the heat capacity at very high temperatures increases very weakly with *T*. This casts new light on an old controversy which arises from the large discrepancy of the literature data, some of which show a dramatic increase of $c_p(T)$ at high temperatures, and others an almost constant specific heat. In this work, it was proved that the stoichiometric stability of the examined oxide prevents the upswing of the heat capacity, ensuring the persistence of its outstanding thermal isolation properties up to temperatures near the melting point.

- The thermal diffusivity and the heat capacity of uranium dioxide was finally measured from 500 K to 2900 K. The heat capacity function $c_p(T)$, which in UO_2 exhibits above 1500 K a sharp upswing, mainly due to oxygen Frenkel pair formation, continues to increase even at temperatures above the lambda transition (~2670 K), across which the defect concentration in the oxygen sublattice increases abruptly. The inverse thermal diffusivity shows a linear dependence on temperature up to the lambda-transition, whilst at higher temperatures negative deviations from the extrapolated straight line are observed. According to the simplest phonon scattering model, the linear dependence of $1/a$ on T entails that the defect concentration and the elastic properties of the lattice are approximately constant over a very broad temperature interval. This is an indirect confirmation of the almost step-like increase of the Frenkel pair concentration across the second-order lambda transition. Above 2200 K the measured thermal diffusivity decreases below the currently recommended curve, which is, however, strongly affected by previous spurious measurements. A new expression for the thermal

conductivity as a function of temperature is finally proposed, which is corroborated by some theoretical considerations on the underlying heat transport mechanisms.

REFERENCES

1. S.R. De Groot and P. Mazur, *Non-Equilibrium Thermodynamics* Chapter XI, North-Holland Publ. Co., Amsterdam NL (1962).
2. R. A. Hein, L. H. Sjodahl, and R. Szwarc, *J. Nucl. Mater.* **25,** 99 (1968).
3. R.A. Hein, P.N. Flagella, Report GEMP-578, General Electric Company, Cincinnati, Ohio, USA (1968).
4. *Standard Terminology relating to Thermal Insulating Materials*, ASTM Designation C 168-90, Annual Book of Standards, Vol. 04.06. American Society for Testing and Materials, West Conshohocken, Pa (1995).
5. Tye, *Thermal Conductivity*, Vol. 1 and 2, ed. P.Tye, Academic Press, New York (1969).
6. Y.S. Touloukian, R.W. Powell, C.Y. Ho, and M.C. Nicolaou, *Thermal Conductivity in Thermophysical Properties of Matter*, Vol. 2, IFI Plenum, New York (1970), p. 1a.
7. K.D.Maglic, A. Cezairliyan and V.E. Peletsky, *Compendium of Thermophysical Property Measurement Methods*, Vol. 1 Survey of Measurement Tecniques, and Vol. 2. Recommended Measurement Techniques and Practices, eds. Plenum, Newyork (1984).
8. H.L. Callendar and J.T. Nicholson, *Brit. Assoc. Adv. Sci., Rept. Ann. Meeting* 418 (1987).
9. F. Kohlrausch, *Sitz. Berlin. Akad.* **38,** 711 (1899).
10. W.J. Parker, R.J. Jenkins, C.P. Butler, and G.L. Abbot , *J. Appl. Phys.* **32,** 1679 (1961).
11. H.S. Carslaw and J.C. Yeager, *Conduction of Heat in Solids*, Oxford U.P., England (1959), p. 101.
12. H.L. Lee, and P.H. Hasselman, *J. Am. Ceram. Soc.*, **68,** C-12 (1985).
13. M.J. Wheeler, *Brith. J. Appl. Phys* **16,** 365 (1965).

14. L.P. Phyllipov in *Compendium of Thermophysical Property Measurement Methods*, Vol. 1. Survey of Measurement Tecniques, K.D.Maglic, A. Cezairliyan and V.E. Peletsky, eds. Plenum, Newyork (1984), p.337.

15. R. De Coninck and V.E. Peletsky in *Compendium of Thermophysical Property Measurement Methods*, Vol. 1. Survey of Measurement Tecniques, K.D.Maglic, A.Cezairliyan and V.E. Peletsky, eds. Plenum, Newyork (1984), p.367.

16. J.C. Van Craeynest and J.C. Weilbacher, *J. Nucl. Mater.* **26**, 132 (1968).

17. C. Starr, *Rev. Sci. Instrum.* **8**, 61 (1937).

18. R.W. King, *Phys. Rev. Ser. 2* **6**, 437 (1915).

19. L.P. Phylippov, *Teplofiz. Vys. Temp. (High temp. Thermophys.)* **2**, 817 (1964).

20. M.M. Mebed, R.P. Yurchak, and L.P. Phylippov, *High Temp-High Press.* **5**, 253 (1973).

21. A.A. El-Sharkawy, R.P. Yourchak, and S.R. Atalla, *Thermal Conduct.* **14**, 209 (1976).

22. E.M. Kravchuk, *Inzh.-Fiz. Zh.* **5**, 59 (1962).

23. E.M. Kravchuk, *Inzh.-Fiz. Zh.* **6**, 3 (1963).

24. W.J. Parker, *Proc. 2nd Conf. On Thermal Conductivity*, Ottawa, Ontario, (1962) p. 33.

25. J.A. Cape and G.W. Lehman, *J. Appl. Phys.* **34**, 1909 (1963).

26. R.D Cowan, *J. Appl. Phys.* **34**, 926 (1963).

27. W.J. Parker and R.J. Jenkins, *Advanced Energy Convertion*, **2**, 87 (1962).

28. A.R. Mendelsohn, *Appl. Phys. Letters*, **2**, 19 (1963).

29. D.A. Watt, *Br. J. Appl. Phys.* **17**, 231 (1966).

30. A.B. Donaldson, *J.Appl. Phys* **43**, 4226 (1972)

31. L.M. Clark III and R.E. Taylor, *J. Appl. Phys* **46**, 714 (1975).

32. A. Degiovanni, *High Temp-High Press.* **17**, 683 (1985).

33. H.S. Carslaw and J.C. Yeager, *Conduction of heat in Solids*, Oxford U.P., England (1959) p. 126.

34. R.C. Heckman, *Proc. of 14th Int. Thermal Conductivity Conference*, ed. P.G. Klemens, and T.K. Chu, Plenum Press, New York, (1976) p.491.
35. R.C. Heckman, *J. Appl. Phys* **44**, 1455 (1973).
36. H.M. James, *J. Appl. Phys* **51**, 4666 (1980).
37. D.L. Balageas, *High Temp-High Press.* **21**, 85 (1989).
38. J. Gembarovic and R.E. Taylor, *Rev. Sci. Instrum.* **65**, 3535 (1994).
39. T.L. Shaw and W.E. Ellis, *High Temp-High Press.* **30**, 127 (1998).
40. R.E. Taylor and J.A. Cape, *Appl. Phys. Letters* **5**, 212 (1964).
41. K.B Larson and K. Koyama, *J. Appl. Phys.* **38**, 465 (1967).
42. R.E. Taylor and L.M. Clark III, *High Temp-High Press.* **6**, 65 (1974).
43. T. Azumi and Y. Takahashi, *Rev. Sci. Instrum.* **52**, 1411 (1981).
44. C.B. Vining, A. Zoltan and J.W. Vandersande, *Int. Journ. of Thermophys.* **10**, 259 (1989).
45. R.E. Taylor, Report PRF-6764, Available from NTIS PB 225 591/7AS, National Technical Information Service, Springfield, Virginia (1973).
46. A. Cezairliyan, T. Baba, and R. Taylor, *Int. Journ. of Therm.* **15**, 317 (1994).
47. K. Beedham and I.P Dalrymple, *Rev. Int. Hautes Tempér. Réfract.* **7**, 278 (1970).
48. J.T. Schriempf, Report of NRL Program, Naval Research Laboratory (1972).
49. J.T. Schriempf, *Rev. Sci. Instrum.* **43**, 781 (1972).
50. J.A. Mackay and J.T. Schriempf, *J. Appl. Phys.* **47**, 1668 (1976).
51. T. Baba, M. Kobayashi, A. Ono, J.H. Hong, and M.M. Suliyanti, *Thermochimica Acta* **218**, 329 (1993).
52. J. Xue and R. Taylor, *Int. Journ. of Thermophys.* **14**, 313 (1993).
53. J. Xue *High Temp-High Press.* **17**, 691 (1985).
54. Y. Agary, A. Ueda, S. Nagai, *J. of Polymer Science; Part B; Polymer Physics* **33**, 33 (1995).
55. J.W. Vandersande, A. Zoltan, C. Wood, *Int. Journ. of Thermophys.* **10**, 251 (1989).

56. Y. Takahashi, *J. Nucl. Mat.* **51**, 17 (1974).

57. Y. Takahashi, H. Yokokawa, H. Kadokura, Y. Sekine, and T. Mukaibo, *J. Chem. Thermodyn.*, **11**, 379 (1979).

58. Y. Takahashi, K. Yamamoto, T. Ohsato, H. Shimada T. Terai, *J. Nucl. Mat.* **167**, 147 (1989).

59. T. Baba *Proc. of 11th Japan Symposium on Thermophysical Properties,* Tokyo, November 6-8, (1990), p.449.

60. G. He, J. Tao, D. Cao, S. Dong, and B. Zhou, *Proc. of 1st Asian Symposium on Thermophysical Properties,* China Academic , Beijing (1986), p 321.

61. G. He, J. Tao, D. Cao, S. Dong, and B. Zhou, in *Proc. of 1st European Conference on Thermoelectrics*, ed.D.M. Rowe, Peter Peregrinus, London (1988), p. 142.

62. Y. Qingzhao and W. Likun, *Proc. of the 1st Asian Symposium on Thermophysical Properties,* China Academic , Beijing (1986) p 325.

63. H.S. Carlslaw and J.C. Jaeger, *Conduction of Heat in Solids*, Claredon, Oxford, England, (1971) Chap.XIV, Sect. 14.3.

64. R. Fletcher, U.K. Harwell Report AERE 6799 (1971).

65. R.A. Fisher *Statistical Methods for Research Workers*, Oliver and Boyd, Edinburgh, (1950).

66. E. Fitzer, AGARD Advisory Report AR 31-71, Neuilly-sur-Seine, France (1971).

67. E. Fitzer, AGARD Advisory Report, Neuilly-sur-Seine, France AR 38-72 (1972).

68. E. Fitzer, AGARD Advisory Report 606, Neuilly-sur-Seine, France (1973).

69. E. Fitzer, AGARD Advisory Report 12, Neuilly-sur-Seine, France (1967).

70. A.D. Little, Technical Report AFML-TR-69-2, (June 1969).

71. R.E. Taylor and H. Groot, *High Temp.-High Press.* **12**, 147 (1980).

72. R. Taylor, *Proc. of 17th Int. Thermal Conductivity Conference,* G. J. Hust, ed. Plenum, New York (1983), p. 753.

73. M. Sheindlin, D. Halton, M. Musella, C. Ronchi, *Rev. Sci. Instrum.* **69**, 1426 (1998).

74. L. Latiev V. Petrov, V.Y. Chekhovskoy and E. Shestakov, Radiation Properties of solids, Moscow, Energia (1974).

75. A. Cezairliyan and F. Righini, *Rev. Int. Hautes Temp. Refract.* **12**, 124 (1975).

76. A. Cezairliyan and A.P. Miiller *Int. Journ. of Thermophys.* **6**, 3, 285 (1985).

77. JANAF, IVTANTHERMO Database ©, ed. L.V.Gurvich, Thermocenter, Russian Academy of Sciences, Moscow (1993).

78. C.F. Lucks, H.W. Deem, and W.D. Wood, *Am. Ceram. Soc. Bull.* **39**, 313 (1960).

79. E.D. West and S. Ishihara, *3rd ASME Symposium*, Lafayette, Ind., 146 (1965).

80. T. Baba and A. Cezairliyan, *Int. J. of Thermophys.* **15**, 343 (1994).

81. R. Brandt and G. Neuer, *Proc. of 17th Int. Thermal Conductivity Conference,* G. J. Hust, ed. Plenum, New York (1983), p. 117.

82. E. Fitzer, S. Weisenburger, *Proc. of 12th Int. Thermal Conductivity Conference,* H.J. Sauer Jr., ed. R.L Reisbig (1974), p. 26.

83. M. Minges, *Int. J. Heat Mass Transfer*, **20**, 1161 (1977).

84. C.H. Liebert, *Thin Solid Films* **53**, 235 (1978).

85. V.Y. Chekhovskoy, V.Y. Zukhova and V.D. Tarasov, *Tepl. Vys.Temp.* **17**, 754 (1979).

86. C.D. Pears, U.S. Report ASD-TDR 62-765 1-420 (AD 298 061) (1963).

87. C. Ronchi, J.P. Hiernaut, *J. Alloys and Comp.* **240**, 179-185 (1996).

88. L.B. Pancratz, E.G. King and K. Kelley, US Bur. Mines, Rept. Invest. 6033 **1**, 8 (1962).

89. C. Ronchi, G.J. Hyland, *J. Alloys and Comp.* **213/214**, 159 (1994).

90. M. Faucher, F. Cabannes, A.M. Anthony, B. Piriou, and J. Simonato, *Rev. Int. Hautes Temp. Refract.* **7**, 290 (1970).

91. P. Morrell and R. Taylor *High Temp-High Press.* **17**, 79 (1985).

92. L. Pawlowsky, D. Lombard, A. Mahlia, C. Martin, and P. Fauchais, *High Temp-High Press.* **16**, 347 (1984).

93. V.Y. Chekhovskoy, A.M. Banaev, *Heat and Mass Transfer* Vol. VII, Ed. Acad. A.V.LIKOV, "Nauka I Tekhnika" , URSS, Minsk (1968), p. 591.

94. M. Bober, H.U. Karow, and K. Müller, *High Temp.-High Press.* **12**, 161 (1980).

95. J.B. Conway, R.M. Fincel and R.A. Hein, *Trans. Amer. Nucl. Soc.* **6**, 1553 (1963).

96. J.A. Christensen, *J. Amer. Cer. Soc.* **40**, 607 (1963).

97. D.G. Martin, *J. Nucl. Mater.* **152**, 94 (1988).

98. M.T. Hutchings, *Chem. Soc. Faraday, Trans. II* **83**, 1083 (1987).

99. J.P. Hiernaut, G.J. Hyland, and C. Ronchi, *Int. J. Thermophys.* **14**, 259 (1993).

100. L. Leibowitz, L.W. Mishler, and M.G. Chasanov, *J. Nucl. Mater.* **29**, 356 (1969).

101. J.B. Conway and R.Hein, *J. Nucl. Mater.* **15**, 142 (1965).

102. G.E. Moore and K. Kelley, *J. Am. Chem. Soc.* **69**, 2105 (1947).

103. A.E. Ogard and L. Leary, *Thermodynamics of Nuclear Materials*, IAEA, Vienna (1969), p.651.

104. C. Affortit, *High Temp.-High Press.* **1**, 27 (1969).

105. C. Affortit, J.P. Marcon, *Rev. Int. Hautes Temper. Et Refract.* **7**, 236 (1970).

106. R. Brandt, G. Haufler and G. Neuer, *Thermal Conductivity and Emittance of Solid UO2*, CINDAS Purdue University Indiana, (1976) p. 42.

107. G.J. Hyland and R. Ohse, *J. Nucl. Mater.* **140**, 149 (1986).

108. T.G. Godfrey, J.A. Woolley, and J.M. Leitnaker, Report ORNL-TM-1596, Oak Ridge National Laboratory, Oak Ridge, Tennessee (1966).

109. G.J. Hyland, *J. Nucl. Mat.* **140**, 149 (1986).

110. J.K. Fink, M.G. Chasanov, and L. Leibowitz, *J. Nucl. Mater.* **102**, 17 (1981).

111. J.K. Fink, *Int. J. Thermophys.*, **3**, 165 (1982).

112. J.K. Fink, M.C. Petri, Report ANL/RE 97/2 Argonne National Laboratory, Illinois, USA (1997).

113. JANAF, IVTANTHERMO Database ©, ed. L.V.Gurvich, Thermocenter, Russian Academy of Sciences, Moscow (1993).

114. J.C. Weilbacher, *High Temp.-High Press.* **4,** 431 (1972).

115. J.L. Bates, Report BNWL-1431 Battelle Memorial Institute, Pacific Northwest Laboratory, Washington, USA (1970).

116. J.C. Stora, B. Desigoyer, R. Delmas, P. Deschamps, B. Lavaud, C. Ringot, Report CEA-R-2586, Commissariat à l'Energie Atomique, Fontenay-aux-Roses, France (1964).

117. V.I. Kolyadin, Eh.P. Il'in, A.G. Kharlamov, V.V. Yakovlev, Report IAE-2227 Gosudarstvennyj Komitet po Ispol'zovaniyu Atomnoj Energii SSSR, Moscow. Inst. Atomnoj Energii, USSR (1972).

118. J-Å. Gyllander, *Report AE-411*, Aktiebolaget Atomenergi, Studsvik, Nyköping, Sweden (1971).

119. M.F. Lyons, R.L. Straley, D.H. Coplin, B. Wiedenbau, and T.J. Pashos, *Trans. Am. Nucl. Soc.* **6** 152 (1963).

120. D.R. De Halas, *Nucleonics* **21,** 92 (1963).

121. A.D. Feith, Report GEMP-296 General Electric Company, Ohio, USA (1964).

122. D. Susnik, U. Runfors, Report AE RMB 1035 AB Atomenergi, Sverige (1968).

123. J.C. Weilbacher, Report CEA-R-4572 Commissariat à l'Energie Atomique, Fontenay-aux-Roses, France (1974).

124. T.P. Salikhov, V.V. Kan, and C. Ronchi, *Proc. of 5th International Workshop on Subsecond Thermophysics*, Aix-en-Provence, France, June 16-19 (1998).

125. C. Ronchi, *J. Phys. Cond. Matter* **6,** L561 (1994).

126. C. Ronchi, J.P. Hiernaut, R, Selfslag, G.J. Hyland, *Nucl. Sci. & Engin.* **113,** 1 (1993).

127. H.A. Tasman, Report TUAR88, European Commission, Joint Research Centre, Karlsruhe, Germany (1988).

128. IAEA Panel Report "*Thermal Conductivity of Uranium Dioxide*", Technical Reports Series No.59, IAEA, Vienna, Austria (1966).

129. M.F. Lyons, D.H. Coplin, T.J. Pashos, B. Weidenbaum, Report GEAP 44624, General Electric Company, California, USA (1964).
130. J.L Bates, *Nucleonics* **19**, 83 (1961).
131. J.A. Christensen, WCAP-2531 (1963).
132. J.L.Bates, *Thermodynamics II* IAEA, Vienna (1965) p.73.
133. I.C. Hobson, R. Taylor, and J.B. Ainscough, *J. Phys.* **D7**, 1003 (1974).
134. J.C. Killeen, *J. Nucl. Mater.* **92**, 136 (1980).
135. D.G. Martin, *J. Nucl. Mater.* **110**, 73 (1982).
136. G. J. Hyland, *J. Nucl. Mater.* **13**, 125 (1983).
137. J.H. Harding, and D.G. Martin, *J. Nucl. Mater.* **166**, 223 (1989).
138. J.A. Stoddard and N.J. McCormick, *Nucl. Sci. Eng.* **3**, 126 (1970).
139. E.E. Anderson, *Nucl. Technol.* **30**, 65 (1976).
140. M. Bober, *Proc. 8th Symp. on Thermophysical Properties*, NBS Gaithersburg, Maryland, (1981) (unpublished).
141. J.M. Casado, J.H. Harding and G. J.Hyland, *J. Phys. Cond. Matter,* **6**, 4685 (1994).
142. D.J. Ecsedy and P.G. Klemens, *Phys. Rev.* **B15**, 5957 (1977).
143. J. Ranninger, *Phys. Rev.* **140A**, 2031 (1965).
144. D. G. Martin, Report BPC/P(89) 393, United Kingdom (1989).
145. B. Schulz, in "*Gmelin Handbook of Inorganic Chemistry, U*", Supplement Vol. C5, Springer, Berlin, Germany (1986), p.168.
146. G.J. Hyland and J. Ralph, *High Temp.-High Press.* **15**, 179 (1983).
147. Y.S. Touloukian, D.P. DeWitt, *Thermal Radiative Properties, Non Metallic Solids,* Vol.8, Ifi/Plenum, New-York, Washington (1972).
148. Private communication.
149. R. Taylor, *Brit. J. Appl. Phys.* **16** 509 (1965).
150. R.F. Bulmer, R. Taylor, *High Temp.-High Press.* **6**, 491 (1974).
151. R. Taylor, *High Temp.-High Press.* **4**, 649 (1972).
152. W.N. Dos Santos, R. Taylor, *High Temp.-High Press.* **25**, 89 (1993).

153. D.C. Oates, W. Nice, R. Taylor, W. Hanson *High Temp.-High Press.* **27/28,** 339 (1995/1996).

154. R. Brandt, G. Neuer, R. Taylor, *High Temp.-High Press.* **8,** 469 (1976).

155. H.Szelagowski, R. Taylor, *High Temp.-High Press.* **30,** 343 (1998).

156. Z. Fang, R. Taylor, *High Temp.-High Press.* **19,** 29 (1987).

157. H.A. Tasman, D. Pel, J. Richter, H.E. Schmidt, *High Temp.-High Press.* **15,** 419 (1983).

158. D. Schwingel, R. Taylor, J. Wigren, *High Temp.-High Press.* **30,** 253 (1998).

159. D. Schwingel, C. Persson, R. Taylor, T. Johannesson, J. Wigren, *High Temp.-High Press.* **27/28,** 273 (1995/1996).